UNCLASSIFIED

AD NUMBER

AD919993

NEW LIMITATION CHANGE

TO

Approved for public release, distribution unlimited

FROM

Distribution authorized to U.S. Gov't. agencies only; Test and Evaluation; FEB 1974. Other requests shall be referred to Air Force Materials Lab., AFSC, Wright-Patterson AFB, OH 45433.

AUTHORITY

AFWAL ltr, 1 Mar 1984

THIS PAGE IS UNCLASSIFIED

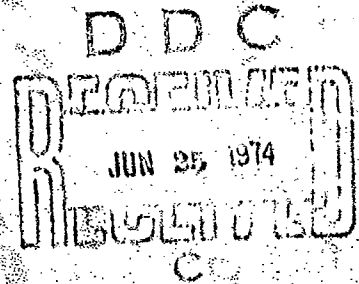UNCLASSIFIED

AD _9/9 993_

AUTHORITY: _AFWAL LTR_
1 MAR 84

AFML-TR-74-10
Volume I
D6-26271-6

AD919993

SLEEVE COLDWORKING FASTENER HOLES

Volume I—Discussion and Summary

Joseph L. Phillips
Manufacturing Research and Development
Boeing Commercial Airplane Company

D D C

JUN 25 1974

C

TECHNICAL REPORT AFML-TR-74-10, VOLUME I

February 1974

NOTICES

When Government drawings, specifications, or other data are used for any purpose other than in connection with a definitely related Government procurement operation, the United States Government thereby incurs no responsibility nor any obligation whatsoever; and the fact that the Government may have formulated, furnished, or in any way supplied the said drawings, specifications, or other data, is not to be regarded by implication or otherwise as in any manner licensing the holder or any other person or corporation, or conveying any rights or permission to manufacture, use, or sell any patented invention that may in any way be related thereto.

Many of the items compared in this report are commercial items that were not developed or manufactured to meet Government specifications, to withstand the tests to which they were subjected, or to operate as applied during this study. Any failure to meet the objectives of this study is no reflection on any of the commercial items discussed herein or on any manufacturer.

SLEEVE COLDWORKING FASTENER HOLES

Volume I—Discussion and Summary

Joseph L. Phillips

FOREWORD

This technical report covers all work performed under Contract F33615-72-C-1630 from 1 June 1972 to 30 November 1973. This manuscript was released for publication by the author in February 1974.

This contract with The Boeing Commercial Airplane Company was initiated under Manufacturing Methods Project 746-2, "Sleeve Coldworking Fastener Holes." It was conducted under the technical direction of Captain Carlan Silha, Metals Branch (AFML/LTM). Manufacturing Technology Division, Air Force Materials Laboratory, Wright-Patterson Air Force Base, Ohio.

This program was accomplished at The Boeing Commercial Airplane Company in Seattle, Washington, with Mr. Richard G. Christner as program manager, Mr. Joseph L. Phillips as principal investigator, and Mr. Ray Hendricks as primary coordinator and director of the testing program. Other personnel that supported the program in Boeing were DeVere Lindh, Dave Reese, Tom Kane, Burke Dykes, Walt Swift, and Merrell Christianson.

Publication of this final technical report does not constitute Air Force approval of the report's findings or conclusions. It is published only for the exchange and stimulation of ideas. Your comments are solicited on the potential utilization of the information contained herein as applied to your present and/or future production and/or your maintenance rework. Suggestions concerning additional manufacturing methods on this or other subjects will be appreciated.

This program was accomplished as part of the Air Force Manufacturing Technology Program, the primary objective of which was to develop on a timely basis, manufacturing processes and techniques for use in economical production of USAF materials and components for aircraft production.

This technical report has been reviewed and approved for publication.

H. A. JOHNSON
Chief, Metals Branch
Manufacturing Technology Division

ii

ABSTRACT

In this 21-month program, optimized process parameters for sleeve coldworking of fastener holes have been developed, and the effects of process and application parameters on structural performance have been defined for selected aluminum, titanium, and high-strength steel alloys. The sleeve coldworking process for fastener holes is a process that uses a tapered mandrel in conjunction with a disposable, prelubricated sleeve to compressively prestress a significant size zone around each hole which offsets the stress concentration of the hole itself. The sleeve method allows higher degrees of prestressing than possible with other methods and offers potential for significant improvements in fatigue performance. In addition, it does not require precision controls germane to other fatigue-rated hole preparation/fastener installation systems. This technical report covers the results of this 21-month program. In addition to definition of optimized methods and the effects of process and application variations upon structural performance, the results include performance and economics comparisons for the process with other fatigue-rated hole preparation/fastener systems. Volume II contains test data sheets and other supporting data.

TABLE OF CONTENTS

TABLE OF CONTENTS—Concluded

LIST OF FIGURES

LIST OF FIGURES--Continued

LIST OF FIGURES - Continued

LIST OF FIGURES--Continued

LIST OF FIGURES—Concluded

ABBREVIATIONS

ann	annealed
cl	clearance
config	configuration
C/W	coldwork
dia	diameter
E/M	edge margin
exp	expansion
hd	head
HLT	high load transfer
HSS	high-speed steel
interf	interference
K_t	stress concentration factor
LLT	low load transfer
R	stress ratio (min stress/max stress)
Rc	Rockwell hardness, C-scale
RHR	roughness height rating
S-N	maximum stress versus stress cycles to failure
SEM	scanning electron microscope
STA	solution treated and aged
STOA	solution treated and overaged
Ti-6Al-4V	6 aluminum, 4 vanadium titanium alloy
Ti-6Al-6V-2Sn	6 aluminum, 6 vanadium, 2 tin titanium alloy
ZLT	zero load transfer

SECTION I

INTRODUCTION

In a stressed component, a fastener hole creates a significant concentration of stresses; that is, the gross area stresses are magnified at the hole. If these stress concentrations are not reliably compensated for, critically stressed aircraft components will suffer premature failures under cyclic loading conditions. In addition, the methods of generating the holes, especially in higher strength metals, can lead to finish and metallurgical conditions that will amplify the problem.

The sleeve coldworking process offers what appears to be one of the most foolproof systems of compensating for these problems. This system utilizes a high-interference tapered mandrel with a disposable, prelubricated sleeve to prestress a significant-sized zone around each fastener hole. This zone is prestressed with a high-order compressive hoop stress that effectively mitigates the stress concentration. The process does not demand precision controls required for other fatigue-rated hole generation/fastener systems.

In this program, optimized process parameters for use of the process in 2024-T851 and 7175-T736 aluminum, Ti-6Al-4V and Ti-6Al-6V-2Sn titanium, and 300M steel have been developed. Additionally, the effect of process and application parameters upon performance have been defined. Phase I of this 21-month program covered development of the optimized process parameters; phase II covered definition of the effect of process variations and application parameters upon performance.

Phase I optimized mandrel taper angles, hole expansion values, sleeve design, sleeve lubricant, mandrel finish, hole sizing requirements and methods, multimaterial stack techniques, and inspection methods, and defined portable equipment, force requirements, edge bulging parameters and distortion parameters. Optimization was based on pull forces, sleeve thinout, hole profile, surface upset, and fatigue performance for 3/8- and 3/4-inch-diameter holes. Phase II primarily utilized fatigue coupon testing plus some stress corrosion and photostress testing to assess the effect of process and application parameters upon performance. This included effects of edge margin, hole spacing, load transfer, adjacent noncoldworked holes, sleeve-split orientation, sleeve design, subsequent hole sizing amount, filled versus nonfilled holes, fastener interference, countersink and countersink angle, countersink/coldworking sequence, differential growth, surface upset, joint prestress, prior hole processing, prior hole fatigue cycling, prior hole damage, subsequent hole damage, and material thickness.

This program was coordinated with contract F33615-71-C-1548, "Precision Hole Generation Methods," conducted at McDonnell Aircraft Company in St. Louis, Missouri. Hole generation criteria for certain specimens and fatigue specimen design were coordinated to allow valid comparisons of results.

SECTION II

SUMMARY

This program has taken the process of sleeve coldworking for fastener holes, as originally developed and utilized for aluminum structure, and refined it with regard to processing and application parameters in aluminum, titanium, and steel. Detailed results from the phase I process refinement effort are extensive and included in the body of this report; in summary, this effort produced the following results:

1) A change in mandrel taper from 0.015 inch/inch to 0.045 inch/inch that allows less back-side clearance and a significant reduction in force requirements

2) Definition of force requirements for different hole diameters and stack thicknesses in the program materials

3) Definition of optimum coldworking expansion values for different hole diameters in the program materials within the restraints of process capability, such as limits imposed by mandrel breakage above certain expansion values in the high-strength steel

4) Definition of surface upset profiles and hole axial profiles with regard to further definition of allowable part gapping, fretting shim requirements, and postsizing requirements

5) Definition of the effect of the process upon part growth, edge bulging, and distortion

6) Development of a successful sleeve process with a pull mandrel for the high-strength steel; albeit, the pull process has a capability to produce only one-half the retained expansion for an equivalent initial theoretical interference as the solid carbide mandrel push process

7) Definition of the current sleeve design, sleeve-split width, and internal sleeve lubricant as optimum for the process

8) Demonstration of the capability of the process to easily accomplish its beneficial prestressing in multimaterial stacks of aluminum and titanium

9) Definition of finite postsizing recommendations and initial hole size recommendations to assure that enough metal remains for full cleanup postsizing (Note: the phase II results indicate that postsizing or full cleanup may not be necessary for many zero- to low-load-transfer applications)

10) Detailed definition of portable tool requirements

11) Detailed listing of commercially available portable tools with specific capabilities designated

12) Definition of a suitable inspection procedure to assure proper processing has been accomplished

The phase II effort on application parameters is probably of the most interest. The results have shown many elements of definite significance, including several that were not anticipated. These results and/or interpretations are summarized in the following:

1) Fatigue test results for reamed only and honed only holes in this program were comparable to those achieved in the McDonnell Aircraft Company Precision Hole Generation Program (AFML-TR-73-135 report) even though testing speeds were different. Thus, performance results can be directly compared.

2) With small test specimens, in some metals, the use of net areas rather than gross areas (for calculating applied load stress) allows a properly prestressed fatigue specimen with a fastener in it to produce fatigue values better than base metal values.

3) The previous proved to be possible with the 2024-T851 aluminum alloy, but was not achieved with the Ti-6Al-4V titanium alloy and the 300M (270-300 ksi) steel. This might indicate that equivalent levels of prestressing (based on strength levels of the alloys) may not have been achieved in the titanium and steel. Edge strain measurements indicate that this was probably the case for the titanium, but not for the steel. The titanium, however, disclosed an erratic performance (wide scatter) at higher levels of coldworking interference.

4) In the 2024-T851 aluminum, a straight shank bolt in a coldworked hole produced a fatigue performance equivalent to a properly installed taperlok in zero-load-transfer as well as in high-load-transfer applications. The high-load-transfer application required some additional bolt interference (0.002 inch) to achieve equivalency. With the so-called "optimum" coldworking interference, however, an interference-fit bolt reduced performance of a zero-load-transfer application.

5) A flush installation tapered shank fastener proved to be inadequate in protecting the countersink in aluminum alloy installations, whereas, a coldworked hole that was postcountersunk had a fatigue performance slightly better than a noncountersunk hole. The flush tapered shank fastener in titanium installations, however, showed only a slight loss in performance over the protruding head versions in zero-load-transfer applications. The countersunk and coldworked holes in titanium still showed better performance than the tapered shank fasteners in the zero-load-transfer applications; however, the sequence of coldworking and countersinking was reversed in terms of best performance. This possibly is the result of inadequate prestressing in the titanium. It should be noted that the best

4

performance of all in the titanium (under zero-load-transfer conditions) was achieved by using an interference-fit bolt in a coldworked hole. The tapered shank results in titanium were very erratic and scattered.

6) In the high-strength steel, countersinking before coldworking was detrimental to fatigue performance, whereas, countersinking after coldworking produced the best overall results with zero load transfer.

7) Deletion of postreaming in coldworked holes demonstrated no influence upon fatigue performance of open holes or upon low-load-transfer specimens in the 2024-T851 aluminum. In the Ti-6Al-4V titanium, deletion of postreaming produced no change in open-hole performance, but some improvement over postreamed holes with low load transfer. Only open-hole performance of nonpostreamed holes was assessed in high-strength steel; in this case, it showed a significant improvement over coldworked and postreamed holes (which were no better than reamed only holes), but only a slight improvement over coldworked and postreamed holes produced in "as-drilled" (versus prereamed) holes.

8) Postreaming allowances for oversizing appear to be quite wide in aluminum and titanium with no significant difference in open-hole performance up to the 1/16 inch (on the diameter) removed in this program. The 300M (270-300 ksi) steel is more sensitive to the open-hole testing and shows a loss in performance at 1/64-inch removal, recovery at 1/32 inch, and a loss again at 1/16 inch. This is not necessarily illogical in view of the increase in performance achieved in countersinking the steel. That is, this more notch-sensitive material probably reacts to the loss of the initial, highly stressed compressive surface layer in terms of crack initiation. Further metal removal very likely reduces compression and tension prestress levels without reducing the size of the compressive zone and, in turn, may achieve a better balance of stresses to reduce crack propagation rates.

9) The span between "worst" performance and "best" performance was least with the aluminum and most with the steel. The worst performance in the aluminum is registered with zero load transfer, open, reamed only holes; whereas, in the titanium and steel, high-load-transfer applications produced drastic reductions in fatigue performance for all conditions. The best high-load-transfer performance in the titanium was achieved with the tapered shank fasteners. The tapered shank fasteners were not tested in the steel. Coldworking produced a 4 to 1 improvement in high-load-transfer applications in the steel at 110 ksi maximum-net test stress and a 20 to 1 improvement with zero load transfer at the same test stress.

10) In aluminum, surface upsetting appeared to cause no loss of performance from fretting in zero-load-transfer and low-load-transfer applications, but did produce some loss of improved performance with high-load-transfer applications. The use of a thin, micarta interface shim eliminated this fretting and the performance loss in aluminum. In titanium, high-load-transfer performance was best without the shim; in the steel it made no difference.

5

11) Open-hole-testing appears to be a valid approach for comparisons in aluminum, but raises questions of value with the more notch-sensitive materials. The author would definitely recommend that only filled-hole testing be used for future comparisons.

12) The stress corrosion tests of coldworked holes in the 300M (270-300 ksi) steel showed absolutely no problem with stress corrosion cracking after completion of almost 900 hours of alternate immersion testing in a 3-1/2% salt-water solution.

13) The lack of countersink protection from a tapered shank fastener and from coldworking where the countersink already exists (with exception to the titanium) means that neither would be worthwhile applying to flush installations in repair work on aluminum and steel structure where countersinks already exist. An exception would be an application whereby the underlying structure requires the protection.

14) Edge margins and hole-spacing variations showed no effect upon fatigue performance gains for coldworked holes in all materials beyond normal scatter bands with edge margins down to 1-1/2D and hole spacing down to 3D.

15) The 7175-T736 alloy showed appreciably better base metal fatigue performance than the 2024-T851, but was only slightly better in reamed, open and filled holes and in coldworked open holes. In coldworked and filled holes, it had slightly less performance than the 2024-T851.

16) The STA and STOA heat treat conditions for the Ti-6Al-4V titanium alloy did not produce as good fatigue performance as the annealed alloy under any test condition, including base metal.

17) None of the heat treat conditions for the Ti-6Al-6V-2Sn titanium alloy had better performance in any condition than the annealed Ti-6Al-4V titanium.

18) The STOA heat treat for the Ti-6Al-6V-2Sn titanium alloy showed slightly better fatigue performance than the annealed or STA conditions for the same alloy in the base metal tests and the reamed, filled holes. Neither the STA or the STOA were as good as the annealed condition with coldworked, filled holes.

19) The pull process with a sleeve developed in this program for the 270-300 ksi steel application produced the following relative fatigue performance at 110 ksi maximum-net area test stress with filled holes and zero load transfer:

    a) Reamed only   80,000 cycles

    b) C/W with steel mandrel and sleeve   150,000 cycles

    c) C/W with carbide mandrel   300,000 cycles

6

20) With unsupported thin aluminum material (0.060 inch), the high-interference coldworking process produced dishing of the material around the hole and no gain in fatigue performance from loss of prestress. In titanium, the loss was slight, and in steel there was no loss. The relative differences may be a result of differing material stiffness and also the differing sensitivity of the titanium and steel to open-hole testing. Stack sandwiching might also alter the aluminum result.

21) Post damage by scoring coldworked holes showed no loss in improved fatigue performance in any of the alloys indicating that the process would not be sensitive to damage caused by bolt installation or reaming.

22) The location of the sleeve split caused no loss of performance in zero-load-transfer testing of the aluminum, titanium, or steel. The discontinuity in the surface upset caused by the sleeve split may create localized interface fretting with aluminum under high-load-transfer conditions. Use of the previously mentioned micarta shim technique would avoid this problem.

23) Photostress analysis of precountersunk and coldworked specimens indicated that the sleeve-split discontinuity may be the determining factor in not providing protection for the countersink in aluminum. A solid sleeve may prove to be better for rework purposes where a countersunk already exists.

24) Proper drilling prior to coldworking was not detrimental to fatigue performance, but abusive predrilling was detrimental in aluminum and titanium. Both proper predrilling and abusive predrilling proved to be better than prereaming in coldworked holes in the 300M steel. This bears more investigation in terms of its potential for reducing current costs for critical hole generation controls in high-strength steel.

25) Prior fatigue cycling followed by sleeve coldworking and prior small fatigue cracks followed by sleeve coldworking resulted in no loss of fatigue performance for the aluminum, titanium or steel over that expected with unfatigued or uncracked holes.

26) The process displayed excellent repeatability of results without extreme care required in processing and provided protection for flush installations when correctly sequenced.

27) Cost analysis shows that provision of reliable coldworking protection is significantly less than that for the tapered fastener system and slightly more than a straight shank, interference-fit bolt system. The latter, however, is practically limited by diameter, whereas, the high interference, sleeve coldworking system is not.

SECTION III

PROGRAM PLAN

The program consisted of a two-phase effort. Phase I included eight separate tasks that developed optimized process parameters for applying the sleeve coldworking process to aluminum, titanium, and steel. Phase II included five separate tasks that defined the effects of process and application parameters upon the performance of these alloys—primarily with regard to fatigue. The basic intents of the program were: (1) to demonstrate that this process is a relatively low-cost, reliable process to assure repeatable, required performance of critical aircraft structure and components, and (2) to develop and define the necessary parameters to allow optimized use and application. A tabulation of the specific tasks is shown in figure 1. A more detailed delineation for each task follows.

1.   PHASE I: PROCESS PARAMETERS

a.   Task I—Optimum Mandrel Taper Angle

In this task, 3/8-inch- and 3/4-inch-diameter holes were coldworked to three different expansions with each of three different taper angles on the coldworking mandrels. This was accomplished in 2024-T851 aluminum, the Ti-6Al-4V titanium (annealed) and the 300M steel (270-300 ksi). Test materials were 3/8 and 1-1/2 inch thick for the 3/8-inch-diameter tools to provide both partial and full engagement of the mandrel tapers. Test material was 2 to 2-1/2 inches thick for the 3/4-inch-diameter tools to assure full engagement.

The coldworking was performed with the test material and a standard pull gun mounted in a Tinius-Olsen tensile/compression test machine (for aluminum and titanium). The test machine was used to push the carbide push mandrels for steel. A minimum of five holes was coldworked per condition to assess scatter. Pull forces were recorded for the different materials, thicknesses, mandrel taper angles, and hole/mandrel interferences. Coldworked holes were measured for surface upsetting, hole profile, and retained expansion. Coldworking sleeves were measured for thinout. Analysis of these data resulted in selection of a preferred mandrel taper angle for each metal.

1)   Test materials

   a)   3/8-inch-diameter tests

      i)   3/8-inch-thick 2024-T851 aluminum

      ii)   1-1/2-inch-thick 2024-T851 aluminum

      iii)   3/8-inch-thick Ti-6Al-4V annealed

9

  iv) 1-1/2-inch-thick Ti-6Al-4V annealed

  v) 3/8-inch-thick 300M steel (270-300 ksi)

  vi) 1-1/2-inch-thick 300M steel (270-300 ksi)

 b) 3/4-inch-diameter tests

  i) 2-1/2-inch-thick 2024-T851 aluminum

  ii) 2-1/2-inch-thick Ti-6Al-4V annealed

  iii) 2-1/2-inch-thick 300M steel (270-300 ksi)

2) Test mandrels

 a) Aluminum and titanium tests (H-11 steel, nitrided, pull design)

 b) Steel tests (883 carbide, push design)

3) Test sleeves

 a) Aluminum tests

  i) 3/8-inch-nominal diameter, axial split, 0.010 inch thick, 1-1/2 inch long, 301 stainless, 1/2 hard, internal Fel Pro 300 lubricant

  ii) 3/4-inch-nominal diameter, axial split, 0.015 inch thick, 1-1/2 inch long, 301 stainless, 1/2 hard, internal Fel Pro 300 lubricant

 b) Titanium and steel tests

  i) 3/8-inch diameter—as above, except full hard

  ii) 3/4-inch diameter—as above, except full hard

4) Test values

 a) Mandrel hole interferences (nominal)

  i) 3/8-inch diameter—0.009, 0.012, and 0.019 inch

  ii) 3/4-inch diameter—0.022, 0.026, and 0.032 inch

10

b) Mandrel tapers

    i) 3/8-inch diameter 0.015, 0.030, and 0.045 inch/inch on diameter

    ii) 3/4-inch diameter 0.020, 0.030, and 0.045 inch/inch on diameter

b. **Task 2—Optimum Mandrel/Hole Interference**

In this task, mandrels with optimum taper angles, based on task 1 tests, were utilized to coldwork fatigue coupons. The coupons used for testing are shown in figures 2 and 3 and were a zero-load-transfer type with two open holes. Fatigue coupon designs were coordinated with those used in the McDonnell Aircraft Company program, "Precision Hole Generation Methods," (contract AF33615-71-C-1548). These coupons were tested on the equipment shown in figures 4 and 5. Loads were selected on the basis of past testing experience to provide approximately 100,000 cycles to failure. Primary test variable was mandrel-hole interference values; four different interference values were used for each hole diameter (3/8- and 3/4-inch diameter). Selection of these values was based on prior test experience.

All fatigue test coupons were shot peened prior to coldworking the holes to ensure that fatigue testing measured hole performance rather than non-associated surface problems. Coupons were tested with tension-tension loading to a stress ratio of $+0.1$; stresses for loading were based on net areas. Only three coupons per condition were tested, unless scatter of results dictated the need for additional quantities.

Selection of optimum hole-mandrel interference values was based jointly on fatigue performance and an assessment of surface upsetting and operational forces required.

1) Test coupons

    a) 3/8-inch-diameter holes

        i) 1/4-inch-thick 2024-T851 aluminum per figure 2

        ii) 1/4-inch-thick Ti-6Al-4V annealed per figure 2

        iii) 1/4-inch-thick 300M steel (270-300 ksi) per figure 2

    b) 3/4-inch-diameter holes

        i) 3/8-inch-thick 2024-T851 aluminum per figure 3

        ii) 3/8-inch-thick Ti-6Al-4V annealed per figure 3

        iii) 3/8-inch-thick 300M steel (270-300 ksi) per figure 3

2) Test mandrels (as specified for task 1)

3) Test sleeves (as specified for task 1)

4) Test values

    a) Mandrel taper (as selected in task 1)

    b) Hole/mandrel interference

        i) 3/8-inch-nominal-diameter holes

            2024-T851 aluminum 0.010, 0.015, 0.020, and 0.025 inch

            Ti-6Al-4V titanium 0.010, 0.015, 0.020, and 0.025 inch

            300M steel 0.010, 0.015, 0.020, and 0.025 inch

        ii) 3/4-inch-nominal-diameter holes

            2024-T851 aluminum 0.025, 0.030, 0.035, and 0.040 inch

            Ti-6Al-4V titanium 0.025, 0.030, 0.035, and 0.040 inch

            300M steel 0.020, 0.025, 0.030, and 0.035 inch

    c) Miscellaneous parameters

        i) Sleeve-split orientation on coupon axis for all holes

        ii) Holes reamed to coldwork dimension prior to coldworking

        iii) Initial hole sizes selected to allow approximately 0.010-inch ream (on diameter) to nominal hole size after coldworking

c. Task 3—Pull Mandrel for High Strength Steel

The radial compression forces involved in coldworking holes in 270-300 ksi steel to high-expansion values have been estimated to be in the order of 500 ksi. This radial loading plus tensile or compressive axial loading to pull or push a mandrel through a hole creates a biaxial loading situation that is extremely rigorous. For 270-300 ksi steel, limited, previously conducted tests had not uncovered any combinations of material and design that would allow use of a pull-type mandrel without catastrophic mandrel failure. Existing techniques required use of a carbide, push-type mandrel. A pull-type mandrel, however, was extremely desirable since it would be more amenable to assembly operations. The push-type mandrel requires one of the following: (1) access for a squeeze yoke, (2) suitable attachment for thrust equipment, or (3) disassembly capability for press operations.

The intent of this task was to conduct tests with specific mandrel materials that had not been tested before and which appeared to have some potential for this type of operation. In addition, hole/mandrel interference values were varied starting at a low value to determine if there is an upper limit for this type of operation which is below the optimum fatigue value defined with carbide mandrels in task 2. Test criteria were based on mandrel failure, mandrel diameter retention, and retained hole expansion observations.

1) Test material

    a) 1-inch-thick 300M steel (270-300 ksi)

    b) 2-inch-thick 300M steel (270-300 ksi)

2) Test mandrels

    a) AISI 9260 threaded pull type

    b) Vascojet MA threaded pull type

    c) M42 HSS threaded pull type

3) Test sleeves

    a) 3/8-inch-nominal diameter, 0.010-inch wall, axial split, 301 stainless, full hard

    b) 3/4-inch-nominal diameter, 0.015-inch wall, axial split, 301 stainless, full hard

4) Hole/mandrel interference

    a) 3/8-inch-nominal diameter: start at 0.005 inch and proceed in 0.005 inch increments to optimum value defined in task 2

    b) 3/4-inch-nominal diameter: start at 0.010 inch and proceed in 0.005 inch increments to optimum value defined in task 2.

d. **Task 4 – Physical Effects and Remaining Mandrel/Sleeve Parameters**

This task included definition of:

1) Impact of sleeve coldworking to optimum values upon part growth, distortion, edge bulging and center line shifting as affected by edge margin, hole spacing, and/or countersink

2) Effect of part taper upon centerline shifting and retained expansion

3) Subsequent diameter creep relative to ultimate fastener fits

4) Optimized callouts for:

    a) Sleeve-split geometry

    b) Sleeve lubricant

    c) Mandrel

Test utilized growth, distortion, edge bulge, centerline shift, and diameter-creep measurements of coldworked specimens and holes to define general parameters for growth and distortion, application, and projected fastener fits. Measurements of pull forces in conjunction with a general analysis of operational factors defined the optimum sleeve-split configuration, sleeve lubricant, and mandrel finish.

It should be noted that the lubrication tests were relatively limited in lubricants being tested, only because a significant number of selected lubricants were already tested by the contractor in the original development of the process. Comparative data on the previously tested lubricants are included in this report.

1) Test materials

    a) Growth, distortion, edge bulge parameters

        i) 3/8-inch-diameter holes

            – 3/8- x 1-1/2- x 15-inch 2024-T851, Ti-6Al-4V, and 300M

            – 3/8- x 1-1/8- x 15-inch 2024-T851, Ti-6Al-4V, and 300M

            – 3/4- x 1-1/2- x 15-inch 2024-T851, Ti-6Al-4V, and 300M (tapered 2° and 4°)

        ii) 3/4-inch diameter holes

            – 3/4- x 3- x 15-inch 2024-T851, Ti-6Al-4V, and 300M

            – 3/4- x 2-1/4- x 15-inch 2024-T851, Ti-6Al-4V, and 300M

    b) Sleeve/mandrel parameters

        i) 3/8-inch-thick 2024-T851, Ti-6Al-4V, and 300M

2) Test mandrels

    a) As defined in previous tasks

b) As defined in previous tasks, but vapor blasted

3) Test sleeves

a) 3/8-inch-nominal diameter, 0.010-inch wall, 301 stainless, 1/2 hard, axial split, Fel Pro 300 lubricant

b) 3/4-inch-nominal diameter, 0.015-inch wall, 301 stainless, 1/2 hard, axial split, Fel Pro 300 lubricant

c) As in a), but full hard

d) As in b), but full hard

e) As in a), but lubricated with Dow Molycote "G"

f) As in a), but lubricated with Lifelube LLC-30

g) As in a), but lubricated with Lifelube LLC-36

h) As in a), but with helical split

i) As in a), but with scarfed axial split

e. Task 5—Multimaterial Stack Parameters

The intent of this task was to define the parameters or techniques required to sleeve coldwork fastener holes in assembly stacks of combination materials such as titanium and aluminum. Primary criteria for assessment of process were analysis of retained hole expansion, sleeve removal characteristics, and postsizing dimensions.

1) Test materials

a) 1/4- x 12- x 12-inch Ti-6Al-4V ⎤
    1- x 12- x 12-inch 2024-T851 ⎥ Stack
    1/4- x 12- x 12-inch Ti-6Al-4V ⎦

b) 1/4- x 12- x 12-inch 2024-T851 ⎤
    1/4- x 12- x 12-inch Ti-6Al-4V ⎥ Stack
    1/4- x 12- x 12-inch 2024-T851 ⎦

2) Test mandrels (as defined in previous tasks)

3) Test sleeves

a) 3/8-inch-nominal diameter, 0.010-inch wall, axial split, 301 stainless, full hard, Fel Pro 300 lubricant

f. Task 6 – Postsizing Parameters

The intent of this task was to define and verify both the methods and quantities required to reliably assure cleanup of as-coldworked holes to a consistent, precise diameter. The primary method evaluated was reaming; broaching was included for aluminum sizing. The slight bellmouthing of the hole created by the coldworking operation plus the slight ridge from the sleeve created a potential tool misalignment problem relative to defining minimum quantities required for cleanup. The tests involved use of coldworked specimens from previous tasks to define minimum quantities required to assure cleanup of the hole profile.

g. Task 7 – Portable Equipment Definition

This task primarily involved documentation of test work, knowledge, and experience that already existed in the design and use of in-line and offset pulling guns, associated sleeve containment nosepieces, and special portable power sources.

h. Task 8 – Inspection Methods Definition

This task involved defining an inspection system that would provide adequate assurance to the user that proper performance results would be achieved.

2. PHASE II: APPLICATION AND PERFORMANCE PARAMETERS

In this phase, the relative effects of process and application parameters upon performance were defined. The primary mode of evaluation was constant amplitude fatigue testing supplemented by some stress corrosion testing, edge strain testing, and analysis of photostress specimens. This phase consisted of five tasks. The last task consisted of comparative cost and performance analyses relative to other fatigue-rated hole/fastener systems.

Most of the fatigue testing was conducted on the Amsler Vibraphore fatigue test machines shown in figures 4 and 5. However, Richle-Los hydraulic fatigue test machines, similar to figure 6, were used on the low-load-transfer and the high-load-transfer specimens to avoid specimen heating with its lower frequency capability. In addition, micarta shims were used in some of the high-load-transfer specimens to avoid premature failures from interface fretting. Other basic parameters used in the fatigue testing program follow:

1) All comparisons and testing were based on net area calculated stress.

2) All coupons were shot peened to assure performance measurement of hole treatment.

3) Primary process and application parameter testing used zero-load-transfer type specimens with both open and filled holes.

4) An S-N curve was produced for base metal, standard open hole, coldworked open holes, standard hole with straight shank fastener, tapered hole with tapered fastener, and coldworked hole with straight shank fastener in:

   a)   300M steel

   b)   Ti-6Al-4V annealed titanium

   c)   2024-T851 aluminum

5) S-N curves were based on use of four selected test stresses.

6) All other process and application performance parameter testing utilized selected singular test stresses to provide comparison ratio indicators.

7) Limited range S-N curves were extrapolated on the basis of the singular stress tests and related family S-N curves generated in the program.

8) Net stress values for singular stress tests were selected to provide approximately 100,000 cycles to failure for a "mean" condition and then utilized for all tests within an alloy series to allow direct comparisons.

9) Fatigue test loading was constant amplitude, tension-tension to a stress ratio of +0.1.

10) All filled holes used equivalent fastener torque.

11) Each test condition used three fatigue test coupons; more were used only if good grouping of test results did not occur.

12) All fasteners in the aluminum and titanium were cadmium-plated titanium; fasteners in the steel coupons were cadmium-plated steel.

13) Unless otherwise noted, axial split in sleeves were in line with coupon axis.

14) Unless otherwise noted, all coupons with holes had 2D edge margins and 4D hole spacings.

15) Primary coldworking method for tests in the 300M steel used the carbide push mandrel; comparative performance tests with the pull/sleeve process were also conducted.

a.   **Task 1--Base Metal Fatigue Values**

The purpose of this task was definition of the fatigue performance for the base metal being used in this program. Base metal values were considered necessary to allow

comparisons of improvements achieved with coupons that had holes in them (and associated stress concentrations). These tests provided assurance that "real world" base metal values were obtained for the specific heats of metal being tested in the program because metal thickness, coupon fabrication, coupon design, and coupon test methods can create significant differences from handbook values. The coupons used were without holes in the test area but were otherwise equivalent to that shown in figure 2.

1) S-N test materials

    a) 300M (270-300 ksi) steel

    b) Ti-6Al-4V annealed titanium

    c) 2024-T851 aluminum

2) Single stress comparison materials

    a) Ti-6Al-4V STA and STOA titanium

    b) Ti-6Al-6V-2Sn annealed STA and STOA titanium

    c) 7175-T736 aluminum

b. **Task 2—Basic Open-Hole Fatigue Values**

In this task, a series of fatigue tests was conducted to establish basic and comparative performance parameters for standard straight holes and sleeve coldworked holes using the optimized techniques defined in phase I. All coldworked holes were reamed prior to coldworking. All tests used the 3/8-inch-diameter hole, zero-load-transfer coupon shown in figure 2. These tests are outlined for all alloys and heat treats as follows:

1) 300M and Ti-6Al-4V annealed

    a) Single stress comparison test of honed open holes to verify compatibility of McDonnell and Boeing results

2) 300M, Ti-6Al-4V annealed and 2024-T851

    a) S-N test of standard, reamed, open holes

    b) S-N test of optimum sleeve coldworked and postreamed open holes

    c) Single stress comparison test of "as-coldworked" open holes

3) All other alloys and heat treats

    a) Single stress comparison of standard, reamed, open holes

b) Single stress comparison of optimum sleeve coldworked and postreamed open holes

c. Task 3—Basic Filled-Hole Fatigue Values

The intent of this task was to obtain basic and comparative fatigue performance for standard, reamed, straight holes with a net-fit fastener installed; tapered holes with tapered fasteners; and optimum coldworked and postreamed straight holes with net-fit fasteners. All tests in this series used the 3/8-inch-diameter hole, zero-load-transfer coupon shown in figure 2. Both flush and protruding head tapered fasteners were included for later process and system comparisons.

1) Ti-6Al-4V annealed and 2024-T851

a) S-N tests of protruding head Taperloks

b) Single stress comparison test of 100° flush head Taperloks

2) 300M, Ti-6Al-4V annealed and 2024-T851

a) S-N tests of standard, reamed holes with net-fit, protruding head Hi-Loks

b) S-N tests of sleeve coldworked and postreamed holes with net-fit, protruding head Hi-Loks

3) All other alloys and heat treats

a) Single stress comparison test of standard, reamed holes with net-fit, protruding head Hi-Loks

b) Single stress comparison test of sleeve coldworked and postreamed holes with net-fit, protruding head Hi-Loks

d. Task 4—Application and Process Parameter Effects

This task contained many different tests and types of test coupons to provide answers for the effects of process and application parameters. Unless otherwise noted all holes were sleeve coldworked and postreamed approximately 0.010 inch on the diameter. Each particular process or application parameter tested is delineated in each test description. All fatigue tests in this task utilized the single-stress comparison test method. Only the baseline materials used for primary comparisons (300M, Ti-6Al-4V annealed, 2024-T851) were included.

1) Zero-load-transfer fatigue coupon per figure 2

a) 300M

i) Filled holes coldworked with pull-type steel mandrels with sleeves using 0° and 90° split orientations

b) Ti-6Al-4V and 2024-T851

    i) Open holes with 90° orientation of axial split in sleeve during coldworking

c) 300M, Ti-6Al-4V annealed and 2024-T851

    i) Open holes abusively drilled prior to sleeve coldworking

    ii) One of two open holes scored after sleeve coldworking and postreaming

    iii) Filled holes that were precracked in fatigue prior to sleeve coldworking

    iv) Filled holes that were fatigue cycled prior to sleeve coldworking

    v) Open holes with subsequent sizing or postreaming of 1/64, 1/32, and 1/16 inch (on diameter) after sleeve coldworking

    vi) Open holes sleeve coldworked in thin (0.060 inch) material

    vii) Open holes sleeve coldworked with helical sleeve

    viii) Filled holes with 0.002-inch clearance and 0.002-inch, interference-fit Hi-Loks; holes sleeve coldworked

    ix) Filled holes with net-fit, 100° head Hi-Loks in holes sleeve coldworked prior to and after countersinking

    x) Filled holes with net-fit, 70° head Hi-Loks (70° csk) in holes sleeve coldworked prior to countersinking

    xi) Filled as-reamed hole adjacent to sleeve coldworked hole (use standard filled-hole tests as baseline)

2) Zero-load-transfer fatigue coupon per figure 7

a) 300M, Ti-6Al-4V, and 2024-T851

    i) Open-hole edge margin tests with sleeve coldworked holes and nominal edge margins of 1-1/2D, 2D, and 2-1/2D.

    ii) Open hole tests with sleeve coldworked holes and nominal hole spacings of 3D, 4D, and 5D

20

3) Low-load-transfer fatigue coupon per figure 8

    a) 2024-T851/2024-T851

        i) Filled holes with net-fit, protruding head Hi-Loks in sleeve coldworked and postreamed holes. Holes drilled, reamed, coldworked, reamed and filled one at a time to evaluate low load transfer and provide baseline for differential growth test comparison.

        ii) Filled holes with net-fit, protruding head Hi-Loks in sleeve coldworked and postreamed holes. Holes generated and filled with production-type process, i.e., produce, coldwork and fill end holes and center hole first then produce, coldwork and fill all remaining holes.

        iii) As in d.3)a)ii) above, but holes not postreamed

    b) Ti-6Al-4V/Ti-6Al-4V

        i) As in d.3)a)ii) above

        ii) As in d.3)a)iii) above

    c) Ti-6Al-4V/2024-T851

        i) As in d.3)a)ii) above

4) Zero-load-transfer fatigue coupon per figure 9

    a) Ti-6Al-4V and 2024-T851

        i) Filled holes with net-fit, protruding head Hi-Loks in sleeve coldworked and postreamed holes

5) High-load-transfer fatigue coupon per figure 10

    a) 300M, Ti-6Al-4V annealed and 2024-T851

        i) Filled holes with net-fit protruding head Hi-Loks in reamed only holes. Baseline for comparison. Run with micarta shims.

        ii) Filled holes with net-fit, protruding head and 100° head Hi-Loks in sleeve coldworked and postreamed holes. The purpose was to assess effect of load transfer on coldworked hole performance. Run with micarta interface shims.

        iii) Filled holes with 0.002-inch clearance and 0.002-inch interference-fit Hi-Lok fasteners (separate tests) in sleeve coldworked and postreamed

holes to assess the effect of fastener fit in coldworked holes under high-load-transfer conditions. Run with micarta shims.

iv) Filled holes with protruding-head and 100° flush head Taperloks (separate tests) in taper-reamed holes to obtain comparative performance values. Run with micarta shims.

v) Filled holes with net-fit, protruding head Hi-Loks in sleeve coldworked and postreamed holes. Fatigue tests to be run without interface shims and two surface conditions: surface upset remaining and removed.

6) Stress corrosion testing with coupon per figure 11

Only the 300M was investigated with regard to the potential effect of sleeve coldworking on stress corrosion characteristics. This approach was based on the contractor's extensive stress corrosion testing experience. Previous tests with coldworked holes in 2024-T3 and 7075-T6 aluminum have never produced any stress corrosion cracking, even when short transverse grains have been favorably exposed. The titanium alloys were not included since they are insensitive to low-temperature stress corrosion cracking. The steel stress corrosion specimen shown in figure 11 has hole edge margins of 2.0- and 1.6-inch diameters; this produced residual tensile prestresses at the specimen edge of approximately 90 ksi and 160 ksi when the holes were coldworked. The specimens were immersed in 3-1/2% salt-water bath every hour and then exposed to laboratory air. Specimens were checked for evidence of stress corrosion cracking daily with the test terminated at approximately 1000 hours of exposure.

7) Edge strain testing with coupon per figure 12

The edge strain tests were intended to produce supplementary data to help explain specific fatigue test results. In this test the coupons were strain guged at the edge of each coupon adjacent to one of two axially aligned holes and at the edge of each coupon in between the two holes. Each coupon was first tensile loaded to produce a graph of load versus strain. Each coupon was then unloaded and sleeve coldworked while unloaded. The tensile strain at each coupon edge, induced by the sleeve coldworking, was then measured. The true strain at the edge was then measured by tensile loading the coupon as before and recording load versus strain. This was repeated after postreaming; a filled hole was also included for the aluminum.

8) Photostress testing

Photostress coupons (plain plates) were fabricated with various conditions of hole spacing, edge margins, countersink/coldwork sequence, adjacent noncoldworked holes and postreaming amounts. Photostress patterns were recorded and analyzed for both entry and exit sides.

e.   Task 5—Cost and Performance Evaluation

This task involved analyzing the accumulated data and summarizing it for comparative performance with the baseline tapered fastener system. It also involved cost comparison evaluations of the sleeve coldworking system with the tapered fastener system and other established fatigue-rated hole/fastener systems.

SECTION IV

PHASE I: PROCESS PARAMETERS–DETAIL RESULTS AND DISCUSSION

This section comprises the detailed results and associated discussions for each task in phase I.

Test reports for the basic material properties of the 2024-T851 aluminum, the Ti-6Al-4V titanium, and the 300M steel used in this program are contained in volume II of this report. Data sheets with detailed test descriptions and test results for all tests in both phase I and phase II are also contained in volume II. Because of the large number of figures contained in this report, they have been placed in one group at the end of the text.

1. PHASE I: TASK 1–OPTIMUM MANDREL TAPER ANGLE

a. Taper Angle

The primary factor used to define the best taper angle for coldworking mandrels was the force required to either pull or push the mandrel through a hole with various interferences in the materials of concern. Additional factors considered were variations produced in sleeve thinout, hole profile, and surface upsetting. Test plates, test setup, tools, sleeves, and equipment are shown in figures 13 through 16. A surfanalyzer for measuring surface upset is shown in figure 17.

In all materials, the steeper taper angles produced the lowest forces, with the largest differences noted at the higher interferences. The degree of sleeve thinout, hole radial variation (profile), and surface upsetting was not significantly affected by variations in mandrel taper angle. It should be noted that the scatter in pull force results was relatively low when coldworking the aluminum, but increased in the higher strength materials and higher interferences—especially with the lower taper angles. As a result of these tests, the 0.045 inch/inch taper angle was initially selected as the optimum mandrel taper angle for coldworking mandrels for use in all materials. Taper angle selection for carbide mandrels to coldwork 270-300 ksi steel is further covered in the phase II, task 2 discussion (section V).

Pull forces for varying taper angles, varying diameters, varying interferences and varying material stack thicknesses are shown in figures 18, 19, and 20 for 2024-T851 aluminum; in figures 21, 22, and 23 for annealed Ti-6Al-4V titanium, and in figures 24, 25, 26, and 27 for 270-300 ksi 300M steel.

b. Pull/Push Force Requirements

All aluminum and titanium taper angle tests utilized steel pull-type mandrels; push-type carbide mandrels were used in the high-strength (270-300 ksi) steel. Axial-split, half-hard 301 stainless steel sleeves were used for the aluminum material, and axial-split,

full-hard 301 stainless steel sleeves were used for the titanium and steel materials. All sleeves were internally prelubricated with a baked-on Fel Pro 300 dry lubricant. The primary testing in the steel was done without sleeves and with Fel Pro 300 baked directly in the holes. Push force and retained expansion comparison tests with sleeves were also conducted in this task; further tests with pull-type mandrels are reported in phase I, task 3.

Measured maximum pull or push force requirements for the diameters and stacks tested are shown in figure 27 for all three basic materials. Forces also proved to be dependent on stack thickness. With the larger diameter holes, forces increase with stack thickness and reach a plateau when full-taper engagement thickness is reached; forces increase beyond this point with increasing stack thickness in the smaller diameters (when using a sleeve). It is believed that this is a result of the thinner walled sleeves used in smaller diameter holes being axially compressed during coldworking, thus providing a braking action on the shank of the mandrel. Effect of stack thickness on forces is shown in figure 28 and projected force requirements for various hole diameters as influenced by stack thickness are shown in figure 29 for aluminum, titanium, and steel. Selection of equipment based on these plots should allow for some process and equipment variation. It should also be noted that these force requirements are for the specific alloys and heat treats tested; different strength alloys or heat treats within these alloy families may make some difference in requirements.

The effect on push forces using a sleeve versus no sleeve in the 270-300 ksi steel is shown in figure 30. As indicated, there is no significant difference at the lower interferences, but the forces are significantly less without a sleeve at the higher interferences.

c.   Mandrel Materials

The phase I, task I, tests were not basically intended to evaluate mandrel materials, but the testing did disclose some definite trends. That is, the current Boeing standard H-11 steel mandrel with a nitrided surface showed no undesirable characteristic such as excessive scatter in forces, obvious wear, or swaged reductions in diameter when used to prestress (coldwork) holes in aluminum. However, when used in the Ti-6Al-4V titanium, the H-11 nitrided mandrels suffered some initial loss in diameter in the order of a few thousandths of an inch. This was not a wear loss since it appeared to diminish to zero after the mandrel apparently work hardened itself to a sufficiently high strength.

For this reason, mandrels of AISI 9260 and Vascojet MA fabricated for pull mandrel development tests with 270-300 ksi steel were also used to coldwork holes in titanium. These mandrels proved to be adequate for the task and did not suffer any loss in diameter. It should be noted that these mandrels were not nitrided on the surface; this difference in surface treatment did not produce any noticeable difference in forces. AISI 9260 and Vascojet MA mandrels did not disclose any problems in their fabrication. As a result of this test data, it appears advisable to change the current mandrel material callout from H-11 to either AISI 9260 to Vascojet MA or equivalent strength alloys.

In coldworking holes in the 270-300 ksi steel, the 883 carbide mandrels showed a definite tendency towards unpredictable breakage, primarily with the higher interference

26

values and thicker stacks. The failure was not a compression type of failure per se, but a clean transverse rupture perpendicular to the mandrel axis. Some previous tests with other, especially selected, higher transverse rupture strength carbides (outside the confines of this program) did not disclose this transverse rupture problem at similar interferences. Test work in coldworking high-load-transfer specimens (3/8-inch hole diameter; 0.023-inch interference; 3/4-inch stack of 3-1/4-inch plates) for phase II, task 4 showed that this condition was extremely marginal with regard to breakage of the 883 carbide. It also showed that the transverse rupture was not totally a function of differential radial pressures from the high-interferences alone; i.e., breakage usually occurred only when the push forces rose significantly from lubricant film breakdown. Thus, the rupture was caused by a resultant of a biaxial stress condition. Higher strength carbides may help, but lubricant film breakdown after one or two holes at higher interferences in thicker stacks may be the primary limiting factor in interference selection. Tests using a lower interference mandrel as a first step did not provide any reduction in forces or lubrication breakdown rate for the final mandrel.

Results of the pull mandrel tests in 270-300 ksi steel holes will be covered in the task 3 discussion.

d. **Retained Expansion**

Knowledge of the amount of expansion retained after the mandrel is pulled through the hole is useful for defining reamer pilot sizes or for general quality control.

Figure 31 is a plot of the retained expansion versus the initial mandrel/sleeve interference for 3/8- and 3/4-inch-diameter holes in all materials tested. The plot also includes a 1-1/2-inch-diameter hole in aluminum from another program. It is very interesting to note that the retained expansion versus initial interference is the same for the aluminum, titanium, and 270-300 ksi steel for equivalent efficiency processes, even though these metals have significantly different yield strengths and elasticity moduli. The smaller diameters do seem to fall on a different curve and, with the exception of the aluminum, did not appear to be stack dependent. There is a slight transition in values between the 3/8- and 3/4-inch diameters, but all diameters from the transition upward fall on the same line—as noted by the 1-1/2-inch diameter hole data point. The maximum retained expansion for the task 3 pull mandrel is also shown and will be discussed under task 3.

As previously pointed out, the retained expansion appears to be equivalent for all materials for equivalent mandrel/hole interference values. Further examination of test data from other programs indicates that this result and the sweeping conclusions that might be drawn from it may purely be the result of a circumstantial combination of alloys. That is, although the results derived were valid in themselves, they should not be used to indicate that the same values will be obtained for all alloys within a family. The probability is: less retained expansion (greater springback) will be encountered for alloys with higher yield strengths within a family that has an equivalent modulus of elasticity. This variance will probably be small, and since the high-interference, sleeve coldworking process uses a postsizing operation, the variance will probably be of no major significance. If the starting-hole values recommended herein are used (based on certain minimum values for postsizing removal), the variance should not cause any problem.

Figure 32 is a bar chart of retained expansion in the 270-300 ksi steel as a function of mandrel/sleeve combinations. Here it is shown that there is some loss of retained expansion when the carbide push mandrel is used with a sleeve versus no sleeve, and approximately a 45% loss when the pull mandrel is used with a sleeve. Test results in phase II will show that this also results in only a 50% gain in fatigue performance relative to that achieved with the carbide mandrel.

e. Hole Finish

The effect of the sleeve coldworking process upon the prior hole finish is shown in figures 33 through 35. The data show that coldworking improves the hole finish by a factor of 2 regardless of the starting finish. This fact is probably of no significance, but has been recorded for possible future reference.

f. Radial Variation

Knowledge of the probable radial variation in a coldworked hole as a function of the "hourglassed" hole profile from coldworking is useful in defining minimum chip loads to assure full cleanup for final sizing. The maximum radial variation for all materials is shown as a function of conditions and diameters in figures 36 through 38. The indications from these plots are that an increase in the minimum diameter in the order of 1/64 inch should provide both assurance of cleanup and a minimum practical chip load for all diameters of normal concern. Postsizing requirements are further discussed under task 6.

A typical hole profile trace in aluminum is shown in figure 39. This trace was produced with the Brush Surfanalyzer shown in figure 17.

g. Surface Upset

Surface upsetting or part thickening is inherent to the hole coldworking process and is something that must be understood or contended with in use or application of the process. Surface upsetting occurs on both the entrance and exit sides of a hole and is always greater on the exit side. Upsetting that occurs at an interface is usually less than that produced on a free surface, but not always necessarily so, as shown herein by the titanium data for thick stacks. Nevertheless, this upsetting (if not removed) will cause some gapping of stacked details, although not at the fastener holes. To date, this surface upsetting has not shown any detrimental effects on fatigue performance of low-load-transfer joints in aluminum; its effects in high-load-transfer joints will be covered in the phase II discussion.

Typical traces of hole axial profile and surface upsetting on entrance, interface, and exit surfaces for 2024-T851 aluminum, 300M steel (270-300 ksi), and Ti-6Al-4V annealed titanium are shown in figures 40 through 57. It should be noted that the scale is highly magnified on these traces for precision and should be referred to for proper perspective.

If results shown herein are compared, it can be seen that surface upset values for equivalent interferences are greater for titanium and steel than those for aluminum. Figures 58 through 65 show that subsequent sizing will not significantly alter or remove this upset.

The values for distance of upset away from the hole also give some idea of the significant size of the zone that is affected by the high-interference, sleeve coldworking process. Further evidence of this is shown in figure 66, a laser holograph of a hole as it was being coldworked in 7075-T6. This holograph was produced at Wright-Patterson AFB by Dr. Adams with our support. The technique uses diffraction of a laser speckle pattern to show strain. Some difficulty was encountered in attempting to use this technique because of the magnitude of the strains that occur during the coldworking process. Elastic strain is shown by the fringe patterns; plastic strain could not be picked up and is depicted by the nonfringed zone around the hole. Thus, this photograph supports previous contentions that a yielded zone (that goes into compression after coldworking) exists that is one radius or more away from the edge of the hole; in fact, it appears to be more on the order of one diameter.

Figure 60 shows the effect of mandrel taper angle on surface upset amount in Ti-6Al-4V titanium. As can be seen, the lower taper angles (the longer ramps) produced greater amounts of surface upset. This was not particularly evident in the aluminum test data but definitely supports the decision to use the steeper taper for force reduction and mandrel length reduction.

Figures 61 and 62 show that thickness of material also affects the amount of upset for the same diameter and mandrel/sleeve-to-hole interference. Upset is increased with the thicker material. This is in line with the higher degree of retained expansion shown for thicker material.

Figure 63 shows both free surface upset values, as well as interface values, for a 3/4-inch-diameter hole in Ti-6Al-4V. The reason for the interface exit value being the highest is not logically explainable; nevertheless, it did occur.

Figure 64 shows the general effect that interference levels for coldworking have on the amount of surface upset produced. It also shows some effect of stack thicknesses and hole diameters for equivalent interferences.

Figure 65 gives the upset values for a 3/8-inch-diameter hole in 300M steel (270-300 ksi). These results are approximately equivalent to those encountered with titanium. It should be noted that all of these results were obtained using mandrel/sleeve-to-hole interference values that were considered optimum for fatigue performance. Changes in interference will have a direct effect upon surface upset. Since the optimum values for 300M steel have been adjusted upwards from the values shown in this figure, the upset values will also be slightly higher.

2. PHASE I: TASK 2—OPTIMUM EXPANSION

Figures 2 and 3 fatigue coupons were used to evaluate the effect of four different initial expansion values on open-hole fatigue performance. Hole expansion values equal to original process values, plus values 0.005 and 0.010 inch over and 0.005 inch below the

original process values were generally approximated for the aluminum and titanium and 0.005 inch over and 0.005 and 0.010 inch below for the steel. The tests were not only designed to define optimum values, but also to show any indication of diameter effect.

Test results for the 2024-T851 aluminum are plotted in figure 67. The plot shows a definite trend for improved fatigue performance with increasing interference. What appears to be a difference in slope of cycle improvement with interference increase between the small and large diameters is purely a function of not using increases in interference increments equivalent to the diameter ratio. When this is accomplished, the extrapolated slope for the 3/4-inch-diameter hole is equivalent to the 3/8-inch-diameter hole. The fatigue cycles also show a leveling off towards the upper end tested. As a result, the maximum values were not selected as "optimum" values since the increased impact of the maximum interference upon upset, forces, and other parameters did not appear to justify the slight fatigue improvement. Thus, a 0.019-inch interference value was selected as optimum for a 3/8-inch diameter and 0.030 inch for the 3/4-inch diameter. An adjusted plot of recommended coldworking interferences versus hole diameters for 2024-T851 aluminum is shown in figure 68.

Test results from this task for the 300M steel are shown in figure 69. The original plan for the 3/8-inch-diameter holes in the 300M steel optimum expansion tests included values for 0.009-, 0.014-, 0.019-, and 0.024-inch expansion or mandrel/hole interference. The values of 0.021 and 0.023 inch were added when a significant difference in performance improvement was noted between the 0.019- and 0.024-inch interference levels (approximately 70,000 cycles versus 200,000 cycles). The results indicate that a minimum of 0.023-inch interference is needed to gain this significant benefit with the 3/8-inch-diameter holes.

The 3/4-inch-diameter hole results for the 300M steel in figure 69 show a basically equivalent performance for the lower levels of interference to those obtained with the 3/8-inch-diameter hole specimens. Thus, we can assume that the base metal is equivalent for the two hole diameters. However, the same problem of using equivalent increments of interference rather than double increments, which would equate to the doubled diameter, exist here as in the aluminum (and titanium) tests. Therefore, the improvement slope does not appear to be equivalent for the larger diameter, whereas, extrapolation based on double increments shows it to be basically equivalent. The projected optimum interference versus hole diameter curve that results from this extrapolation, however, has a steeper slope than those projected for the 2024-T851 aluminum.

This projected optimum interference curve is shown in figure 70. There is a secondary curve shown on this plot. This secondary curve is a projected probable practical limit for interference that is well below the projected optimum from approximately 5/8-inch-diameter holes on up. This secondary curve is based on the breakage in carbide mandrels that has occurred above this line. The breakage is a function of the directly increasing, high radial pressures with increasing interference that results in breakdown of the Fel Pro 300 lubricant and transverse rupture of the carbide mandrels. Higher rupture strength carbides than the Carboloy 883 used might help if the lubricant breakdown doesn't excessively amplify the biaxial stresses.

30

Note: Test work in another (concurrent) progra.n has shown that Carboloy 55B or Carboloy 248 carbide are superior to the Carboloy 883 carbide for this usage.)

It should be noted that even though optimum interference values for the different alloys appear to be relatively equivalent for the smaller diameter holes, this again may be a circumstantial situation for the particular alloys tested. For a lower yield strength alloy with the same modulus of elasticity in a basic metal family, the optimum interference values might be slightly lower.

One other point relative to optimum interference testing is worth discussing. There was some question if the open-hole specimen fatigue test for optimum inter ;rence values was truly valid for filled holes (with fasteners). It now appears that the open-hole specimen test is a reasonably valid test for this purpose with aluminum since concurrent tests at Lockheed (in Georgia) with the sleeve coldworking process, disclosed basically equivalent optimum interference values for filled holes with up to 50% load transfer in 7075-T6 specimens. Their values were:

Hole diameter (inches)	Optimum interference (inches)
1/4	0.014
5/16	0.017
3/8	0.021
1/2	0.024

Further test work later in this program with titanium and steel indicates, however, that open-hole comparisons may not be meaningful with regard to ultimate filled-hole performance. In fact, the stress amplification of an open hole coupled with greater notch sensitivity of these and other metals may totally mask significant improvements that might be achieved with filled holes. Thus, the author believes that open-hole testing should not be used for such evaluations in the future.

The optimum interference fatigue performance data for the Ti-6Al-4V annealed titanium is shown in figure 71. Three items presented some difficulty in attempting to interpret these data:

● The generally lower fatigue performance of the 3/4-inch-diameter hole specimens

● The different slope on fatigue improvement with increasing mandrel/ sleeve-to-hole interference for the 3/4-inch-diameter hole specimens

● The relatively large scatter in results at higher mandrel/sleeve-to-hole interference values not evident at lower values.

The following presents results of further investigations relative to the foregoing items and of further analyses aimed at establishing a reasonable optimum interference curve.

3

a. 3/8- Versus 3/4-Inch Holes (Ti-6Al-4V)

The mandrel/sleeve-to-hole interference values used in these tests were selected on the basis of limited work conducted previous to this program that indicated that optimum interference levels for aluminum and steel might be relatively close to one another. The equivalent retained expansion values for the aluminum, titanium, and steel obtained in this program also indicated that a good baseline value for interference with the steel and titanium was the optimum value defined for aluminum. The test plan then included one increment below this value and two above for the titanium and two below and one above for the steel. The latter decision was based on the probability that practical limits on high interference would occur with the high-strength steel. Interference values for the 3/4-inch-diameter hole specimens were selected using the same slope on the interference versus diameter curve for aluminum (based on equivalent strain calculations).

The initial reaction, when the 3/4-inch-diameter hole titanium specimens failed at a generally lower level than the 3/8-inch-diameter hole specimens, was that the titanium required a different slope curve for diameter. Further examination of the data disclosed, however, that the entire band of data for the 3/4-inch-diameter hole specimens is shifted downward toward lower performance. Observation of the fracture faces from the fatigue tests also showed an obvious difference in visual appearance between the 3/8- and 3/4-inch-diameter hole specimens (fig. 72). The 3/8-inch-diameter hole specimen had a granulated, large grain appearance, and the 3/4-inch-diameter hole specimen had a laminar, fine grain appearance. In phase I, the 3/8- and 3/4-inch-diameter hole specimens were not fabricated from the same heat of material as all specimens were in phase II. A spectrographic analysis of the two materials (fig. 73) showed some difference, but each was within alloying specifications. Metallurgical sections (figs. 74 and 75) show a more laminar grain structure for the 3/4-inch-diameter hole specimens, but neither metallurgical structure is considered abnormal for Ti-6Al-4V titanium.

Scanning electron microscope photos of the two fracture faces (figs. 76 through 79) show some difference in appearance at high magnification, but nothing of great significance. The conclusion that must be drawn from these observations is that a phenomenon known as texturing in titanium alloys is present and is causing a difference in fatigue performance. Thus, this factor or phenomenon must be taken into consideration when allowables are defined.

The possibility that larger diameter holes in titanium and steel do not follow the same interference increase requirement for larger diameter holes in aluminum was also investigated. A number of specimens were fabricated to analyze strain patterns using a Moire fringe pattern technique. This included specimens of 3/8- and 3/4-inch-diameter holes in aluminum and titanium, plus one with a 3/8-inch-diameter hole in steel. The specimens were prepared by applying a 400-line/inch linear grid in one direction before coldworking. After coldworking, the specimens were placed in a vacuum frame, and a matching 400-line/inch film grid was registered with the specimen grid. The specimen was then photographed at a scale of 1:1 while the film grid was held in contact by the vacuum system. The film grid was then adjusted to give a rotational mismatch of 16 fringes per inch, and this pattern was photographed. The photographic negatives were then enlarged in a rear projection system at

a magnification of 4.85:1. The density of the enlarged image was scanned with a motor-driven photoelectric pickup. The scanning aperture was a rectangle, 0.05 inch wide by 0.015 inch long. All scans were made in the Y direction as referenced on the specimen, i.e., perpendicular to the grid lines. Plots of density versus position were recorded on an X-Y plotter. The position scale was adjusted to a magnification of 10:1; i.e., 1 inch on the plot was equivalent to 0.10 inch on the specimen.

The half- and full-order fringe positions were located on the plots, and surface displacement curves were drawn with each fringe equal to 0.0025 inch of displacement. The slope of the displacement curve then represented the strain. Photographs of the fringe patterns are shown in figure 80. The top photograph represents the method described; the bottom represents a 90° placement of the grid to assist in orientation of the strain field through angular shift of the grid lines. Figure 81 is a plot of the actual strain data taken at the edges of the hole. As can be seen from these data, the affected zone is in general agreement with the laser holograph; i.e., it is roughly equivalent to one diameter away from the edge of the hole. Also, no significant pattern emerges on tangential stresses (the ones considered important to fatigue) other than some loss in the larger aluminum holes where performance was considered equivalent. The radial strains are much higher in the titanium and steel than in the aluminum, but the tangential strains appear to be basically equivalent. Thus, no definite requirement for higher interferences in larger diameters (for the titanium and steel) can be drawn from these data.

b. Scatter at Higher Interferences (Ti-6Al-4V)

Since the yield strength of titanium is relatively close to the ultimate strength, the scatter in fatigue performance with the highest mandrel/sleeve-to-hole interferences used raised the question of whether the coldworking operation itself was causing surface microcracks in the holes at these values. To resolve this question, specimens of holes coldworked to these high interferences were submitted to the Boeing Commercial Airplane Company quality control research organization for examination. As defined in figure 82, a number of eddy current and penetrant inspection methods were used to inspect these specimens, including a "wink" method wherein the specimen is loaded in bending to open up any cracks that may exist but are closed by compressive stresses. None of these tests disclosed any evidence of surface cracking in the holes. Nevertheless, the higher interference values were avoided in the projected optimum interference curve until more performance data are available.

c. Interference-Versus-Diameter Curve (Ti-6Al-4V)

The values for mandrel/sleeve-to-hole interference for optimum performance are the crucial elements of concern. Further examination of the data discloses that shifting data points to use increases in interference increments that are pertinent to diameter increases, plus shifting the loss due to "texturing" of the metallurgical structure, plus discounting the high end of the interference (on the basis of scatter) results in selection of a curve for optimum interference in Ti-6Al-4V titanium that is equivalent to that for the 2024-T851 aluminum. Such a curve is shown in figure 83. Test work in phase II, "Application and Performance Parameters," used interference values selected from this curve.

33

3. PHASE I: TASK 3—PULL MANDREL DEVELOPMENT

The high-strength steels selected for fabrication of experimental pull mandrels for use in coldworking 270-300 ksi steel were AISI 9260, Vascojet MA, and M-42 HSS. All of these alloys have yield strengths above that for the 300M steel heat treated to 270-300 ksi. All tests run with these test mandrels used disposable, full-hard 301 sleeves.

The M-42 alloy proved to be too difficult to work with in fabrication and was discarded. Mandrels of AISI 9260 and Vascojet MA were fabricated. These mandrels did not have a nitrided surface as the standard H-11 mandrel does. Data from Alloy Digest for these alloys and 300M steel are shown in volume II for comparison and reference purposes.

The test results and conclusions for this task follow:

- It is possible to use a pull mandrel with a sleeve to coldwork the 270-300 ksi 300M steel; but the lower modulus of a high-strength steel mandrel (versus carbide), coupled with sleeve thinout, results in roughly one-half the retained expansion that is obtained with a carbide mandrel for equivalent mandrel-to-hole interference (theoretical).

- The Vascojet MA alloy was the best alloy tested and also proved to be practical to fabricate.

- The Vascojet MA mandrel does not require nitriding as the previous H-11 or H-13 mandrels do for sleeve coldworking in aluminum.

- Since the now standard H-11 or H-13 mandrels are not adequate for titanium, on the basis of diameter loss reduction, it appears that a Vascojet MA mandrel is a good material selection not only for use in high-strength steel, but also as a standard for all uses (lack of nitriding requirement compensates for higher material cost).

- The radial pressures in coldworking the high-strength steel are still sufficient to cause initial surface yielding of the Vascojet MA mandrels, with a resulting diameter loss of a few thousandths, but this decreases to zero through work hardening of the mandrel surface if the interference is kept within limits. Thus, mandrels for this purpose should be made oversize and preconditioned by coldworking prior to production usage.

- The limits for use of the steel pull mandrel in high-strength steel (or in carbide) are not totally defined but are probably equivalent to the interference values defined for aluminum, up to a probable limiting interference of 0.025 inch.

- The pull force for the steel mandrel and sleeve is reduced by the same ratio as the retained expansion, i.e., to one-half of that required for the carbide push mandrel for the same theoretical interference (based on initial dimensions).

34

● The degree of fatigue improvement that can be obtained by this method is reduced by approximately the same ratio as the retained expansion is reduced (from results in phase II, task 4).

4. PHASE I: TASK 4—PHYSICAL EFFECTS AND REMAINING MANDREL/SLEEVE PARAMETERS

a. Lineal Growth

The lineal growth of aluminum, titanium, and steel material with varied edge margins and hole spacings for 3/8- and 3/4-inch-diameter holes as a function of high-interference sleeve coldworking is plotted in figures 84 through 89. Values are shown in lineal growth per foot of part length for three conditions: (1) after coldworking, (2) after coldworking postream, and (3) after postream and countersink.

A three-diameter versus a four-diameter hole spacing seemed to have little effect on results; whereas, edge margin was more significant (for a stringer type of part). No definite trend could be observed relative to subsequent operations such as postreaming and countersinking. The parts with larger diameter holes had significantly less lineal growth per foot. This is probably due to the interference values for the larger diameters not being in direct ratio to the increase in diameter (see fig. 83). The lineal growth for the titanium and the steel are significantly greater than that shown for aluminum. As with any interference system, this growth must be tolerated in tooling systems and methods, in structural design, and in operations technique. For instance, with the relatively standard two-diameter edge margin and four-diameter hole spacing in the 2024-T851, the lineal growth for a 100-foot-long part with 3/8-inch-diameter holes would be on the order of 1 inch (for a part such as a stringer or a spar chord). Obviously, this value would be somewhat reduced by constraint of attached skins or webs; nevertheless, tooling must provide allowances. In addition, critically located parts may require location after all of the growth has been encountered and mismatch of holes in different parts must be prevented by using a technique of "spot" completion. That is, every fifth or 10th hole (or some other number) is coldworked, postreamed, and filled prior to coldworking the remainder.

b. Bow or Distortion

As with lineal growth, edge margin had more effect on degree of bow than hole spacing. Bow was more significant in the thinner gages and was approximately equivalent for the aluminum and titanium before countersinking, but it was approximately twice as great in the steel (higher interference). The amount of bow for different edge margins, hole spacings, hole diameters, and specimen thicknesses is shown before and after countersinking for aluminum, titanium, and steel in figures 90 through 95. It should be pointed out that many interference-fit fastener systems, including Taperlok, will cause some bow in unrestrained specimens, although some systems such as uniformly squeezed slug rivets minimize the effect. The previous evidence of higher retained expansion and greater surface upsetting on the exit side of the hole showed up in the direction of bow. In all cases, the bow was concave away from the exit or pull side of the hole. Since a pull-type operation would normally be an external operation on a countersunk part, such as a wing skin, the

countersink was kept on the coldworking exit side in all cases. Since the countersinking partially removed some of the compressive material, it reduced the bow. This was more significant in the thinner gages of aluminum than in the thicker and even resulted in zero-to-negative bow in the titanium. This definite effect on material bow from removing this countersink material certainly raises some question on how significant an effect it may have upon fatigue performance—especially since the Moire strain data did not show a significantly different tangential strain on the exit side. This certainly lends some credence to the proposal that a 70° countersink may be more advantageous than a 100° countersink. The effect of countersink sequence and countersink angle is covered in phase II.

c. Edge Bulge

Values for edge bulging with 1-1/2D and 2D edge margins in 3/8- and 3/4-inch-diameter holes at 3D and 4D hole spacing are plotted for the aluminum, titanium, and steel in figures 96 through 98. Edge bulge of some degree will always occur with normal edge margins and is a factor that must be understood as an acceptable item with coldworking or other interference-fit fastener systems. Normal bulge is not a cosmetically unacceptable item to casual observation, although it can be seen by the naked eye if one sights along an edge (see fig. 196). The 1-1/2D edge margins do have some increase in edge bulge, but, as can be seen in the figures, the increases as well as the overall values are relatively small. Thus, there may be some difference in fatigue performance with 1-1/2D versus 2D edge margins, but probably not in the order of major significance. The fact that the 3/4-inch-diameter holes are showing a greater bulge for equivalent edge margins (based on diameter) tends to indicate that the interference levels being used for the larger diameters is not out of order, as was questioned earlier. Edge bulge also represents a tensile stress condition at the edge of a part that could raise questions about its effect upon stress corrosion with certain alloys. Previous tests at Boeing with aluminum, including 7079 material with transverse end grains unfavorably exposed, have disclosed no problems with stress corrosion when using the high-interference, sleeve coldworking process. Stress-corrosion tests with the sleeve coldworking process and other interference-fit fastening systems reported in reference 1 indicate that the sleeve coldworking process is outstandingly better than all the other systems evaluated when tested in 7075-T6. Tests in phase II will show that favorable stress-corrosion performance can be achieved with 300M steel.

d. Surface Taper Effect

In this portion of task 4 (phase I), holes were coldworked in aluminum, titanium, and steel with surface tapers of 2° and 4° to determine if there was any serious effect on the uniformity of the coldworking near the surface. This was done with 3/8-inch-diameter holes using basically a 0.019-inch mandrel/sleeve-to-hole interference. The resulting retained expansion should normally be in the order of 0.012-inch for this expansion (0.006-inch per side). The results are plotted in figure 99, and some typical rotary traces taken on a Moore precision measuring machine are shown in figure 100. These measurements showed the centerline shift at the taper surface entry to be on the order of 0.003 inch for both the 2° and 4° tapers. Thus, the coldworking retained expansion is roughly 50% of normal at the high side of the hole on the tapered surface. This shift should cause no postsizing difficulties in production; in addition, it should cause no difficulties with fatigue performance since the

area of reduced retained expansion is in line with the normal direction of stress relative to taper.

e. Diameter Creep

A check was made with 3/8-inch-diameter holes in aluminum and titanium to determine if there was any significant degree of diameter creep after coldworking. The results of these measurements are shown in figure 101. The hole diameters were checked immediately after coldworking, 1 hour after coldworking, and 24 hours after coldworking. Only 0.0001-inch loss in diameter occurred within the first hour; this result was the same for both materials. No further detectable changes occurred in the next 24 hours. In the past, installation difficulties have been reported when bolts were not installed on the same day, but the data seem to refute the contention that this problem was based on creep. Furthermore, creep would result in a change in prestress and would require an evaluation of time effects on fatigue performance. This limited test indicates, however, that time and creep do not seem to be problems.

f. Sleeve Lubricant

The sleeve lubricant selected as a standard lubricant for the process early in its development was Fel Pro 300. This is a solid-film molybdenum disulfide type of lubricant that comes in air-dry or bake-on versions. Of the two, the latter performs best and has been used as the standard. Prior to the initiation of this program, some difficulties were experienced with high forces and force variations in coldworking 9/16-inch-diameter holes in thick stacks of material. At that time, an evaluation of numerous alternatives to the Fel Pro 300, or combinations with the Fel Pro 300, was conducted. The earlier tests, as with those within this program, were conducted on a Tinius Olsen setup as shown in figure 14. In this setup, an actual pull gun is used to pull the mandrel through the hole at the same rate that occurs in normal use with the machine registering the forces involved. Some typical mandrels and sleeves used in this type testing are shown in figure 15.

The previous testing was fairly extensive and concentrated heavily on the long-chain alcohols since cetyl alcohol was proven to be such an outstanding lubricant for mandrel coldworking of holes. In this program, two versions of a new lubricant, which supposedly combines with the surface and a molybdenum disulfide paste, were evaluated. Results of both the previous tests and the program tests are shown in figures 102 through 106.

Figure 102 shows that the baked-on Fel Pro 300 was superior to the LLC 36 dry lube and the Moly Kote G paste in this extreme pressure situation. It should be noted that the 2024-T851 test also represented the lowest demand of the materials of concern in this program. The tests produced loud, snapping sounds with the LLC 36 and the Moly Kote G paste, indicating a slip-stick action from complete breakdown of the lubricant.

Figure 103 shows some basic variations in sleeve lubricants; it also shows why some attention was paid to the long-chain alcohols, since the cetyl alcohol is quite close to Fel Pro 300 in performance. Nevertheless, nothing surpassed the Fel Pro 300, although

driving off any absorbed moisture in the Fel Pro 300 just before use did help some. The benefit, however, was not sufficient to merit the special handling that would be involved. It should be noted that the Fel Pro 300 is designated, in figure 103, as being properly mixed. Figures 104 through 106 show variations with Fel Pro 300, including some in which the Fel Pro 300 is not properly mixed. The mixing turned out to be very important since the lubricant has some heavy metallic elements that settle out very rapidly if the liquid is not agitated continuously.

Close observation of the test results, which included 32 lubricant variations, shows that only two were slightly better than properly mixed Fel Pro 300. These were cetyl alcohol and paraffin in combination with improperly mixed Fel Pro 300. The slight improvement was not sufficient to justify the complexity involved in application. As a result, the Fel Pro 300 baked-on version continues to be the standard for the coldwork sleeves. The manufacturer of the sleeves was contacted as a result of the previous evaluation, and a system to ensure continuous agitation of the lubricant in the automatic application system was installed.

g.   Mandrel Finish

Previous work with mandrel-only processes in aluminum showed that some reduction in pull force could be achieved by vapor blasting the mandrel to provide a "grip" for the cetyl alcohol lubricant. Vapor-blasted mandrels for use in the sleeve coldworking process were evaluated in this program. The mandrels were first vapor blasted and then treated by baking on a coat of Fel Pro 300. They were then tested in coldworking aluminum and titanium by the sleeve method and compared with standard mandrels. The results are shown in figure 107. As can be seen, the treatment did produce a slight reduction in pull force, but it was not significant enough to justify the extra processing.

h.   Sleeve Configuration

The standard sleeve process uses a sleeve with an axial split in it as shown in figure 15. The width of the split is established at a value that will produce a minimum-width ridge in an as-coldworked hole but wide enough to prevent the edges of the thinned-out sleeve from being jammed together by hole springback (after the mandrel passes by) causing the sleeve to be locked into the hole. A typical ridge in a thick stack is shown in figure 108 where two nonaligned split sleeves were used in conjunction with each other to handle the stack thickness. This ridge produces a surface discontinuity in strains (part surface, not hole surface) as evidenced by the Moire data but does not necessarily represent a zone that has not been adequately prestressed. The hoop expansion results in a hoop strain that is apparently sufficiently uniform since previous tests have shown no detrimental effect from this ridge or its location. Test work in phase II verified this contention, in general, but photostress tests in phase II disclosed some limitations relative to precountersunk holes (see phase II for more detail).

Actually, the width of the split in the sleeves, as previously defined, proved to be adequate for all but the very highest interferences attempted in this program. Since these maximum values of interference were not selected for use, the existing sleeve design appears to be adquate.

As now configured, the sleeves also have different thicknesses. Actually, they could all be of a singular thickness of a high value, but this would make them more difficult to manufacture in the smaller diameters and very difficult to put onto a mandrel in the smaller diameters. Consequently, the sleeve thickness starts at 0.006 inch for a 3/16-inch-diameter mandrel and progresses in increments up to 0.018 inch for a 1-inch-diameter mandrel. The 0.018-inch thickness also happens to be the maximum limit for the axial split sleeve with the current manufacturing equipment; thus, if a one-sided operation is to be used, another sleeve configuration with thicker walls must be used for mandrels over 1 inch in diameter. The incremental thickening of the sleeve wall is necessary to allow one-sided entry of the mandrel into the hole and achieve the necessary diameter-related interference (through sleeve thickness) on mandrel withdrawal.

Use of thin walls to facilitate sleeve manufacture and placing a sleeve on a mandrel leads to one other requirement. The thin wall has a low column strength, and nosepiece jaws in the pull gun (to restrain the sleeve) are not adequate alone with the thinner sleeves if the sleeve does not grip the hole with a high friction component. The presence of any lubricant, either on the outside of the sleeve or in the hole from drilling, may cause the sleeve to cripple and result in a rejection. Therefore, the current sleeves are lubricated only on their internal surfaces; the Boeing process specification stipulates that holes to be coldworked must be drilled with a noncontaminating cutting fluid such as Freon TB-1. Use of oils, paraffin, or cetyl alcohol that are not cleaned from the hole may lead to difficulties.

Practice has also disclosed a further refinement in the axial-split sleeve configuration that is desirable. Since the sleeve wall is relatively thin in smaller diameters, the nosepiece jaws are not as reliable when the sleeve does not have a flare on its one end. This flare not only decreases the probability of slippage, but it also enhances the operation of putting a sleeve on the mandrel by providing an entry taper. It also makes it relatively easy to use simple tools to hold the sleeves for placing them on mandrels. Since a singular sleeve length is probably adequate for most stacks in smaller diameter holes, a nonflared sleeve in smaller diameters (for end-to-end stacking) is probably not a serious requirement.

This discourse has been aimed at providing an understanding of the parameters involved in current sleeve configurations. Within this program, other configurations were evaluated. They are as follows:

(1)   Scarfed Axial-Split Sleeve

The concept here is to continue use of the current axial-split sleeve but to scarf the edges of the split at an angle (instead of 90°). Theoretically, this should allow use of a narrower split and should prevent inadvertent difficulties in sleeves that jam in holes at high interferences because the edges of the split should ride over one another when they close together. The current manufacturing technique for the sleeves, which uses a pull-through cutoff tool to part the sleeve material, also appeared to be amenable to producing this configuration.

As stated previously, no jamming difficulties with the standard sleeves was encountered, and it was difficult to provide any comparisons of improvement without

significantly altering mandrels and starting hole sizes. This was not done because microscopic examination of the "scarfed" splits showed that it was process-critical and would require further development to gain the quality and uniformity deemed essential.

(2) Helical-Split Thin-Wall Sleeves

This concept was evolved before the contract, although only partially tested. The sleeve is wound from strip material as a spring is wound and then cut into individual length sleeves. Several as-wound strips are shown in figure 109. As can be seen, there is a probable maximum strip width for a specific diameter since the wider strip has an anticlastic saddling that could present some difficulties. The theory of the helical-split sleeve is that it does not have to be precise, the split is not critical, it can be easily wound, it can accommodate diameters that are close (but different), and it should not leave as significant a ridge in the hole. Figure 110 shows some helical sleeves cut to length; it also shows the two major problems of helical sleeves: (1) the ends of the helix have a tendency to spring outward and present problems on inserting a mandrel/sleeve combination into a hole, and (2) the deburring evident on the sleeves represents an unsolved problem relative to a practical, high-rate cutoff method that does not require subsequent deburring.

Figure 111 shows the minimal ridge that this type of sleeve leaves in a hole. Test work in this program also showed that the helical, thin-wall sleeve was easier to put on the mandrel and to remove from the holes. Retained expansion and thinout were no different than axial-split sleeves, as should be expected. The fabrication problems, however, still retard practical adoption of this type sleeve.

(3) Square-Wire Sleeve

This is a further evolution of the helical sleeve conceived before this program and only partially evaluated. In this concept, the helical material is a square or rectangular wire that can be fabricated close coiled on a conventional spring machine and the end cut to length in the conventional fashion that a spring is. A number of such sleeves are shown in figure 112. The potential advantages of this sleeve are that it can be fabricated with standard, low-cost techniques and equipment, it can be cut to length with no difficulty, it can be made heavy enough so that it should resist buckling on its own without lubricant restraints, and it should be able to accommodate variations in diameter close to its nominal diameter.

Tests with this sleeve concept (in this program) have disclosed a number of problems. The first problem is that of putting the sleeves onto the mandrel. This has proven to be very difficult and would require further development of a special loading device that unwinds and enlarges the sleeve diameter in a quick and easy fashion for mandrel placement. The second is not as complex; it was encountered in fabricating aluminum fatigue coupons for phase II. In this problem, a square-wire sleeve was extended because the jaws let it slip through. This resulted in very wide gaps that did not get coldworked. The solution appears to be a modification of the nosepiece jaws to accommodate the thicker sleeve material in a way that the jaws will not tip and allow the sleeve to slip by. The third problem is

trapezoidal tipping of the square wire elements under the frictional faces encountered in attempting to coldwork titanium. This problem totally voids its consideration for this type application without use of heavier elements. The fourth problem was breaking of the rings that extend beyond the hole so that a housekeeping problem is generated.

One further factor deserves to be mentioned about helical sleeves in general; the tests disclosed that they produce less difference in axial radial variation than the standard axial-split sleeves.

5.   PHASE I: TASK 5—MULTIMATERIAL STACK PARAMETERS

This task involved reaming, sleeve coldworking, and postreaming multimaterial stacks of titanium and aluminum to define the feasibility and practicality aspects of such an operation. The stacks selected consisted of nominal thicknesses as follows:

1/4-inch Al + 1/4-inch Ti + 1/4-inch Al
1/4-inch Ti + 1-inch Al + 1/4-inch Ti

The task was somewhat simplified by the selection of equivalent interferences for each alloy as optimum interferences. Hole diameter was 3/8 inch. Figure 113 shows the retained expansion obtained at different interference levels in the specific stacks, and figure 114 shows the preream, as coldworked, and postream diameters for the specific stacks at the optimum interference.

Even though the previous retained expansion curves plotted from individual plates of material showed basically equivalent values for the different materials, the combination stacks produced retained expansion values in the titanium that were 0.0015 to 0.002 inch smaller than those for aluminum. The preream and the postream operations, however, were within 0.0005 to 0.001 inch of each other, with the titanium actually ending up slightly larger in all cases. Freon TB-1 was used for all reaming and may have had an influence because titanium often ends up smaller in reamed holes in titanium/aluminum stacks. Nevertheless, no significant problem occurred in final hole size, in the coldworking operation, or in the removal of the disposable sleeves. It should be noted that the sleeves could not be removed easily from the holes in the normal fashion with fingers alone; they did require the use of pliers in most cases. Helical sleeves could rectify this situation if their other associated problems were solved.

6.   PHASE I: TASK 6—POSTSIZING PARAMETERS

This task was aimed at defining the minimum allowances for postreaming or postbroaching to ensure cleanup of the surfaces in all cases. To some degree, a portion of this task, and perhaps the most difficult, was already covered in the multimaterial stack effort. The data sheets in volume II show that holes in the aluminum, with 0.003-inch minimum (on the diameter) and 0.007-inch maximum to be removed (as a result of hole

profiling) were consistently reamed to final hole size with full cleanup in every case when using piloted reamers. Holes in titanium were consistently reamed to final hole size with piloted reamers with only 0.002-inch-minimum removal and 0.005-inch-maximum removal. These values are considered to be excessively low in terms of a 100% assurance that cleanup will always occur, although the tests did show that this performance could be obtained. Nevertheless, we have defined 0.010 inch and 0.015 inch (on the diameter) as minimum removal values for holes less than 1/2 inch and more than 1/2 inch, respectively. Charts that define the relative starting-hole sizes to ensure these cleanup amounts are provided in figures 115 and 116.

If hand-held power equipment is used for reaming, tests have disclosed that a long pilot is required on the reamer for guidance. Broaching can also be used for sizing, but it is practical only in aluminum. Care must be exercised in broaching thick stacks relative to ensuring cleanup, since the hole profile and the sleeve ridge in the hole prevent having a close-fitting pilot to assure angular alignment. Consequently, the teeth on the broach must be ground in a certain manner to provide the required alignment. That is, the broach must be ground with teeth in sets of three that all cut to the same diameter before the next set increases an increment of diameter. A broach that cuts bigger with every tooth does not seem to line up as well with an existing coldworked hole axis as the previously specified type.

It should also be noted that this task placed some emphasis on assurance of cleanup; phase II results indicate that lack of postsizing or full cleanup is actually not detrimental to fatigue performance of zero- and low-load-transfer applications. The advantage of postsizing is elimination of requirements for precise starting holes and precise knowledge of springback to produce finite finished holes (no postsizing); nevertheless, phase II results indicate that full cleanup is not totally necessary for many applications and should be so specified in pertinent specifications.

7. PHASE I: TASK 7–PORTABLE EQUIPMENT DEFINITION

Depending on specific performance requirements, the sleeve coldworking process can be basically considered a process that is very amenable to assembly and rework operations with portable tools. Most individuals that are exposed to the actual coldworking operation are usually impressed with its simplicity. The basic elements of the tooling to accomplish sleeve coldworking are:

- Mandrel

- Sleeve

- Nose cap and jaws

- Pull gun

- Hydraulic power pack

- Postsizing reamers or broaches

The process is patented and licensed to a manufacturer for sale of the elements to anyone that wishes to use the process. The licensee is listed under reference 2.

It should be noted that the mandrels and sleeves now carried as standards by this supplier basically reflect the Boeing system as originally developed. The standard tools now being offered do not necessarily include the changes that may be advisable as a result of this program. However, provision of sleeves and mandrels to revised designs and dimensions on the basis of either this program or the procuring organization's desires appears to be no major problem.

Selection of tools for sleeve coldworking operations requires knowledge of:

- Diameters of holes to be coldworked

- Interference to be used

- Stack thickness of the parts to be coldworked

- Material to be coldworked

From this knowledge and the data contained herein, the type of sleeve, size of sleeve, size of mandrel, pull gun size, and starting hole size can be defined. For instance, the type 301 half-hard stainless sleeve is normally used for aluminum coldworking, and the type 301 full-hard sleeve is required for coldworking titanium (or steel if a lower performance pull process is used). Actually, the full-hard sleeve can be used for all materials if it proves to be advantageous from a cost factor in separation and stocking. The Vascojet MA mandrel will be required for sleeve coldworking titanium or steel. It is not currently a standard at the supplier, although it will probably become the standard for all mandrels in the future.

Sleeves can be procured in various lengths in 1/16-inch increments between 1/4 inch (minimum) and 1-1/2 inches (maximum). For specific diameters, there is a fixed price for sleeves from 1/4 inch to 3/4 inch in length and a slight increase in price for sleeves from 3/4 inch to 1-1/2 inches in length. Practice has shown that it is advisable to procure the sleeves in standard singular lengths of 3/4 inch or 1-1/2 inches. Excess sleeve sticking beyond the stack will cause no problem unless there is a limited clearance situation on the far side of the hole. Thicker stacks than 1-1/2 inches are accommodated by stacking nonflared sleeves end to end. The 0.045-inch/inch taper should be specified on the mandrels since it will significantly reduce force requirements and shorten mandrel ramp length. The latter can be critical with limited back-side clearance restrictions. It should be especially noted that all of the charts compiled in the remainder of this section for equipment selection are based on use of the 0.045-inch/inch mandrel taper.

Mandrels can also be procured with a threaded tang or a collet-type tang. The latter is shown on the mandrels in figure 15. The collet tang is a holdover from the original mandrel-only, low-interference, coldworking process in which the entire mandrel must be passed through the hole, grasped by the collet in the pull gun, pulled, and automatically released from the gun to repeat the cycle. The type of gun and collet are evolutions of the CP 659 and CP 660 broach pullers shown in figures 117 and 118. These pull guns have a longer stroke than is normally required for most coldworking operations but can be used if they are available. With the sleeve coldworking system, the operation is a simple one-sided operation whereby the sleeve is placed on the mandrel, the mandrel/sleeve combination inserted into the hole to be coldworked, and the mandrel withdrawn by actuating the pull gun. The sleeve stays in the hole during the operation and is manually extracted later and discarded. Consequently, for this type of operation, the mandrel should stay affixed to the pull gun continuously, except when the mandrel diameter is to be changed. This means that, if a collet system is being used, the gun must be set up so that the collet does not automatically bottom out and release the mandrel on extension. Setting the gun up this way, however, requires removal of the entire nose barrel to actuate the collet for mandrel changes. For this reason, it appears advisable to use a simple threaded adapter on the pull gun with a threaded tang on the mandrel. Such a mandrel is easier to change, and the adapter costs less than the collet. One further aspect needs to be considered, however. As will be noted in the offset attachments shown later in this section, a collet-type tang may be advantageous for limited access, quick attachment situations. Consequently, a combination tang that meets both requirements is proposed in figure 119.

The nose cap design is also deserving of some comment. The current standard available uses a singular nose cap with interchangeable jaws or inserts to handle various diameters of mandrels. These jaws or inserts are segmented (in four pieces) to accommodate the change in mandrel diameter and held together with springs or O-rings. The jaws are necessary to support the end of the sleeve and prevent sleeve slippage. The design of the jaws and nose cap also provides flush support of the structure being coldworked adjacent to the hole by both the jaws and the nose cap. A typical nose cap and jaw assembly is shown in figure 120. The feature of having a singular nose cap that can accommodate different jaw inserts has proven to provide some difficulties in use. If the particular combination of mandrel length, gun barrel length, and gun stroke results in the mandrels withdrawing totally into the barrel, the current system requires the operator to hold his hand over the inserts to keep them from popping out when the mandrel re-extends. This occurs because there is a tipping moment on them that cannot be accommodated properly with the universal cap. Consequently, the nose cap design needs to be revised to prevent this—the obvious solution is a nose cap/jaw assembly for each diameter range.

Figure 121 is a tabulation of pull guns that are available, their designations, stroke, force capacity, and oil volume requirement. Figure 121 also includes a squeeze-yoke setup for pushing carbide mandrels. In addition to this chart, figure 122 gives the diameter capacity for each unit in different materials and stacks, and figure 123 gives the material stack or thickness capacity for each unit. The latter takes into account the stroke limits of each unit versus the total stroke capability required for specific stacks and specific diameters. Photographs of this equipment are shown in figures 117, 118, and 138 and also in figures 124 through 131.

44

Figure 132 lists puller unit accessories for offset and angle situations where an in-line pull on the tool is restricted by space limitations. The accessory designation, critical dimensions, use with designation, stroke, and force capacity are given. Photographs of these accessories are shown in figures 133, 135, 136, and 138 and schematics of some in use in figures 134 and 137.

Figure 139 provides a listing of various types of power sources that have been used with these pull or squeeze devices. It provides their designation, maximum pressure, volume flow at maximum pressure, oil available per cycle, type of action, input power, type unit, approximate weight, and 1973 list price. Photographs of most of the units are shown in figures 140 through 145. It should be pointed out that any hydraulic power source can be used, including the simple hand pump shown in figure 146. The latter may be quite adequate for a simple rework job, but is totally impractical for production usage. One other fact must be pointed out. Figure 147 shows a schematic of the internal construction of a broach puller unit (similar to the coldwork tool pull guns). These guns are operated for pulling action by hydraulic pressure. Return stroke is provided by air pressure. Therefore, a small air pressure line to the gun is required in addition to the hydraulic line. For practicality, even the hand pump setup shown in figure 146 should have an air bottle hookup for stroke return. Because air is normally readily available in most plants and maintenance areas, most of the power packs shown are either pneudraulic or pneumatically operated. A further factor must be considered if the standard actuation system on the pull gun is to be used. Each gun, as shown in figure 147 has three attachment ports. The larger one is for the hydraulic supply, one of the smaller ports is for the return air supply, and the second small port is for supply actuation. This is a small air line to the power supply. Depression of the gun's trigger bleeds pressure from the actuation line and causes a pressure-drop valve to actuate the power supply. The CP 805 pneudraulic power supply shown in figure 140 is equipped with this remote control system that is compatible with the guns as a standard feature. Most other power sources will require this remote control modification. A schematic of such a modification is shown in figure 148.

The standard hose systems normally provided with the CP 805 system and pull guns are believed to be especially cumbersome, as shown in figure 140. An even more cumbersome hose setup with a heavy air hose used is shown in figures 144 and 145. This problem can be reduced by using smaller diameter lines, as shown in figures 141 and 142, since the flow requirements for this operation are not high. The small pneudraulic power supply shown in figures 142 and 143 would not be recommended for production work, but it has proven to be useful for field rework kit applications.

8. PHASE I: TASK 8—INSPECTION METHODS DEFINITION

Test work in this task was limited to tests with eddy current probes to determine if this method could be used satisfactorily to detect that coldworking had not only taken place in a hole, but also to what degree. These tests were totally unsatisfactory   no detection of coldworking was possible within the scope of using available equipment and probes.

The above test work was aimed at providing a possible end-item inspection tool for an inspection system to be defined in this task. The remainder of the task effort was directed to analysis and observation to define a practical inspection system in lieu of the probe detection system. Such a system, however, must be in-process controlled.

Since the primary criteria for fatigue performance with the process is the amount of mandrel/sleeve-to-hole interference used for a specific diameter of hole, this interference must be controlled. As now established, the process uses a 0.003-inch, maximum-tolerance, precision-drilled hole. Thus, the interference is controlled basically within a 0.003-inch band since the sleeve thickness and mandrel dimensions are usually very close and consistent.

Nevertheless, the only way that the required interference can be ensured is to require inspection and recording of the starting hole dimensions. With good equipment setups, this can definitely be done on a sampling basis with the sample size defined by continuing experience with a particular setup. Inspection and recording of dimensions on mandrels and sleeves in use are also essential.

The question that most often arises with regard to inspection of coldworking is: "How can you tell that the hole has been coldworked?" If the hole has been coldworked and postreamed without an intermediate inspection step, it may prove to be difficult, although the surface upset at the higher interferences usually has a discontinuity where the axial split was located. If there is a serious question when such a situation arises, close observation of the surface at the hole periphery should disclose the upset and the discontinuity. If other suitable inspection has not ensured that the appropriate coldworking has taken place and no surface upset can be detected, then the hole may require oversizing and recoldworking.

In practice, a reasonably practical system has evolved for inspection control of the process. After recording starting-hole and tool sizes, the mechanic performing the coldworking operation leaves the sleeves in the holes he has coldworked as a guide to himself on what holes he has coldworked. The sleeves could be left in the holes as an indicator to the inspector that the holes had been coldworked and not removed until "bought off." If a further check is desired at this point, the inspector can spot check for presence of a definite ridge in the holes. This is easy to spot and provides definite assurance that coldworking has taken place.

If the starting-hole dimensions have been properly checked and recorded, the inspector could also spot check for proper interference by checking the as-coldworked hole against the retained expansion values defined in this report to determine if the hole is within the proper range. This technique is not being advocated as a standard method, but it is available if serious questions arise.

Finally, the postreaming or postbroaching operations can be controlled to some degree by requiring that the reamers or broaches have noncutting pilots of a specific diameter that will only enter a hole if it has been coldworked. Again, recording tool dimensions is essential to control and ensuring that they are truly being used is another. Unfortunately, it is a weak control because it is difficult to provide assurance that the proper reamer was used.

Consequently, the strong elements of an inspection system must be control of starting-hole sizes and coldwork tools and intermediate inspection prior to final sizing to ensure that coldworking has been accomplished.

SECTION V

PHASE II: APPLICATION AND PERFORMANCE PARAMETERS—

DETAIL RESULTS AND DISCUSSION

The work in this phase was primarily fatigue testing to define the performance parameters of the sleeve coldworking process in various types of applications and its relativity to standard fastening systems and other fatigue-rated systems. In addition, the effects of process and control variations were also assessed relative to fatigue performance. This work was complemented by additional studies relative to stress corrosion, relative strain (using photostress and strain gage coupons), and comparative costs.

The reports for the basic material properties of the 2024-T851 aluminum, the Ti-6Al-4V titanium, and the 300M steel used in this program are contained in volume II of this report. Data sheets with detailed test descriptions and test results for all tests in both phase I and II are also contained in volume II. Because of the large number of figures contained in this report, they have been placed in one group at the end of the text.

The primary data were procured with the three major alloys: 2024-T851 aluminum, annealed Ti-6Al-4V titanium, and 300M steel (270-300 ksi). With these alloys, multistress fatigue data were procured for base metal, basic open holes, and basic filled holes. S-N curves were plotted for these data (tasks 1 through 3). All other process and application variations and the additional alloys and heat treats (Ti-6Al-4V STA, Ti-6Al-4V STOA, Ti-6Al-6V-2Sn annealed, Ti-6Al-6V-2Sn STA, Ti-6Al-6V-2Sn STOA and 7175-T736) were all tested at a singular test stress. This stress was selected from the previously generated S-N curves so that a singular test stress could hopefully be used for all variations so that direct "across-the-board" comparisons could be made. The original intent was to select a stress for each condition that would produce approximately 100,000 cycles fatigue performance; this was discarded in favor of the singular stress approach since it allowed direct comparisons and since the high-speed Vibraphore test machines could handle large-value cycles quickly. Thus, 30 ksi was the maximum net area stress used for the aluminum comparisons; 70 ksi was the maximum net area stress used for the titanium comparisons; and 110 ksi was the maximum net area stress used for the 300M steel comparisons. The stress ratio (R) was 0.1 for all tests. For comparison purposes, extrapolated S-N curves have been generated for major single-stress variations and plotted on overall summary plots.

All figure 2, 3, and 7 configuration specimens were tested on the Amsler Vibraphore machines at 4000, 5000, or 6000 cpm. All of the aluminum specimens of these configurations were tested on the 36 kip Vibraphore machine shown in figure 4. All of the figure 2 titanium and steel specimens were also tested in the 36 kip Vibraphore. All figure 3 and 7 specimens in titanium and steel were tested in the 100 kip Vibraphore shown in figure 5. All figure 8, 9, and 10 specimens were tested in Riehle-Los equipment similar to that shown in figure 6. Test speed in these machines was set at 600 cpm. The Riehle-Los equipment was used for these tests to handle the coupon size and to provide a lower testing

speed so that overheating from interface fretting would be less of a potential problem. The maximum part temperature that ever occurred in any of these lower speed tests was 200° F (300 M steel).

Data sheets on each test (contained in volume II) also include sketches depicting origins of all failures. Failure origins are also summarized for each metal family, but the data sheets should be referred to if there are any questions relative to origins, failure and parameter conclusions, or specific numerical values for fatigue cycles. Summary fatigue cycle sheets are also contained in volume II for ease of reference.

It should be noted that all fatigue specimens in this program have been shot peened before testing. This was done to prevent premature surface failures and to ensure definition of maximum benefits to be gained from coldworking of the holes. Admittedly, this will improve the fatigue life of the base metal specimens as well, but this is probably appropriate since the author believes that most truly fatigue-critical structural components should be shot peened where it is possible and practical.

Where fasteners were used, the same standard torque value was used for all nuts. No variation in fastener preload or use of high preloads was used in the program. All fasteners used in the aluminum and titanium were cadmium-plated Ti-6Al-4V; fasteners used in the steel were cadmium-plated steel. The use of Hi-Loks for the straight shank fastener system should not be construed to mean that this fastener was selected for any particular structural fatigue performance attributes; it was selected only because it is a relatively common straight shank fastener system.

In phase II, all specimens of a specific alloy have been fabricated from a single heat of material. Where different thicknesses of material were used, the material has been machined (not rolled) to that thickness. The 2024-T851, Ti-6Al-4V, and Ti-6Al-6V-2Sn were machined from plate stock and the 7175-T736 and 300M were machined from forged stock. Where the test plan called for annealed, STA, and STOA heat treat conditions of the Ti-6Al-4V and Ti-6Al-6V-2Sn alloys, each material was fabricated as a special heat, a portion of this heat was mill annealed and the remainder was solution treated and aged (STA) by the vendor. Part of the latter portion was overaged at Boeing to put it into the STOA condition. Much of the STA material, as received from the vendor, was warped from the heat treatment. The worst of these were selected for the STOA condition, given a protective coating, overaged in a hot flattening press and then chemically etched to remove any alpha case.

The original plan called for use of all aluminum and titanium materials in the as-rolled condition, but this was impractical since the surfaces were too badly pitted and scored to assume that the shot peening alone would mask or alleviate these potential sources of failure initiation. Consequently, all aluminum specimens were machined to thickness during specimen fabrication, and all titanium and steel specimen blanks were ordered ground to thickness by the vendor. The 300M steel specimens were heat treated to 270-300 ksi after machining to configuration using copper plating for decarburization control.

50

A word of caution: care should be exercised in studying the plotted fatigue results because the logarithmic scale on fatigue cycles foreshortens the larger values and can be misleading to an uncritical observer. For proper perspective, one should compare the actual values because the graphic scale often makes the differences appear to be small when they are not.

For ease of discussion and to allow grouping of results displayed in the figures by major metal groups, the following material is divided into major groups by metals as first headings.

1. ALUMINUM

a. Phase II: Task I—Base Metal Performance (Aluminum)

Values for base metal fatigue performance are plotted for the 2024-T851 aluminum in figure 149. These values were obtained with figure 2 type test coupons (without holes in the test section) that were 1/4-inch thick. These values may not be equivalent to handbook values, which are usually obtained with 0.060-inch-thick electro-polished specimens, but they are "real-world" test values for this heat and thickness of metal albeit, the results may also be influenced by the friction grip loading in the test machine and the relationship of part thickness to this method of loading. The static load test values for this heat of 2024-T851 are given in volume II.

The test values in figure 149 are plotted as an S-N scatter band curve. The scatter band shown is purely a graphic interpretation; it does not represent a statistical calculation of probable limits based on test quantities and deviations. A graphic "mean" S-N curve for these data is plotted in figures 153 and 154 for comparison with other open- and filled-hole S-N data. Figure 153 is plotted on the basis of net area stresses. Figure 154 is plotted on the basis of gross area stress since many individuals find it difficult to accept net area stress comparisons. More on this subject will be discussed later.

A 30 ksi maximum net stress (R = 0.1) comparison of the base metal fatigue performance for 2024-T851 and 7175-T736 aluminum is shown in the first line of figure 158. At this comparative stress, the 7175-T736 is significantly better in fatigue performance than the 2024-T851 a mean of approximately 500,000 cycles in one case and 8-10 million cycles in the other. The notch sensitivity and fracture mechanics differences in these two alloys might not have produced this significant difference in performance without the shot peening. The better fatigue performance of the base metal 7175-T736 should be expected (especially with the surface protected by shot peening) since its typical yield strength (72 ksi) is well above that for 2024-T851 (60 ksi). The higher yield strength also indicates that a higher coldworking interference may be required in this equivalent modulus alloy to get the same degree of final compressive prestressing for fatigue improvement.

b. Phase II: Task 2—Basic Open-Hole Data (Aluminum)

Scatter band S-N curves for as-reamed open holes and sleeve coldworked open holes are shown in figure 150. The open holes are 3/8-inch diameter and the holes are coldworked to the 0.019-inch optimum interference value selected in phase I and then postreamed to nominal size (dimensions specified in volume II data sheets). It should be noted that all tests and sleeve coldworked holes in phase II used the optimum interference values; the specific value for interference will not be generally defined for each case in the text.

Graphic mean S-N curves for these data are also plotted in figures 153 and 154 for comparison with base-metal and filled-hole S-N data. Discussion of these curves will be covered in the task 3 subsection.

A comparison of open-hole results at the 30 ksi maximum net stress level for 2024-T851 and 7175-T736 is shown on lines 2 and 3 of figure 158. The open reamed hole results indicate that the 7175-T736 is more notch sensitive since its fatigue performance with a notch (the open, untreated hole) is now only slightly better than the 2024-T851; whereas, its base metal performance is significantly better (as shot peened). When the holes are sleeve coldworked, the 30 ksi maximum net stress performance improves from an approximate mean of 40,000 cycles for a reamed hole to 300,000 cycles for the coldworked hole in the 2024-T851; for the 7175-T736, it goes from approximately 50,000 cycles to 500,000 cycles. This is maintaining, more or less, the same ratio of performance and indicates the possibility that insufficient interference is being used in coldworking the 7175-T736 since the type of improvement shown possible with the "unnotched" base metal specimen is not being achieved. It could also indicate that an open-hole test is too severe an evaluation with more notch-sensitive material.

Basically, all of the tests conducted within this program and most of the plotted data are based on net area stresses. These are theoretical averaged stresses in the net remaining area since there actually is a gradient of stresses from the notch factor. Because many design considerations for fatigue are related to bending stresses in a wing (with no significant load transfer), many stress engineers use stress levels based on gross areas as being relevant to what the wing panel encounters. The author believes that neither system (net area or gross area) provides the proper visibility for accurate comparisons when using small section coupons. The development of an improved system was not in line with the basic intent of this program and is not included. Nevertheless, the author believes that this very elemental area of need (low-load-transfer applications) should be investigated to explore the use of an equivalent strain concept for useful comparisons and allowables development. That is, when a wing bends, every element in a wing panel within a chordal area strains an equal amount (disregarding twisting loads). Thus, if a large panel with little area removed by fastener holes is strain gaged adjacent to a fastener hole and the strain values are plotted for specific gross area stresses in the panel, these strain values could be used to define loads to produce equivalent strain adjacent to the fastener holes in strain-gaged small specimens. The strain gages are placed next to the holes because this is the area of maximum concern being tested and because the area adjacent to the hole will strain a greater amount than the area between holes in a small specimen. Therefore, when one wants to conduct a test, load values

to use for equivalent gross stress in a large panel would be determined via a chart and used. The results should be truly meaningful and should allow better interchange and application of data.

All failure origins in this task were at the holes. In the reamed holes, the fatigue failure origins were fairly uniformly distributed along the hole surface on the hole centerline 90° to the load axis (as shown in figure 168). In the sleeve coldworked and postreamed holes in aluminum, the failure origins were relatively uniformly distributed as well but with more definite origins at the hole exit corners. As with all coldworked holes in aluminum observed in this program, the longer life coupons had more definite, localized origins that were well defined. In addition, all noncountersunk coldworked hole failure origins were, without exception, located at the coldworking entrance side of the holes.

c. **Phase II: Task 3—Basic Filled-Hole Data (Aluminum)**

Basic S-N data is contained in the scatter zone curves of figures 151 and 152 for as-reamed holes with net-fit protruding head Hi-Lok fasteners, sleeve coldworked and postreamed holes with net-fit protruding head Hi-Lok fasteners, and taper-reamed holes with protruding head and 100° flush head Taperlok fasteners. Graphic mean curves are plotted in figures 153 and 154 as well for comparison with other data.

Filling a reamed hole with a net-fit fastener (in aluminum) provides a significant improvement in fatigue performance over an open, reamed hole, although the scatter in results is rather large at lower stress levels.

The difference in mean performance shows approximately a 300,000 cycle life for reamed filled holes at 30 ksi maximum net stress (versus 40,000 cycles for an open reamed hole) and 900,000 cycles for a sleeve coldworked filled hole (versus 300,000 cycles for a sleeve coldworked open hole). At 40 ksi maximum net stress, the performance of filled reamed and filled coldworked holes is 50,000 cycles and 155,000 cycles, respectively.

The protruding head Taperloks were slightly better than the coldworked holes with net-fit, protruding head Hi-Loks although the Taperloks had a large scatter at lower stresses. The flush head Taperloks, however, had failure origins at the countersink to part surface junction (where no prestressing from the taper shank occurs) with fatigue performance only slightly better than that obtained from a net-fit, protruding head Hi-Lok in a reamed hole. The Taperlok holes were all prepared with care under laboratory conditions to a Boeing class F specification. This specification requires a higher minimum and maximum level for protrusion (effective interference) than the vendor standard and all known industry standards. This Boeing protrusion standard is 0.187 to 0.289 inch for a 3/8-inch fastener; all Taperloks within the program fell between 0.200- and 0.240-inch protrusion values. All Taperlok holes were reamed to size, but no holes were checked for contact with bluing pins. One failure analysis of Taperlok installations in a high-load-transfer coupon did show a corkscrew type of fretting in the shank area even with the care exercised.

The results indicate that, in 2024-T851, proper tensile prestressing via a protruding head Taperlok system is as good or slightly better than a straight shank net-fit fastener in a coldworked hole, although there appears to be more scatter and less confidence

built into the tapered fastener system. The flush head tapered fastener runs into serious difficulties in the nonprestressed countersink; its performance is little better than a conventional flush head fastener installed with a good net fit in a reamed hole. Figures 155, 156, and 157 are photographs of typical fracture faces and failure origins.

Figure 158 shows the relative performance of reamed and sleeve coldworked holes filled with protruding head Hi-Loks in 2024-T851 and 7175-T736 aluminum (lines 4 and 5). The reamed holes with Hi-Loks in 7175-T736 show a mean value improvement (at 30 ksi maximum net stress) from approximately 55,000 cycles for open holes to 500,000 cycles for filled holes; the latter value is not significantly better than that achieved for 2024-T851 (a mean of approximately 400,000 cycles). Whereas, the coldworked and postreamed holes in 2024-T851 showed an improvement from 400,000 cycles for open holes to 750,000 cycles for filled holes, the 7175-T736 showed no basic improvement. In fact, the filled coldworked holes in 7175-T736 had lower performance than equivalent installations in 2024-T851. Thus, the benefits potentially achievable with the 7175-T736, as evidenced by the base-metal test values, are not being reached with the coldworking interferences used. Either the notch sensitivity is too critical or the prestressing (via interference) is not adequate for this alloy. Further S-N type testing and optimum interference testing with open and filled holes appear necessary for this alloy to resolve the questions not answered by the planned tests in this program.

d. Phase II: Task 4—Application and Process Performance Parameters (Aluminum)

In this phase, variations in application such as edge margin, hole spacing, adjacent noncoldworked holes, and load transfer plus process variations and controls such as countersink sequence, hole finish, prior damage, subsequent damage, and split orientation are evaluated for their impact on fatigue performance. The task also included some strain effect and photostress testing (covered in the "All Alloy - General" subsection).

All data that follow are solely for 2024-T851 aluminum; it was all obtained by testing at 30 ksi maximum net stress (R = 0.1).

(1) Hole Finish and Program Correlation (Aluminum)

The program included specimens with both as-reamed holes and honed holes (no coldworking) with the latter to serve as a test method check against results from the "Precision Hole-Generation Methods" contract, F-33615-71-C-1548 conducted at McDonnell Aircraft Company. This was aimed at providing a proper reference for comparisons and correlations. The McDonnell program, however, used honing in only its titanium and steel test work; comparisons will be made in the subsections on titanium and steel (which do show that results are directly comparable).

The open as-reamed and as-honed results shown in lines 2 and 3 of figure 159 for 2024-T851 indicate that improving the hole finish from approximately 55 RHR (as reamed) to 25 RHR (as honed) does not result in any improvement in fatigue performance. The use of an as-drilled hole versus a reamed hole prior to sleeve coldworking, as shown in lines 2 and 4 of figure 161, did not result in any change of coldworked fatigue performance either; actually, the finish of each type of precoldwork hole was relatively equivalent (40-50

RHR). The use of a very dull drill (line 5, figure 161) for abusive drilling immediately prior to coldworking produced hole finishes of 125, 130, and 145 RHR. The open-hole fatigue performance of these holes was 287,000, 110,000, and 93,000 cycles, respectively, relative to a coldworked open-hole fatigue performance of 200 to 400,000 cycles for properly prereamed or properly predrilled holes. It is interesting to note that the loss in performance was relative to the degree of increase in finish above 125 RHR (with the 125 RHR specimen showing no loss in performance). Further examination of the data in volume II for this set of abusively drilled specimens shows that the retained expansion from coldworking was greater than should be expected (as previously determined and charted). Thus, the heat generated in the abusive drilling operation (with a very dull drill) was apparently able to accomplish some overaging and loss of strength in the material immediately surrounding the hole with a resultant loss in fatigue capability (regardless of coldworking).

These results indicate that a 125 RHR finish limitation is still probably a practical overall limit; any finish beyond 125 RHR may indicate other damage and should be cause for rejection and reaming of the hole to the next oversize to remove damaged material. Further, it may be wise to limit the number of holes that approach 125 RHR to a specific percentage to ensure good process control. This should present no practical problems since standard precision drilling processes for the 0.003-inch total tolerance hole now generally specified in aluminum will normally produce hole finishes in the 40-60 RHR range.

(2) Starting-Hole Tolerance (Aluminum)

The phase I optimum interference data for the 2024-T851 are repeated in lines 4 through 7 of figure 159 for 3/8-inch-diameter holes. In figure 68, a proposed interference-versus-diameter curve was plotted for 2024-T851. This was based on analyses of the performance data and selection of a 0.019-inch interference for 3/8-inch-diameter holes as a reasonable optimum and 0.030-inch interference for 3/4-inch-diameter holes and applying a downward hole tolerance of 0.003 inch to these values. Further examination of these data indicates that, if the starting-hole tolerance of 0.003 inch is to be maintained without causing the process to become tolerance critical in performance, the interference range for the 3/8-inch hole should probably be shifted from the originally projected 0.016 to 0.019 inch to one of 0.018 to 0.021 inch.

(3) Sleeve-Split Location (Aluminum)

As shown in figure 160, the axial split in the coldworking sleeve leaves a ridge in the hole after coldworking. In all tests to this point, this ridge has been aligned at 0° to the axis of loading to place it in a noncritical zone in the zero-load-transfer specimens. In this test, the split in the sleeves was aligned at 90° to the load axis in the most critical zone of the holes in each specimen. Lines 2 and 3 of figure 161 compare the results for the 0° orientation and the 90° orientation. The results show that the split location has no detrimental effect whatsoever on the fatigue performance with the results falling well up in the 0° scatter band. In fact, the ridge not only displayed no adverse effect, but all failure origins were on the side of the holes opposite the location of the ridge.

For load-transfer applications, the location of the split in the sleeve or its mere existence might cause some problems. That is, the surface upsetting generated in coldworking displays a discontinuity at the split location. This discontinuity could accentuate interface fretting under conditions of load transfer. Methods of offsetting fretting problems are covered under the subsection on high-load-transfer testing in task 4.

(4) Process Predamage (Aluminum)

This subject has already been covered in the subsection on hole finish.

(5) Process Postdamage (Aluminum)

In this test, holes that had been sleeve coldworked and postreamed were deeply scored with a sharp tool at the most critical position, 90° to the load axis and in line with the hole axis. Only one of the two holes in each specimen was so scored. The test results are shown on line 7 of figure 161. Since all failure origins were in the nonscored holes, it must be assumed that a sleeve coldworked and postreamed hole has a relatively high tolerance for postdamage—especially for the conventional scoring or rifling that might be encountered in standard reaming and broaching processes. No significance is especially attached to all failures occurring in nonscored holes; this is probably a statistical anomaly and should not be construed to indicate that scoring is beneficial.

The actual fatigue performance values (with one exception) fell within the desired scatter band. The one low value (in a nonscored hole) showed evidence of fretting products from drilling that had migrated into the fatigue fracture interface. This indicates that the presence of such aluminum oxide fretting particles may influence the crack propagation rate by acting as wedges or props in the crack. This subject may deserve further exploration since many of the so-called noncontaminating solvent-type cutting fluids used for precision drilling of aluminum alloys often produce some fretting products.

(6) Postreaming Allowables (Aluminum)

In this series of tests, the open-hole fatigue performance with no postream and postreams of 1/64, 1/32, and 1/16 inch on the diameter were compared to results obtained with a standard postream. The standard postream is currently on the order of 0.006 to 0.010 inch on the diameter. The results are shown on lines 6 and 8 through 10 of figure 161 and should be compared to the standard shown on line 2 of the same figure. As shown, no postreaming produces results towards the high end of the scatter band and a 1/64-inch postream toward the low end of the scatter band. The increased postreams of 1/32 and 1/16 inch actually showed a progressive improvement in results, all within the scatter band limits. Thus, these results would indicate that a number of successive oversizing operations could be exercised for repair or rework without recoldworking the hole. Since the test results did not show any loss in performance up to a full 1/16-inch removal, the maximum limit has not been defined; however, a practical allowable has. The results also indicate that no postreaming should be necessary for holes in aluminum that remain open—such as clearance and drain holes.

(7) Square-Wire Sleeve (Aluminum)

The concept of a square-wire sleeve was covered in the phase I discussion. This concept appeared to offer some potential for sleeve fabrication improvement and process flexibility. In this test, its capability to provide equivalent fatigue performance was to be verified. The results of the test are shown on line 11 of figure 161. Of the three specimens tested, two produced acceptable fatigue results within the defined scatter band (line 2). One specimen, however, had reduced performance (still well above the reamed-only performance shown on line 1). In this specimen, the square-wire sleeve slipped through the nose piece and helically extended within the hole. As a result, a specific helical zone within the hole received a reduced amount of coldworking, resulting in a loss in performance.

This problem can probably be averted in the future by revising the ledge in the nose cap jaws or inserts to fully support the thickness of the square wire. The jaws used were designed for the thinner sheet metal split sleeve; the eccentric load condition with the thicker sleeve caused them to tip and allow the sleeve to slip through. In addition, the square-wire sleeve proved to be very difficult to place on the mandrel compared to a regular split sleeve. A special sleeve handling tool will be required to overcome this problem before further consideration can be given to this sleeve concept. In addition, difficulties experienced with this sleeve concept in titanium (discussed later) indicate that potential application would probably be restricted to aluminum structure.

(8) Material Thickness (Aluminum)

Material thickness of the part being coldworked has previously been shown to influence surface upset amount and retained expansion values. In this test, specimens were fabricated from 0.060-inch-thick 2024-T851 and sleeve coldworked and postreamed. Open-hole fatigue results for these specimens are shown on line 4 of figure 162 and compared to base-metal coldworked and reamed-only results in 0.250-inch-thick 2024-T851 in lines 1, 2, and 3 of the same figure. The results show a serious loss in performance compared to the thicker material, with only a slight improvement over that to be expected with a reamed-only hole.

Observation of the specimens disclosed that the material gage allowed it to achieve its condition of lowest potential energy via oil-canning or dishing at each hole, thus, practically eliminating any beneficial compressive prestressing at the hole. This test has disclosed that a serious limitation may exist in applying this process to thin gages, especially those in sandwich structures. It is highly probable that the flattening of such dished zones, when clamped by a fastener into a thicker stack, would reestablish the desired performance improvement, but that was not tested in this program. In addition, the limit on gage for aluminum where this loss of performance in unsupported structure ceases to be a problem has not been defined. Both deserve further exploration. Tests discussed in later sections for the steel and titanium show that their higher modulus (greater stiffness) diminished this problem.

(9) Edge Margin and Hole Spacing (Aluminum)

Since the sleeve coldworking process is a high-expansion process that depends on an external tensile tangential prestress within the part to maintain an internal compressive tangential prestress, some consideration must be given to edge margin limitations, especially for rework situations. For this test, a special specimen more representative of actual edge margin conditions, per figure 7, was used. All tests were conducted with open holes. Edge margins were varied between 1-1/2, 2, and 2-1/2D. Hole spacing, at 2-1/2D edge margin was varied between 3, 4, and 5-1/4D. Test results are given in figure 163. Of these conditions, the only one that showed some loss in performance from the standard of 2D edge margin and 4D hole spacing was the 1-1/2D edge margin condition. The best results (although only slightly so and with more scatter) were obtained with the 2-1/2D edge margin and the wide 5-1/4D hole spacing. Some other tests conducted within Boeing have indicated that the limit for the beginning of performance loss with edge margin is at 1-3/4D, although the loss suffered at 1-1/2D was not severe. Therefore, hole spacing down to 3D and edge margin down to 1-3/4D should be considered no problem.

(10) Type Fastener System—Zero Load Transfer Application (Aluminum)

The 30 ksi maximum net stress test values from task 3 are included for net-fit, protruding head Hi-Loks in reamed holes and coldworked holes and for protruding and flush head Taperloks in lines 2 through 5 of figure 164 for comparison. This graphically shows the large scatter in results with reamed-only holes and with tapered fastener holes, although the scatter band for the latter is admittedly high in overall performance. It also shows the loss in performance suffered by the flush head Taperlok through countersink failure origins that make its performance almost equivalent to that which can be expected from a good net-fit, straight shank fastener in a reamed hole.

(11) Countersink and Countersink Sequence (Aluminum)

The previous subsection defined the effect of a countersink on a Taperlok system. In this test, the effect of a 100° countersink and its preparation sequence (before or after coldworking) on the fatigue performance of a flush head Hi-Lok in a sleeve coldworked hole was assessed. The results are shown on lines 6 and 7 of figure 164.

When the countersink is produced after the sleeve coldworking operation, the area that is being countersunk has already been prestressed. Admittedly, a significant amount of metal is removed from this zone in the countersinking operation, but apparently a sufficient prestress remains since the performance is actually better than that shown in the scatter band for protruding head Hi-Loks in coldworked holes. The fact that these results are slightly better with a high metal removal, plus the fact that the protruding head Taperloks are also somewhat better, indicates that the improvement may be related to a lesser tensile prestress in the edges of the specimen. In fact, it leads one to question the possible merit of using a high coldworking interference to achieve a sizable affected zone coupled with a significant postream to reduce the outer tensile prestress levels. The trend toward improved performance with increasing postream amounts tends to support this hypothesis.

When the 100° countersink is produced prior to coldworking, the result with net-fit Hi-Loks in the holes is a serious loss in performance (shown on line 7 of figure 164) from a mean value of approximately 1,000,000 cycles to individual values of 169,000, 213,000, and 508,000 cycles. All failure origins were at the countersink-to-part surface juncture. Performance loss was basically equivalent to that suffered by the flush head Taperloks.

The need to countersink in a separate operation is not desirable since a one-shot drill/countersink operation is preferable from the point of flow time and assured hole/countersink concentricity. Nevertheless, it is a firm requirement if the intended fatigue improvement is to be achieved. Such countersinking operations should be performed with good-fitting pilots on the tools; a nonrotating pilot would be best. An even better approach with regard to concentricity control and lowest labor costs would be to incorporate the countersink with the reamer for a one-shot postream/countersink operation.

The requirement to countersink after coldworking indicates that use of the sleeve coldworking process for a rework situation, where a countersink already exists, is not a valid application—especially with zero to low load transfer and hard, nonupsetting fasteners. A valid solution is not clear-cut and there are a number of alternatives. However, all of them require verification or qualification beyond the scope of this program (as originally defined).

(12) Countersink Angle (Aluminum)

Since a 100° countersink has a relatively large major diameter, its outer boundaries cut well into the previously prestressed zone. In the planning of this program, it was anticipated that a 70° countersink (with a 70° head fastener) would remove less of this beneficially prestressed zone and would, thus, prove to be advantageous. This test was designed to confirm or disprove that theory. The results are shown on line 8 of figure 164.

The test produced some totally unanticipated results. A severe loss in fatigue performance occurred with the 70° countersunk hole that fell into the zone of performance one would expect for an unfilled (open) coldworked hole. Observation of the fracture faces disclosed a severe fretting and erosion at the bottom of the countersinks on the 90° and 270° sides relative to load axis. Further investigation disclosed that the actual countersink included angle was 73° and the fastener head was 69° which led to contact primarily at the bottom of the countersink. The failure origins, however, were not located at the area of fretting but at the top edge of the countersink. Thus, the lack of support was more severe than the fretting.

Further investigation of the previous 100° included angle countersink installations disclosed that there was a discrepancy in angles there also. In this case, the countersink was 102° and the head was 100°. The same type of performance result did not occur, however, with the 100° head installations. Analyses indicate that this is probably based on the greater flexibility of the 100° head in allowing the torque preload to seat it and fully support the countersink; whereas, the relative rigidity of the 70° head would not as readily accommodate a mismatch.

Thus, the 100° head design remains as a good choice. However, it has become apparent that closer controls need to be exercised on countersink angles, head angles, countersink perpendicularity, and countersink concentricity than the probable norm in the past.

(13) Fastener Fit—Zero Load Transfer (Aluminum)

All straight shank fastener tests conducted to this point in the program had fasteners installed in a fit as close to net as could be achieved by measuring actual fastener diameters and selecting reamers accordingly. This test series assessed the relative impact of using 0.002-inch clearance fits (on the diameter) or 0.002-inch interference fits in 3/8-inch-diameter holes. This proved to be an important test with some previously unanticipated results. The fatigue test results are shown on lines 9 and 10 of figure 164.

Two of the three clearance-fit fastener installations produced results within the scatter band to be anticipated for net-fit fasteners in coldworked holes and one at the high end of the band for open coldworked holes. All failure origins, however, were at the corners of the specimens (away from the holes); whereas, open coldworked holes always have failure origins at the hole. Fracture analyses of the lower performance specimen disclosed no detectable damage near the edge failure origin that might have precipitated premature failure. It did disclose a fairly large bulge at the corner from shot peening (not uncommon) that may have created an adverse stress condition. Since this failure has no other explanation, this conclusion must be accepted. If it is correct, it would imply that care should be exercised to ensure 45° shot peening of edge corners after the major shot peening is completed. As previously noted, open holes and reduced prestress in countersinks coupled with fastener mismatch have a significant impact upon performance; whereas, a 0.002-inch clearance fit in this case does not. Until more data are available to answer the question of a specific dimensional limit, the 0.002-inch limit will have to be accepted.

The fatigue results with the 0.002-inch interference fit fastener were the lowest of any of this filled-hole series for the figure 2 zero-load-transfer coupons. Previous Boeing-funded test work in 2024-T351 with the lower mandrel-to-hole interference currently in use as a standard did not show any loss in performance when using a low-level interference-fit fastener. Fracture analyses of the interference-fit specimens in this section disclosed that failure origins were all located at the specimen corners. In each case, there were multiple, very definitely defined origins with very short fatigue crack lengths and large-area ductile failures as if the specimen, in general, was overloaded. Apparently, the combination of the tensile prestresses (that support the compressive prestresses) from the so-called optimum interference coldworking, plus the tensile prestresses from the interference-fit fastener, actually did just that overloaded the specimen. Thus, zero-load-transfer applications should not use an interference-fit fastener with optimum interference coldworking and a st   dard postream. Alternatives for interference-fit installations would be use of a larger postream to reduce tensile stresses away from the hole (while still maintaining a large-area compressive zone) or lower interference standards for coldworking similar to those in the Boeing Company's original standards for the process.

60

This brings up another probability on process sequencing or control. When hand-driven rivets are used with coldworking to achieve fatigue performance and the shanks are upset into an 82°/30° countersink, the countersink area will probably see a reasonably high interference whereas the shank area will not. Therefore, it may be advisable to coldwork after countersinking for this type application. Some limited Boeing data with this type of installation and lesser coldworking interference tend to support this probability. These results should not be construed as a blanket indictment of interference fits in optimum coldworked holes. These results are relative to zero or low load transfer. The later section on high load transfer discloses some different results.

(14) Adjacent Hole Not Coldworked (Aluminum)

In the application of a process such as coldworking, there are often finite zones of the structure where its benefits are deemed necessary. On the boundaries of such zones, a transition would be required to noncoldworked hole/fastener installations. It is this transition that was of concern in these tests since some photostress panels in high-strength steel prior to this program showed a possibility that a coldworked hole adjacent to a noncoldworked hole might produce some detrimental stress risers in the noncoldworked hole. In this test, only one of the two holes in each figure 2 specimen was coldworked. The other hole was as-reamed. Each hole had a net-fit Hi-Lok installed in it. The hole spacing was the conventional 4D spacing relatively common in practice and used as a standard within this program, unless hole spacing per se was being evaluated. The intent was to compare the fatigue life performance of the noncoldworked hole (with an adjacent coldworked hole) to that of the reamed, filled-hole specimens tested in task 3. The results are shown on line 11 of figure 164. The performance of these specimens was surprisingly good with the performance of two specimens falling within the scatter band for coldworked, filled holes and the third within the scatter band for an open coldworked hole. Failure origins for the two higher performance specimens were actually in the coldworked holes; failure origin in the lower value specimen was in the noncoldworked hole. Therefore, some benefit from the prestress field was apparently gained in the noncoldworked hole. Since the results from all specimens were above the scatter band to be anticipated for reamed, filled holes, this situation should cause no concern in conventional applications of the process. Hole spacings closer than 4D may require some test verification of application validity.

(15) Prior Fatigue Crack (Aluminum)

Any fatigue improvement fastening system must be considered not only for production applications, but also for field rework, overhaul, and extended-life modifications. In rework, the question arises relative to oversizing the holes (to remove damaged material) and what happens if all of an undetected crack is not removed? In this test, specimens were prepared by drilling an undersize hole and fatigue cycling the specimen to start an actual fatigue crack from a jeweler's saw cut within the hole. The holes were then reamed to precoldwork size, which left approximately a 0.030-inch-long crack at time of coldworking. After coldworking and postreaming, this crack length was reduced to approximately 0.020 inch prior to fatigue testing.

Results (line 12, figure 164) from two of the specimens fell at the low end of the filled-hole coldwork scatter band, with the failure origins along the edge of the

specimen; the original precracks at the hole evidenced no detectable growth. The third specimen had a low-performance equivalent to the low end of the scatter band for a reamed-only filled hole. Failure analyses showed that the original crack was longer than it was thought to be and, in fact, had a belly in the center that made this hidden portion much longer. The relative initial lengths were 0.120 and 0.240 inch, respectively.

(16) Low Load Transfer (Aluminum)

The skin/stringer simulation 15-hole fatigue specimen (fig. 8) was included in the program to assess the effect of low load transfer upon the fatigue performance of coldworked holes and to assess what effects, if any, a production sequence would have on performance. To assess this, one group of specimens was subjected to the total process of hole drilling, coldworking, postreaming, and fastener installation, one hole at a time, to prevent any buildup of differential expansion stresses between the two different width members of the specimen. Another group was assembled with a "production" process; that is, all holes were drilled and then every fifth hole was coldworked, postreamed, and the fastener installed before the remainder of the holes were completed.

In all of these specimens, the holes were postreamed for a close net fit of the Hi-Lok fastener. A further group of specimens was not postreamed and the fasteners installed with a close net fit to the minor diameter of the hourglassed hole. This required adjusting the starting hole and mandrel diameters to utilize standard fasteners. This group of specimens was aimed at assessing the real need for postreaming to achieve a good net fit for the fastener throughout its length under low-load-transfer situations.

One other group of 15-hole specimens that represented only the stringer portion of the dual specimen was run. This specimen is shown in figure 9. The intent of this test was to correlate results based on a different design of specimen and different test speeds with previous zero-load-transfer coupon (fig. 1) test results.

These specimens were not all tested at the same net stress because of operator error between net area and gross area test methods. However, the actual net stresses that resulted were equivalent to a 40 ksi stress level used in S-N testing, and adequate performance comparisons can be made.

Figure 165 data is plotted for this 40 ksi net stress and shows that for this test stress that neither the specimen design, the testing frequency, the load transfer, the assembly sequence nor the lack of a postream had any effect upon altering the performance to be anticipated with a zero-load-transfer single-thickness specimen. The origins of failure in the stringer-only 15-hole specimens were all at the edge corners of the specimen away from the hole. The existence of some interface fretting plus the load transfer in the skin/stringer specimens caused the primary origins of failure to be in the skin at the skin/stringer interface and hole junction. Many of the origins were also at a 45° location to the load axis, which is typical of a load-transfer-type failure. Nevertheless, at this test stress and associated life, the load transfer and fretting were apparently not significant enough to cause any loss in performance.

The fact that differential expansion stresses caused by using a production sequence technique does not cause any change in performance is important to know because a one-hole-at-a-time technique would be totally impractical. The fact that eliminating the postream for this low-load-transfer application did not cause any loss of performance offers some potential for cost savings; further verification at different stress levels appears advisable before such an approach would be used extensively. The actual practicality of not using a postream is also questionable since it would require precise presizing of the starting hole and precise knowledge of springback. The current system allows some flexibility in this regard.

When the net area stress is reduced to 30 ksi (fig. 166), the fatigue performance for the 15-hole load transfer specimen (fig. 8) improves from approximately 150,000 cycles to approximately 265,000 cycles; however, this result is now well below the 600,000 to 800,000 cycles achieved with the zero-load-transfer specimens. Thus, the combination of the load transfer and, possibly, the fretting at the interface is apparently now causing some loss of potential performance at the longer-life stress level. If fretting is causing some of this loss, it can be prevented with the shim technique discussed in the high-load-transfer section. The use or injection of micarta shims may, however, be rather difficult to accomplish in rework situations where parts are not disassembled.

The 15-hole specimens did disclose something else worth noting. The trend in specimen design is to simplify the specimens to reduce size and the number of fasteners in them. However, when a specimen has a large number of holes in it, it has been theorized that the test results should more accurately represent the statistical lower side of the scatter band. The results from these 15-hole specimen tests tend to support this theory since the results were extremely consistent and very tightly grouped.

(17) High Load Transfer (Aluminum)

Load transfer across a joint creates a special problem of stress concentration at the joint interface. Whereas, in a zero-load-transfer situation the failure origin can often be driven away from the hole, this has not proven to be possible with a high-load-transfer situation. An additional problem may reach a level of significance in high-load-transfer joints - fretting at the interface. Under some conditions, the latter situation may become paramount, with the fretting mode of failure masking or superseding all other conditions induced to improve performance. Interface fretting problems are of special importance with sleeve coldworking since the surface upsetting that is produced at each hole can create a condition of localized bearing and high contact pressures. For this reason, the test program included the use of micarta shims at the interface of the joint for most of the test specimens. Some specimens were also run without shims and some without shims and the surface upset removed to assess the comparative effects. The specimen design was a double-shear type per figure 10. Fastener systems included for comparison with zero-load-transfer results and one another were:

- Net-fit, protruding head Hi-Lok in coldworked hole

- Net-fit, flush head Hi-Lok in coldworked hole

- Clearance-fit, protruding head Hi-Lok in coldworked hole

- Interference-fit, protruding head Hi-Lok in coldworked hole

- Protruding head Taperlok

- Flush head Taperlok

The primary shim used with the aluminum specimens was a smooth sheet of micarta 0.010 inch thick. One test used a sand-blasted sheet of micarta 0.050 inch thick, similar to the material often used in grips of fatigue test machines. The design of the specimen was in error relative to evaluation of flush head fasteners since the side plates were equal in thickness to the center plates. Thus, the stress in the side plates was half that of the center; a countersink in a side plate could not achieve major importance under this condition. Subsequent tests in steel and titanium had the side plates reduced in thickness to rectify this situation.

The test results for the high-load-transfer portion of the program are shown on lines 4 through 13 of figure 167. Lines 1 through 3 represent data from zero-load-transfer coupons, per figure 2 for comparison.

For net-fit fasteners in reamed-only holes, the load-transfer situation caused very little loss in performance relative to the zero load transfer. For net-fit fasteners in coldworked holes, the load-transfer situation caused a reduction in the performance band from a range of 600,000 to 950,000 cycles to one of 370,000 to 580,000 cycles. The use of a 0.002-inch clearance-fit fastener reduced this range further to one of 280,000 to 355,000 cycles. Use of an interference fit of 0.002 inch did not have the detrimental effect shown with zero load transfer and actually produced an improvement in performance to a range equivalent to that to be expected with zero load transfer at optimum performance.

Taperloks proved to be equivalent to net-fit Hi-Loks in coldworked holes under the high-load-transfer conditions but not equivalent to the interference-fit Hi-Loks in coldworked holes.

The 0.010-inch micarta shim proved to be very durable in these tests and did not break down sufficiently to allow any metallic contact. It should be noted that the surface upset for 3/8-inch-diameter aluminum holes is on the order of 0.003 to 0.004 inch. Therefore, the 0.010-inch shim would prove to be adequate to prevent metallic contact. Increased upset with large diameter holes or different materials (steel and titanium) may require adjustment of the shim thickness. Tests with a rough 0.050-inch micarta shim were too limited, and results were such that conclusions could not be drawn. The removal of the micarta shims to allow metal-to-metal contact at the interface proved to be detrimental for the 2024-T851, although no more so than using clearance-fit fasteners. Failure analyses of these conditions did show significant fretting at the interface and secondary cracks initiating immediately beyond the fretted zone. Removal of the surface upset and testing without an interface micarta shim produced a definite improvement in fatigue performance over that obtained with the upset not removed and no shims in place; however, the scatter in results was beyond acceptability.

The interface fretting that occurred on specimens without micarta shims was solely on the first hole toward the load and solely on the half of the periphery of that hole toward the load. This certainly indicates that an in-line load transfer joint using hard fasteners is highly questionable in its effectiveness beyond the first fastener; it also indicates that the cost of this type specimen could be reduced by using only four fasteners instead of the eight in the design tested.

The results of this test sequence show that (1) the micarta shim is a definite advantage with sleeve coldworked holes in aluminum structure and (2) an interference fit is also a definite advantage with sleeve coldworked holes under high-load-transfer conditions.

2. TITANIUM

a. Phase II: Task 1—Base Metal Performance (Titanium)

Results from base metal fatigue tests for the annealed Ti-6Al-4V titanium, conducted with figure 2 type specimens (no holes), are plotted as an S-N scatter curve in figure 173. In comparing these results to the 2024-T851 results, the Ti-6AL-4V produces 1,000,000 cycles at approximately 88 ksi whereas the 2024-T851 does so at approximately 27 ksi when there are no stress concentrating factors such as fastener holes involved.

No particular significance is being attached to the base metal values per se in this report. They are intended to serve solely as "real-world" references or baseline values to assess the relative performance of other conditions.

Figure 170 gives comparative base metal values (at 115 ksi maximum net area stress) for the annealed: STA and STOA heat treat conditions of both the Ti-6Al-4V and Ti-6Al-4V-2Sn titanium alloys. For the Ti-6Al-4V, neither the STA or STOA heat treat conditions provides an improved fatigue performance over the annealed condition with the STA condition exhibiting wide scatter and a generally lower log mean performance. The annealed Ti-6Al-6V-2Sn alloy also exhibits a lower performance than the annealed Ti-6Al-4V. The Ti-6Al-6V-2Sn STA heat treat condition is equivalent to the annealed Ti-6Al-6V-2Sn although the STOA condition is better, but only equivalent to the annealed Ti-6Al-4V. Thus, with no stress concentrations from fastener holes, the annealed Ti-6Al-4V titanium appears to be the best selection of all for fatigue performance.

b. Phase II: Task 2—Basic Open-Hole Data (Titanium)

Figure 169 contains S-N scatter band curves for reamed open holes and coldworked open holes in annealed Ti-6Al-4V titanium. These data were generated with figure 2 type coupons. The open holes are 3/8-inch diameter; the coldworked holes are coldworked to a 0.019-inch interference value (selected in phase I) and then postreamed to nominal size (dimensions specified in the data sheets in volume II). It should be noted that all coldworked holes in titanium in phase II were coldworked with this optimum interference value; the specific value for interference will not generally be defined for each case in the text.

Open hole fatigue performance for the annealed, STA and STOA conditions in the Ti-6Al-4V and Ti-6Al-2Sn alloys with open reamed holes and open coldworked/postreamed holes is shown in lines 1 and 2 of figures 171 and 172. These values were generated at a 70 ksi maximum net area test stress (R = 0.1). There are some slight differences between the alloys and heat treat conditions; but basically, the performance of all reamed holes for all conditions fall into one group with a mean performance of approximately 30,000 cycles, and the coldworked holes all fall into another group with a mean performance of approximately 60,000 cycles.

Reference to figure 182 will show that fatigue failure origins for all of the open holes were at the holes and were not localized. In fact, almost all test conditions with titanium specimens resulted in relatively similar failure origin patterns. In general, this lack of finite, localized failure origins would tend to indicate that adequate prestressing (via coldworking) is not being applied. Test work in phase I, however, indicated that higher prestressing tended to produce excessive scatter. As will be seen in later discussion of other tests, results with titanium did not always follow the theoretical pattern that should be expected. This may be a combined result of texturing, material directionality, and a susceptibility to the Bauschinger effect. The latter is a tendency for a material to lose yield strength in one direction when plastic deformation occurs from a stress in the opposite direction.

c. **Phase II: Task 3—Basic Filled-Hole Data (Titanium)**

Baseline S-N scatter curves for filled holes are plotted in figures 173 and 174. As can be seen (by referring to open hole S-N data in figure 169), introduction of a net-fit fastener in the hole boosts the fatigue performance of the Ti-6Al-4V at 70 ksi maximum net stress from 30,000 cycles to 80,000 cycles for reamed-only holes and from 60,000 cycles to 500,000 cycles for coldworked holes.

Figure 174 gives S-N scatter curve data for protruding head and flush head Taperlok fasteners in Ti-6Al-4V. A scatter curve is shown only for the 100° flush head Taperloks since the data for the protruding head version of this fastener was too excessively scattered to plot it. The upper limit for the flush head Taperlok S-N scatter curve is basically equivalent to the upper limit of the S-N scatter curve for the net fit, protruding head Hi-Loks in coldworked holes; however, the Taperlok curve is wider from more scatter. This result, again, is an anomaly for the titanium since flush head Taperloks in aluminum provide little better performance than net-fit fasteners in reamed holes (because of the lack of prestressing in the countersink) and the same loss does not occur in the titanium. The holes prepared for these Taperlok installations were prepared with care under laboratory conditions. Protrusion values and tolerances were equivalent to those specified in the aluminum section.

Alloy and heat treat condition comparisons for basic filled holes are shown in lines 3 and 4 of figures 171 and 172. As with open holes, neither the Ti-6Al-6V-2Sn alloy or any heat treat condition for either alloy produced better results than those achieved with the annealed Ti-6Al-4V alloy. With both alloys the annealed conditions produced the best fatigue performance with coldworked holes.

d. Phase II: Task 4—Application and Process Performance Parameters (Titanium)

With exception of the multimaterial 15-hole skin/stringer coupons of Ti-6Al-4V titanium and 2024-T851, all other Ti-6Al-4V titanium coupons in this section were tested at a maximum net area test stress of 70 ksi (R = 0.1).

(1) Hole Finish and Program Correlation (Titanium)

Open hole values shown in figure 175 were obtained at 65 ksi maximum net area stress for comparisons of results with those obtained in the "Precision Hole Generation" program conducted at McDonnell Aircraft Company (AFML-TR-73-135). Basically, the honed-only open holes were intended as the primary comparison tool. McDonnell test specimens were basically the same configuration as those in this program within the test section of the specimen. The only differences were loading methods (grip design), test frequency, and test equipment. They loaded their specimens with a single large pin in each end, whereas, we used a bolted friction grip. They tested their specimens in Sonntag SF-10 machines at 1800 cpm test frequency; we tested the majority of ours in Amsler Vibraphore machines at 4000, 5000, and 6000 cpm.

The honed hole specimens in our program produced roughly 60,000 cycles at this test stress and the McDonnell specimens roughly 80,000 cycles. This is not a significant difference and can be basically considered equivalent performance—especially in light of some of the material property differences encountered with titanium in this program. Comparisons of reamed-only open holes at 55 ksi bear this assumption out: their results ranged from 65,000 cycles to 80,000 cycles and ours ranged from 55,000 cycles to 105,000 cycles. Thus, across-the-board comparisons of results appear to be valid with no significant impact from testing method or frequency.

The honed-only open holes showed slightly better fatigue performance than the reamed-only open holes although the finish was basically equivalent at 30 RHR. Properly drilled holes had a finish near 55 RHR, and abusively drilled holes a finish between 65-75 RHR. Reference to lines 2 through 5 of figure 176 shows that a coldworked hole that was properly drilled has a fatigue performance basically within the scatter band of results for reamed and coldworked holes; however, the abusively drilled holes do show a slight loss in performance. The finish, though, is not significantly different for the abusively drilled hole and falls well within the 125 RHR finish limit often used for drilled holes. Three possible conclusions arise:

- Finish control for precoldworked holes in titanium is not a meaningful method of control.

- Quality of precoldworked holes in titanium is not significantly important.

- This situation should be assessed with filled holes since the range between open reamed holes and open coldworked holes is not overly large, and small differences could prove to be more significant in filled holes.

Since precise control of drilling operations and tool sharpness is difficult, it would appear wise to require prereaming of holes for coldworking in titanium until more data is available on this subject.

(2) Sleeve-Split Location (Titanium)

Lines 2 and 3 of figure 176 compare orientation of the split location in the coldworking sleeve. Line 2 location is in line with the specimen load axis (the area of minimum stress) and line 3 location is at 90° to the other (the area of maximum stress). The mean performance of the adverse location is actually slightly better, but is within the scatter range and must be considered basically equivalent. Also, failure origins were on both sides of the holes. Thus, as with the aluminum, the titanium material is not sensitive to the location of the sleeve split under zero-load-transfer situations. The previously discussed surface upset discontinuity from the sleeve split might prove to be a problem with load-transfer applications.

(3) Process Predamage (Titanium)

This subject has been covered in the subsection on hole finish.

(4) Process Postdamage (Titanium)

In this test, holes that had been sleeve coldworked and postreamed were deeply scored with a sharp tool at a position 90° to the load axis and in line with the hole axis. Only one of the two holes in each figure 2 specimen was so scored. Holes were tested in the open condition. Results are shown on line 7 of figure 176. All failure origins were at the score, but the fatigue performance of all specimens were equivalent to unscored holes. Again, the coldworking process has demonstrated its lack of sensitivity to the type of damage that can often occur in reaming, broaching, or bolt insertion—an important factor to manufacturing, quality control, and engineering.

(5) Postreaming Allowables (Titanium)

In this series of tests, the open-hole fatigue performance with no postream and postreams of 1/64, 1/32, and 1/16 inch on the diameter were compared to results obtained with a standard postream. The standard postream is currently on the order of 0.006 to 0.010 inch on the diameter. The results are shown on lines 6 and 8 through 10 of figure 176 and should be compared to the standard shown on line 2 of the same figure. As shown, no postreaming produces results towards the high end of the scatter band and a 1/64-inch postream toward the low end of the scatter band. The increased postreams of 1/32 and 1/16 inch showed a very slight loss in results, but within what appears to be acceptable limits. Thus, these results would indicate that a number of successive oversizing operations could be exercised for repair or rework without recoldworking the hole. The results also indicate that no postreaming should be necessary for holes that remain open such as clearance and drain holes.

(6) Square-Wire Sleeve (Titanium)

The square-wire sleeve concept was tested and discussed in some depth in the section on aluminum. When an attempt was made to use it to coldwork holes in Ti-6Al-4V fatigue specimens, the square cross section of the wires in the sleeves were plastically deformed from a square section to a trapezoidal one. Damage to the sleeve was excessive, and the approach must be rated as being totally unacceptable at this time for titanium. Further testing with different size wire cross sections to determine if this difficulty could be averted was not attempted.

(7) Material Thickness (Titanium)

In this test, specimens were fabricated from 0.060-inch-thick Ti-6Al-4V titanium and sleeve coldworked and postreamed. Open-hole fatigue test results for these specimens are shown on line 4 of figure 177 and compared to base metal, reamed-only and coldworked test results in lines 1, 2, and 3 of the same figure. At 70 ksi maximum net area test stress, the reamed holes in the 0.250-inch material gave approximately 30,000 cycles, the coldworked holes in the 0.250-inch material approximately 70,000 cycles, and the coldworked holes in the 0.060-inch material approximately 55,000 cycles. The loss in performance from sheet thickness is not of the magnitude with the titanium that was encountered with the 0.060-inch material in aluminum. The reason for this probably lies with the higher elastic modulus of the titanium, which inhibits dishing around the hole and a resultant loss of prestressing. The real magnitude of the loss (if it would occur at all) should be assessed with filled holes for the aforementioned reasons. The increased stiffness of the titanium coupled with support that might be obtained with dense honeycomb core (for fastened areas) might make coldworking of fastener holes in titanium sandwich a valid application; whereas, in aluminum this did not appear to be possible. As with aluminum, layering of thin titanium with other material in a joint would probably avoid any loss of beneficial prestressing in the thin material.

(8) Edge Margin and Hole Spacing (Titanium)

The results of these tests are shown in figure 178. In these tests the edge margin was varied from 1-1/2 to 2-1/2D and the hole spacing from 3 to 5-1/4D with the special edge margin specimen per figure 9. All holes were tested in the open condition. A thorough analysis of the results indicates that there is no significant difference or trend displayed, including the 1-1/2D edge margin specimens (with exception to exhibiting the most scatter). Thus, a normal 2D edge margin should allow some rework capability without creating problems.

(9) Fastener Fit = Zero Load Transfer (Titanium)

The effect of fastener fit in sleeve coldworked holes is shown in lines 2, 3, and 4 of figure 179. Line 2 represents the standard net fit used as the baseline. Line 3 is a 0.002-inch clearance fit (on the diameter) and line 4 is a 0.002-inch interference fit. Whereas in aluminum, a 0.002-inch clearance fit produced only a slight loss in baseline net-fit performance, the loss in the Ti-6Al-4V titanium is significant. In addition, where the

0.002-inch interference fit in the aluminum produced a significant loss, it produces a reverse effect in the titanium — a significant gain. This is further evidence that the titanium is not coldworked or prestressed to the so-called optimum level (if this is possible).

Nevertheless, if the values for coldworking defined to-date herein are used, bolt installations should be slanted towards a net to interference fit. It should be noted also that the gains in performance that appear possible are generally better than what might be achieved with a tapered fastener installation.

(10) Countersink and Countersink Sequence (Titanium)

In aluminum structure, coldworking to a high interference with the sleeve process prior to countersinking was adequate to protect the countersink. In fact, since the failures were driven away from the hole to the specimen edge, removal of the countersink material lowered the tensile stresses at the specimen edge and produced a small inprovement in performance. When the hole was coldworked after countersinking in aluminum structure, the countersink was not protected and the fatigue performance was only slightly better than a reamed-only, filled hole.

In these Ti-6Al-4V titanium tests, the same is not true (lines 6 and 7 of figure 179). Countersinking before coldworking now produces the best performance (equal to a protruding head installation). Countersinking after coldworking with a 100 countersink produces a loss to a mean of 300,000 cycles at 70 ksi from 900,000 cycles for the reverse sequence versus 85,000 cycles for reamed-only holes. In other words, the result was not only reversed, but the loss was not as significant. Furthermore, countersinking after coldworking with a 70 countersink also caused some loss of performance, but not of the magnitude of the 100 countersink. Reference to figure 182 shows that all failures originated in the shank zone regardless of sequence, indicating that the hole is most critical and sufficient prestressing for total protection is not occurring. Thus, postcountersinking and its associated reduction of prestressing in the shank area, as well, would reduce performance of this zone.

(11) Countersink Angle (Titanium)

Since the sequence result is the reverse of what was anticipated in the titanium, the 70° angle countersink would also have to be generated prior to coldworking to fully assess its potential value. As the results now stand, it is not as good as a 100° countersink generated prior to coldworking (line 8, fig. 179).

(12) Adjacent Hole Not Coldworked (Titanium)

When the adjacent hole to a coldworked hole is not coldworked in titanium, the prestress zones around the coldworked hole do not create any detrimental effects on the noncoldworked hole (loss of anticipated reamed hole performance). This can be seen in line 5 of figure 179. Consequently, no special precautions with application to only specific zones in titanium structure relative to side effects on nearby holes need to be exercised with 4D or more hole spacing.

(13) Prior Fatigue (Titanium)

When some titanium specimens were fatigue cycled first to 80,000 cycles (close to failure) and then coldworked, full life to values within the normal scatter band for nonfatigued holes was achieved. Thus, coldworking of existing holes in a structure that has endured service (without prereaming) can provide a "like new" performance. This approach was evaluated only for holes that were not previously coldworked. It is not known if the same would work for previously coldworked holes. Test results are shown in line 11 of figure 179.

(14) Prior Fatigue Crack (Titanium)

In this test group, actual fatigue cracks were generated in a fastener hole and then the hole was coldworked. Line 12 of figure 179 shows the fatigue cycles achieved in Ti-6Al-4V titanium specimens with three different crack lengths prior to coldworking. It appears that the process is basically capable of mitigating the cracks existence if it is 0.020 inch or less long. Cracks 0.030 inch long resulted in a fatigue performance equal to reamed-only holes (no cracks).

(15) Low Load Transfer (Titanium)

The 15-hole low-load-transfer, skin/stringer type coupons in the titanium evaluation included both specimens with titanium/titanium stacks and titanium/aluminum stacks. Since with the design of this specimen (per figure 8), both components encounter equal strain at the center of the specimens, the aluminum will theoretically reach a fatigue critical strain first (assuming no effect of load transfer). Consequently, the loads for the titanium/aluminum specimen were selected to provide a 40 ksi maximum net area cyclic stress for the aluminum with a resultant stress in the titanium of 64 ksi. All specimens had net-fit, protruding head Hi-Loks installed; specimens tested in this subsection were:

- 15-hole single coupon per figure 9 with holes coldworked and postreamed

- 15-hole titanium/titanium coupon per figure 8 with holes coldworked and postreamed with production technique (see aluminum section for explanation)

- 15-hole titanium/titanium coupon per figure 8 with holes coldworked and not postreamed using production technique

- 15-hole titanium/aluminum coupon per figure 8 with the aluminum in the stringer component and holes coldworked and postreamed with the production technique

Results are shown in figure 180 along with results from zero-load-transfer, two-hole coupons for comparison (both aluminum and titanium). The two-hole zero-load-transfer coupons indicate that the titanium at 70 ksi should have appreciably better fatigue life than the aluminum at 40 ksi. With the respective stresses in the dual-material coupon 64 and 40 ksi, the performance of the titanium should be even better.

Results from the single-strap 15-hole zero-load-transfer coupon on line 3 of figure 180 show, however, that the titanium in this case has a fatigue performance significantly lower than the zero-load-transfer 2-hole coupon for the same 70 ksi stress. In the aluminum tests (wherein failure origins can be driven away from the fastener hole when coldworked and filled), the performance of the 15-hole coupon was equivalent to the 2-hole coupon. This raises the question of effect of testing speed upon relative performance since the 15-hole coupon was cycled at 600 cpm in the Riehle-Los equipment and the 2-hole coupon at 4000 cpm in the Vibraphores equipment. Testing speed differences that ranged from 1200 cpm to 4000 cpm between McDonnell and Boeing (previously discussed in this section) did not seem to have an impact on results. Furthermore, a titanium check coupon we ran in the Riehle-Los equipment with reamed-only, filled holes to verify loads produced 112,000 cycles, basically equivalent to Vibraphore results shown in line 1 of figure 181. The only remaining difference in the coupons is hole diameter. The 2-hole coupons had 3/8-inch-diameter holes and the 15-hole coupon 1/4-inch-diameter holes. Overall widths of the test sections were inherently different dimensionally, but were equivalent based on both having 2D edge margins. Thus, the only possible conclusion is that the smaller diameter hole (with equivalent edge margins) is more critical.

Further observation of the results shows that the imposition of even a low load transfer has a further impact upon the titanium performance with a coldworked and postreamed hole (see line 4 of fig. 180). The best performance with the low-load-transfer condition was obtained with coldworked holes that were not postreamed as shown in line 5 of figure 180.

Because 1/4-inch-diameter hole coupons in titanium have a generally lower performance and because the titanium is even sensitive to low load transfer (whereas the aluminum is not), the failures in the dual-material titanium/aluminum coupons all initiated first in the titanium component. Results are shown on line 6 of figure 180.

(16) High Load Transfer (Titanium)

If low load transfer caused some loss of fatigue performance in titanium, the high load transfer used in this test series should have an even more serious impact. As with the aluminum, the figure 10 high-load-transfer coupons were run with and without micarta shims in the interfaces. The shims were intended to diminish the potential impact of interface fretting at the coldwork upset around each fastener hole.

Results and test contents can be seen in figure 181. It should be noted that this figure starts at 10^3 cycles instead of the 10^4 cycles used in most of the other figures. This figure shows that at 70 ksi the reamed-only fatigue performance drops from approximately 85,000 cycles for zero load transfer to approximately 15,000 cycles for the high load transfer (with shims). For the coldworked holes the reduction is from approximately 350,000/1,500,000 to approximately 20,000 cycles (with shims), respectively. As can be seen, the performance of the coldworked holes is not appreciably better than reamed-only holes when interface shims are present with high-load-transfer titanium specimens. A clearance-fit fastener in a coldworked hole functions as well as a net-fit

fastener under these conditions although it caused some loss with zero load transfer. As with aluminum though, an interference-fit fastener in a coldworked hole is beneficial under high-load-transfer conditions, although its benefit in the titanium is not overly significant.

Whereas the interface micarta shim proved to be beneficial with aluminum high-load-transfer coupons (eliminated fretting), better performance was achieved in the titanium without it (35,000 cycles). This indicates that the notch sensitivity relative to load transfer is sufficient in the titanium so that it supersedes any potential problems from fretting; in this case, the smooth micarta shim probably enhanced movement of the components and increased the effective load transfer. Removing the surface upset and testing without a shim did not appear to provide any significant improvement over not removing the upset.

The comparative performance of the best coldworked hole situation under high load transfer and reamed-only holes under zero load transfer (70 ksi) is 35,000 cycles and 85,000 cycles, respectively. Protruding head Taperloks showed the best performance in the high-load-transfer titanium tests. Its mean performance was basically 70,000 cycles at 70 ksi.

Both the flush head Hi-Loks in coldworked holes and the flush Taperloks had poor performance in these tests. The failure origins, in these cases, were in the countersunk side plates that were reduced in thickness to produce stresses in them theoretically equivalent to those in the main coupon section. Basically, this didn't appear to be good design per se, since the countersunk left only 0.045-0.060 inch of straight hole. Regardless, the failure origins (fig. 182) were not in this straight portion for either the coldworked or Taperlok installation; the failure origins were actually spread along the countersink. This is not consistent with the zero-load-transfer failure origin locations (all in shank), but indicates that the reduced zone of resistance, in this case, probably resulted in higher effective prestressing of the small remaining straight portion. The load transfer still made the overall situation more critical and the countersinks failed at cycles well below what the straight portions did under zero-load transfer.

3. **STEEL**

a. **Phase II: Task 1—Base Metal Performance (Steel)**

All phase I fatigue tests with coldworked open holes in 300M (270-300 ksi) steel were run at 110 ksi maximum-net stress. The base metal tests with figure 2 coupons run in this phase showed that the base metal endurance limit stress was above 110 ksi. An S-N scatter curve for the 300M base metal fatigue tests is shown in figure 183 with an indication that the endurance limit stress is in the 120 ksi range.

b. **Phase II: Task 2—Basic Open-Hole Data (Steel)**

Figure 184 shows the S-N scatter curve results for open reamed holes in the 300M steel in comparison to the base metal results. Whereas at a stress of 25 ksi the 2024-T851 produced approximately 1,000,000 cycles for the base metal and 60,000 cycles for the

notched metal (reamed holes), the 300M steel at 125 ksi goes from 1,000,000 cycles to 20,000 cycles for the same respective conditions. Figure 185 gives S-N scatter curve values for open holes that have been coldworked and postreamed in comparison to base metal values. These holes were coldworked with a carbide push-type mandrel that had a 0.045-inch/inch taper angle. The coldworking interference value was 0.0245 inches on the diameter for the 3/8-inch-nominal-diameter holes. The fatigue performance of these holes is statistically equivalent to the open reamed holes with no obvious improvement in fatigue performance. This result gave some cause for concern that possibly the previously selected 0.045-inch/inch mandrel taper (selected on the basis of force tests) was causing more axial rather than radial yielding with no benefit to fatigue performance. This concern was investigated further in task 3 and is reported on therein.

c.   **Phase II: Task 3—Basic Filled-Hole Data (Steel)**

Figure 186 gives S-N scatter results for holes that were reamed and filled with net-fit Hi-Lok fasteners and holes that were coldworked and filled with net-fit Hi-Lok fasteners in comparison to base metal S-N values. The reamed and filled holes show no basic improvement in fatigue performance over the previous open-hole tests. The coldworked and filled holes show a definite improvement in performance over the reamed and filled holes. These holes were coldworked with a 0.030-inch/inch taper angle mandrel. The performance improvement, relative to base metal values, is still not of the magnitude that was achieved with the 2024-T851 aluminum.

Figure 187 is a composite plot of open and filled holes. Lines 5 through 10 give comparative values for reamed holes and coldworked holes in 300M steel filled with net-fit Hi-Loks. The coldworked holes were produced at different interferences and with different mandrel taper angles to assess both the suspected critical interference plateau and the mandrel taper angle under suspicion as a result of task 2 test results. The previous indication that there was a definite jump in fatigue performance between 0.020- and 0.025-inch interference (for 3/8-inch-diameter holes) was verified with 0.023 inch appearing to be the minimum value for the better performance. No significant difference in fatigue performance resulted for 0.023-inch versus 0.025-inch interference; however, coldwork processing of the specimens showed another problem: the solid film lubricant was breaking down rapidly at 0.025-inch interference levels. The 0.023-inch interference level and the 0.030-inch/inch mandrel taper were more tolerable with regard to forces and lubrication durability. At this time, it appears that the 0.030-inch/inch mandrel taper may be a better selection for high-strength steel. The previous indications of a practical limit on interference in high-strength steel have also been generally verified.

d.   **Phase II: Task 4—Application and Process Performance Parameters (Steel)**

(1)   Hole Finish and Program Correlation (Steel)

Honed open holes in line 1 of figure 187 have a finish of 20 RHR, but did not produce as good a fatigue performance as reamed open holes—50,000 cycles versus 100,000 cycles at 105 ksi. Both the honed holes and the reamed holes had finishes of 20 RHR. Coldworking these reamed holes resulted in no basic improvement in open-hole

fatigue performance. At 110 ksi this was roughly 60,000 cycles. Good drilled holes had a hole finish of 40 RHR and abusively drilled holes, in the 300M steel, had a hole finish of 60 RHR. Again, all of these finish values fall well within the finish values normally accepted as evidence that good practices have been followed. However, reference to figure 188 (lines 3 and 4) will show that both the good and bad drilled holes had significantly better fatigue performance than reamed holes (even though the drilled hole finish was not as good as the reamed) when the holes were subsequently coldworked. Thus, not only finish must be discarded as evidence of "poor" processing, but also the concept of untempered martensite and overtempering, if the holes are subsequently coldworked. It is evident from previous research that conventional drilling and, certainly, abusive drilling operations will produce some degree of untempered martensite and overtempering in high-strength steel. It now appears that this previously "undesirable" result may be beneficial if the affected zone is appropriately prestressed via coldworking since the material involved may not be as notch sensitive through the overtempering involved. This is an important observation since it offers the possibility of removing stringent controls from hole generation processes in high-strength steel in lieu of subjecting them to a postprocessing operation of coldworking.

The honed hole results shown in figure 187 were run at 105 ksi to allow comparison with the McDonnell tests on their Sonntag equipment at different test frequencies (see finish subsection in titanium). The McDonnell test results (between 40,000 and 60,000 cycles) are equivalent to our test results, which indicates that the results of both programs should be directly comparable for the 300M steel as well as for the Ti-6Al-4V titanium.

(2) Starting-Hole Tolerance (Steel)

Reference to the difference in fatigue performance results for 3/8-inch-diameter holes shown in figure 187 for 0.023-inch versus 0.020-inch coldworking interference indicates that either the upper interference should be increased or the hole tolerance held close to control the minimum interference. Since the high-strength steel imposes its own upper limits with regard to mandrel breakage, the only practical alternative is controlling the hole tolerance range closely (to 0.001 inch). This anticipated tolerance is actually displayed in the projected interference-versus-diameter requirements shown in figure 70 for 300M steel. This conclusion appears to be adverse to the conclusions espoused in the previous subsection; i.e., a predrilled hole may be better than a prereamed hole for 300M steel. In actuality, it may not prove to be excessively difficult to drill close-tolerance holes in high-strength steel, although some development may be required.

(3) Process Predamage (Steel)

The previous subsection has covered this subject.

(4) Process Postdamage (Steel)

– Line 5 of figure 188 shows fatigue test results for open holes that were coldworked and deeply postscored with a sharp tool in line with the hole axis at a point 90° to the load axis (the most critical location). The scoring or "damage" caused no loss in fatigue performance relative to similarly coldworked and postreamed holes—in fact, the

mean performance was improved. It is rather interesting to note that for each material tested (the aluminum, the titanium, and the steel), the fatigue performance of the scored specimens was statistically better than unscored specimens in all cases even though only one hole of two was scored in each specimen. The results certainly indicate, without doubt, that the sleeve coldworking process (with high interference) is relatively immune to normally unacceptable visible hole "damage."

.(5) Postreaming Allowables (Steel)

As has been seen with titanium, open-hole tests are severe tests that may prove to be overly severe with the more notch-sensitive materials. Reference to lines 6 through 9 of figure 188 show the effect of the standard 0.006- to 0.009-inch postream versus no postream versus 1/64-, 1/32-, and 1/16-inch postream (on the diameter) after coldworking 300M (270-300 ksi) steel. With open-hole testing, none of these situations produces less fatigue performance than the standard postream. However, no postream results in a significant improvement in open hole fatigue performance; a 1/32-inch postream is also better, but not quite as good as no postream. The fact that no postream and 1/32-inch postream were significantly better than 1/64- and 1/16-inch postream is not necessarily abnormal. That is, the removal of the initial highly compressive "worked skin" is bound to reduce fatigue performance of an open hole in notch-sensitive material with regard to crack initiation. Removal of more material may effect a better balance of compressive and tensile prestresses with regard to crack propagation rates. This is purely conjecture, yet it is supported by some test results to be discussed later. The point at which this best balance occurs has not been defined for all diameters and may require further testing.

(6) Material Thickness (Steel)

Figure 189 contains fatigue result comparisons for the standard 0.250-inch-thick fatigue specimens primarily used in this program versus the "thin" 0.060-inch specimen tested in this series. Again, this is an open-hole test. Whereas the 0.060-inch-thick aluminum had insufficient rigidity to maintain the prestress from coldworking (material dished around the hole) and no fatigue improvement was achieved, it cannot be finitely concluded that the 300M material has sufficient rigidity even though the open-hole fatigue performance in the 0.060-inch-thick 300M was basically equivalent to the thicker material; i.e., coldworking of open holes produced no basic improvement over reamed-only open holes.

(7) Edge Margin and Hole Spacing (Steel)

Edge margin and hole spacing have not proven to be critical in the previous aluminum and titanium tests. Reference to figure 190 would indicate that this is also the case for the 300M steel. In no case is the open-hole fatigue performance worse than that for the standard 2D edge margin, 4D hole spacing. The fact that a 1-1/2D edge margin, 5-1/4D hole spacing and 2-1/2D edge margin, 4D hole spacing appear to provide the best performance is not logically explainable. Regardless, the indication is that a 1-1/2D edge margin is not critical with 300M steel, at least with open holes.

(8) Pull Process and Sleeve Orientation (Steel)

As previously mentioned, the only coldworking capability that existed for 270-300 ksi steel at the outset of this program was a push process that utilized a carbide mandrel and a dry lubricant baked into the holes. In the course of this program a steel mandrel pull process capability (with a sleeve) was developed. This subsection contains results of tests to assess the relative performance of the pull mandrel/sleeve process for the high-strength steel. To assure that a valid evaluation was achieved, these tests were all conducted with filled holes (net-fit Hi-Lok fasteners). The maximum practical coldworking interference was used for each process: 0.023 inch for the carbide/no-sleeve, push process and 0.019 inch for the HSS mandrel/sleeve pull process. As stated previously, the retained expansion for the pull mandrel/sleeve process was roughly 50% of that for the carbide push mandrel process on the basis of sleeve thinout and elastic mandrel deformation. The fatigue performance was roughly equivalent to the retained expansion achieved (see fig. 191). Reamed-only filled holes were basically 75,000 cycles; carbide push mandrel coldworked and filled holes were 300,000 cycles; steel pull mandrel and 0° split sleeve coldworked and filled holes were 95,000 to 300,000 cycles; and steel pull mandrel and 90° split sleeve coldworked and filled holes were 150,000 cycles. Thus, the steel mandrel/sleeve process did show some capability of providing a fatigue improvement; albeit, only 50% of that possible with the carbide mandrel process, regardless of sleeve split orientation. Admittedly, this result must be qualified, at this time, to zero-load-transfer applications. Later discussion will show that surface upset, per se, with carbide mandrels, had no influence upon high-load-transfer results; however, the effect of the split orientation upon high-load-transfer interface fretting and fatigue performance is not known at this time.

(9) Countersink and Countersink Sequence (Steel)

Sleeve coldworking a precountersunk hole and filling it with a net-fit fastener proved to be of little benefit over reaming alone in aluminum, although countersinking after sleeve coldworking proved to be slightly more beneficial to fatigue performance than sleeve coldworking and filling a noncountersunk hole. Titanium responded in a reverse fashion which further indicates that insufficient interference was used to achieve the "optimum" interference in the titanium. The lower values used in the titanium (because higher values caused excessive scatter) resulted in prestressing levels that were reduced to insufficiently protective levels in the straight hole portion of the hole by postcountersinking. The question is: would the same be true for the 300M steel?

Reference to figure 192 shows that this does not occur with the steel. In fact, countersinking and filling a hole in steel after coldworking and postreaming it produced an outstanding improvement in fatigue performance over noncountersunk-hole performance. Again, this improvement seems to be a function of initially generating a large compressive zone through high interference coldworking and then reducing the levels of compressive prestress and supportive tensile prestress to a better balance without reducing the size of the compressive zone (via metal removal).

Countersinking a hole in 300M (270-300 ksi) steel prior to coldworking proved to be detrimental. In this case, the fatigue performance was significantly less than that achieved with reamed-only, noncountersunk holes. This type of result has been

encountered by Boeing in previous, independent test work. The reduction below reamed-only performance with precountersunk holes was traced to generation of an undesirable tensile stress bulge at the hole/countersink juncture after coldworking.

Consequently, with zero to low load transfer in steel, countersunk holes appear to be definitely preferable in terms of fatigue performance, whether or not flush installations are desired. It is possible that the same results could be achieved via appropriate postreaming, but definition of limits have not been evaluated for filled holes in this program.

(10) Countersink Angle (Steel)

In this test, the 70° countersink angle was evaluated for the steel as it was for the titanium and aluminum. The results (shown in line 5 of figure 192) indicate that 70° postcountersinking is also beneficial to fatigue performance of high-strength steel; however, the 100° postcountersink was definitely superior. Regardless of the reason, a 100° countersink has proven to be a better selection of angle for all alloys tested in this program and should remain as the primary standard for countersink angle.

(11) Fastener Fit (Steel)

The use of a clearance fit or an interference fit did not have any significant effect upon zero-load-transfer performance of straight, coldworked holes in the 300M steel. The interference fit, however, was only a theoretical fit since the steel stregnth and hardness was beyond the ability of a conventional steel bolt to effect such a fit. The result was basically a net fit of a severely scored and broached bolt (see fig. 193). This type installation produced only a slight decrease in the minimum fatigue performance, but did result in a wider scatter in results.

Therefore, a net to 0.002-inch clearance fit appears to be an appropriate call-out for coldworked holes in 300M (270-300 ksi) steel.

(12) One Hole Not Coldworked (Steel)

As discussed in similar, previous subsections, the application of a fatigue improvement process or fastener system will normally be selective with regard to critically stressed zones. Thus, there may be a transitional zone in fastened joints or structure wherein adjacent holes may not be "treated". In the previously discussed aluminum and titanium sections, such a situation (a noncoldworked hole adjacent to a coldworked one) has caused no loss in anticipated performance of the reamed and filled hole. In fact, in both the titanium and aluminum, the performance of the adjacent reamed-only hole was improved. The initial investigation of this consideration was based on a photostress observation in 270-300 ksi steel. This observation (of a possible problem) has now been borne out. That is, the results on line 8 of figure 192 show that such a situation very definitely decreases the reamed-only hole fatigue performance below normally expected levels.

This result was obtained with the standard 4D hole spacing. No evaluation of different hole spacing was included in the program. Wider hole spacing would probably diminish or eliminate this problem. If standard 4D hole spacing is being used, the indication is that the process must be applied in the structure to a point where the diminished, reamed-only result will not be a problem.

(13) Prefatigued Structure (Steel)

Available test results with prefatigued structure of 300M steel, shown in line 9 of figure 192, indicate that 300M material that was cyclic loaded close to origin of fatigue failure can be coldworked (without metal removal to start) and achieve a fatigue performance equivalent to that expected of basically virgin material. This result is important and coupled with the following result could save appreciable time and funds in rework of existing structure.

(14) Prior Fatigue Crack (Steel)

Line 10 of figure 192 gives results from holes that were cracked in fatigue cycling prior to coldworking. With the 0.030-inch-long fatigue cracks used, the result of coldworking these holes was performance-equivalent to virgin metal—a total blunting or mitigating of the prior crack. Coupled with the prior result, this should be useful knowledge for field service operations. It must be pointed out, however, that such results are dependent upon initial crack length. This result only shows a tolerance for the specified crack length at the specific test stress when the hole was coldworked.

(15) High Load Transfer (Steel)

For a proper reference, it should be pointed out that the lowest fatigue cycle scale in figure 194 starts at 1000 cycles rather than the 10,000 cycles normally used in most figures in this report. The impact of high load transfer upon fatigue performance of the 300M steel was severe. The test results show that coldworking does provide some definite benefit in fatigue performance over reamed-only holes; however, the overall level of performance relative to zero-load-transfer is low. The degree of fastener fit in the coldworked holes (at the 110 ksi test stress) did not seem to have any effect under these high-load-transfer conditions. Considering previous results with the titanium and aluminum, the lack of fastener-fit effect in high load transfer is surprising. The results also indicate that the antifretting micarta shim is of no benefit either in enhancing fatigue performance. The slight loss in performance for the flush head fastener is probably a result of the countersink-to-hole ratio in the 0.125-inch-thick side plate.

For this stress level, these results are apparently valid. However, the results are all tightly grouped in a manner indicative of high-stress levels wherein the effect of process variations are diminished as S-N curves tend to converge. The impact of the high-load transfer apparently has put these tests into that position. Thus, lower test stresses probably would define some definite differences for the conditions tested herein.

The fact that the theoretical interference-fit bolt did not have any effect upon performance might be explained by the photograph of such a bolt (after installation) in figure 193. This protograph makes it obvious that such installations are basically impractical.

(16) Failure Origins (Steel)

Figure 195 shows typical failure origin locations for specified test conditions with the 300M steel. Similar charts for the aluminum and titanium are shown in figures 168 and 182, respectively. Other than using these charts to pinpoint specific processing effects, it is interesting to generally compare all three with regard to general characteristics. That is, the 2024 aluminum is not generally regarded as a notch-sensitive material (as evidenced by test results) and its failure origin characteristics are: nonlocalized failure origins without prestressing and very definite, localized failure origins when protection is provided via adequate prestressing. The titanium also displayed the nonlocalized failure origins which would generally indicate that it was not particularly notch sensitive either. In no case, however, were we able to adequately prestress the titanium to localize failure origins. The 300M steel, on the other hand, displayed finite, localized failure origins in all cases, whether prestressed or not. Thus, the steel could be considered to be more notch sensitive to start on this basis alone.

(17) Stress Corrosion (Steel)

The only stress corrosion tests conducted in this program were in the 300M steel. The reasons for this are: previous tests at Boeing have not shown titanium to be susceptible to room temperature stress corrosion and stress corrosion tests of the most stress corrosion susceptible aluminum alloys with coldworked holes and adversely exposed transverse end grains did not result in stress corrosion problems.

In this test, the figure 11 plate, with 1.6D and 2.0D hole edge margins, was coldworked and postreamed and then mounted in a ferris-wheel type of setup that alternately immersed it in a 3-1/2% salt-water solution for 10 minutes and air exposed it for 50 minutes every hour at ambient conditions. After 888 hours of cycling, the test plate was thoroughly examined by dye penetrate inspection with no evidence whatsoever of any cracks. Photographs of the plate before exposure and after exposure are shown in figure 196. The before exposure photograph was taken at an angle to accentuate and disclose the surface upsetting. Some edge bulging is also evident for the 1.6D edge margin holes.

4. ALL ALLOYS--GENERAL

a. Strain Gage Tests (All Alloys)

In this series of tests, specimens of each major alloy, basically similar to figure 12, were strain gaged at the edge of the specimen adjacent to the holes and between the holes. These specimens are shown in figure 197. Edge strain was measured prior to coldworking as the specimen was tensile loaded to specific loads. The specimens were then unloaded and coldworked while still mounted in the tensile test equipment (to avoid setup variations).

The edge strain from coldworking alone was recorded and then the composite edge strain as the specimens were again tensile loaded to the same loads. This was repeated after postreaming. The calculated edge stresses for actual and theoretical values are plotted for areas adjacent to the holes for each alloy in figures 198, 200, and 201. The same is plotted for the edge area between the holes of the 2024-T851 specimen in figure 199.

As can be seen, relatively significant tensile stresses are generated at the specimen edge of a 2D edge margin specimen by the high-interference coldworking process. These stresses are charted along with relative material yield strengths and coldworking interference levels for comparison in figure 202. With regard to the aforementioned probability that the titanium was not adequately prestressed, this chart shows that the tensile prestress at the specimen edge is 30% of yield strength for the aluminum, 23% for the titanium, and 35% for the steel. The charts also show that no decrease in cyclic straining would occur in this tensile prestressed area when the specimen is cyclic, tensile loaded. This is apparently true when the tensile prestress is "propped" by the material itself. It would not necessarily be true for a hole that is externally propped by a fastener such as the Taperlok. Thus, tensile edge stress is important with regard to final results once the failure origin has been driven away from the hole and may help to explain the benefits of postcountersinking for the aluminum and steel.

b. Photostress Coupons (All Alloys)

Aluminum, titanium, and steel coupons were produced with holes that had different spacing and edge margins. These specimens were then coated with photostress plastic and the plastic bored out to prevent direct contact with coldwork sleeves. One hole was precountersunk and most were then coldworked. Two were left uncoldworked, and one coldworked hole was postcountersunk. Photographs of the entrance and exit sides, with overlaid polarizing material to display fringe patterns, of the aluminum and titanium specimens are shown in figures 203 through 206.

Visually, the coupons readily depict the degree of prestressing and the magnitude of the compressive zone. It also shows that a low-level, small compressive zone is created at the specimen edges between the holes. The entire center of each specimen is also at a low level of compression. The impact of precountersinking and of successive postreaming operations can also be dramatically seen. The compressive zone surrounding the hole does not seem to reach the specimen edge until the edge margin is decreased to 1-1/2D. This reinforces the supposition that the compressive zone is 1D in width from the hole edge. The compressive zones also join when the hole spacing reaches 3D. The precountersunk holes do display some surface evidence of a compressive zone: however, there is a discontinuity in this zone at the split location. Therefore, even though the split in the sleeve does not normally present any effect upon fatigue performance of noncountersunk holes or postcountersunk holes, it does appear to be the primary culprit with regard to loss of performance in precountersunk holes. This suggests that a nonsplit sleeve may have some advantages for precountersunk holes and repair work. This theorem certainly must be verified by testing prior to applying it.

c.   Comparative Performance and Cost Analysis (All Alloys)

This subsection contains the results of task 5 in phase II—cost and performance analyses. The performance analysis considers the comparative performance of the coldworking system to the tapered fastener system and relative to its application. The cost evaluation was extended to also include straight shank, interference-fit fastener systems.

Figures 207, 208, and 209 are mean value S-N curves for the aluminum, titanium, and steel that include certain extrapolated curves based on single-stress test results. They include zero-load-transfer and high-load-transfer results, coldworking and tapered fasteners, and different process variations. They graphically and rapidly depict differences. They also show that the range between least performance and best performance is least for the aluminum and most for the steel. Whereas high load transfer had little impact upon the aluminum (when properly handled), it had a serious impact upon the titanium and steel.

Figure 210 is a tabulation of trends in comparative performance and failure origins for the aluminum, titanium, and steel when subjected to various hole processing and fastener treatments. Figure 211 tabulates the comparative performance of the coldworking process to reamed-only holes and tapered fastener installations for aluminum and titanium at zero-load-transfer and high-load-transfer conditions. These tabulations plus previous details analysis show that the sleeve coldworking system is equivalent to the protruding head tapered fastener system in zero- to high-load-transfer applications in aluminum; is superior for all flush head installations in both alloys; is superior to the protruding head tapered fastener system in zero-load-transfer situations in titanium (cycles and scatter); and is not quite as good as the tapered fastener system in high-load-transfer situations in titanium (for the coldworking interference used).

Figure 212 is a tabulation of allowable average stresses within 2D of a fastener to enable each material to produce 100,000 cycles in constant amplitude fatigue loading. The stress is defined in this manner since it is based on net area stresses. As can be seen, it indicates that one can tolerate applied stresses near the hole in aluminum (when the hole is properly prestressed) that are higher than those that the base metal can tolerate. Obviously, gross area loads must be kept within the capabilities of the base metal; nevertheless, the author believes this system is meaningful—it just requires some analysis or test work to define stresses in local areas. The gross area stress system is not precise either, but it does have a conservative element built into it. Analysis of this chart on the basis of relative fatigue performance to metal density for various systems and applications allows one to make weight-effective material selections for fatigue-critical applications.

Figure 213 is a tabulation of a thorough cost analysis of total installed costs for various fatigue-rated fastener systems. The cost elements, detail operation times and the overall analysis are contained in the appendix. The time elements represent a composite of many different production observations. The fastener cost elements also represent a composite of costs as influenced by various conditions such as the user influence and buy size. Admittedly, the costs of these fasteners can vary significantly, but these averaged costs are considered appropriately relative to one another. The analysis was based solely on a

3/8-inch diameter by 5/8-inch grip installation as a typical requirement. Different diameters and grips will affect specific costs, but should not significantly affect the relative cost positions.

The analysis shows that the most cost effective titanium fastener installation in aluminum and titanium structure is a straight shank interference-fit bolt (of appropriate design). If steel fasteners can be tolerated, then the sleeve coldwork system becomes most cost effective. With steel or titanium fasteners, the sleeve coldwork system is significantly lower in cost for all structures than the tapered fastener system. In addition, the straight shank, interference-fit bolt is practically limited to diameters no larger than 3/8 inch. Therefore, above this diameter the sleeve coldwork system becomes the most cost effective overall system.

REFERENCES

1. C. F. Tiffany, R. P. Stewart, and T. K. Moore (Captain, USAF), "Fatigue and Stress Corrosion Test of Selected Fastener/Hole Processes," ASD-TR-72-111, January 1973.

2. Industrial Designers, 6406 South 143rd Street, Tukwila, Washington 98168, (206) 243-2949.

Phase I—Process Parameters

Task 1   Optimum Mandrel Taper Angle

Task 2   Optimum Mandrel/Hole Interference

Task 3   Pull Mandrel for High Strength Steel

Task 4   Physical Effects and Remaining Mandrel/Sleeve Parameters

Task 5   Multimaterial Stack Parameters

Task 6   Postsizing Parameters

Task 7   Portable Equipment Definition

Task 8   Inspection Methods Definition

Phase II—Application and Performance Parameters

Task 1   Base Metal Fatigue Values

Task 2   Basic Open Hole Fatigue Values

Task 3   Basic Filled Hole Fatigue Values

Task 4   Application and Process Parameter Effects

Task 5   Cost and Performance Evaluation

Figure 1.—Task Outline

All dimensions in inches
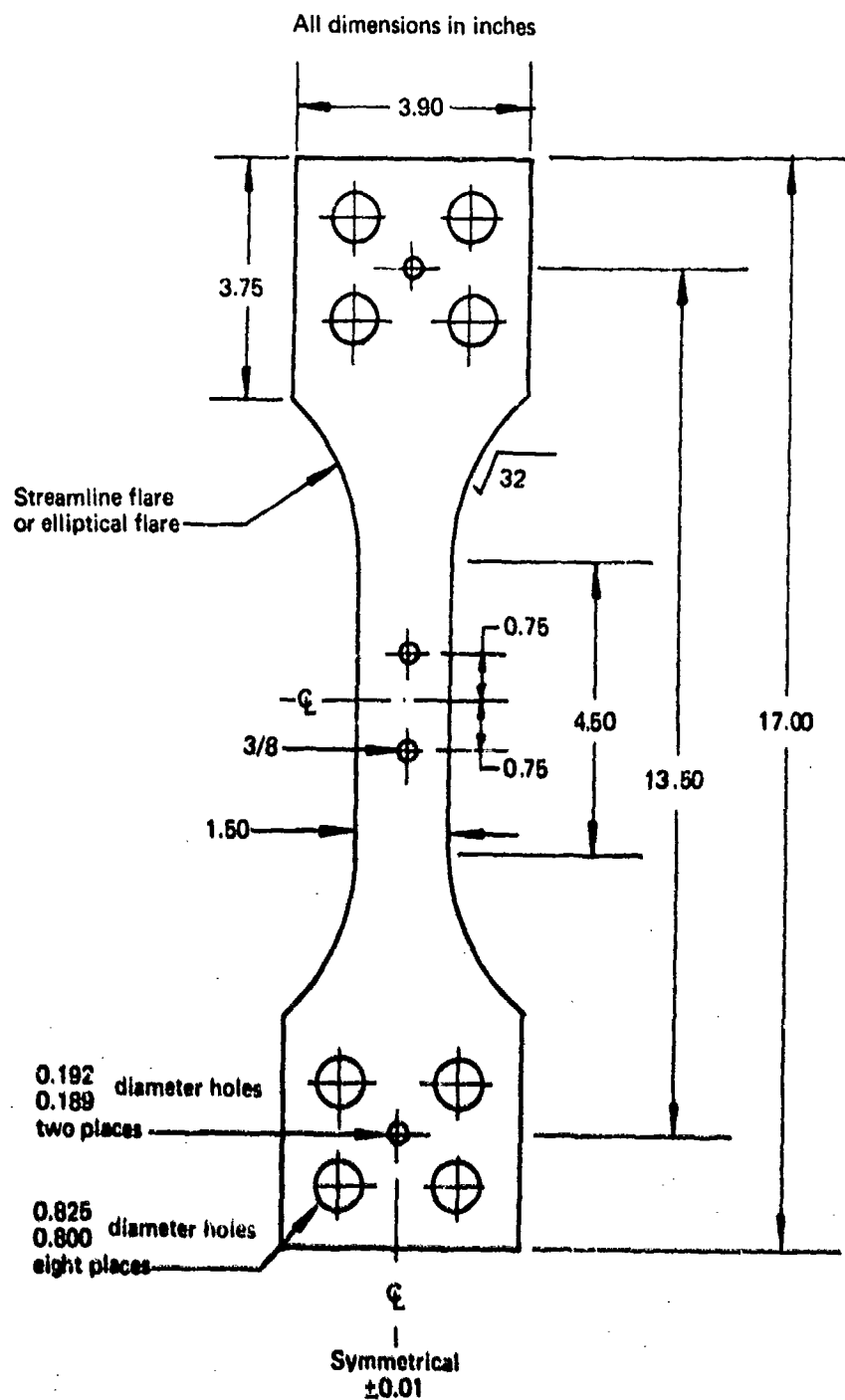
Figure 2. – Zero Load Transfer Baseline Fatigue Coupon – 3/8-In.-Diameter Holes

All dimensions in inches
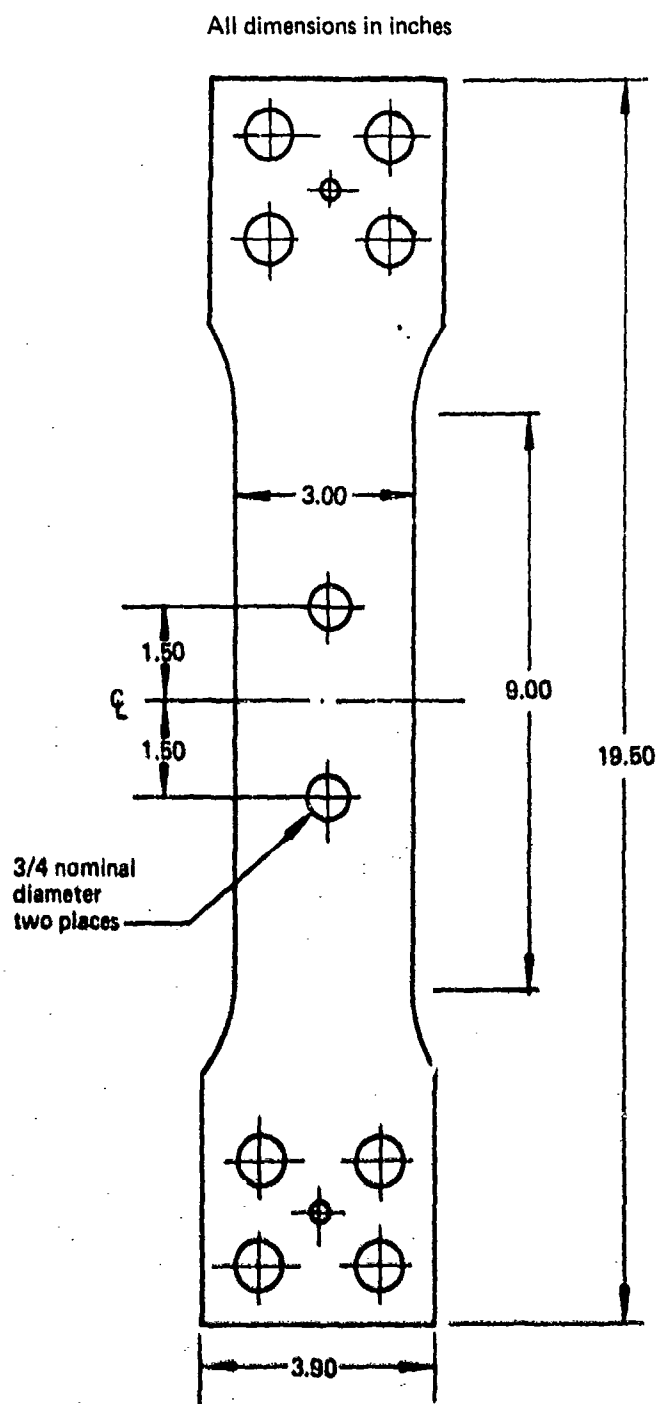
Figure 3.—Zero Load Transfer Baseline Fatigue Coupon—3/4-In.-Diameter Holes
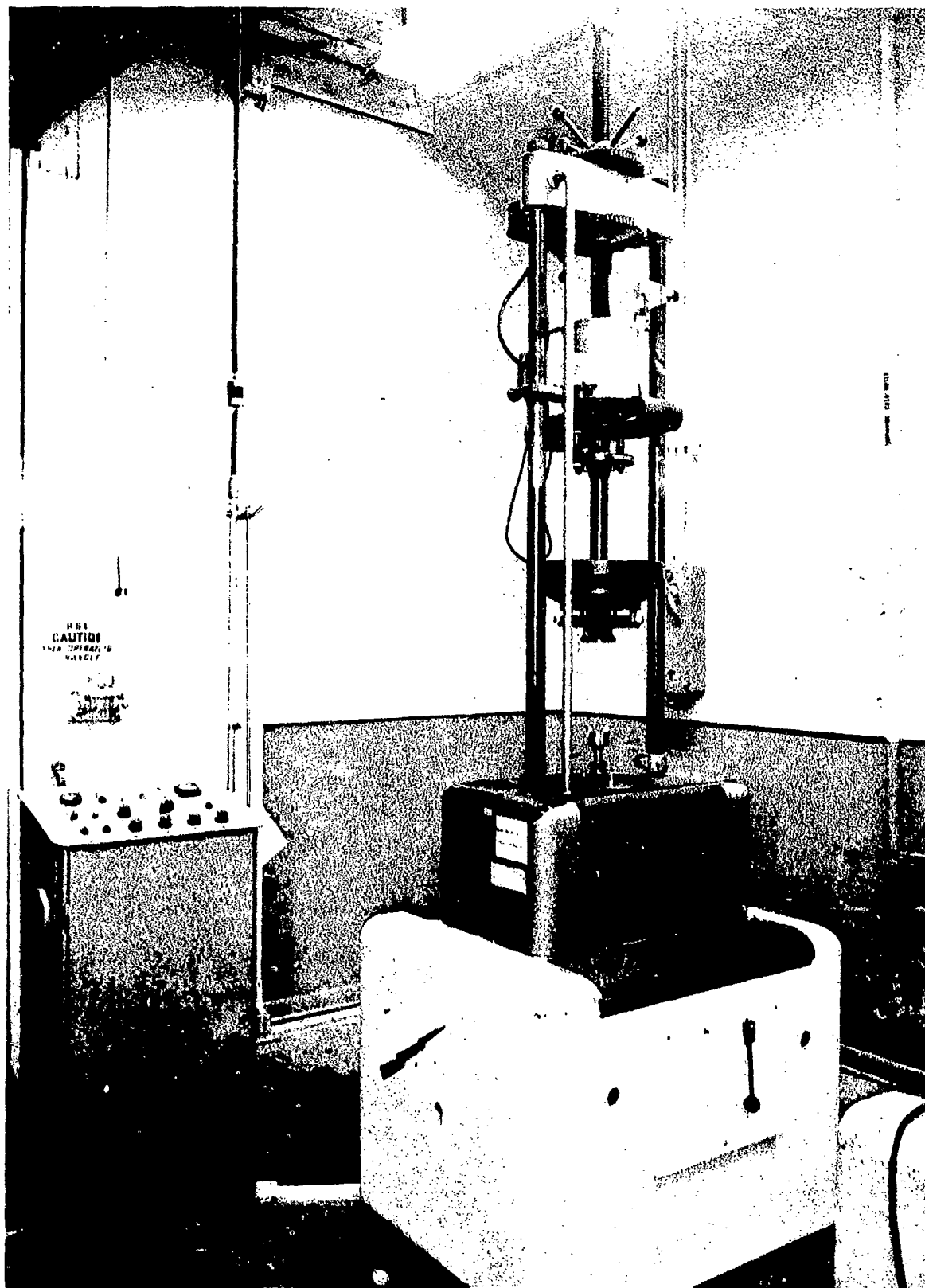
Figure 4. — 36-KIP Amster Fatigue Test Machine
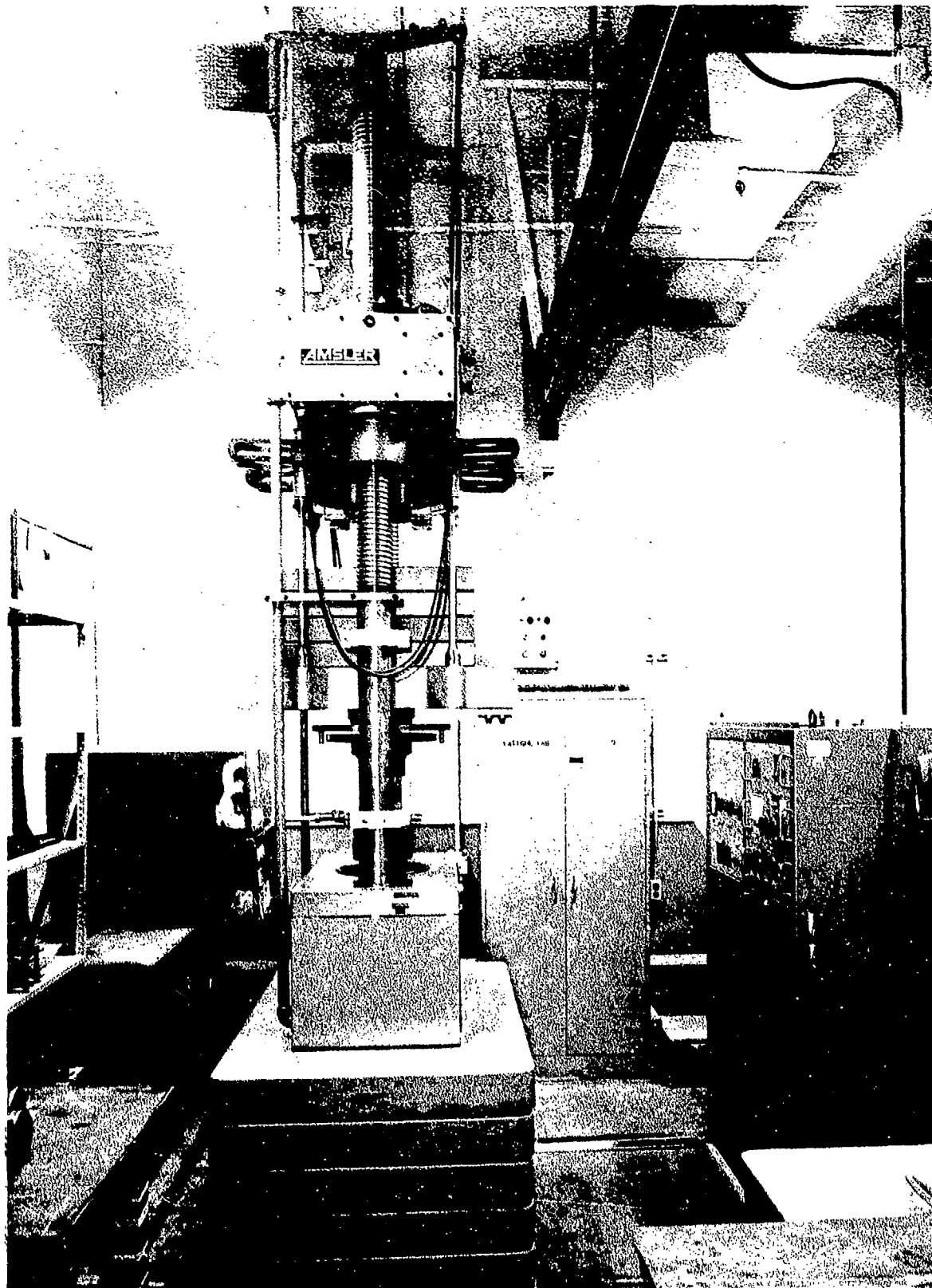
Figure 5. — 100-KIP Amsler Fatigue Test Machine
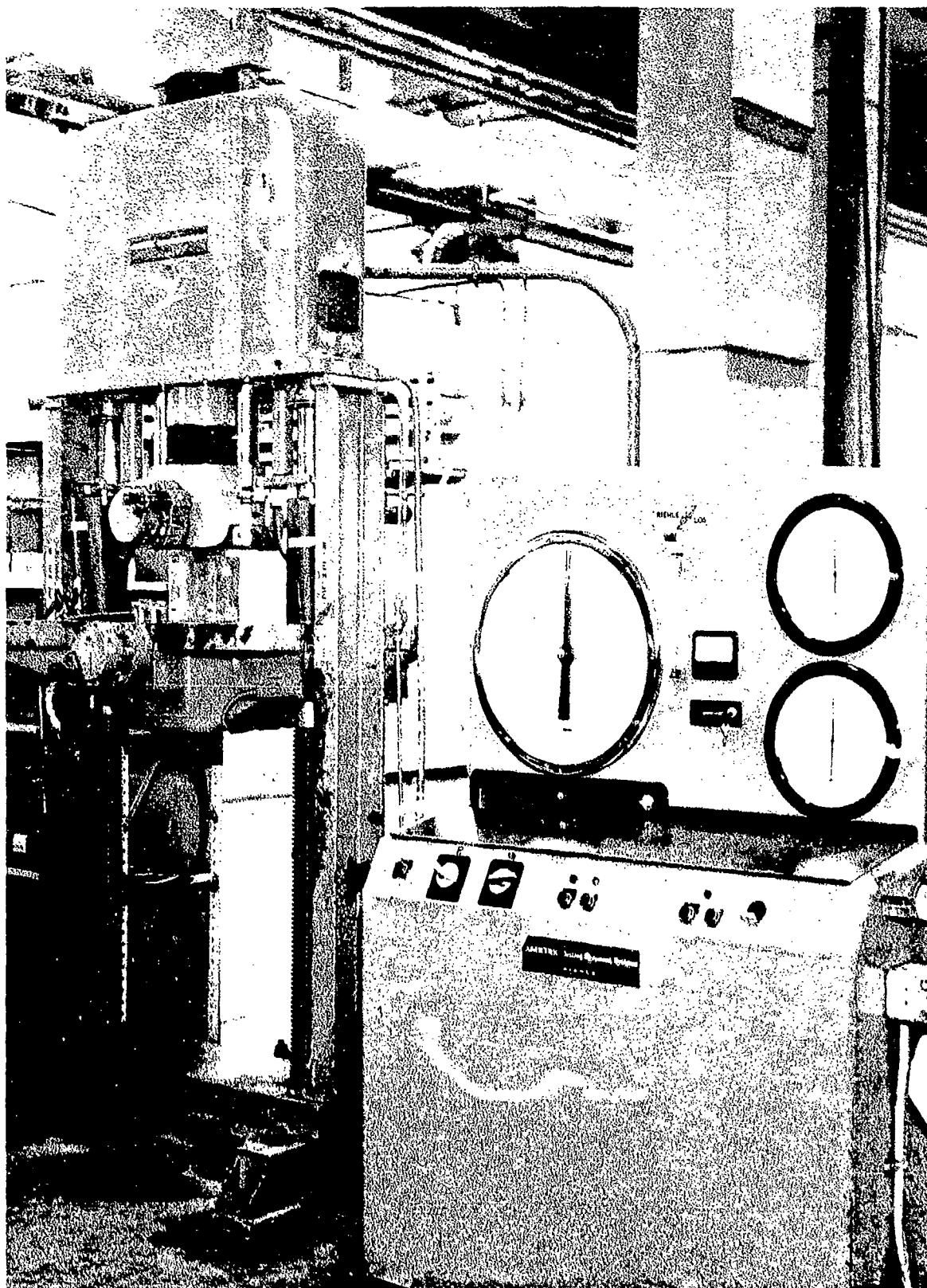
Figure 6. — 60- to 80-KIP Riehle-Los Fatigue Test Machine

All dimensions in inches
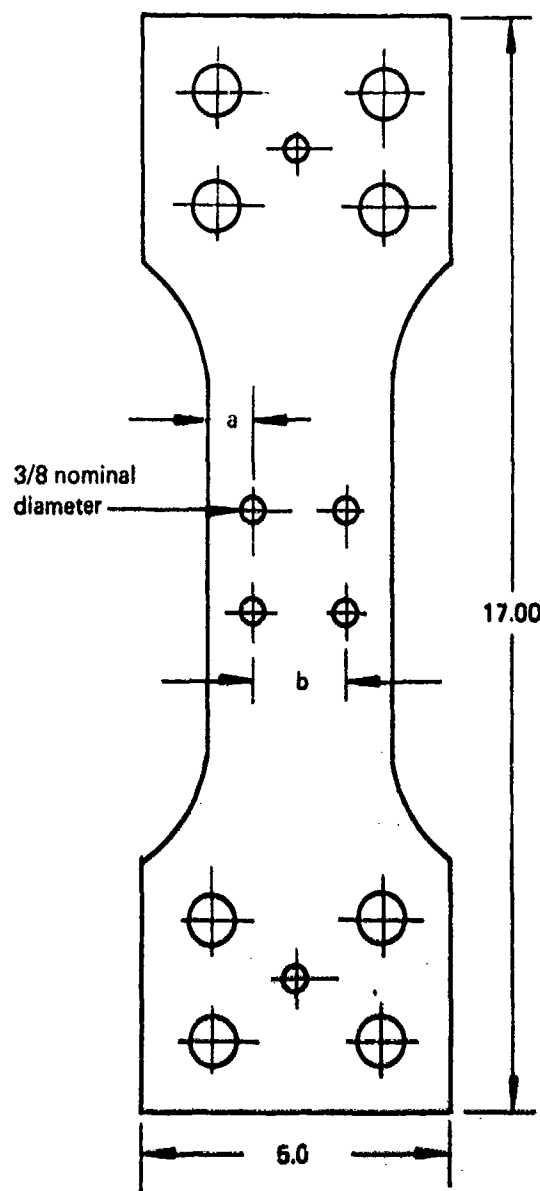
Configuration	Edge margin a (in.)	Hole spacing b (in.)
A	9/16	2
B	3/4	2
C	15/16	2
D	15/16	1-1/8
E	15/16	1-1/2

3/8 nominal diameter

17.00

6.0

Figure 7.—Zero Load Transfer Edge Margin Fatigue Coupon

All dimensions in inches

1/4 nominal diameter
15 places

30.00

1.00

2.50

6.00

10.50

12 R

15 R

1.00 (typical)

3.90

Figure 8. — Low Load Transfer Fatigue Coupon

All dimensions in inches

15 R

1.00

10.50

30.00

1/4 nominal diameter
15 places

1.00 (typical)

3.90
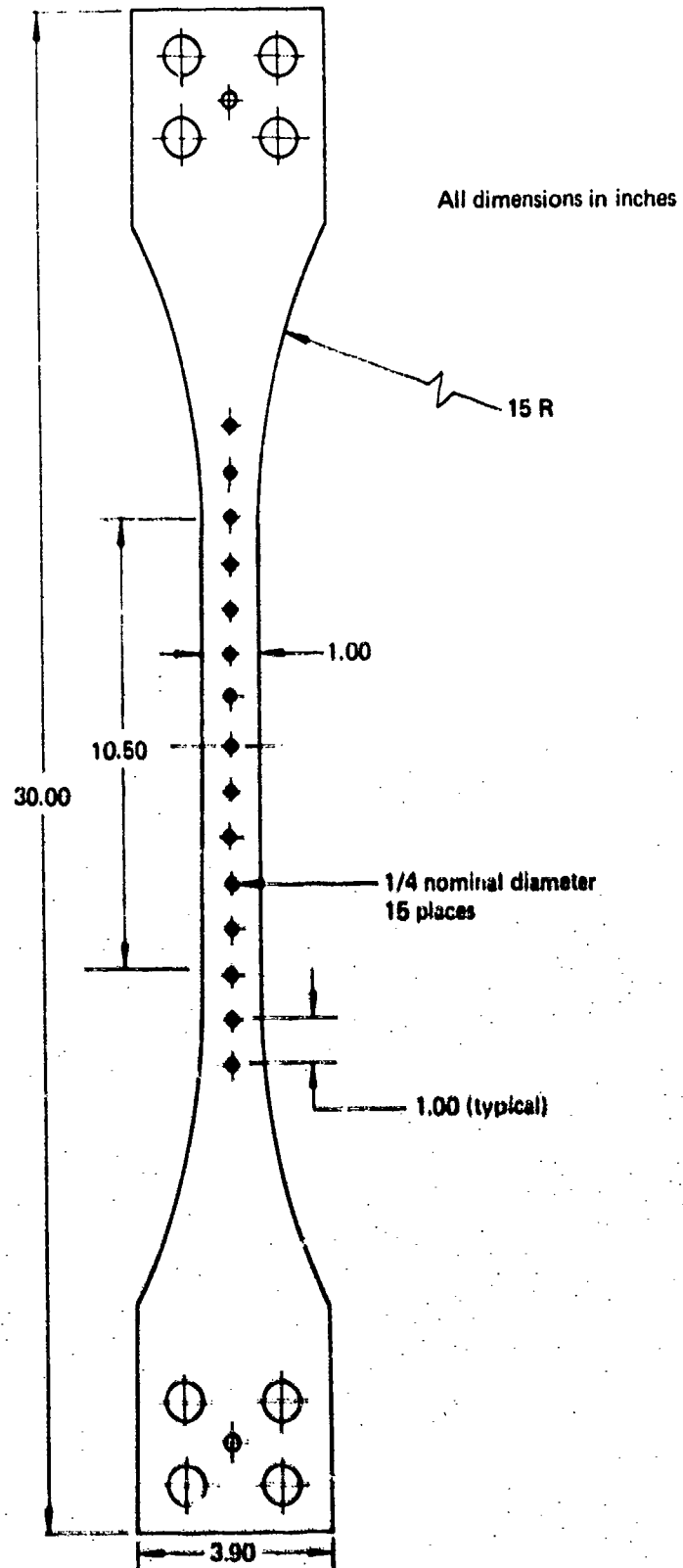
Figure 9.—Zero Load Transfer—15-Hole Fatigue Coupon

All dimensions in inches

16.50

3.00

1.50

3/8 nominal diameter

6.00

1.50

2 splice plates

3.90

Figure 10. – High Load Transfer Fatigue Coupon

Figure 11. — Stress Corrosion Specimen

All dimensions in inches

1 1/2

3/8

3/8 diameter hole

Strain gage

Strain gage

3/8 diameter hole

1 1/2

24"
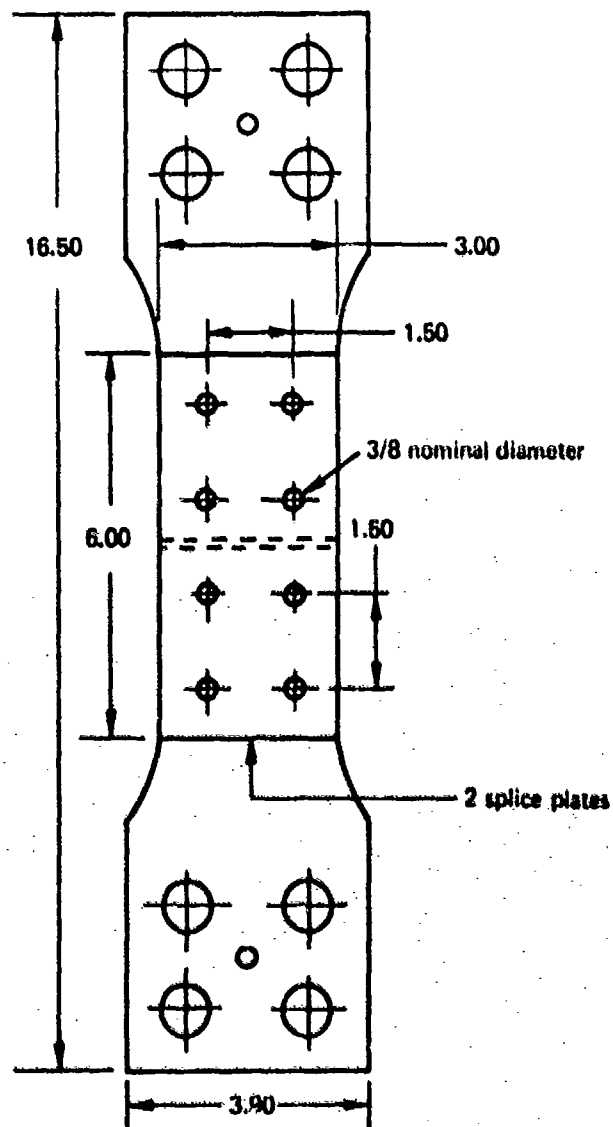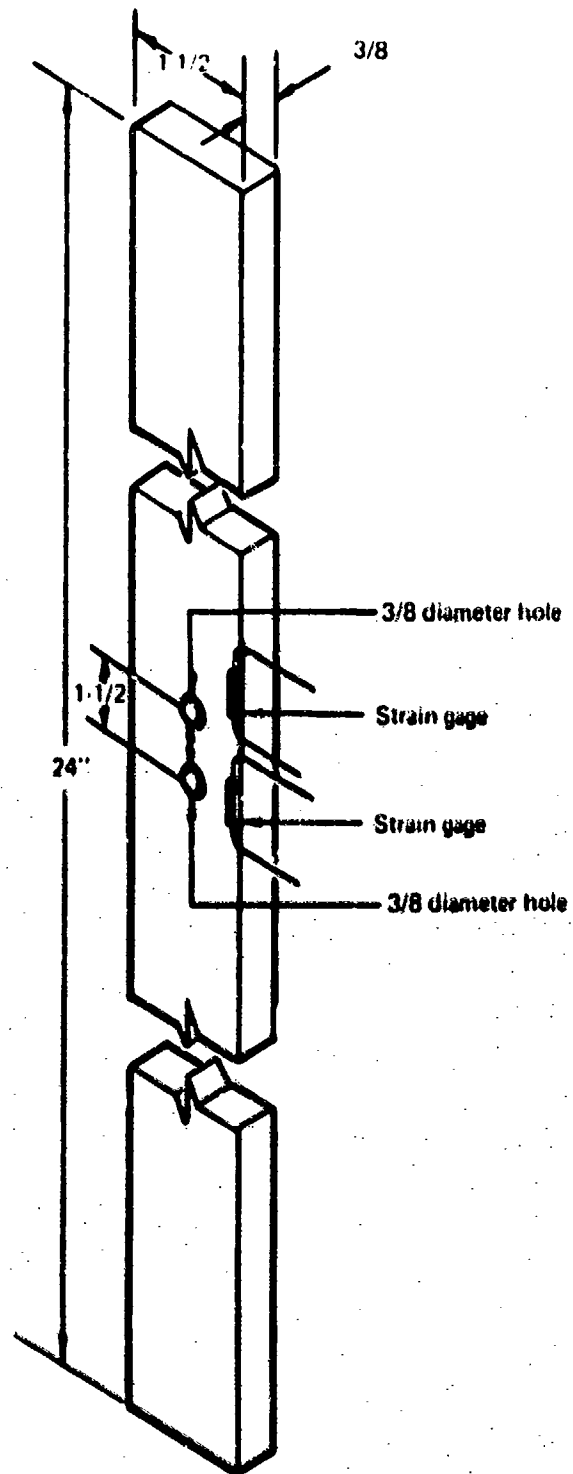
Figure 12. - Edge Strain Coupon

96
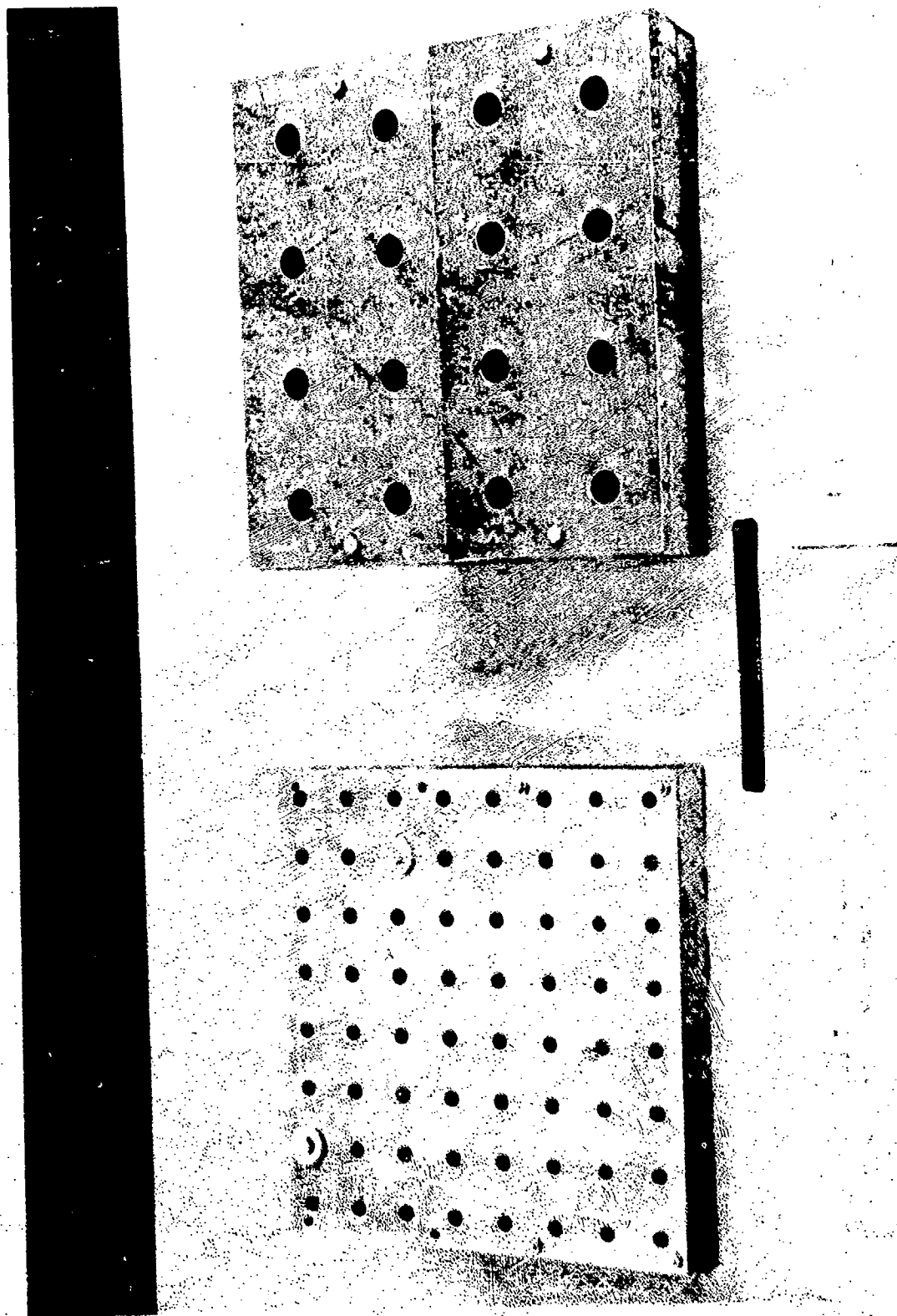
Figure 13. Optimum Taper Test Plates
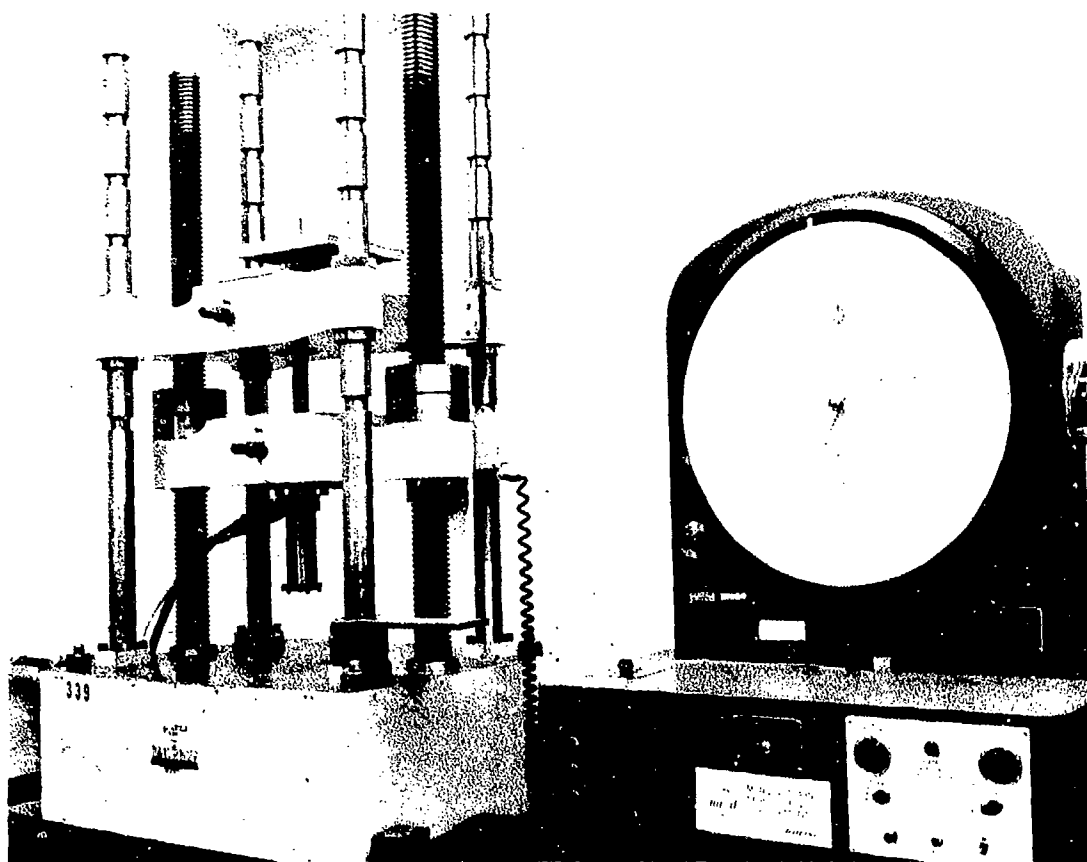
Figure 14.--Tinius Olsen Force and Lubricant Test Setup
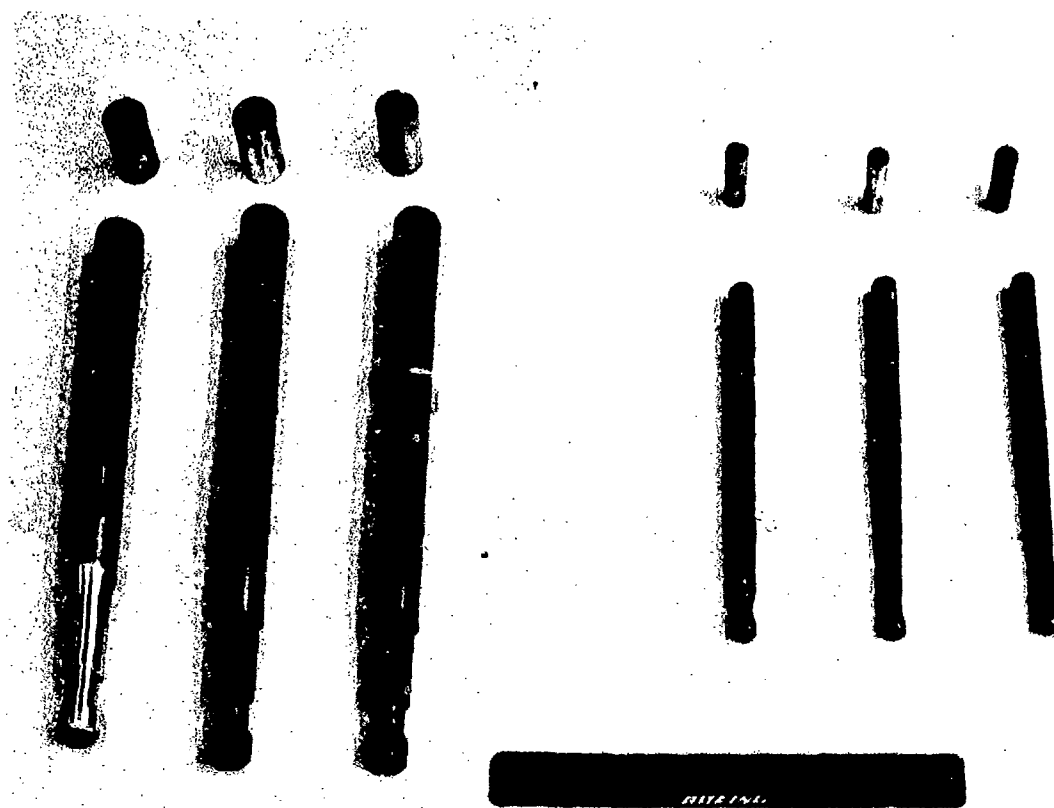
Figure 15. Typical Coldwork Mandrels and Axial Split Sleeves
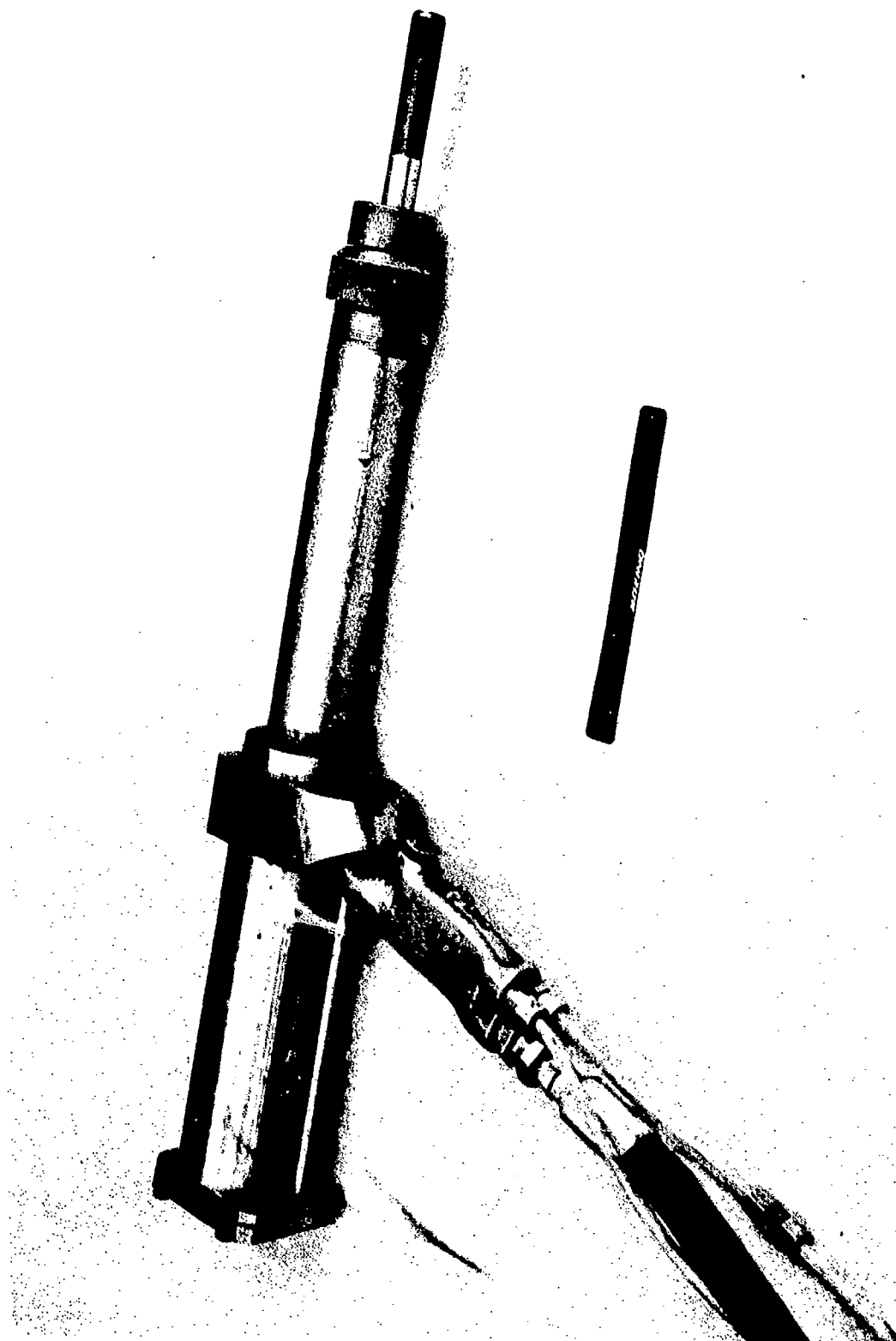
Figure 16. Coldworking Pull Gun
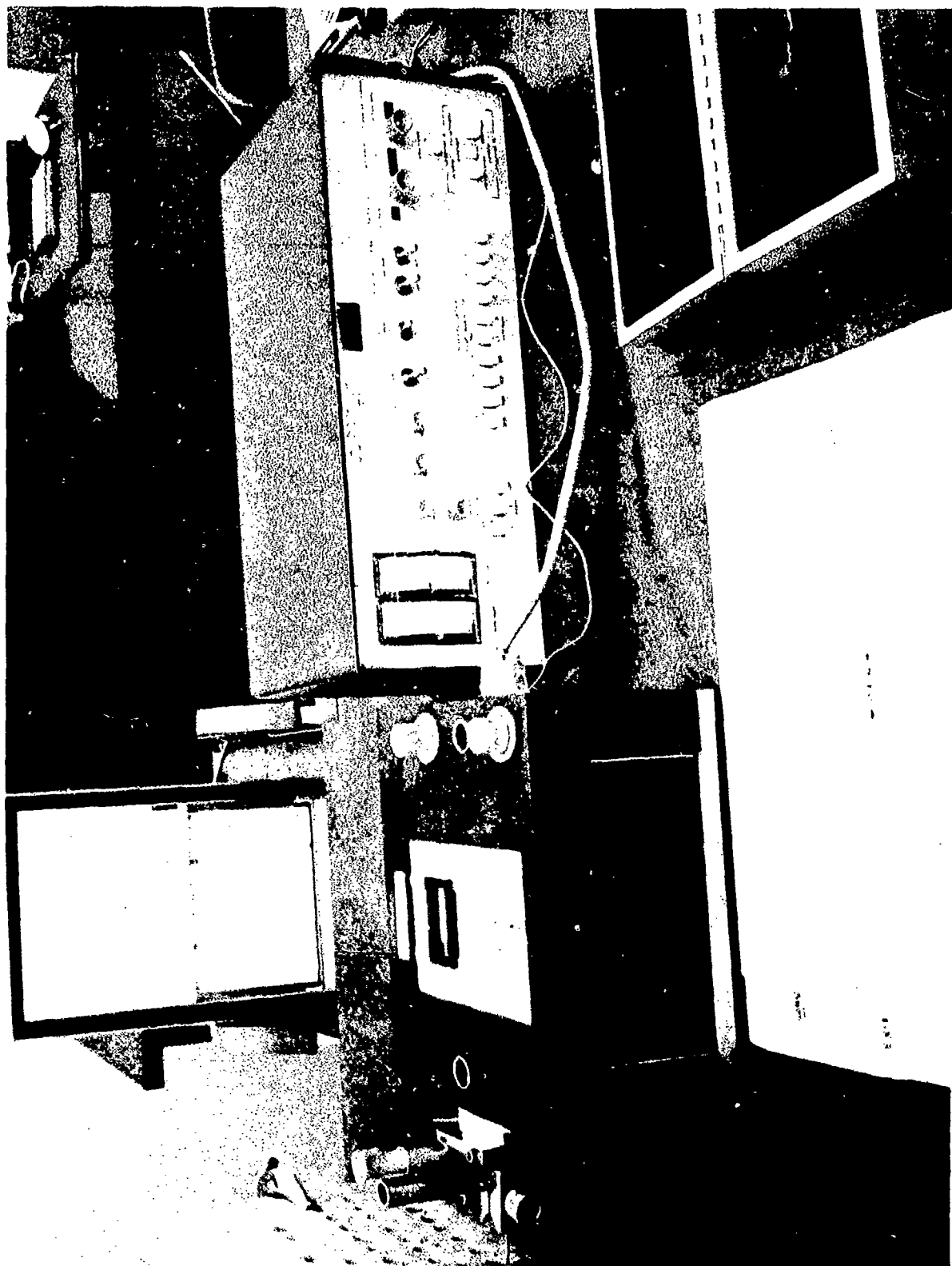
Figure 17. - Traversing 'Recording Surfanalyzer
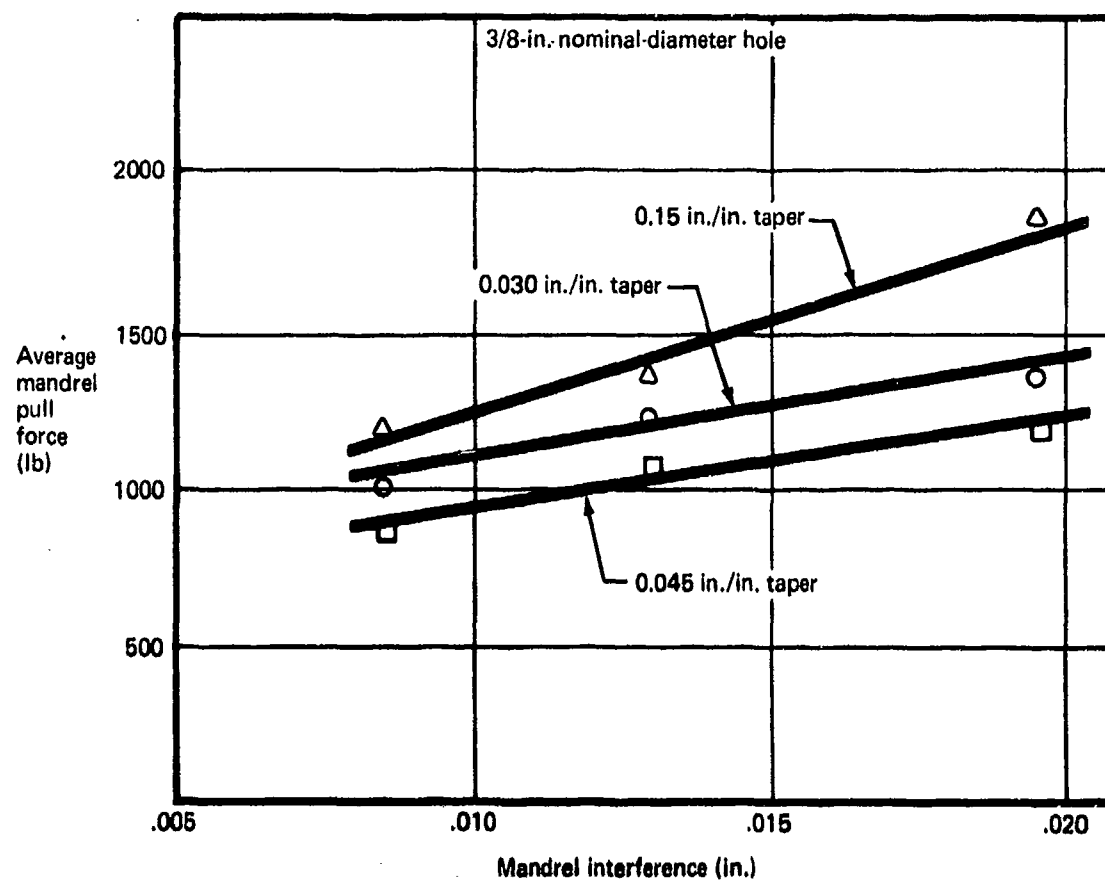
Figure 18.—Effect of Mandrel Interference and Taper on Pull Force—2024-T851, 3/8 In. Thick
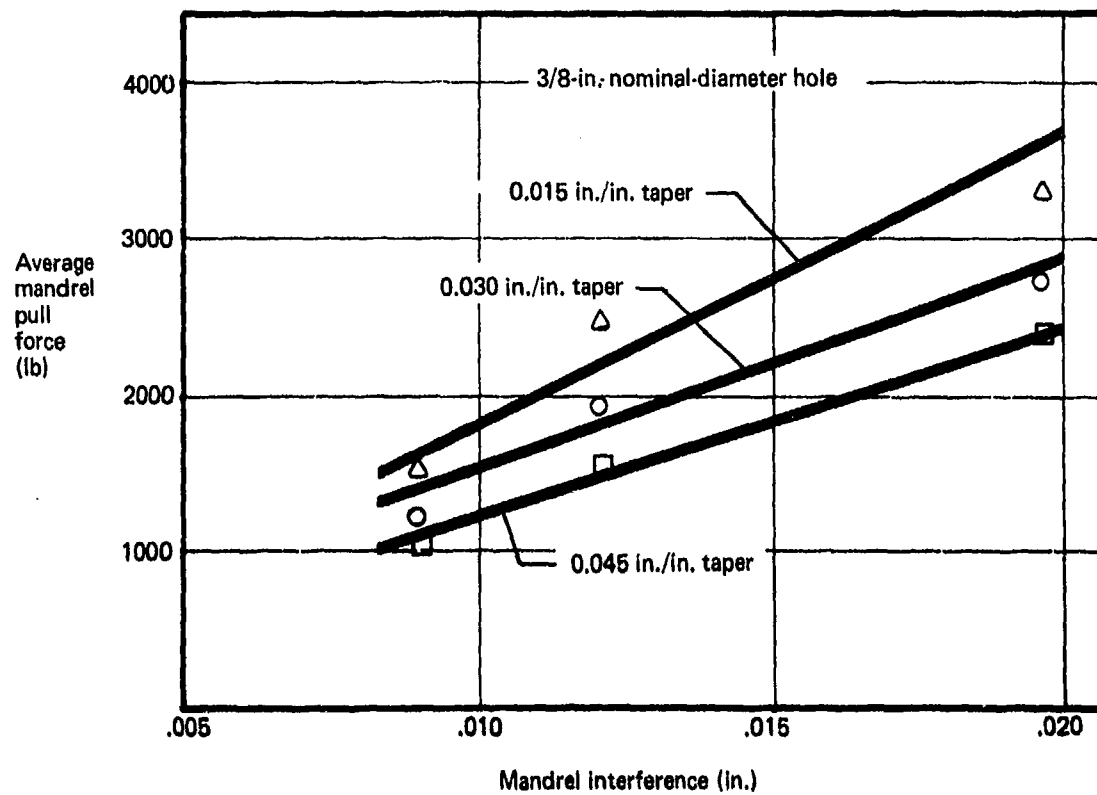
Figure 19.—Effect of Mandrel Interference and Taper on
Pull Force—2024-T851, 1-1/2 In. Thick
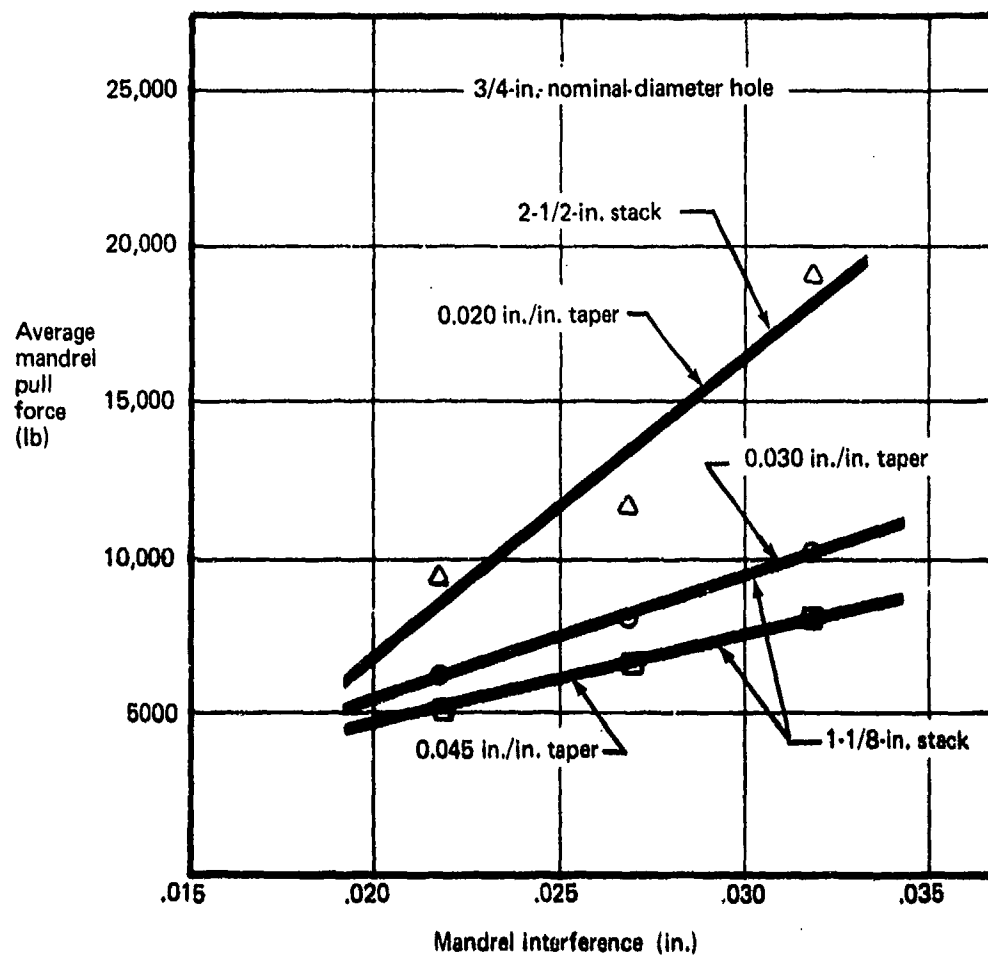
Figure 20.—Effect of Mandrel Interference and Taper on
Pull Force—2024-T851, 2-1/2- and 1-1/8-In. Stack
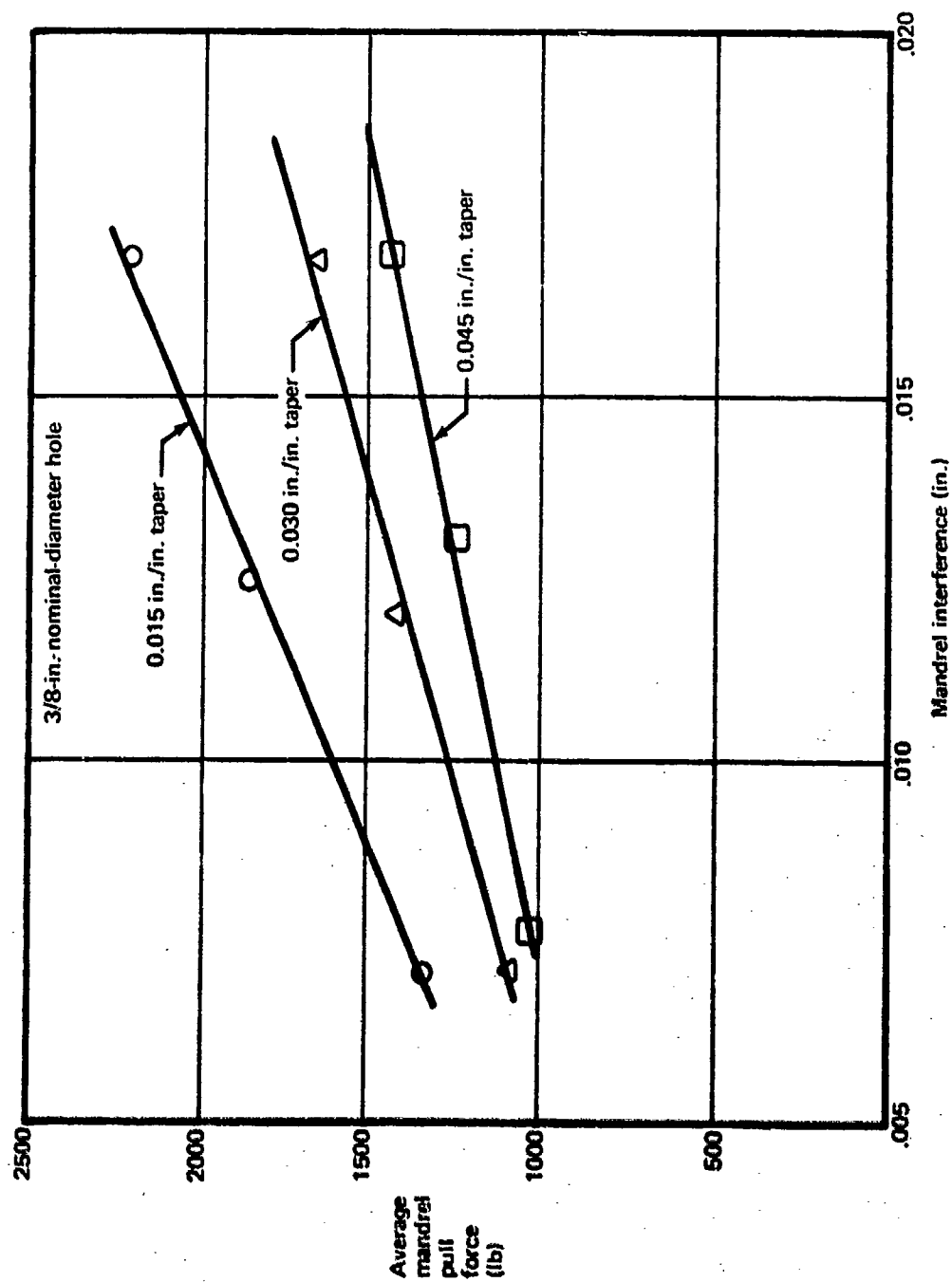
Figure 21.—Effect of Mandrel Interference and Taper on Pull Force—6Al-4V Annealed Titanium, 3/8-In. Thick
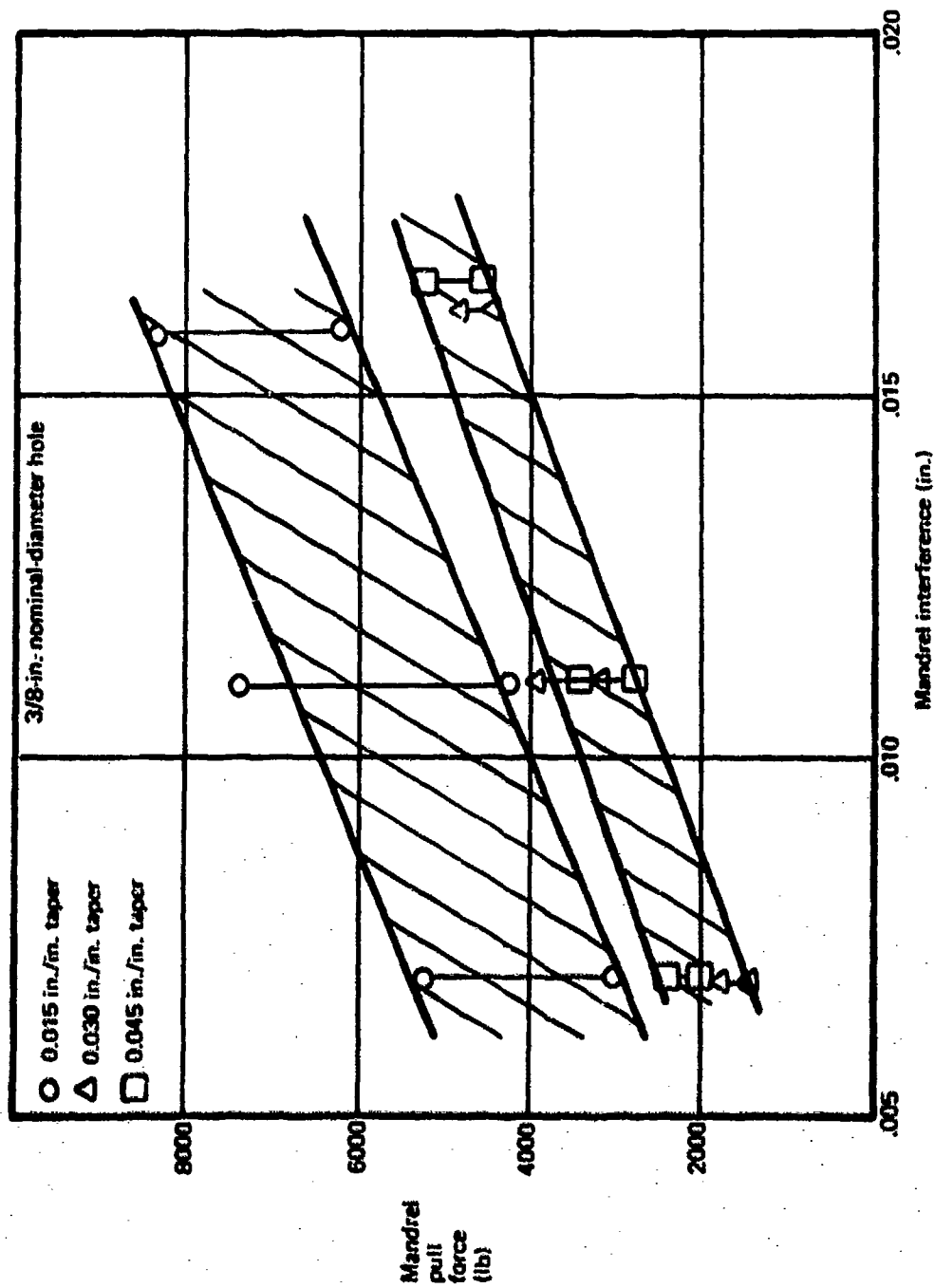
Figure 22. — *Effect of Mandrel Interference and Taper on Pull Force— 6Al-4V Titanium, Annealed, 1-1/2-In. Thick*

Legend (on chart):

3/8-in.-nominal-diameter hole

- O 0.015 in./in. taper
- △ 0.030 in./in. taper
- ▢ 0.045 in./in. taper

Mandrel pull force (lb)

8000
6000
4000
2000

Mandrel interference (in.)

.005   .010   .015   .020
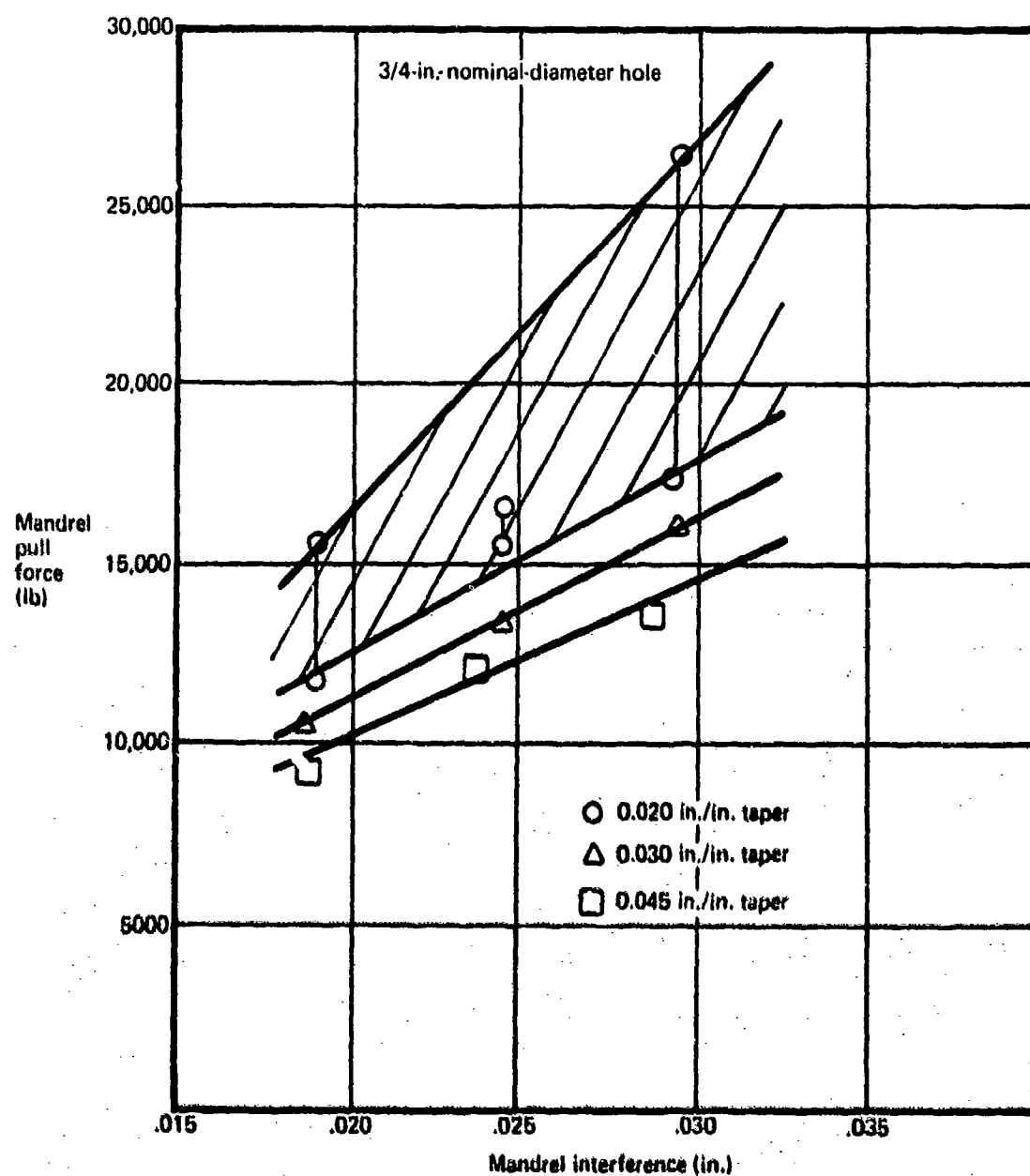
Figure 23. - Effect of Mandrel Interference and Taper on Pull Force--
6Al-4V Titanium, Annealed, 2-In.-Thick Stack
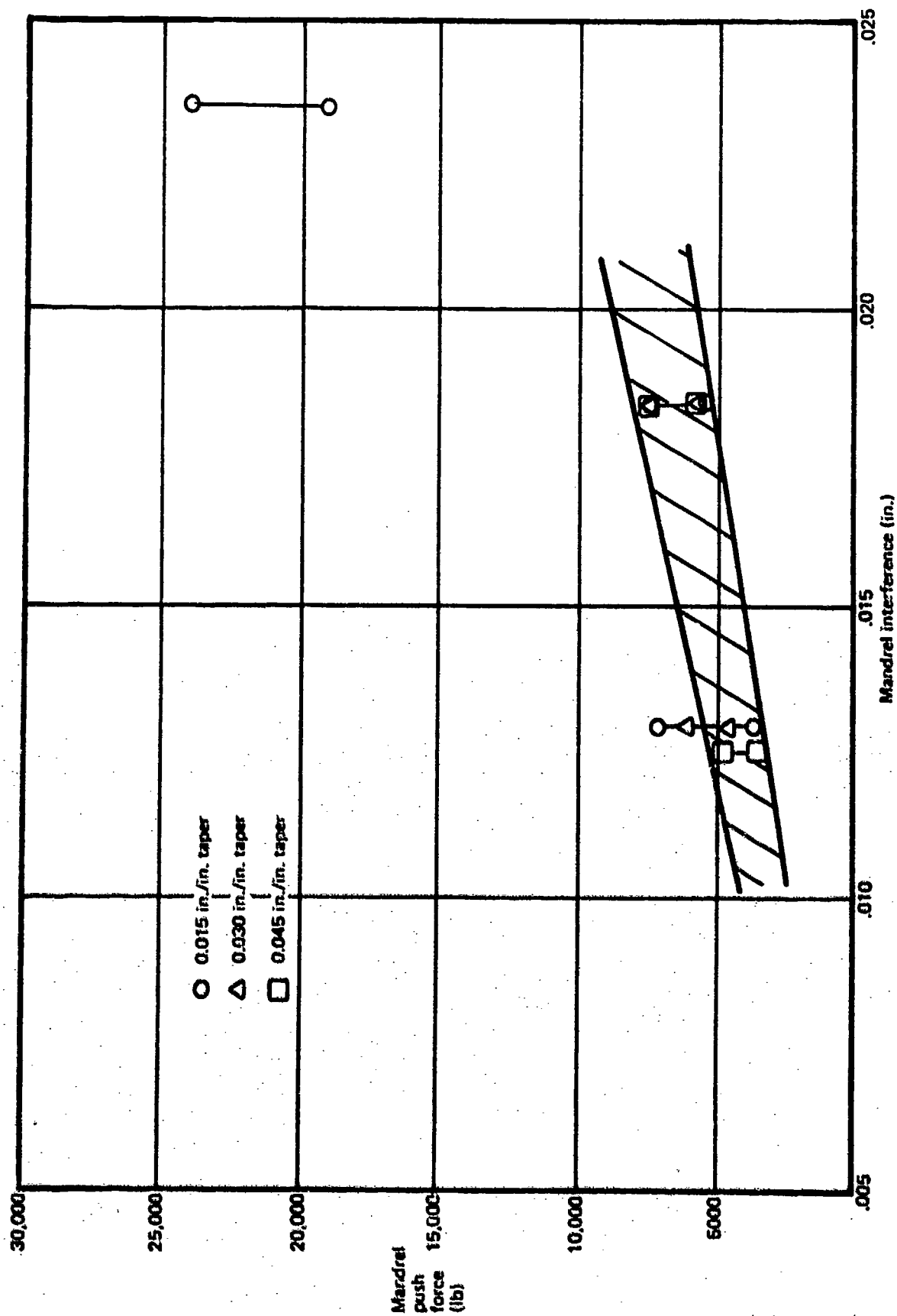
Figure 24. — Effect of Mandrel Interference and Taper on Push Force—270-300 KSI 300M Steel, 3/8-In. Stack
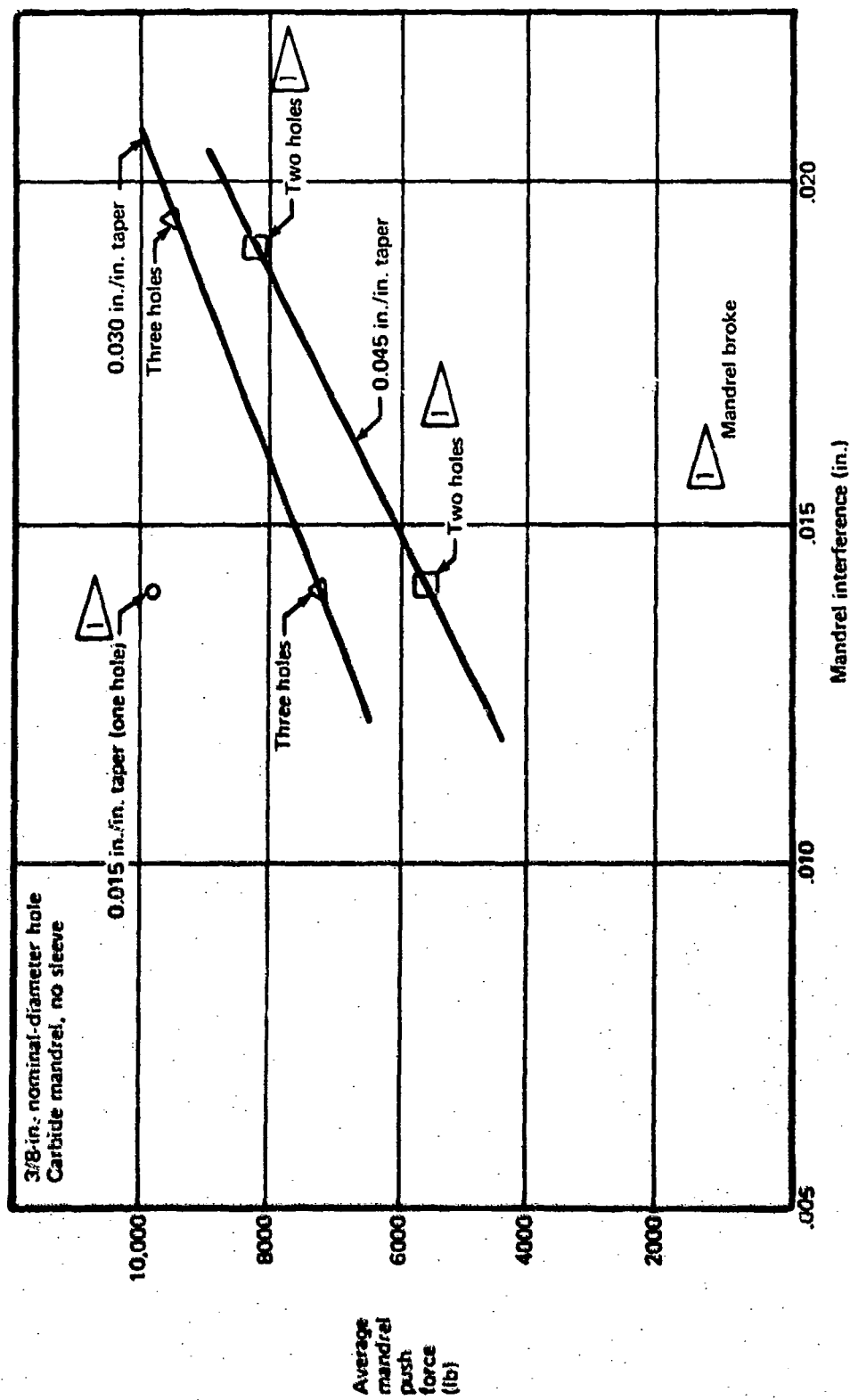
Figure 25. – Effect of Mandrel Interference and Taper on Push Force – 270-300 KSI 300M Steel, 1-3/8-In. Stack

The chart has axes:

Y-axis (left): Mandrel push force (lb) — 50,000 / 40,000 / 30,000 / 20,000 / 10,000

X-axis (bottom): Mandrel interference (in.) — .015 / .020 / .025 / .030 / .035

3/4-in. nominal-diameter hole
Carbide mandrel, no sleeve

Five holes

Five holes

Five holes[a]

Two holes[a]

Four holes

Four holes

Three holes

One hole

Two holes

Legend:
O 0.015 in./in. taper
△ 0.030 in./in. taper
☐ 0.045 in./in. taper
[a] Mandrel broke
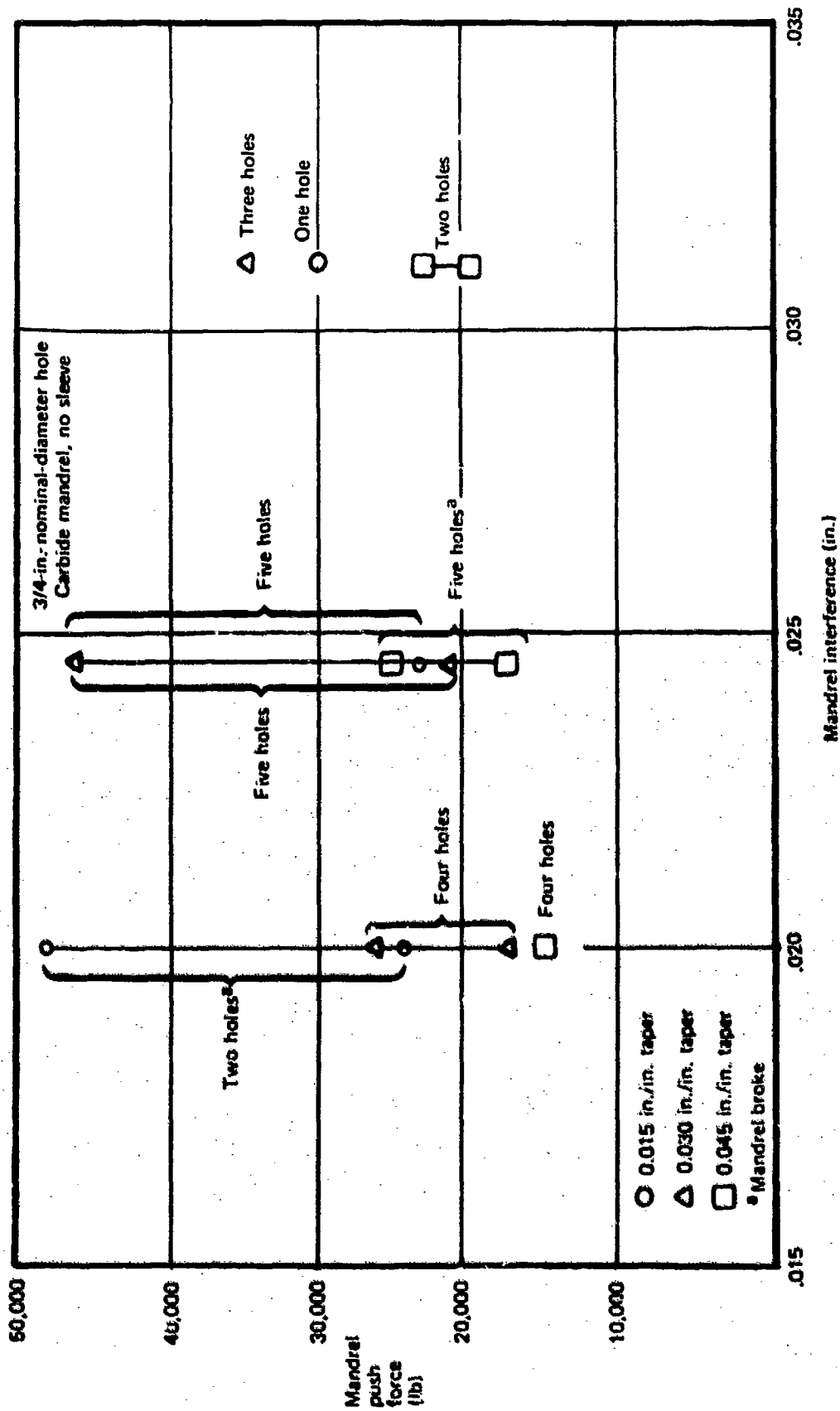
Figure 26. —Effect of Mandrel Interference and Taper on Push Force—270-300 KSI 300M Steel. 2-In. Stack
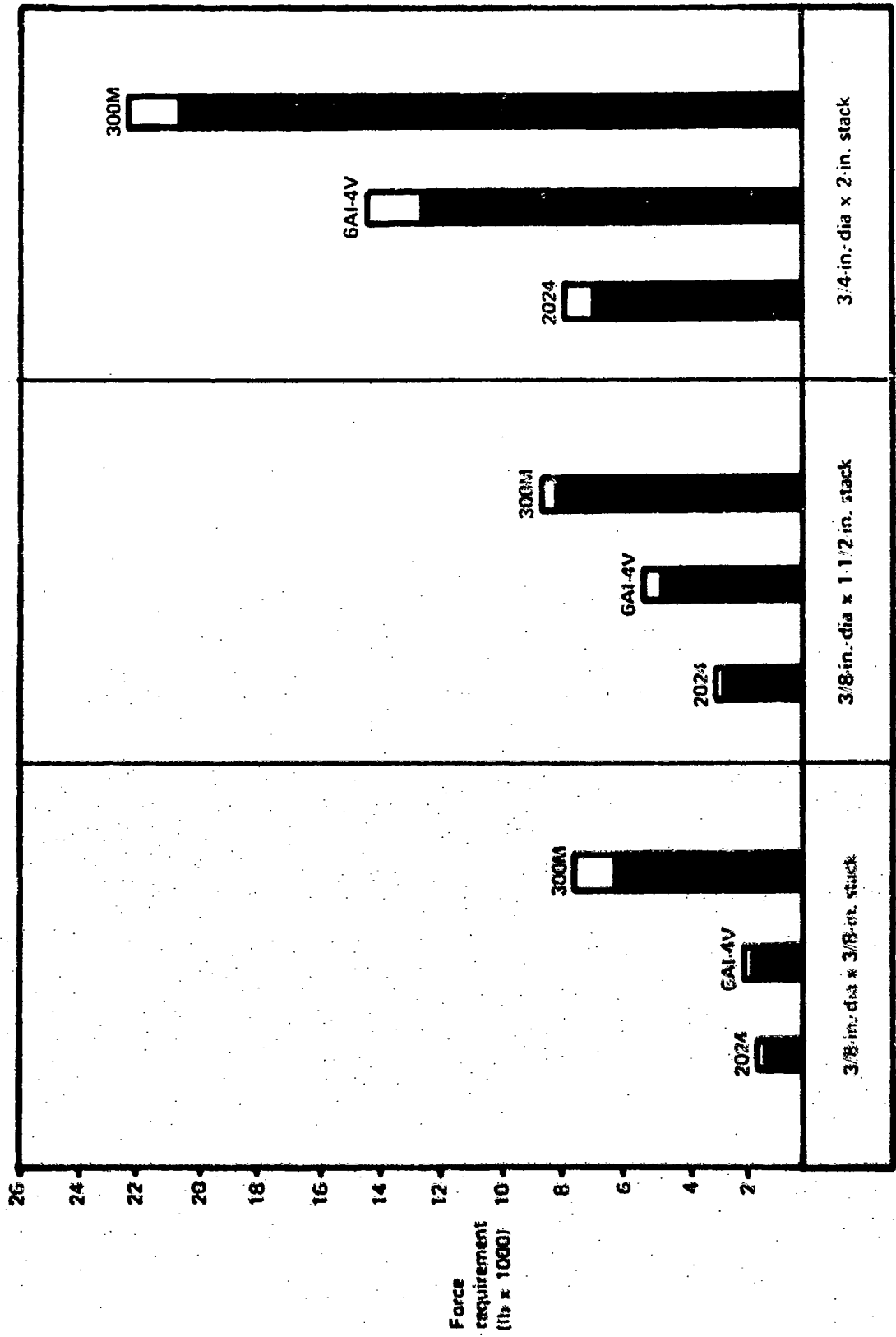
Figure 27. Force Requirement With 0.045-In.-In. Taper Mandrel and Optimum Expansion
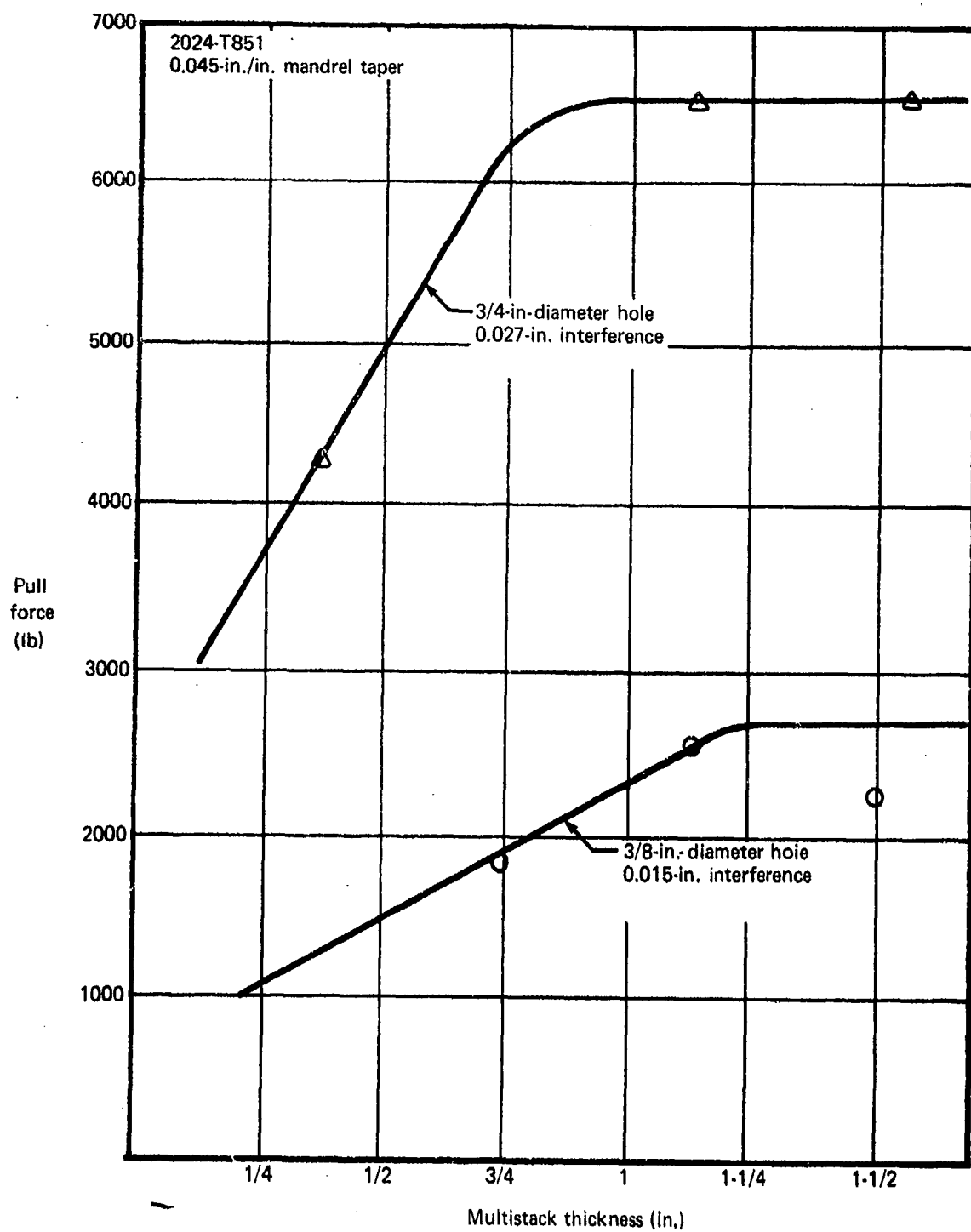
Figure 28.—Effect of Stack Thickness on Pull Force
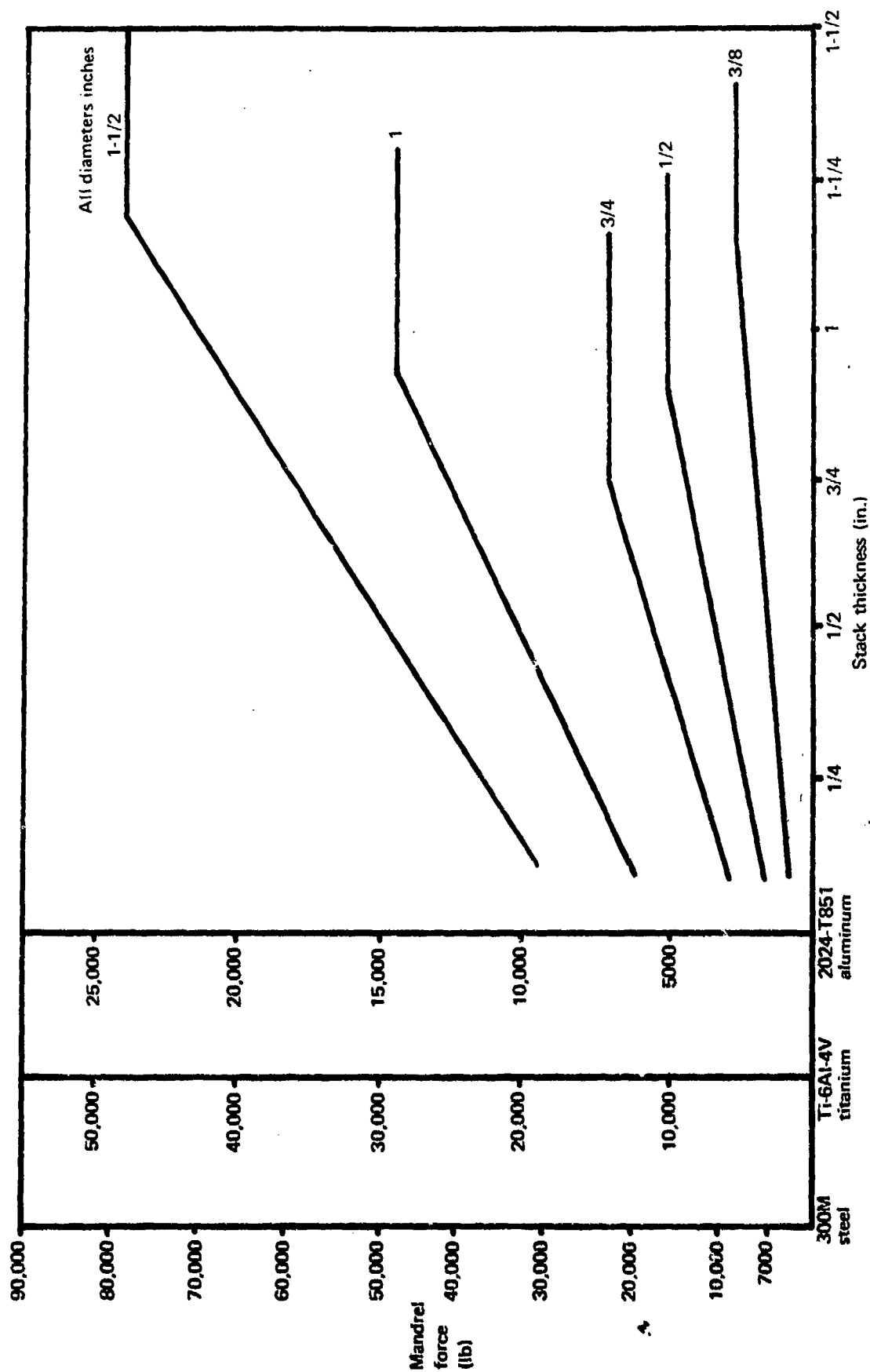
Figure 29. –Projected Stack and Diameter Effect on Force Requirements
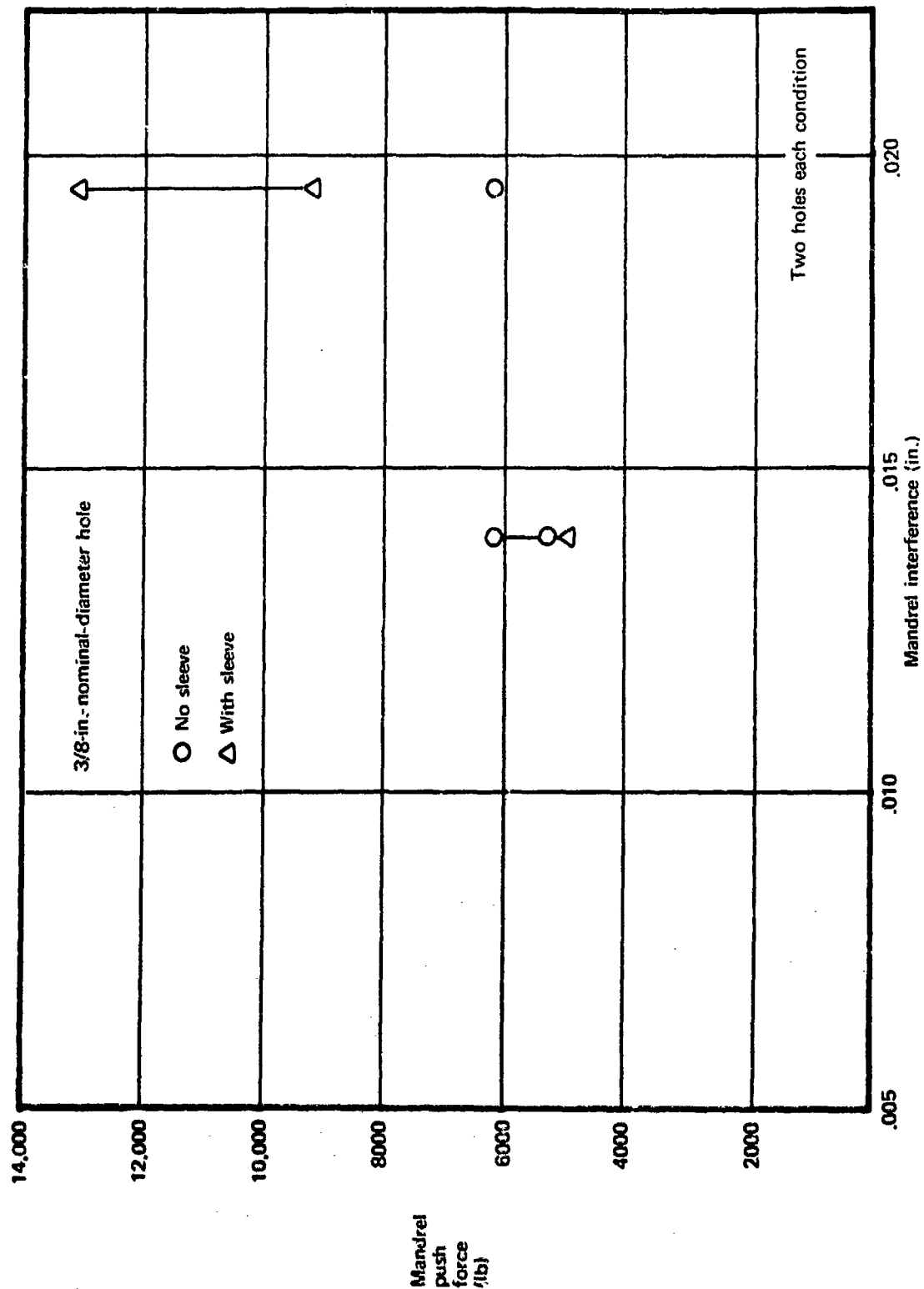
Figure 30.—Effect of Mandrel Interference, With and Without Sleeve, on Push Force—270-300 KSI 300M Steel, 5/8-In. Stack
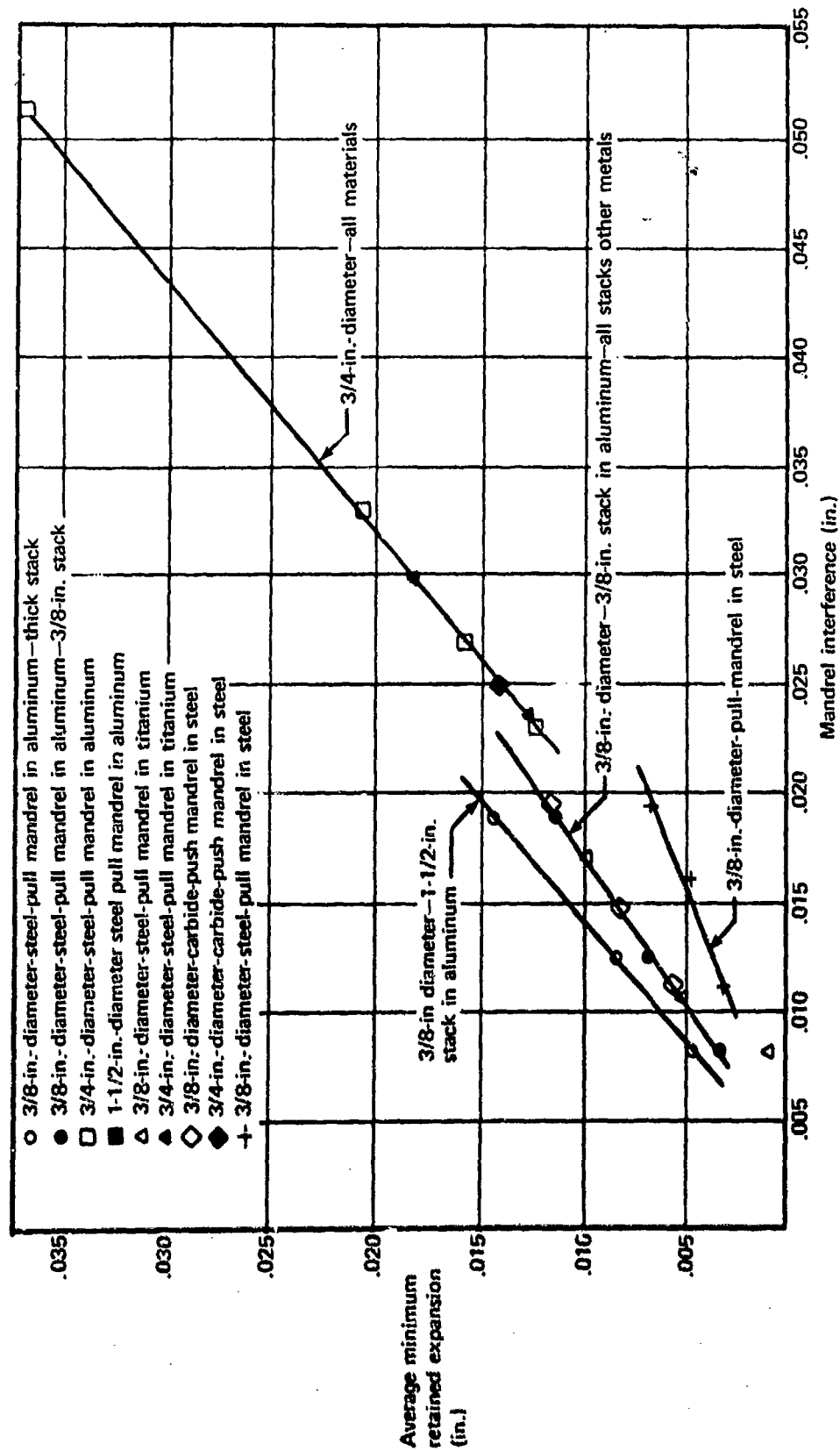
Figure 31.—*Effect of Diameter and Stack on Retained Expansion*
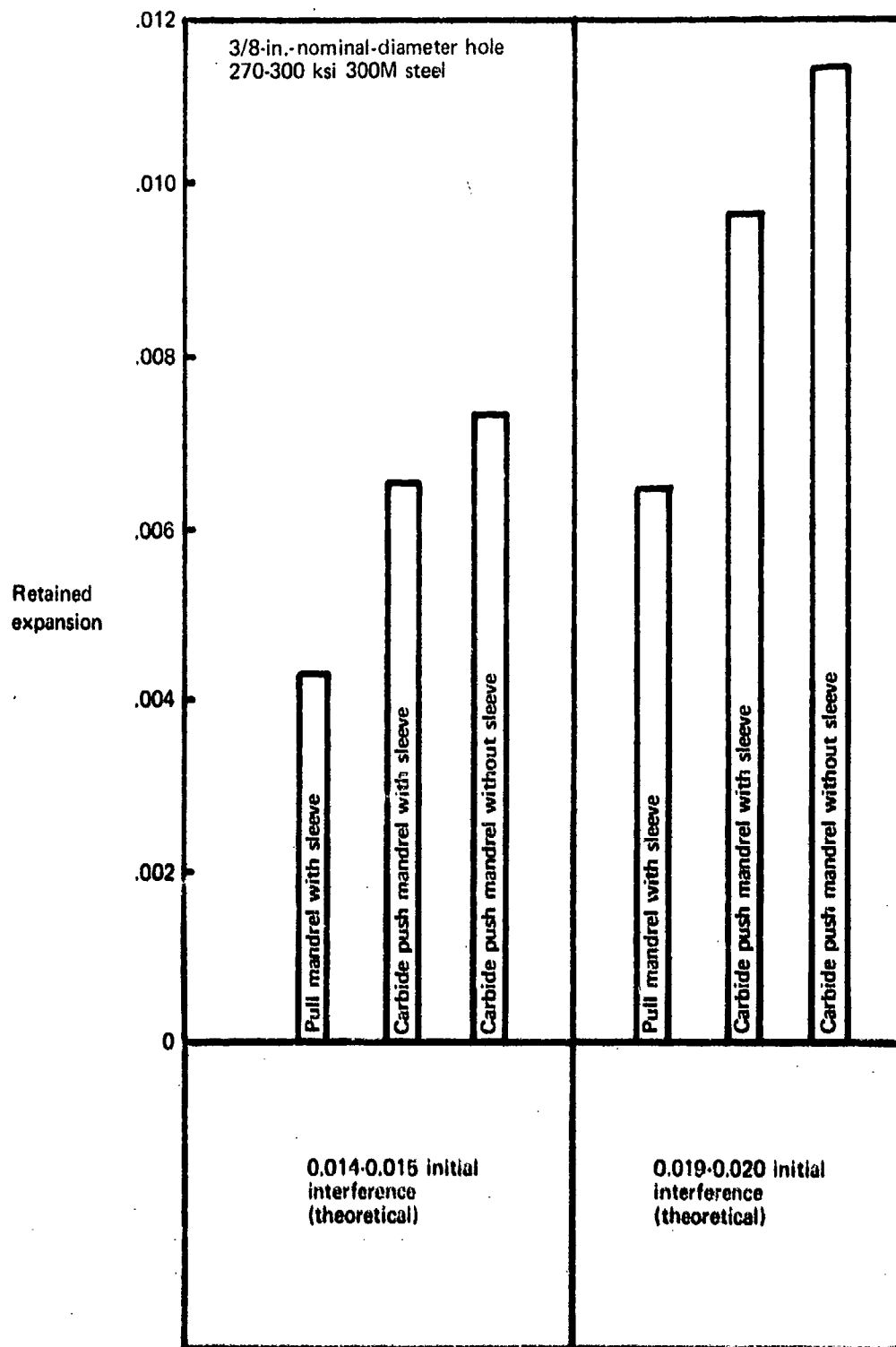
Figure 32. — Effect of Process on Retained Expansion
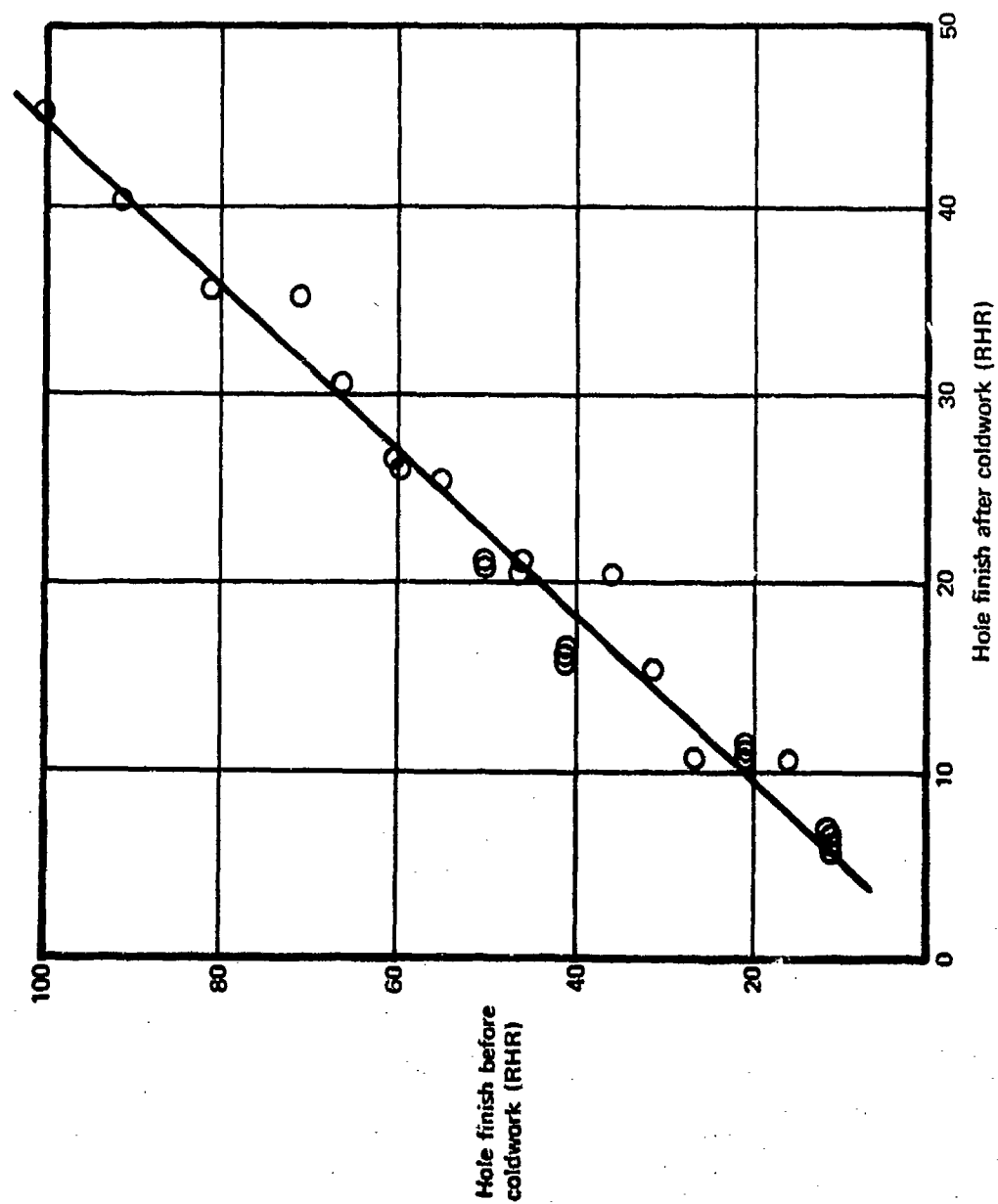
Figure 33. —Hole Finish Before Coldwork Versus After—2024-T851 Aluminum

Hole finish after coldwork (RHR)

Hole finish before coldwork (RHR)
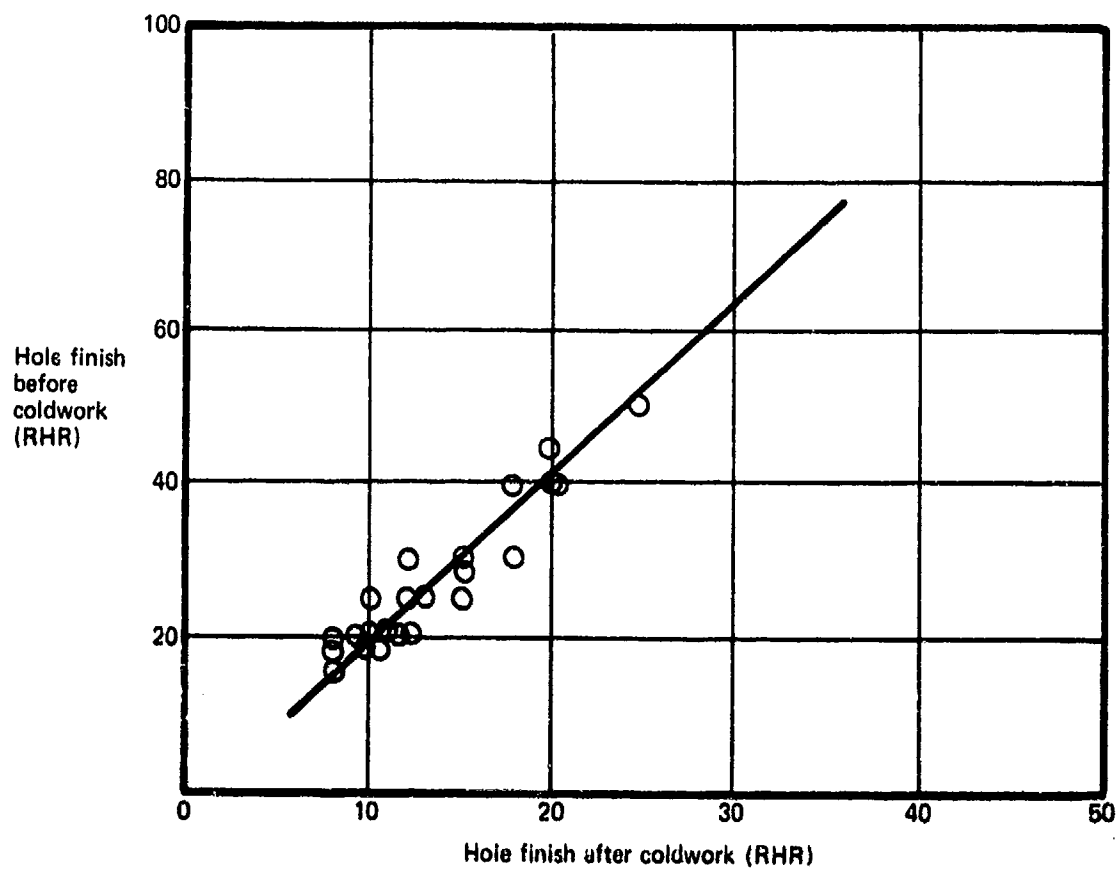
Figure 34.—Hole Finish Before Coldwork Versus After—Ti-6Al-4V Titanium, Annealed
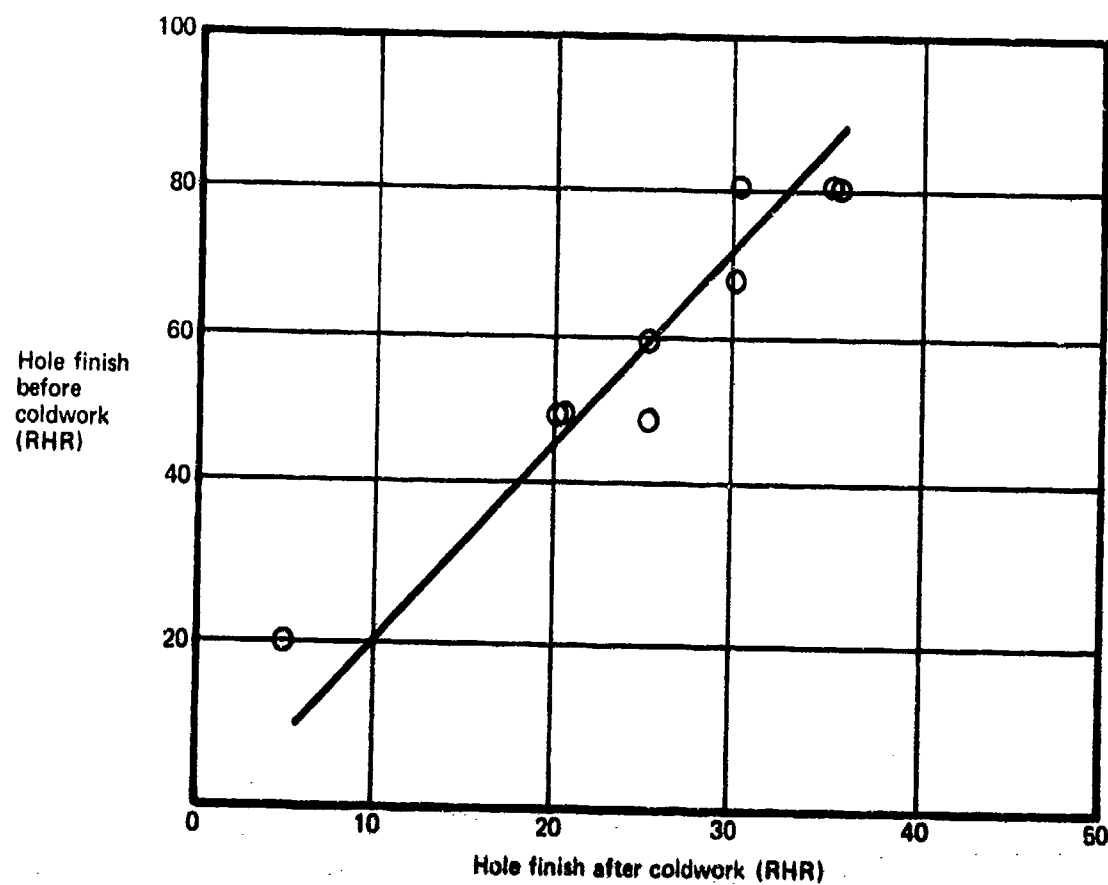
Figure 35.—Hole Finish Before Coldwork Versus After—270-300 KSI 300M Steel

Interference	Min	Max	Max	Min	Max
Taper	Min	Max	Max	Min	Max
Stock thickness, (in.)	3/8	3/8	1-1/2	2-1/2	2-1/2
Nominal diameter (in.)	3/8			3/4	

Maximum radial variation (in.)
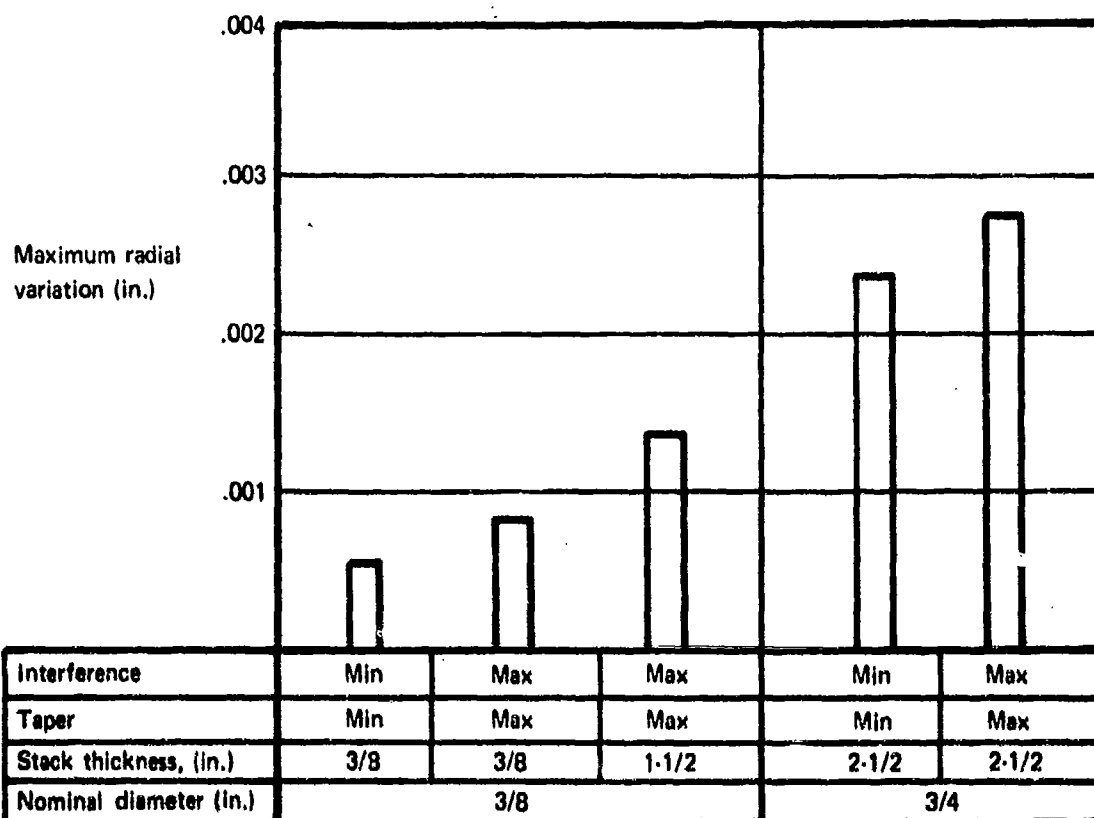
Figure 36.—Maximum Radial Variation—2024-T851

Interference	Min	Max	Max	Max	Min	Max
Taper	Min	Max	Max	Max	Min	Max
Stack thickness (in.)	3/8	3/8	3/8	1-1/2	2	2
Nominal diameter (in.)	3/8				3/4	
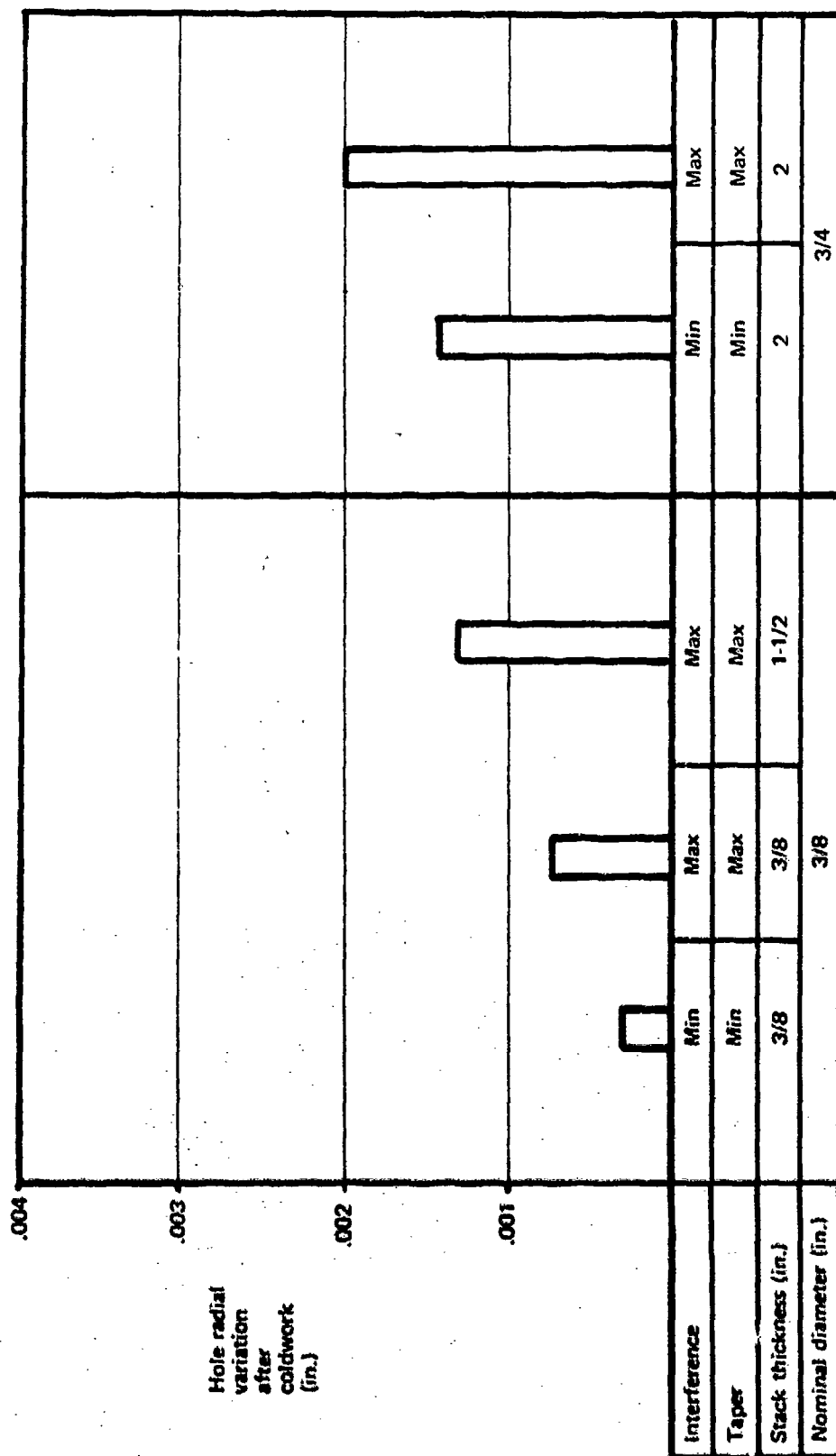
Figure 37. – Hole Radial Variation After Coldwork – Ti-6Al-4V Titanium, Annealed
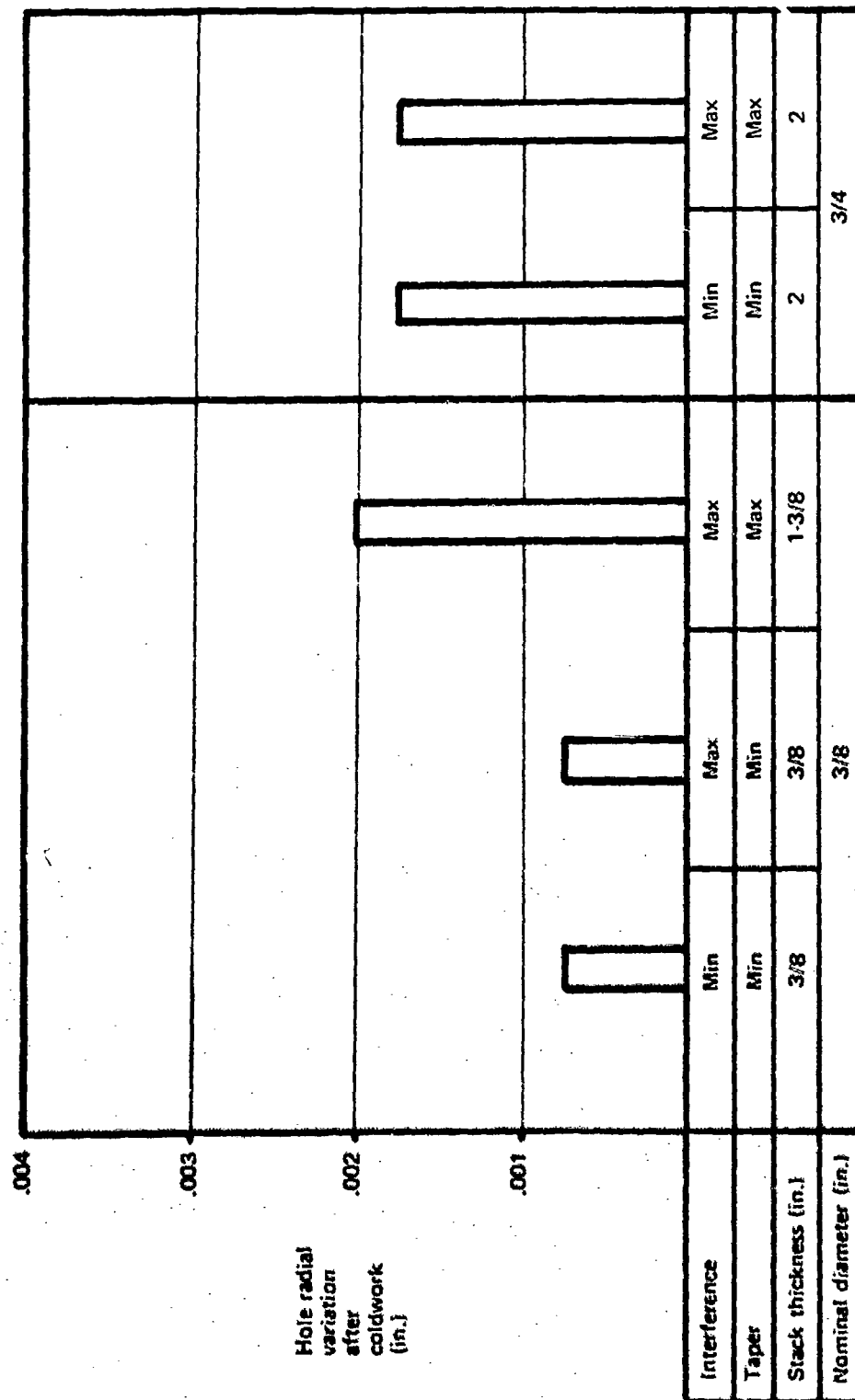
Figure 38. —Hole Radial Variation After Coldwork—270-300 KSI 300M Steel

	Min	Max		Max		Min	Max
Interference	Min	Min		Max		Min	Max
Taper	Min	Min		Max		Min	Max
Stack thickness (in.)	3/8	3/8		1-3/8		2	2
Nominal diameter (in.)	3/8			3/4			

Hole radial variation after coldwork (in.)

.004
.003
.002
.001

AFML CW PROG
TEST PLATE IV
HOLE A-3

MICRO INCHES   CUTOFF   SKID   SKIDLESS

PROFILE ROUGHNESS AVERAGE

PROFILE ROUGHNESS AVERAGE

DATE 8/30/72
PART

TRAVERSE

Figure 39—Typical Hole Profile Trace
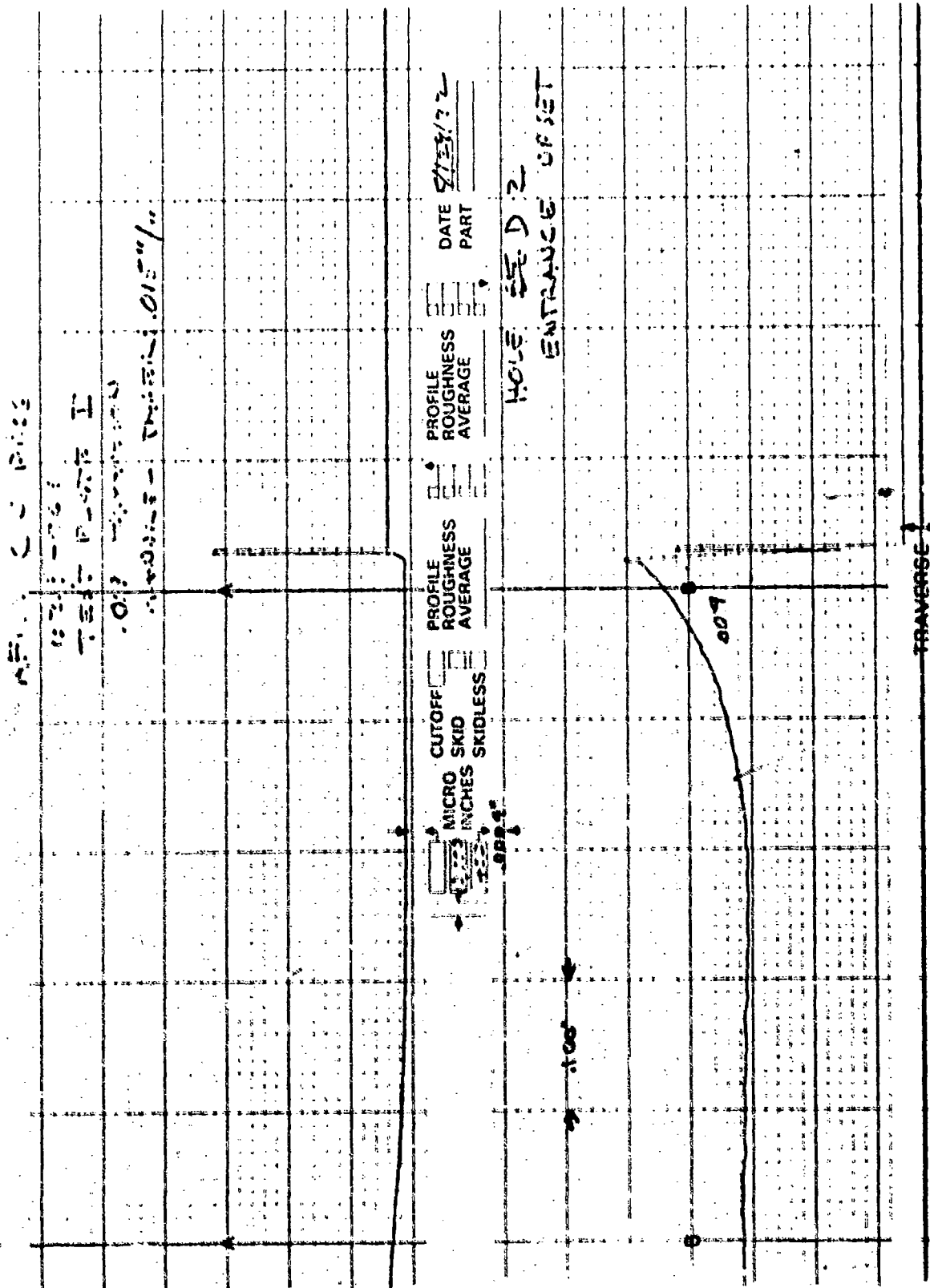
Figure 40. Typical Entry Surface Upset Trace

Figure 41. Typical Exit Surface Upset Trace
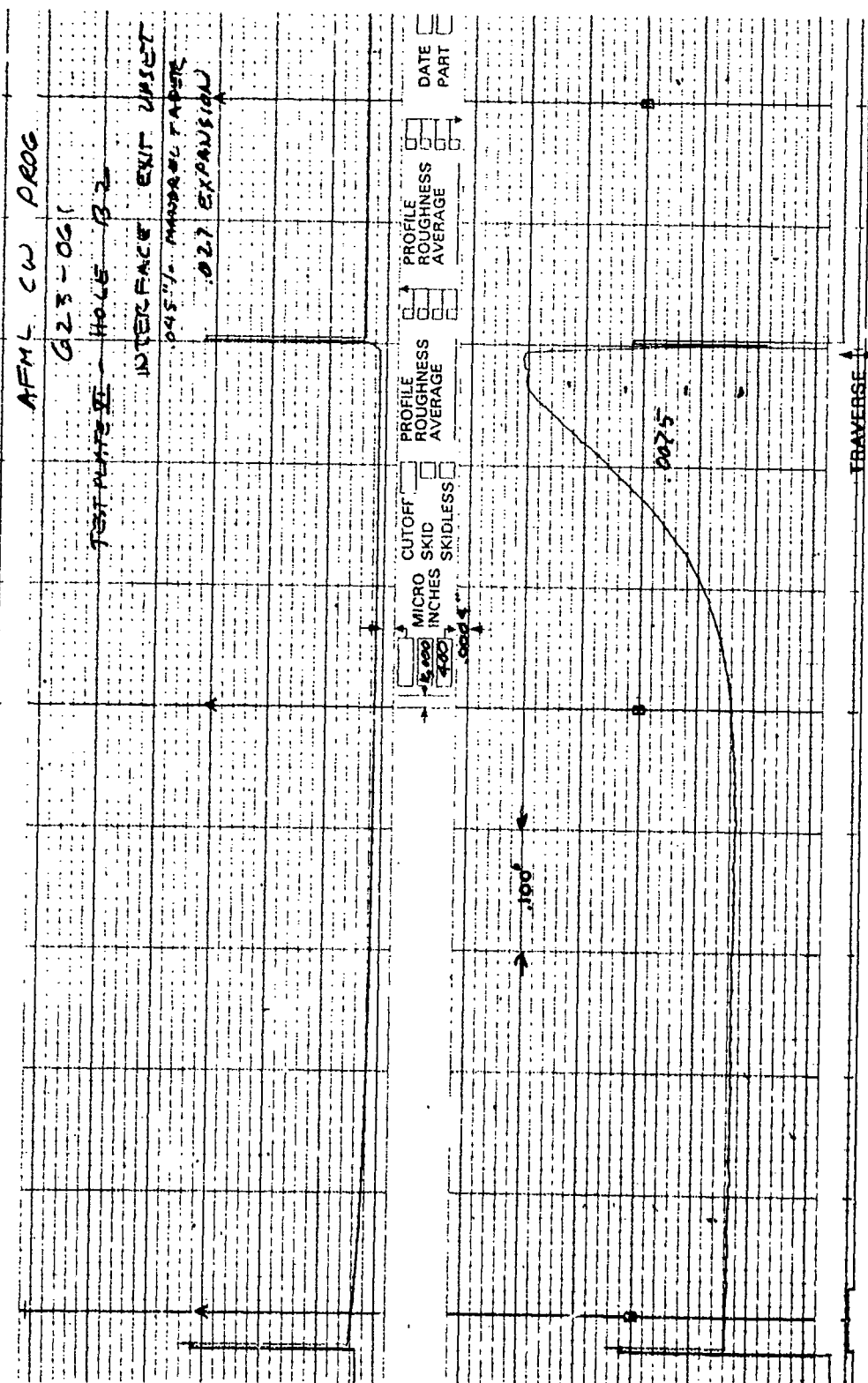
Figure 42. – Typical Interface Entry Surface Upset Trace
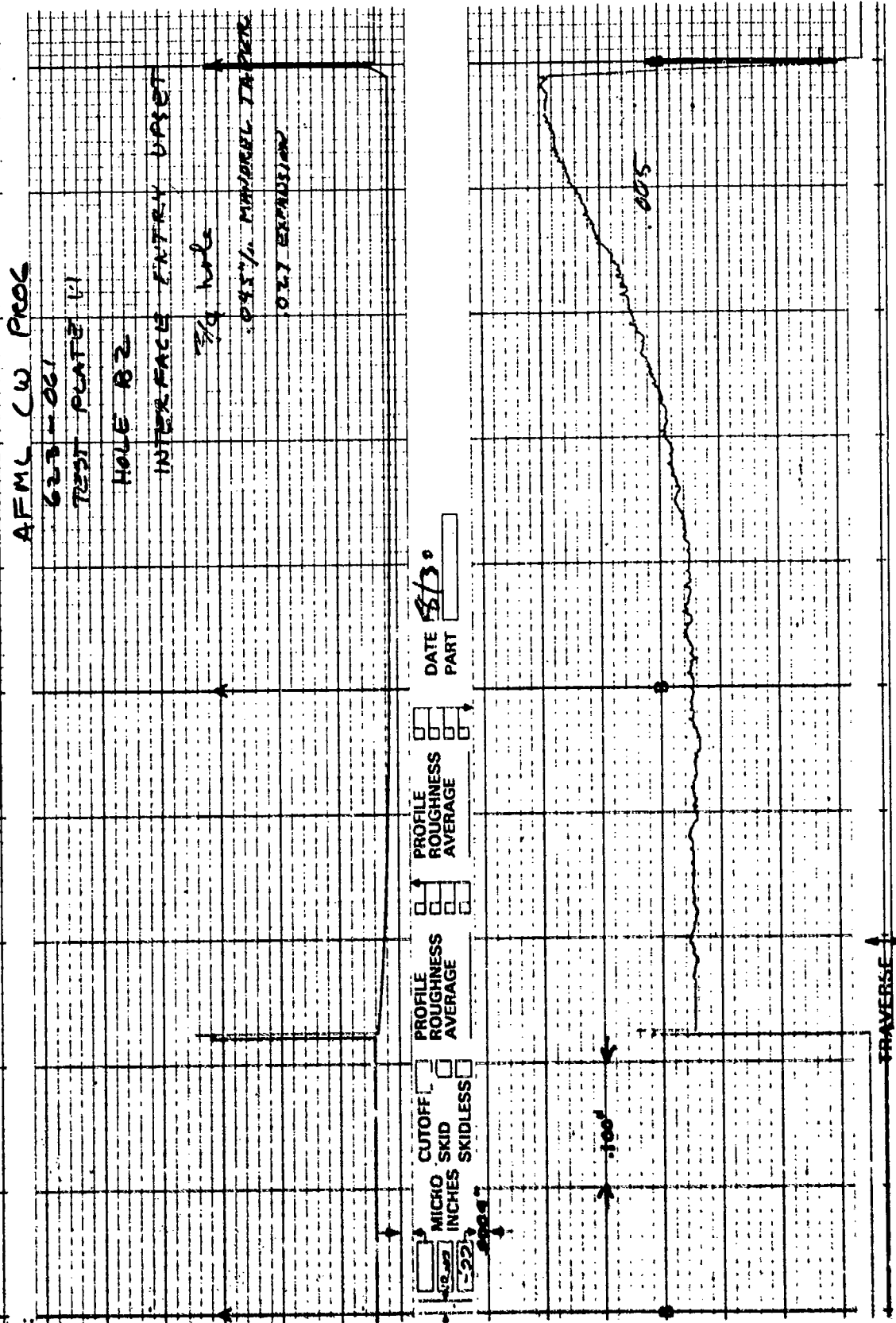
Figure 43. – Typical Interface Exit Surface Upset Trace

127
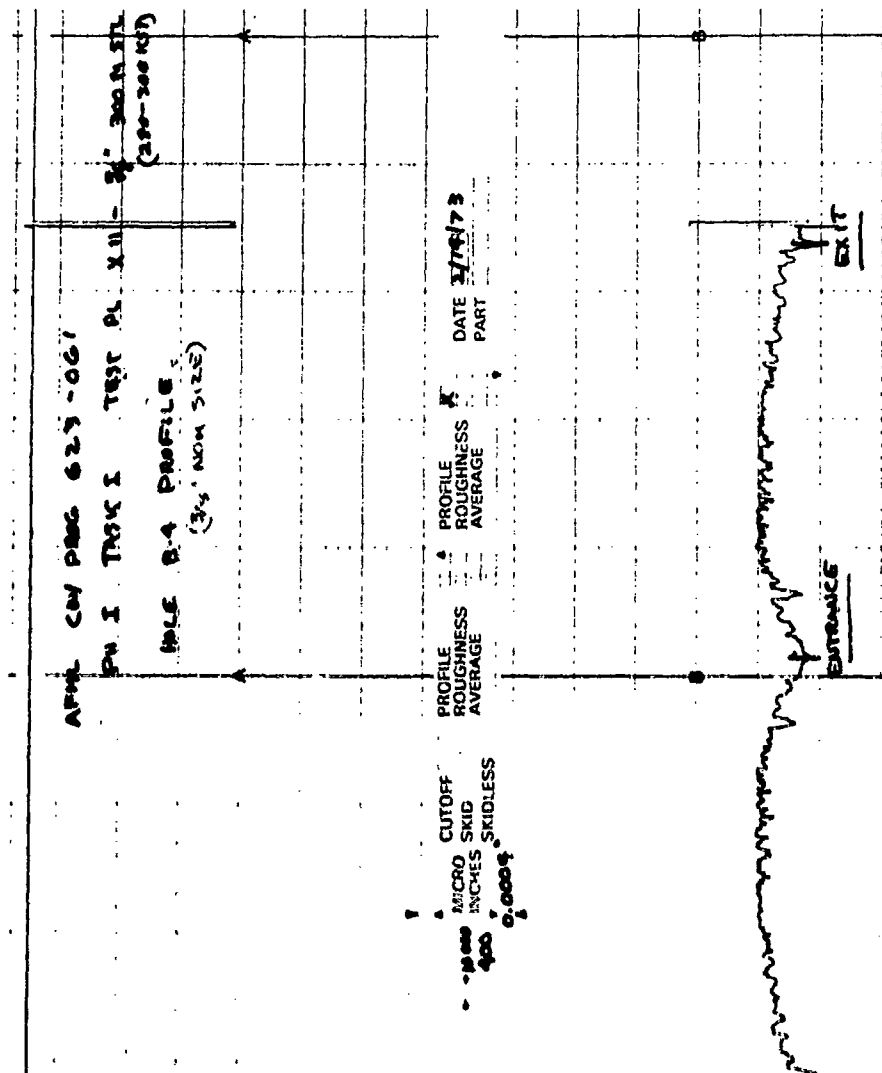
Figure 44.—Hole Profile Trace—3/8-In.-Diameter Hole.
0.0185-In. Interference. 300M Steel

128
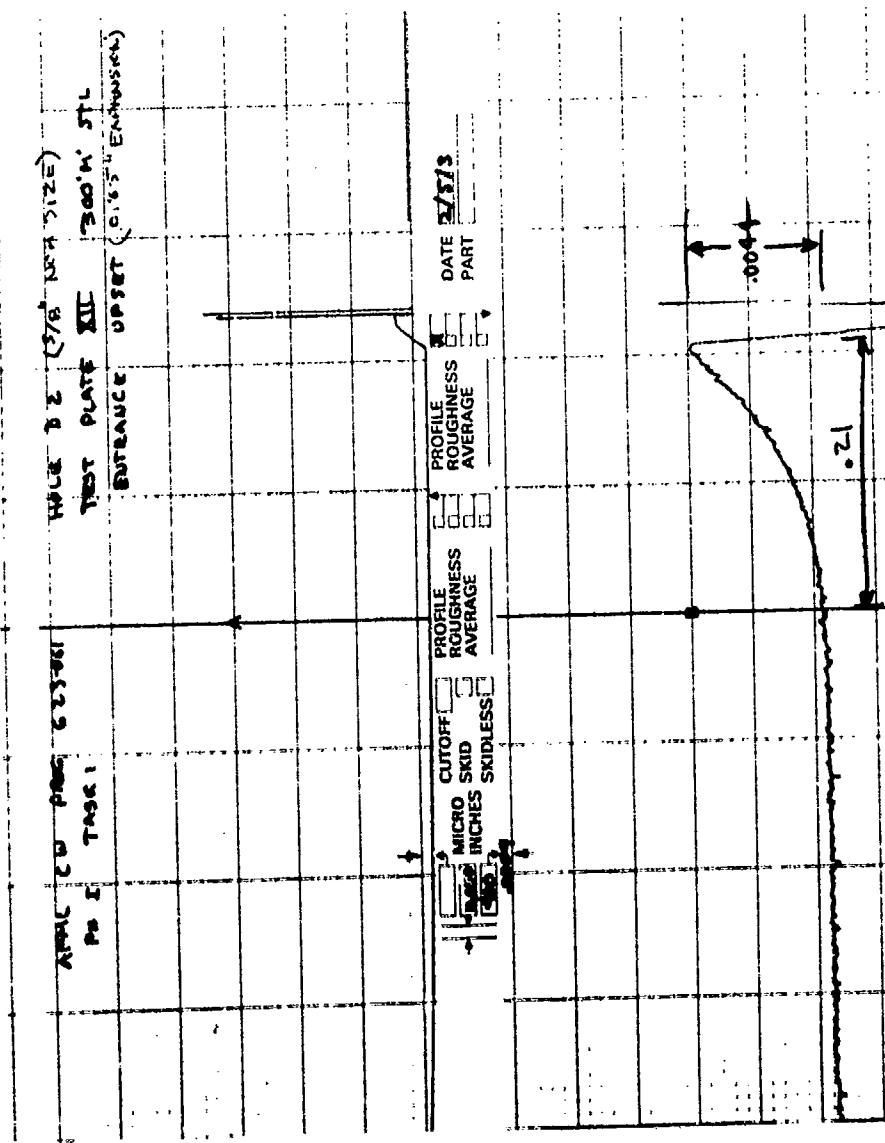
Figure 45.—Entrance Upset Trace—3/8-In.-Diameter Hole, 0.0185-In. Interference, 300M Steel
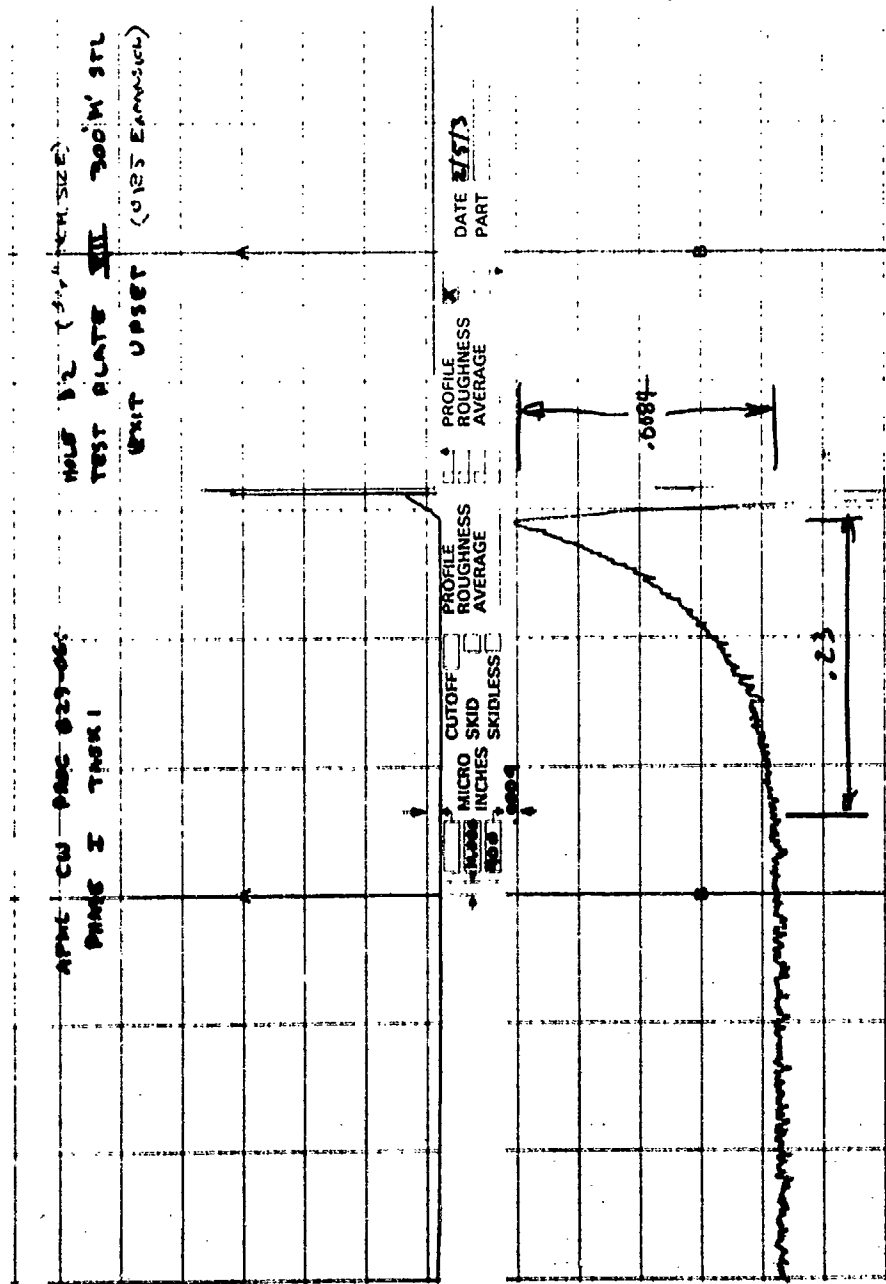
Figure 46.—Exit Upset Trace—3/8-In.-Diameter Hole, 0.0185 In.-
Interference, 300M Steel
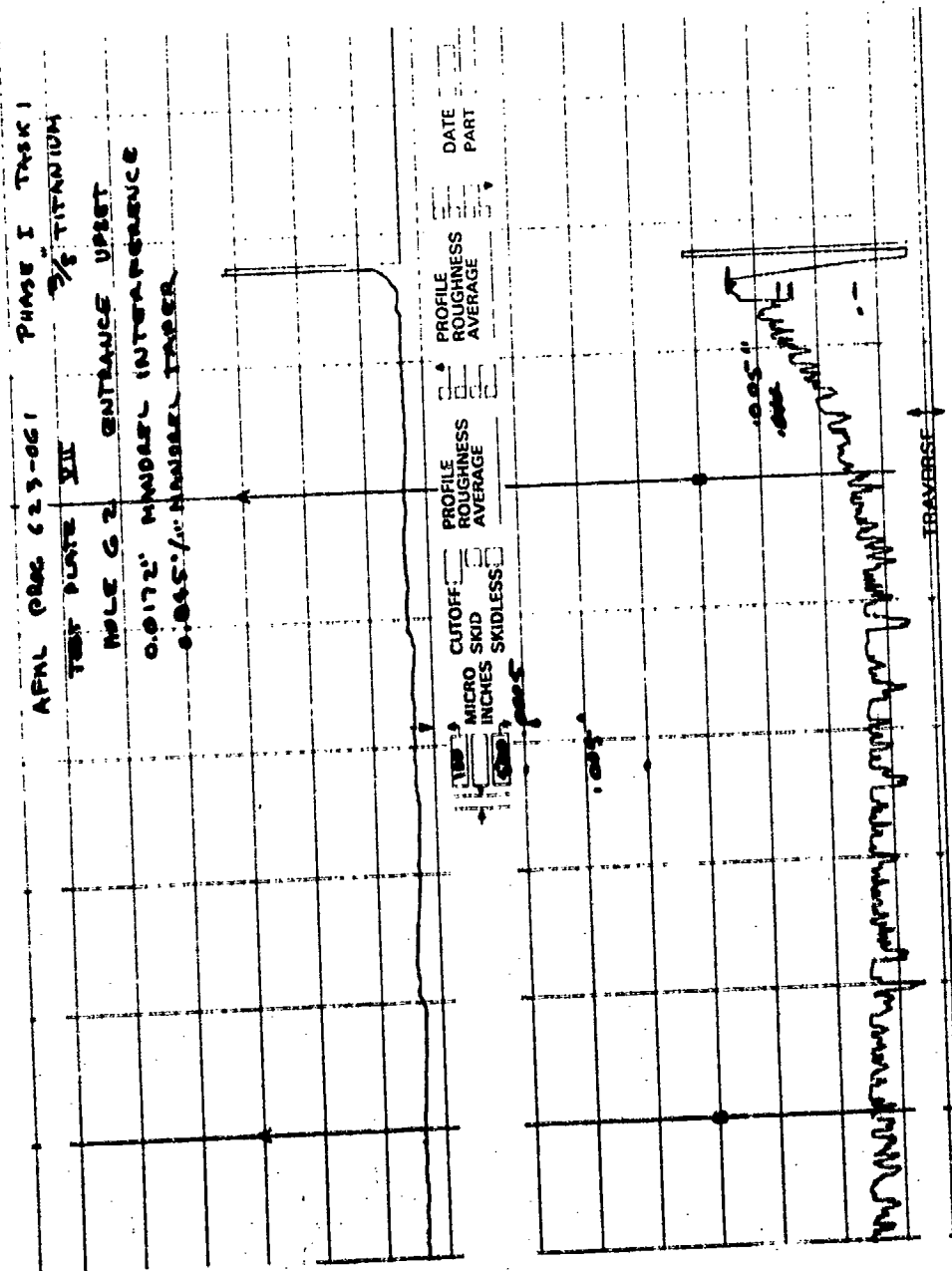
Figure 47.—Entrance Upset Trace—3/8-In.-Diameter Hole, 3/8 In. Plate,
0.0172-In. Interference. 0.045-In./In. Mandrel Taper
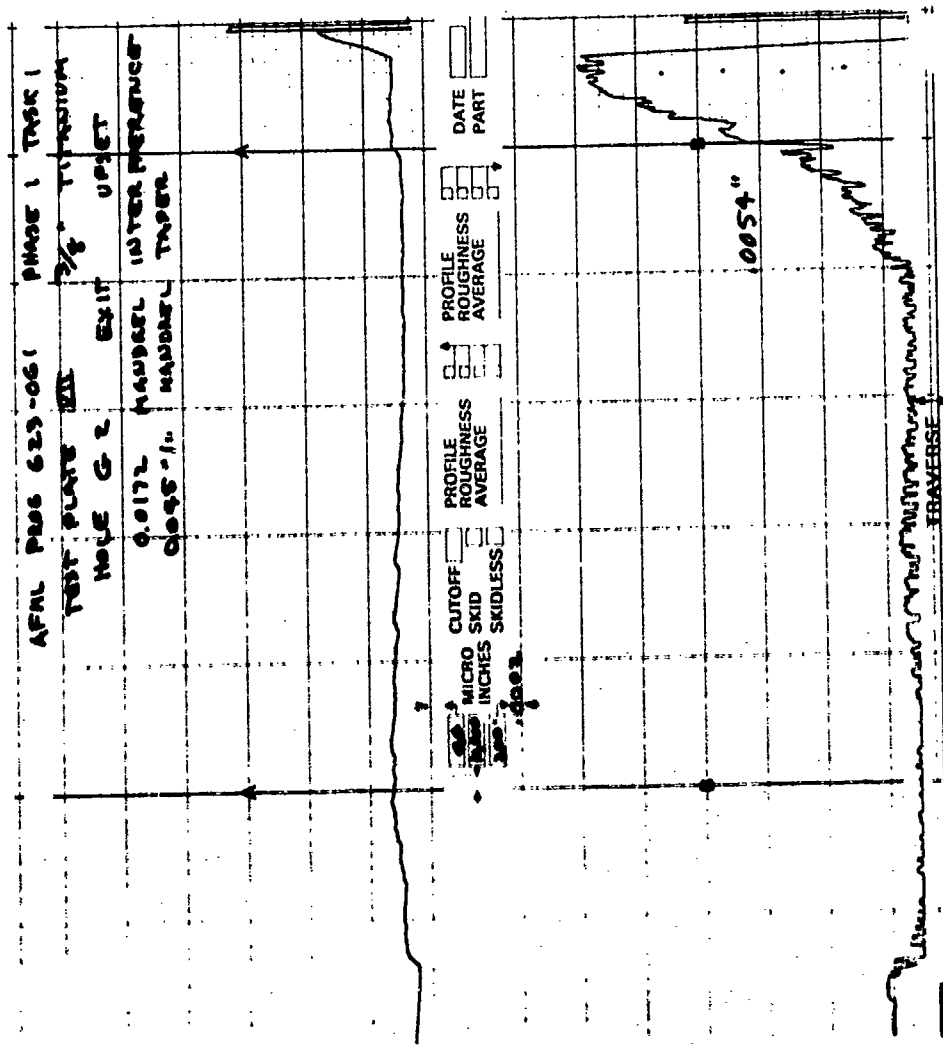
Figure 48.—Exit Upset Trace—3/8-In.-Diameter Hole, 3/8-In. Plate, 0.0172-In. Interference, 0.045 In./In. Taper, Ti-6Al-4V
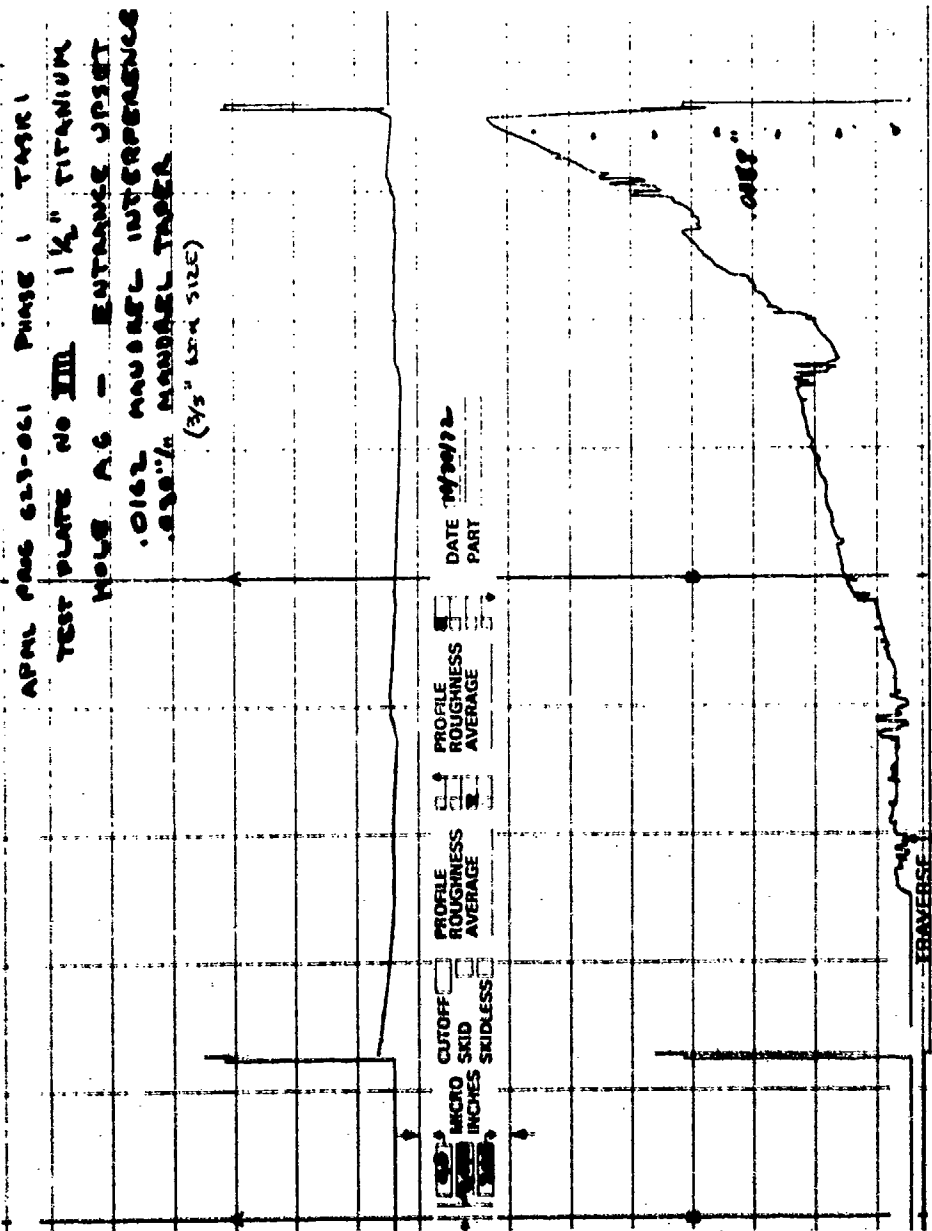
Figure 49.—Entrance Upset Trace—3/8-In.-Diameter Hole, 1-1/2-In. Plate, 0.0162-In. Interference, 0.045 In./In. Taper

133
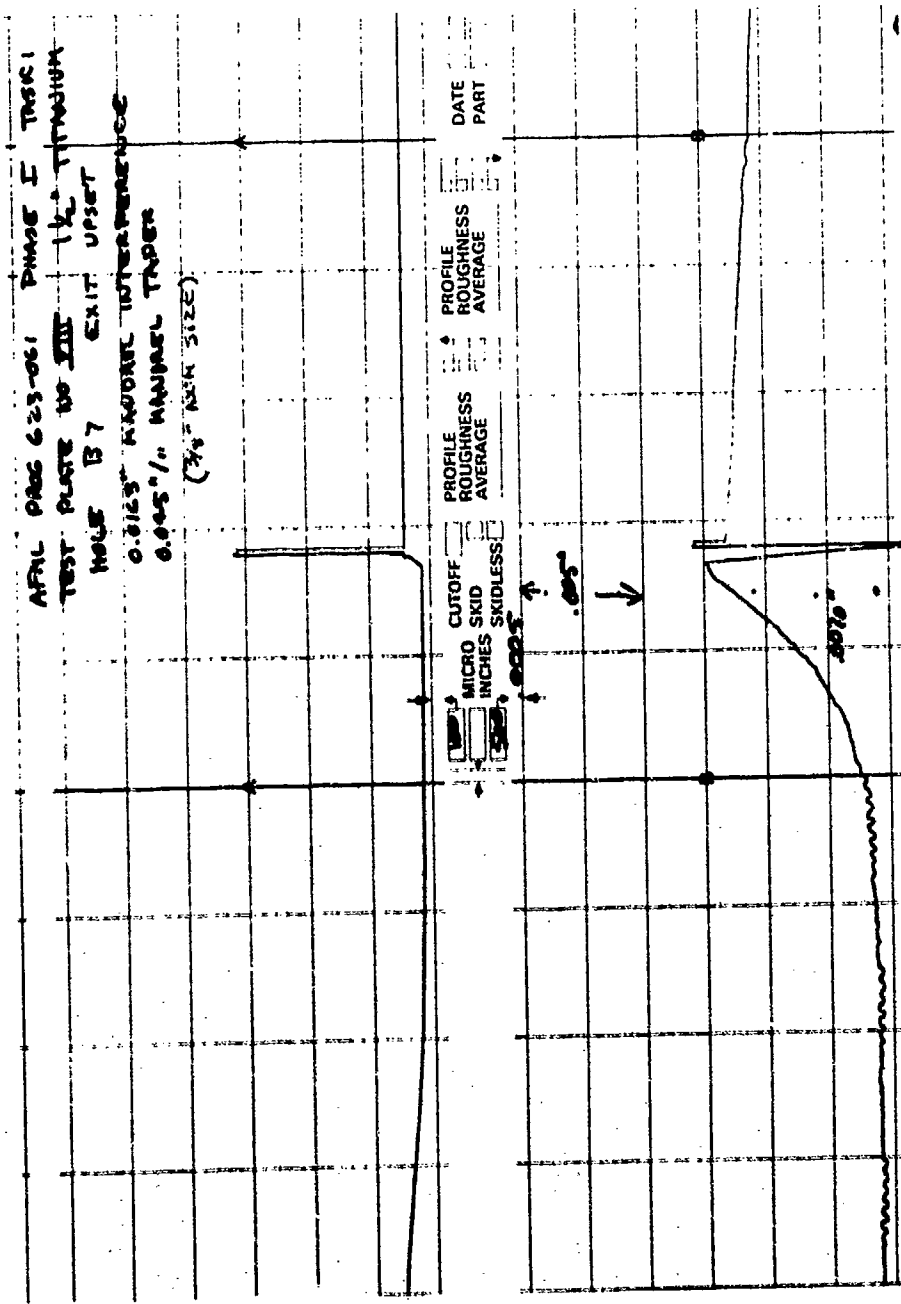
Figure 50.—Exit Upset Trace—3/8-In.-Diameter Hole, 1-1/2-In. Plate, 0.0163-In. Interference, 0.045-In./In. Taper, Ti-6Al-4V
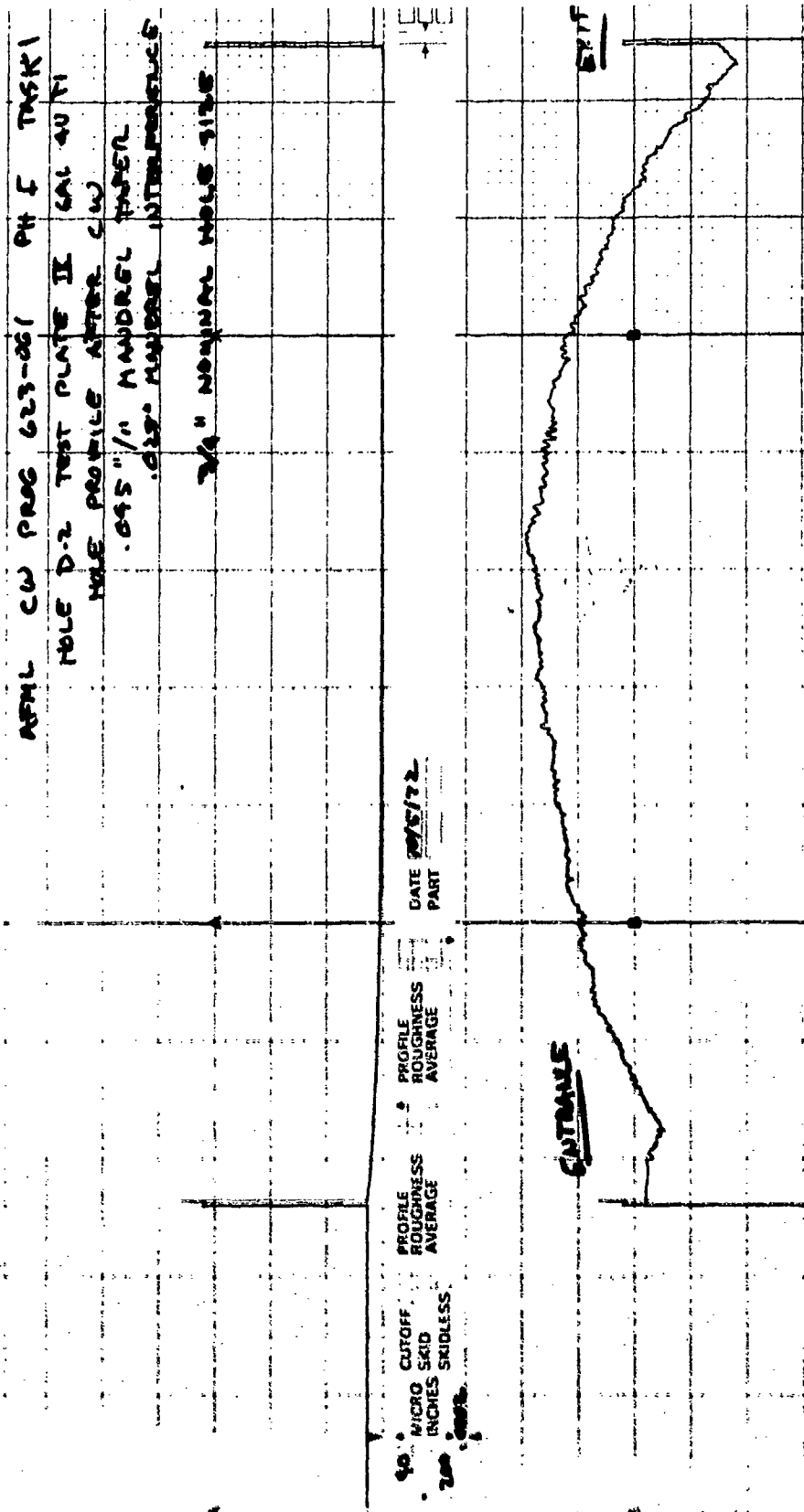
Figure 51.—Axial Hole Profile—3/4-In.-Diameter Hole, 2-In. Stack, 0.028-In.
Interference, 0.045 In./In. Taper, Ti-6Al-4V
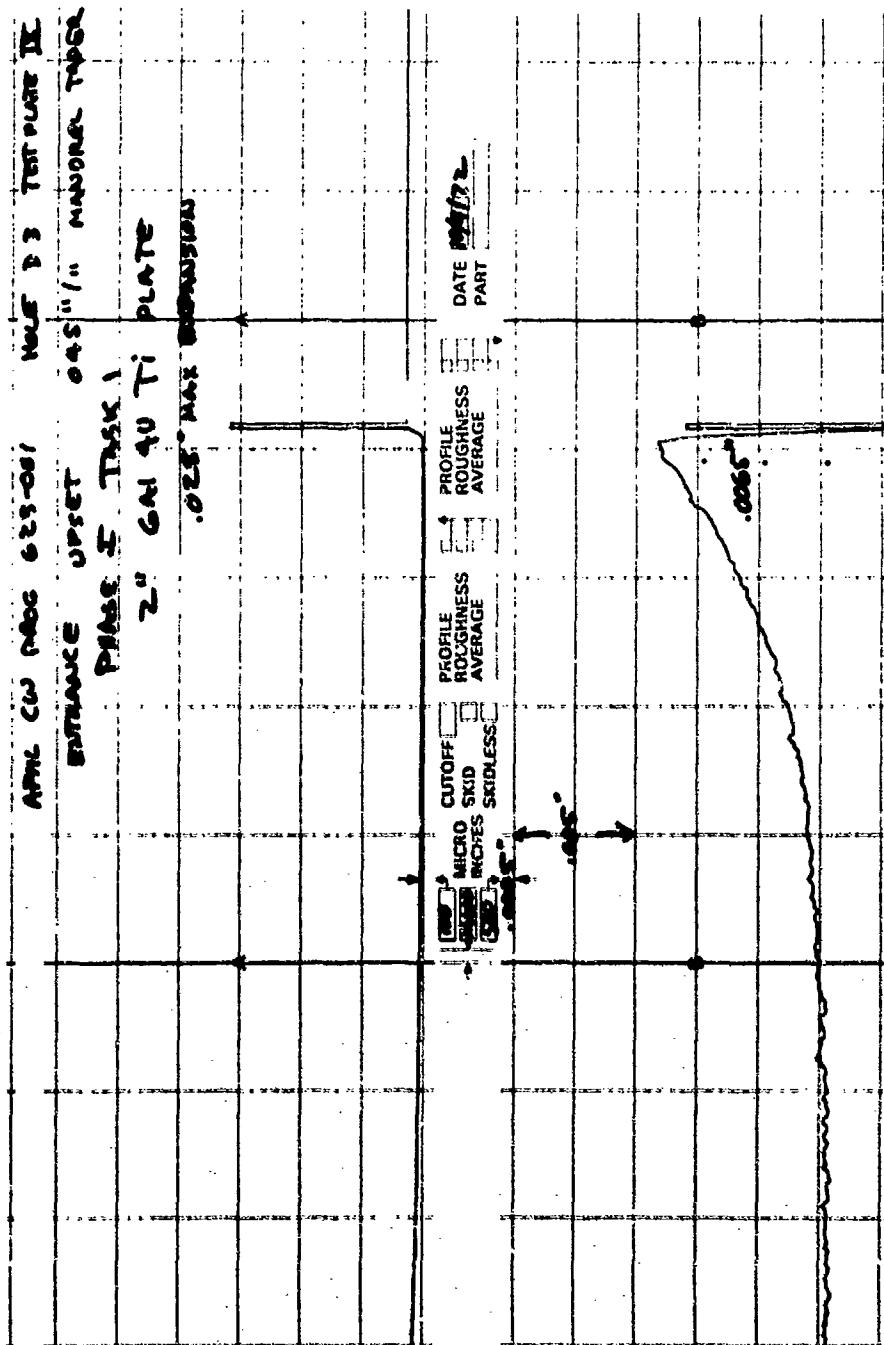
Figure 52.—Entrance Upset Trace—3/4-In.-Diameter Hole, 2-In. Stack, 0.028-In. Interference, 0.045 In./In. Taper, Ti-6Al-4V
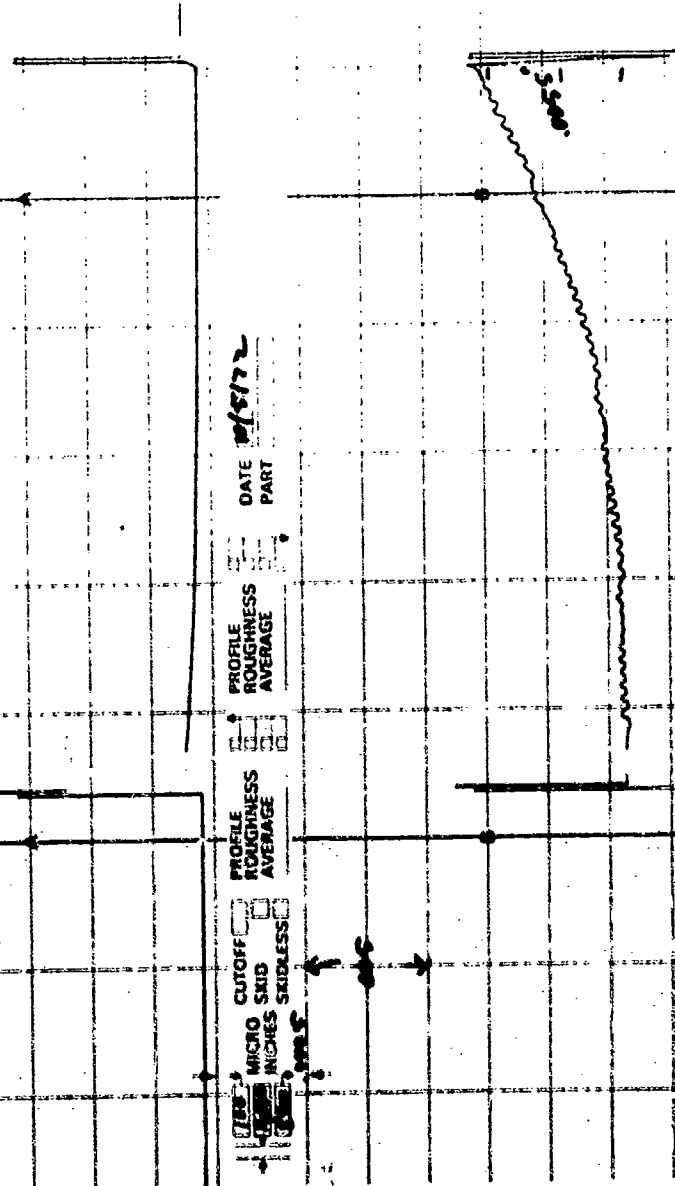
Figure 53.—Interface Entry Upset Trace—3/4-In.-Diameter Hole, 2-In. Stack, 0.028-In. Interference, 0.045 In./In. Taper. Ti-6Al-4V

Figure 54.—Interface Exit Upset Trace—3/4-In.-Diameter Hole, 2-In. Stack.
0.028-In. Interference, 0.045 In./In. Taper, Ti-6Al-4V
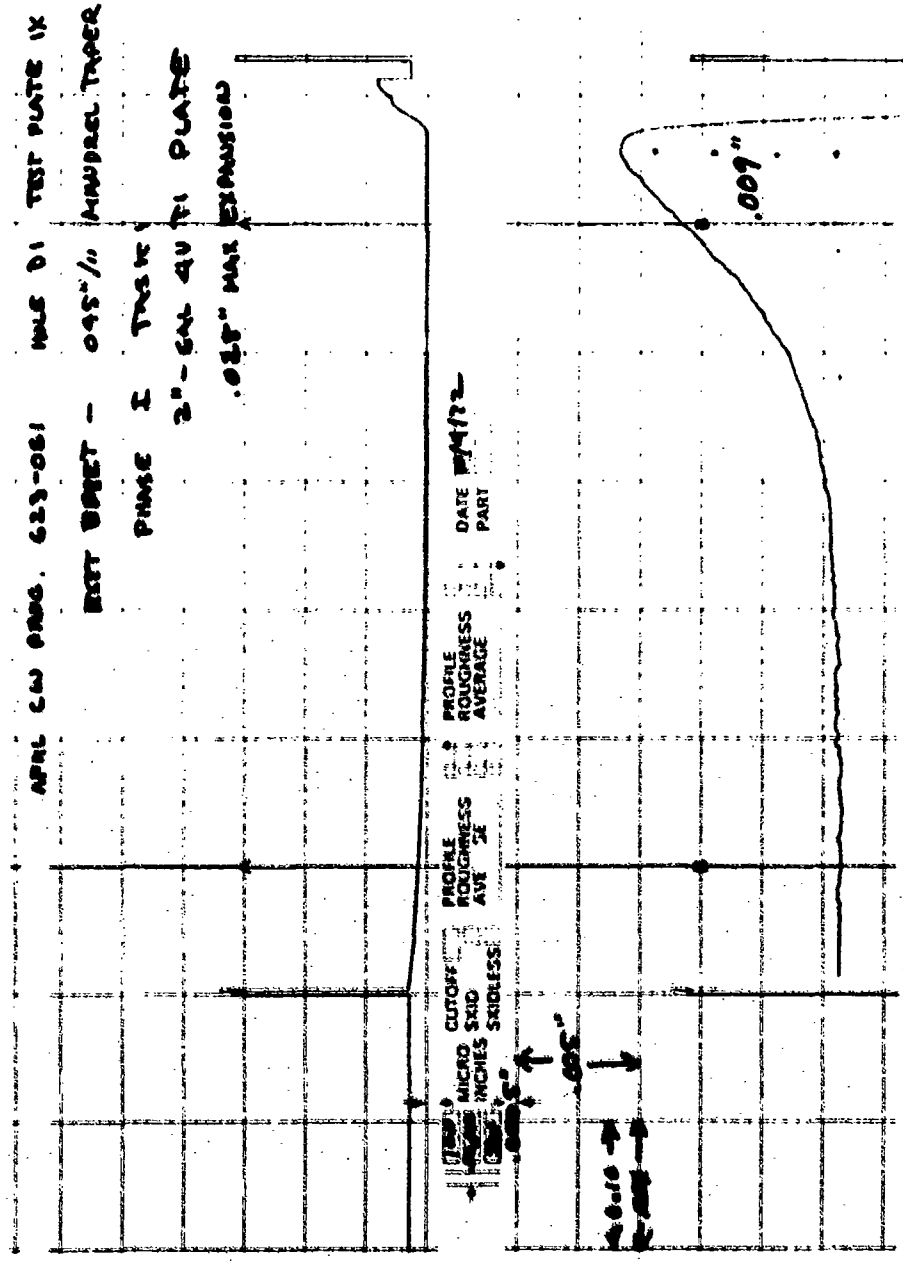
Figure 55. — Exit Upset Trace—3/4-In.-Diameter Hole. 2 -In. Stack. 0.028-In. Interference, 0.045 In./In. Taper. Ti-6Al-4V

Figure 56.—Exit Upset Trace—3/4-In.-Diameter Hole, 2-In. Stack,
0.029-In. Interference, 0.020-In./In. Taper, Ti-6Al-4V

Figure 57.—Exit Upset Trace–3/4-In.-Diameter Hole. 2-In. Stack.
0.030-In. Interference. 0.030 In./In. Taper, Ti-6Al-4V

14
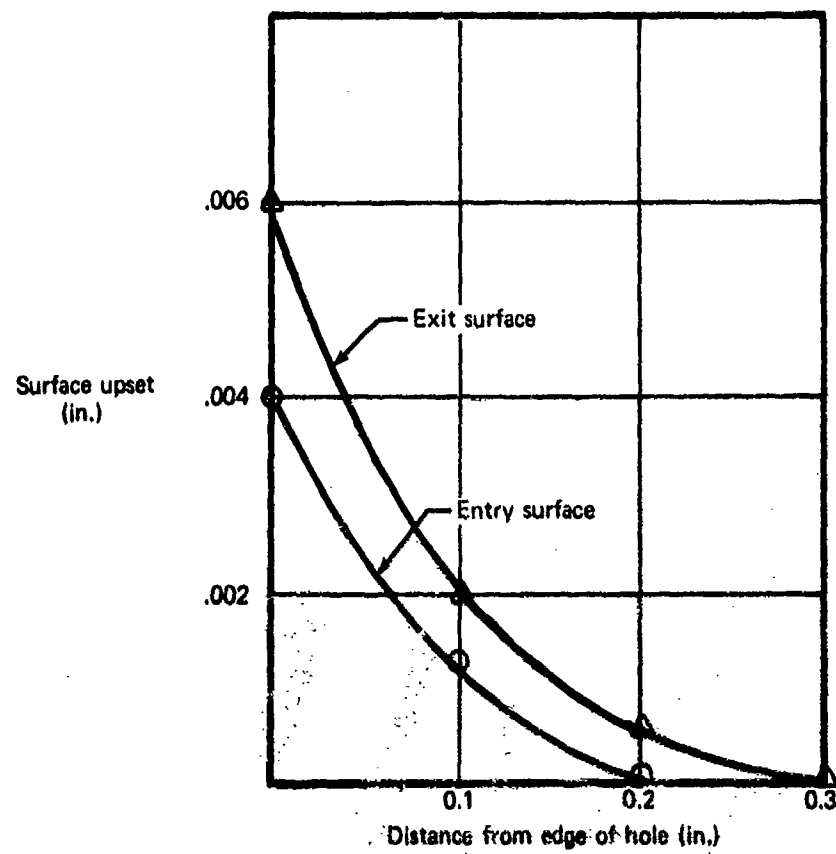
Figure 58.—Surface Upsetting—2024-T851, 3/8-In.-Nominal-Diameter Hole
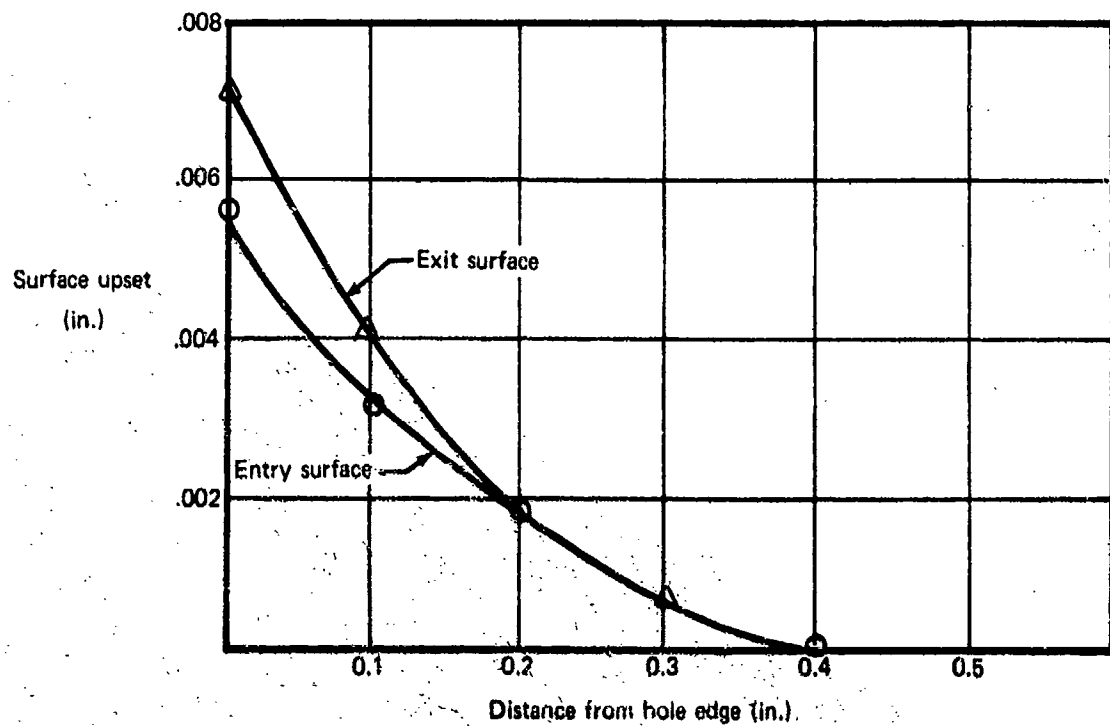
Figure 59.–Surface Upsetting–2024-T851, 3/4-In.-Nominal-Diameter Hole

143
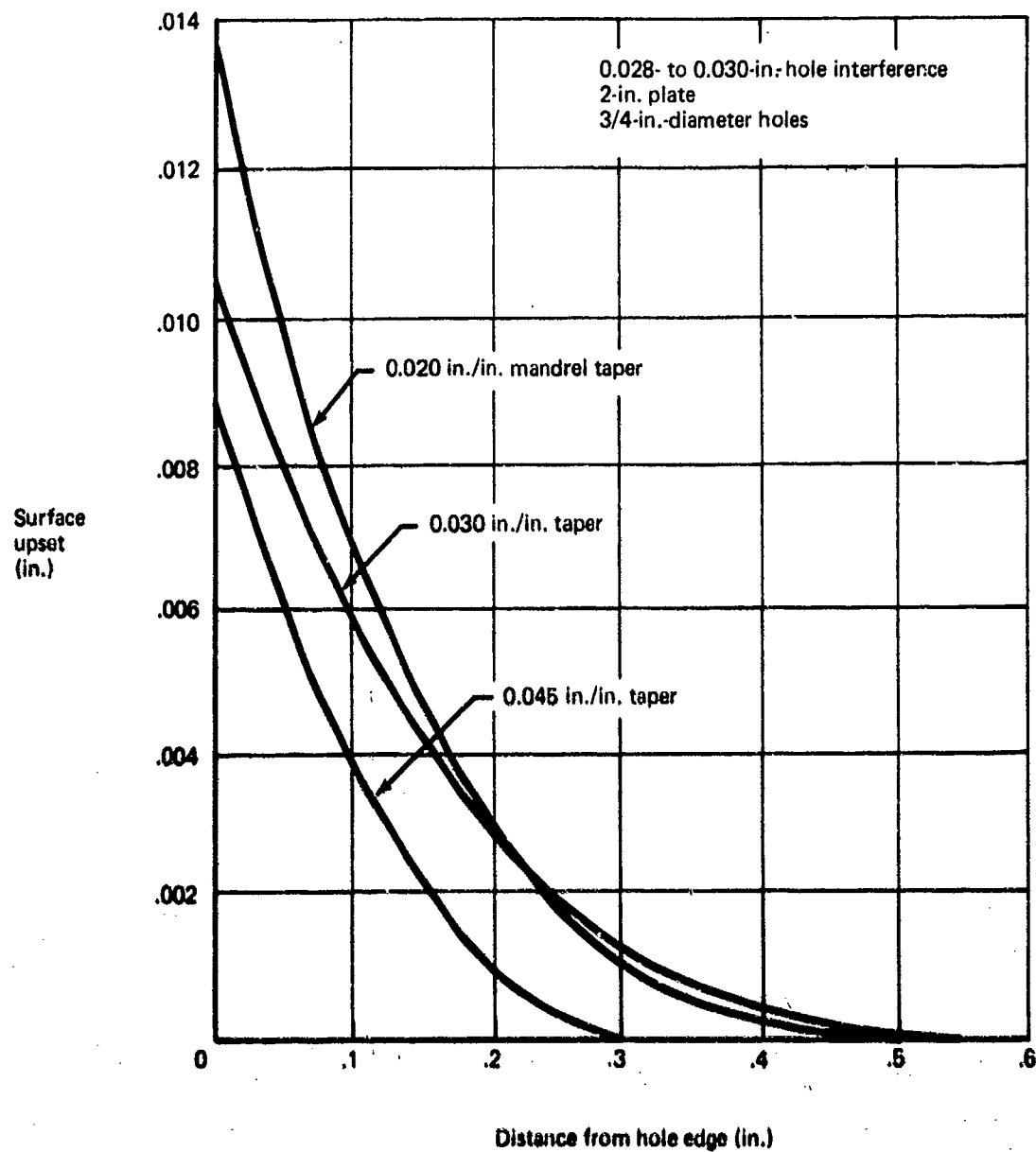
Figure 60. –Mandrel Taper Effect on Exit Upset–Ti-6Al-4V

144
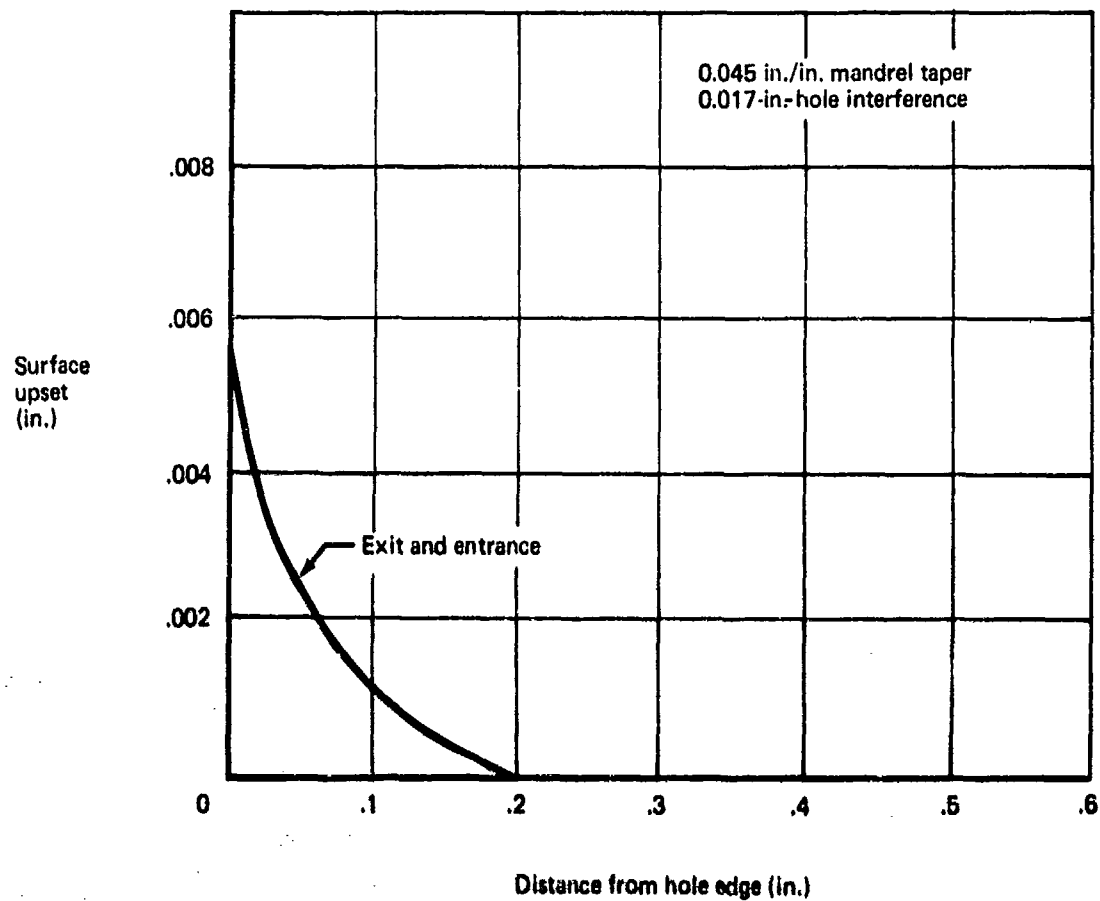
Figure 61.—Surface Upsetting—Ti-6Al-4V, 3/8-In.-Nominal-
Diameter Hole, 3/8-In. Plate
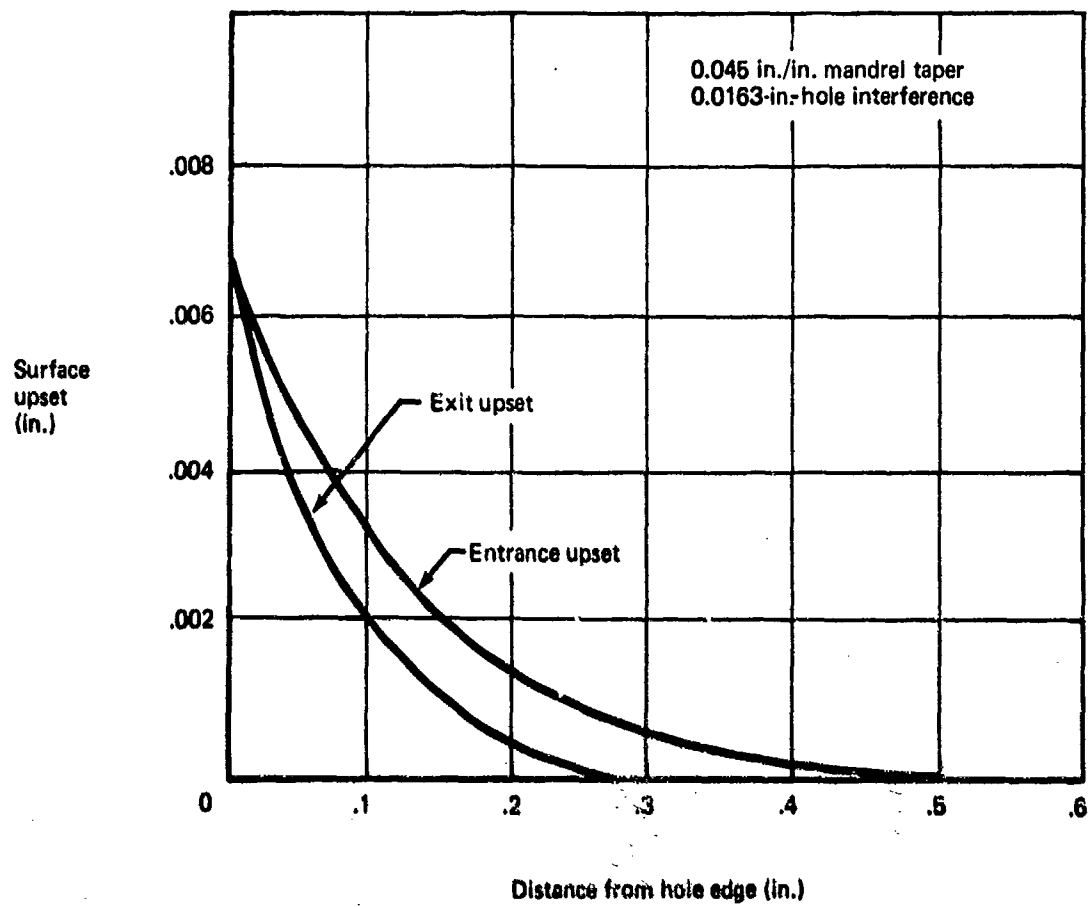
Figure 62. —Surface Upsetting—Ti-6Al-4V, 3/8-In.-Nominal-Diameter Hole, 1-1/2-In. Plate
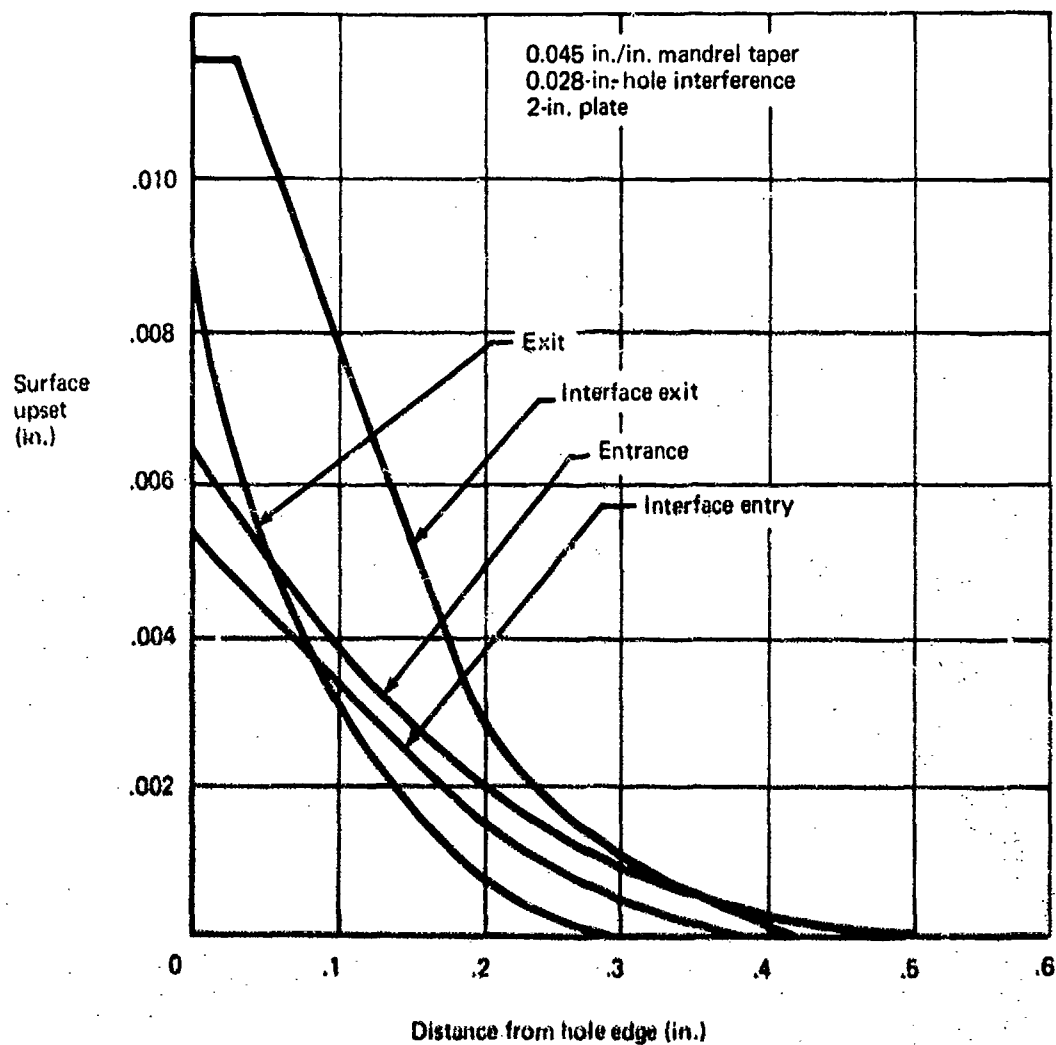
Figure 63.—Surface Upsetting—Ti-6Al-4V, 3/4-In.-Nominal-Diameter Hole
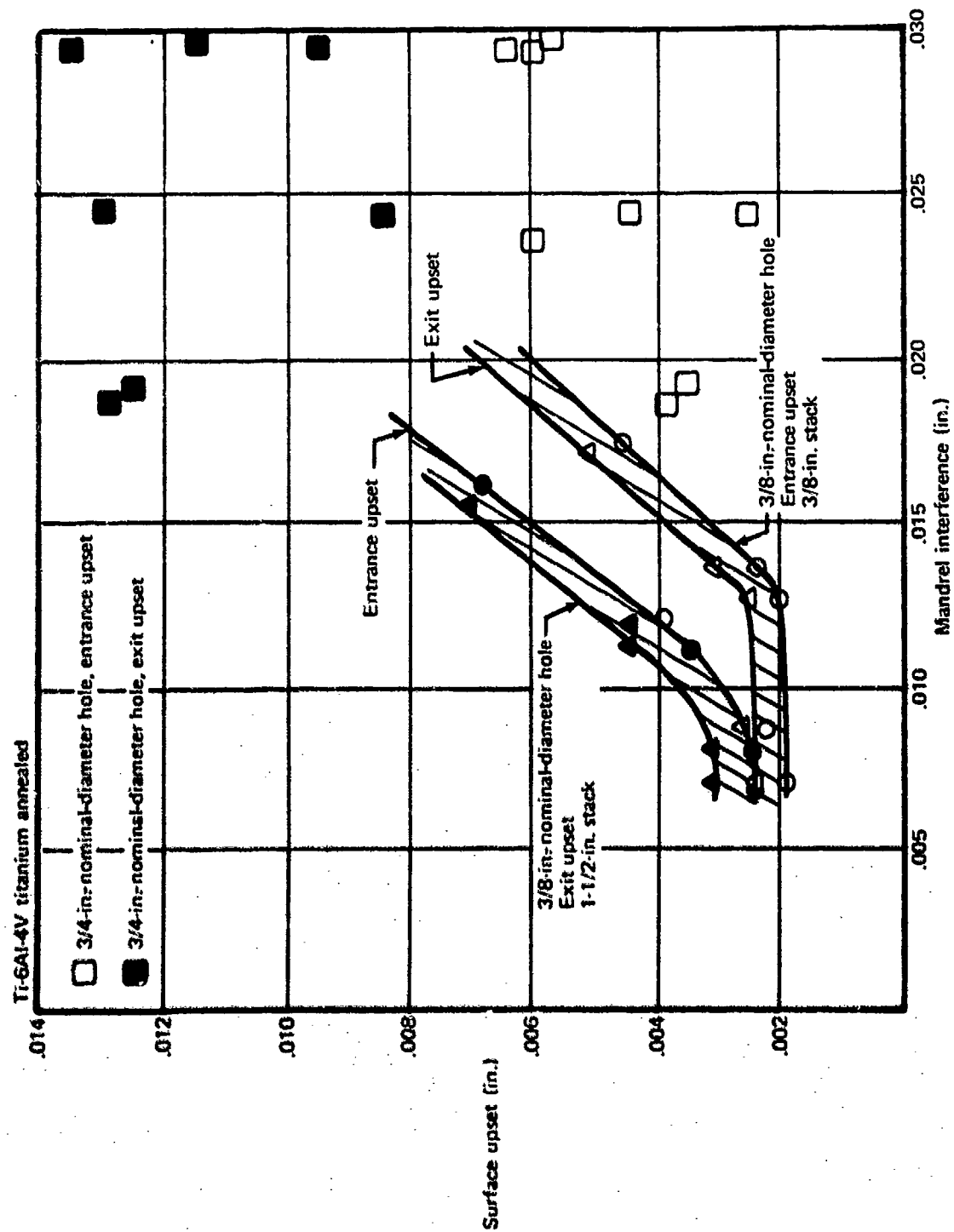
Figure 64. – Effect of Interference on Surface Upset

148

0.045 in./in. mandrel taper
0.0185-in.-hole interference

Exit upset

Entrance upset

Surface
upset
(in.)

Distance from hole edge (in.)
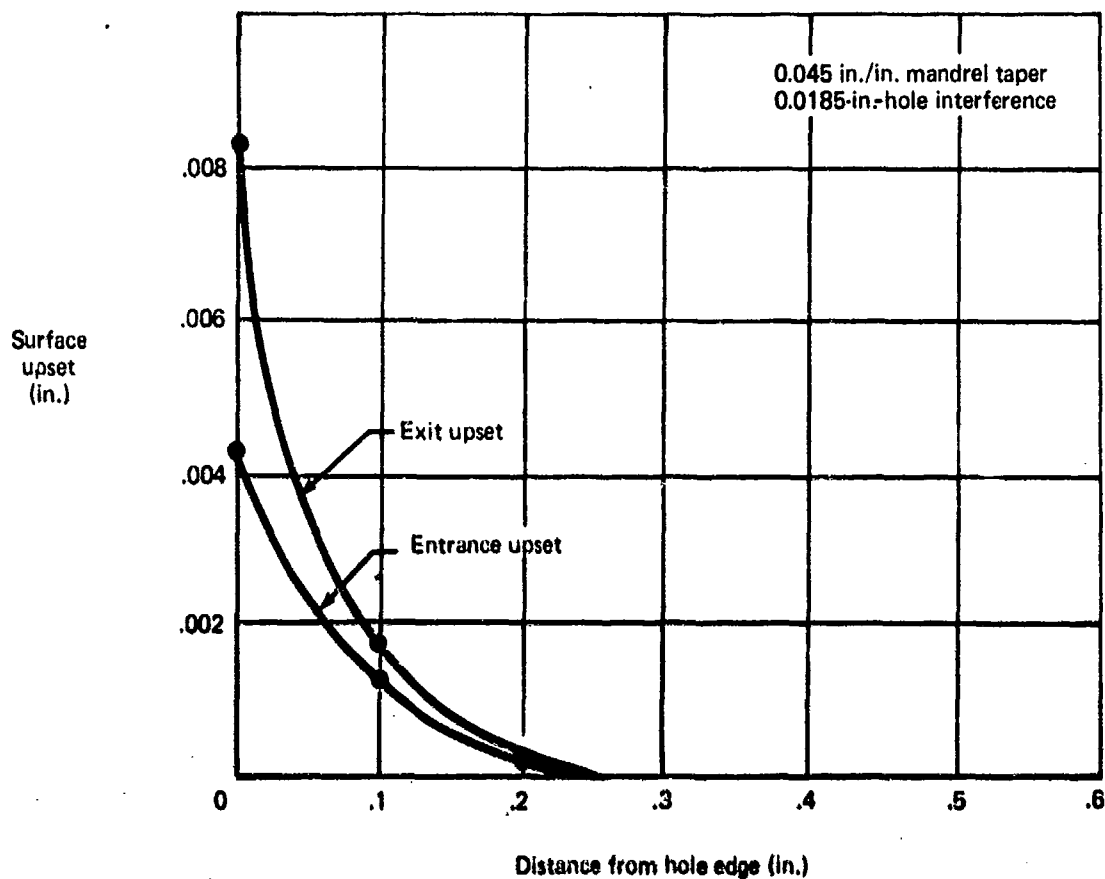
Figure 65.—Surface Upsetting—300M Steel, 270-300 KSI, 3/8-In.-Nominal-Diameter Hole

149
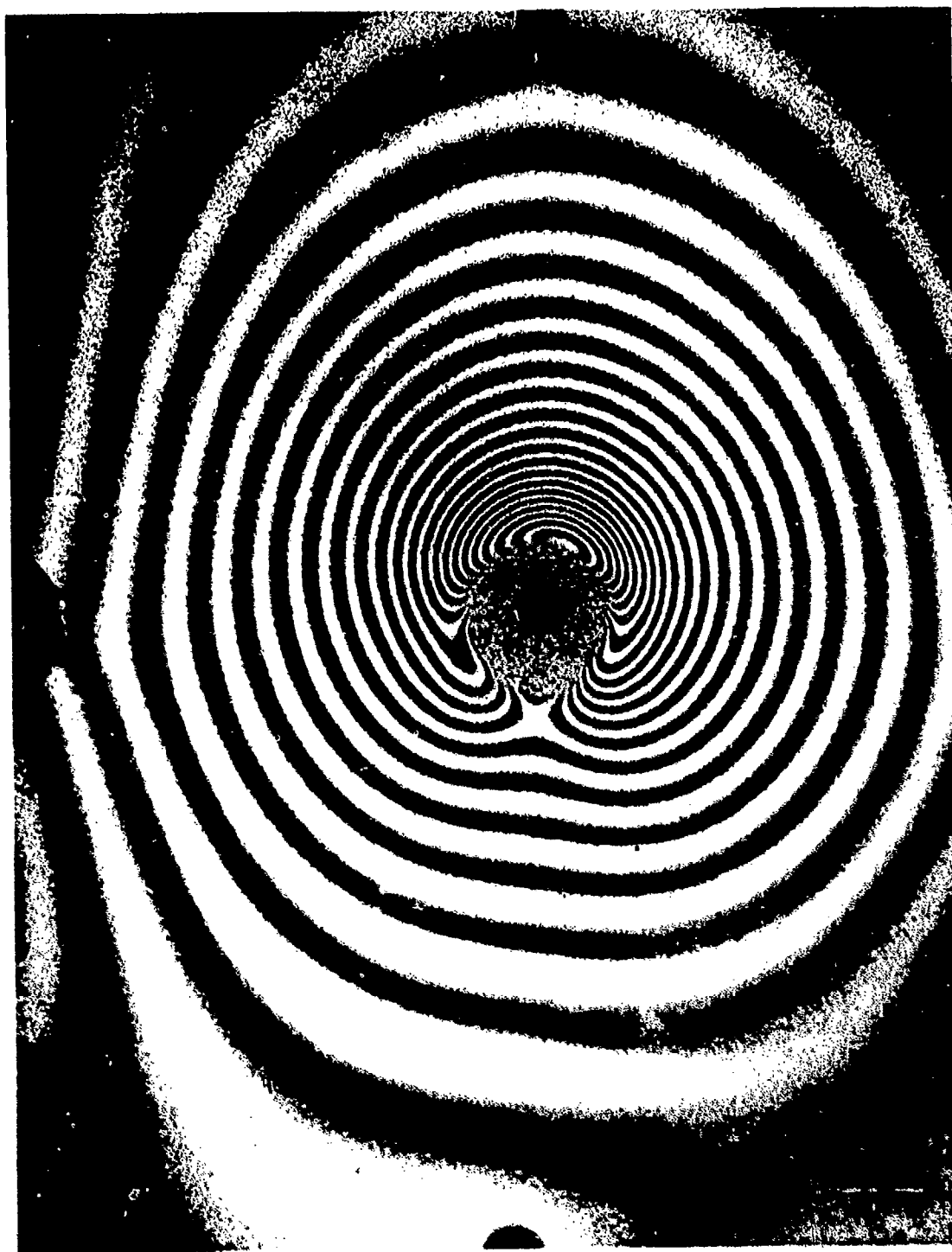
Figure 66. Laser Holograph of Coldwork Strain

Cycles to failure at 30 ksi maximum net stress
R = +0.1, K_t = 2.43

Coldworking interference (in.)	Nominal hole diameter
0.009	3/8
0.014	3/8
0.019	3/8
0.024	3/8
0.023	3/4
0.027	3/4
0.032	3/4
0.035	3/4
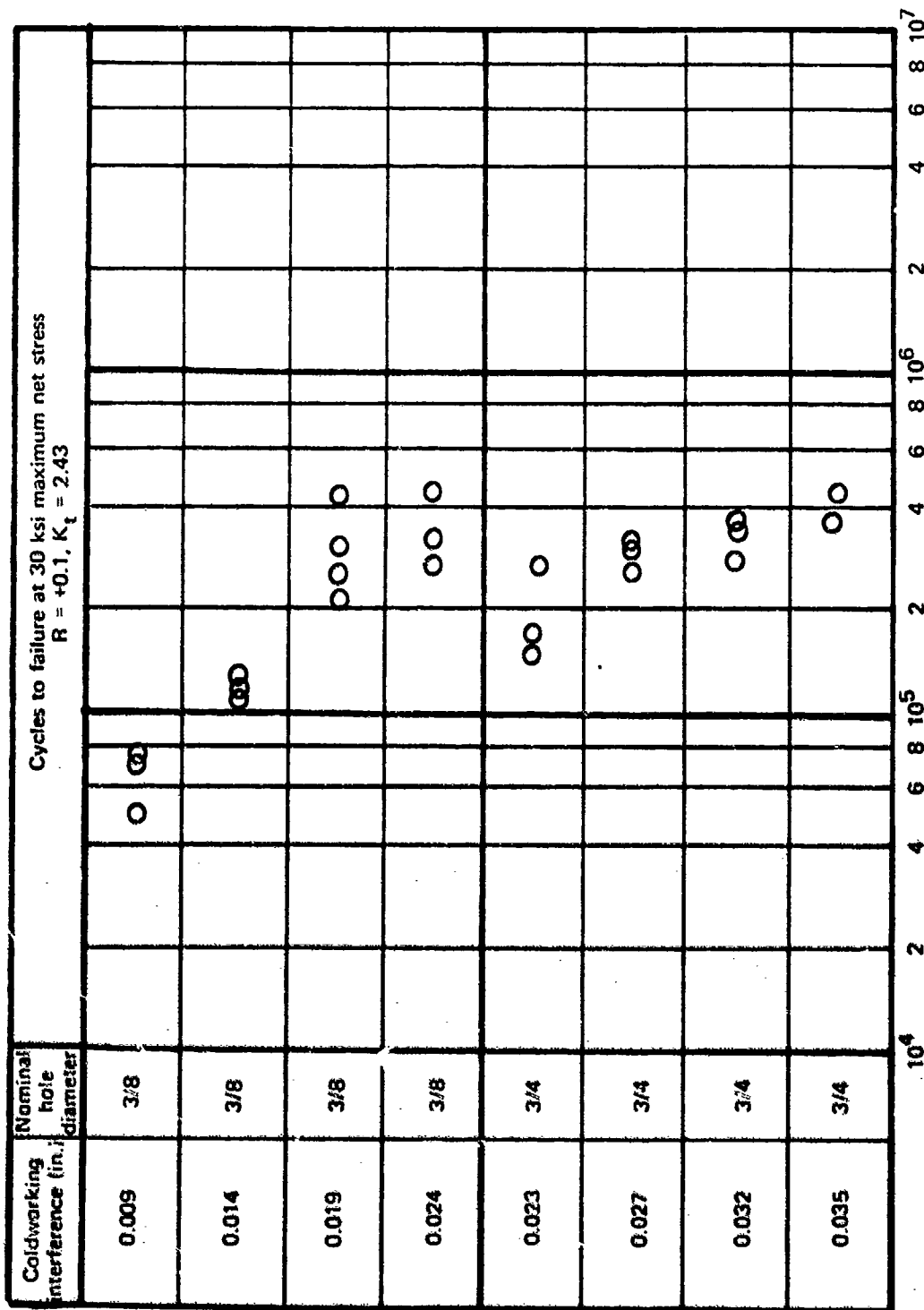
Coldworked and reamed open holes in specimens per figures 2 and 3

Figure 67.—Optimum Coldworking Interference Fatigue Tests—2024-T851
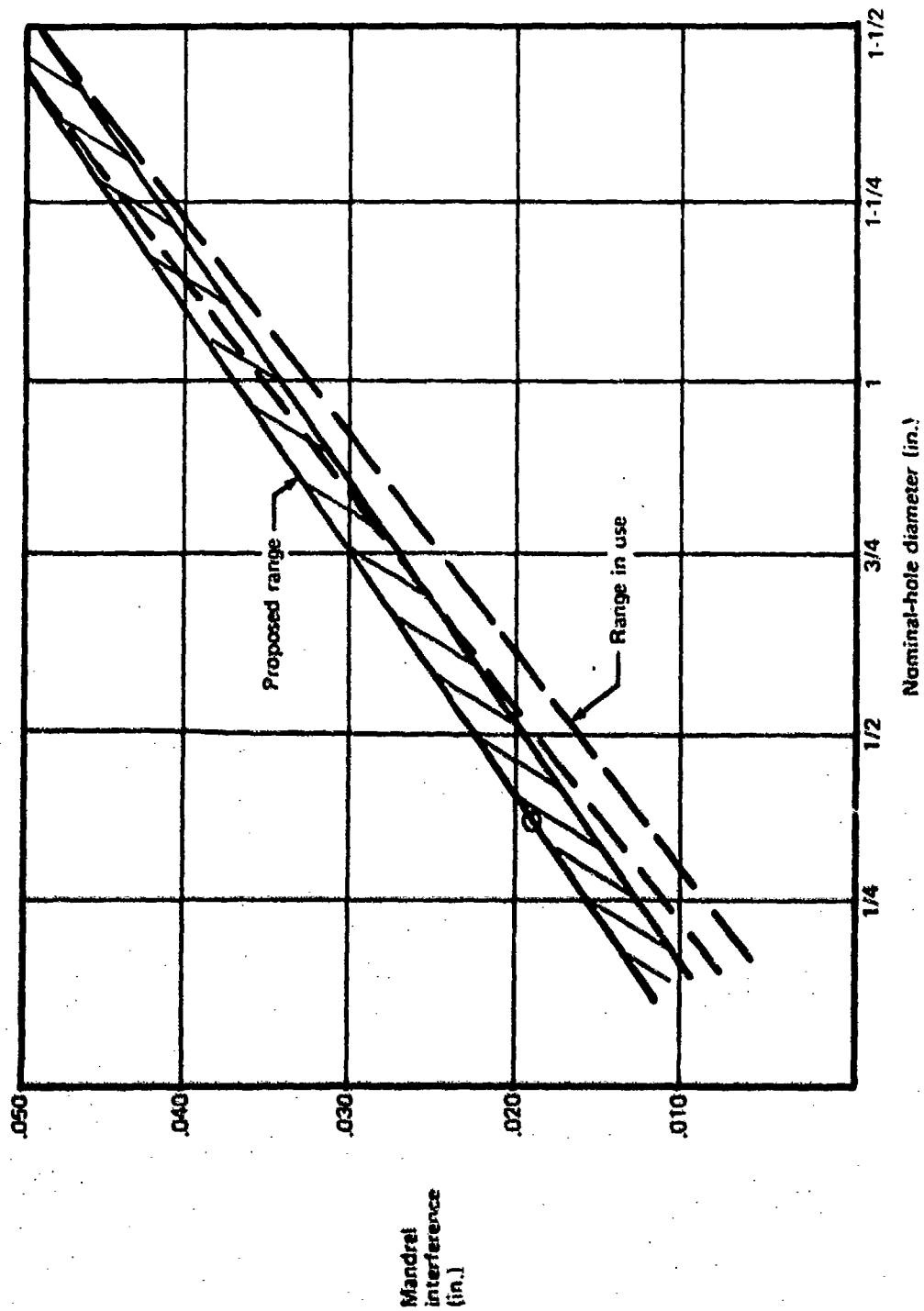
Figure 68.—Projected Optimum Mandrel Interference Versus Diameter—2024-T851 Aluminum

Cycles to failure at 110 ksi maximum net stress

R = +0.1, K_t = 2.43

Coldworking interference (in.)	Nominal hole diameter (in.)
0.009	3/8
0.145	3/8
0.019	3/8
0.021	3/8
0.023	3/8
0.0245	3/8
0.020	3/4
0.025	3/4
0.0295	3/4
0.0355	3/4

Specimens per figures 2 and 3

10^4 2 4 6 8 10^5 2 4 6 8 10^6 2 4 6 8 10^7
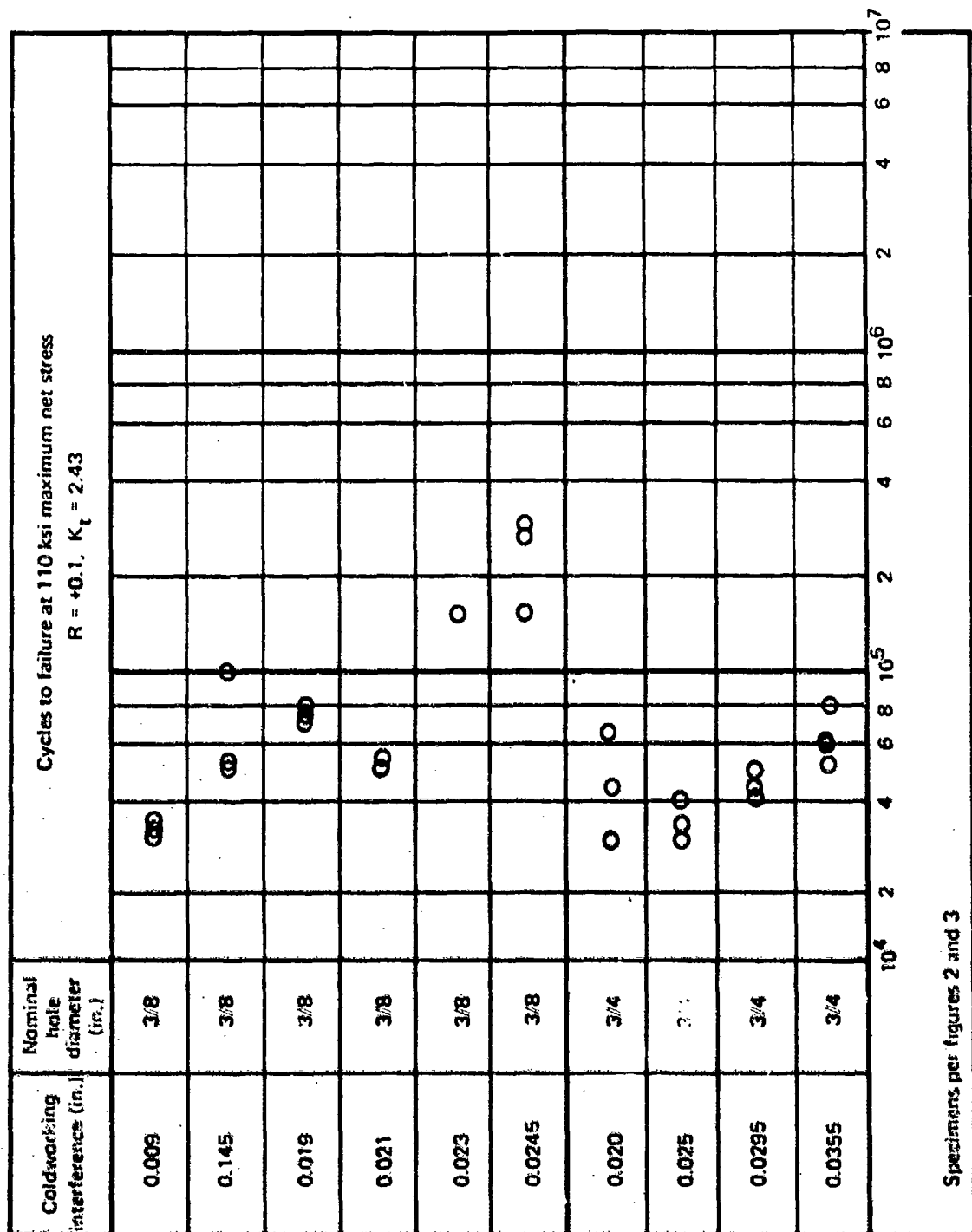
Figure 69.—Optimum Coldworking Interference Fatigue Tests— 300M Steel, 270-300 KSI
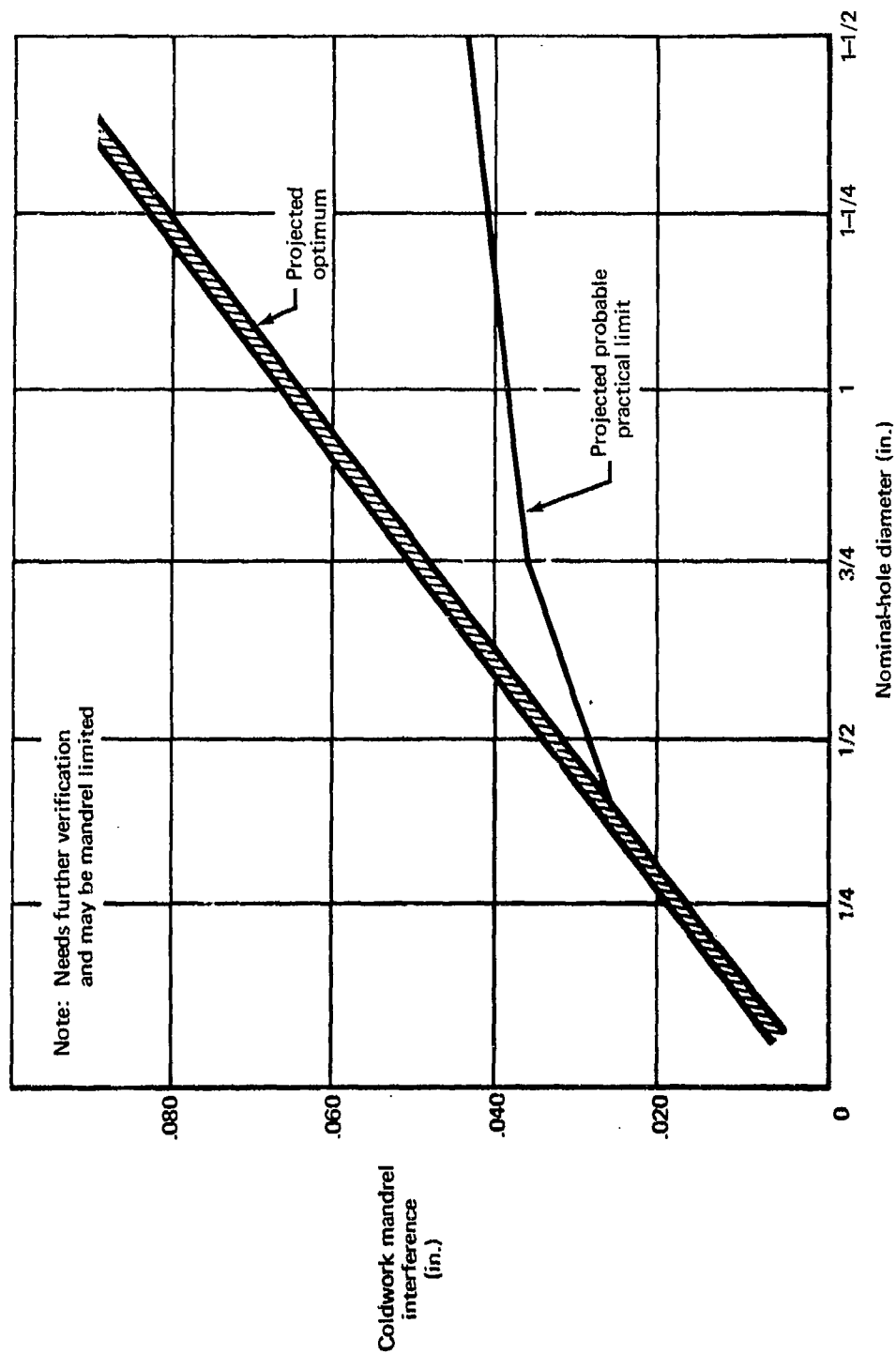
Figure 70. —Projected Optimum Mandrel Interference—300M Steel, 270-300 KSI
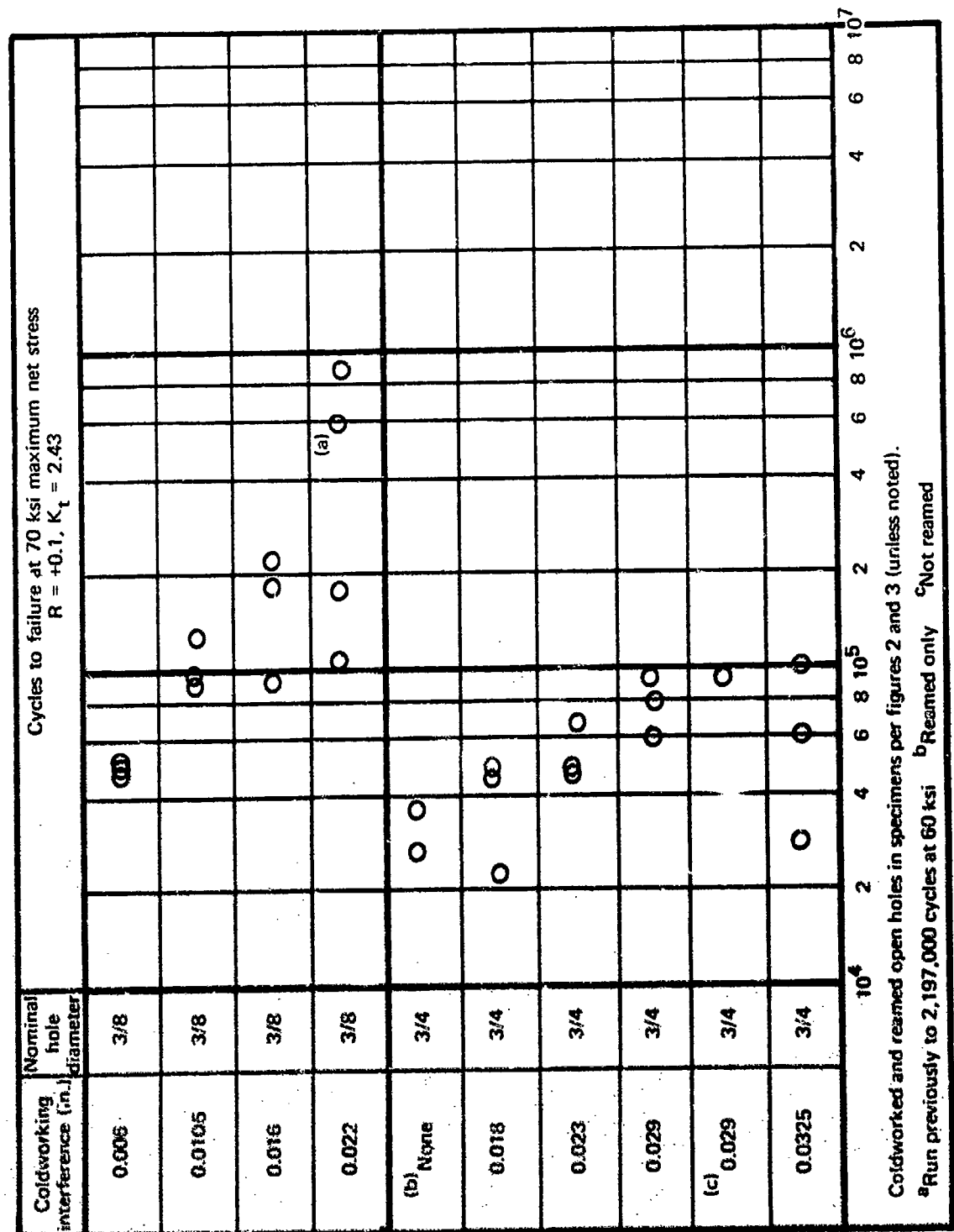
Figure 71.—Optimum Coldworking Interference Fatigue Tests—Ti-6Al-4V, Annealed

Coldworked and reamed open holes in specimens per figures 2 and 3 (unless noted).
[a] Run previously to 2,197,000 cycles at 60 ksi   [b] Reamed only   [c] Not reamed
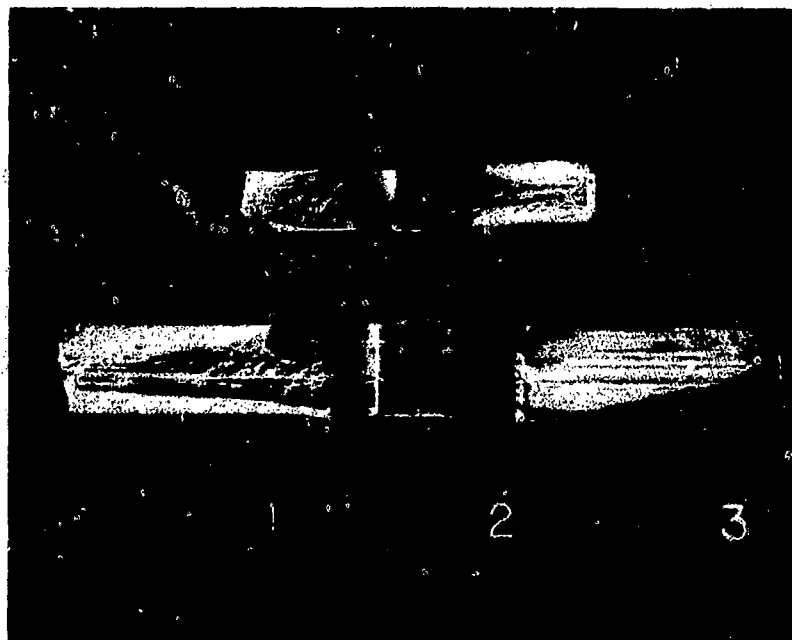
Figure 72.--Photo of Fatigue Fracture Faces 3/8-In.-Diameter Hole and 3/4-In.-Diameter Hole, Ti-6Al-4V Specimens

LABORATORY TEST RECORD L40-141   JOB NO. ___7038___

REF. _____

ASSIGNED TO _____ REQ BY _____ DATE _____

SPEC _____ BATCH/LOT NO _____

MATERIAL _____ PART NC _____

SOURCE _____ WORK ORDER _____ MODEL _____

P O _____ R R NO _____ DATE REC D _____ QTY _____

Sample	H %	O	Al	V	Fe	T
IIJ2	0.0038	0.14	6.3	4.2	0.14	3/4 in. hole
IIN1	0.0055	0.16	6.2	3.8	0.18	3/8 in. hole

MATERIAL CODE NC _____ SAMPLE SIZE _____ DATE REQUESTED _____

Figure 73. –Spectographic Analysis of Ti-6Al-4V Specimens
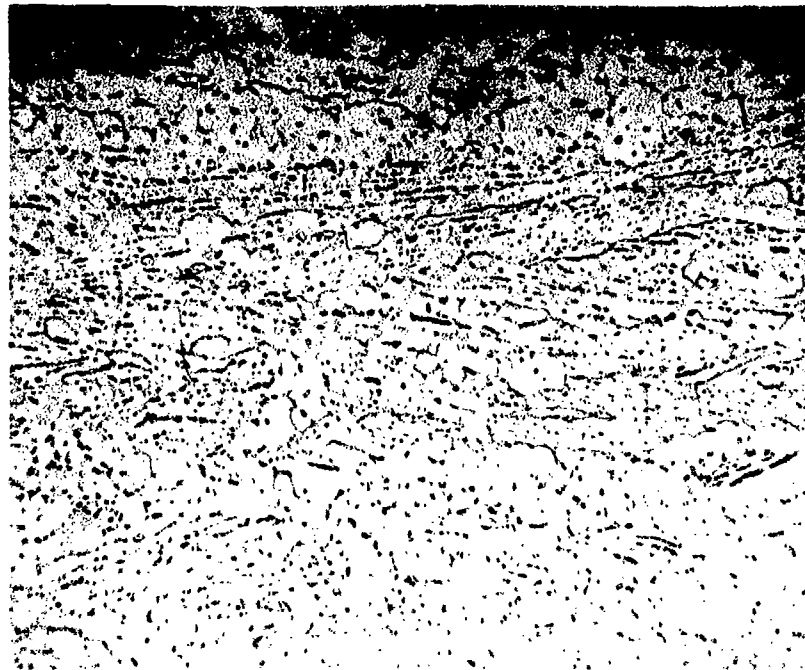
Longitudinal Section--Ti-6Al-4V, Annealed
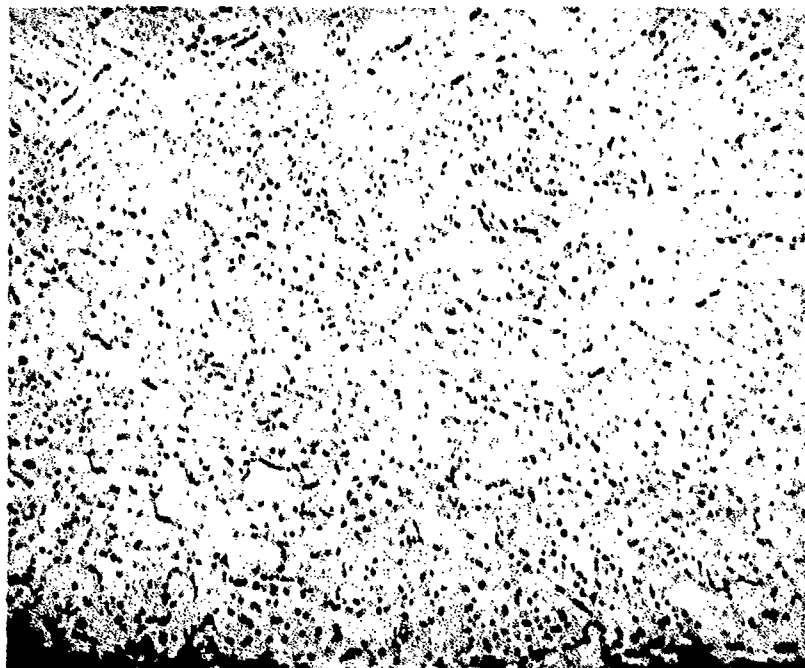
Transverse Section - Ti-6Al-4V, Annealed

Figure 74.—Metallurgical Sections—3/8-In.-Diameter Hole Specimen (500X)

Longitudinal Section—Ti-6Al-4V, Annealed
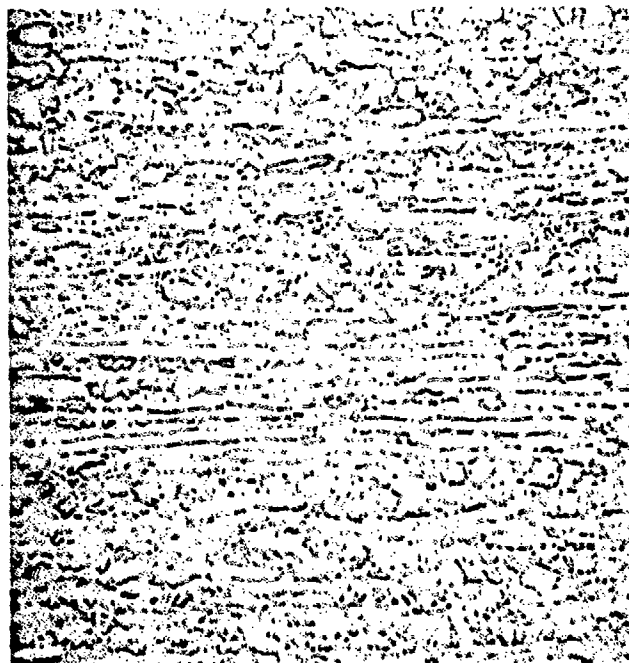
Transverse Section   Ti-6Al-4V, Annealed

Figure 75.—Metallurgical Sections—3/4-In.-Diameter Hole Specimen (500X)

Ductile ← ⊕ → Fatigue   15X

1400X of above
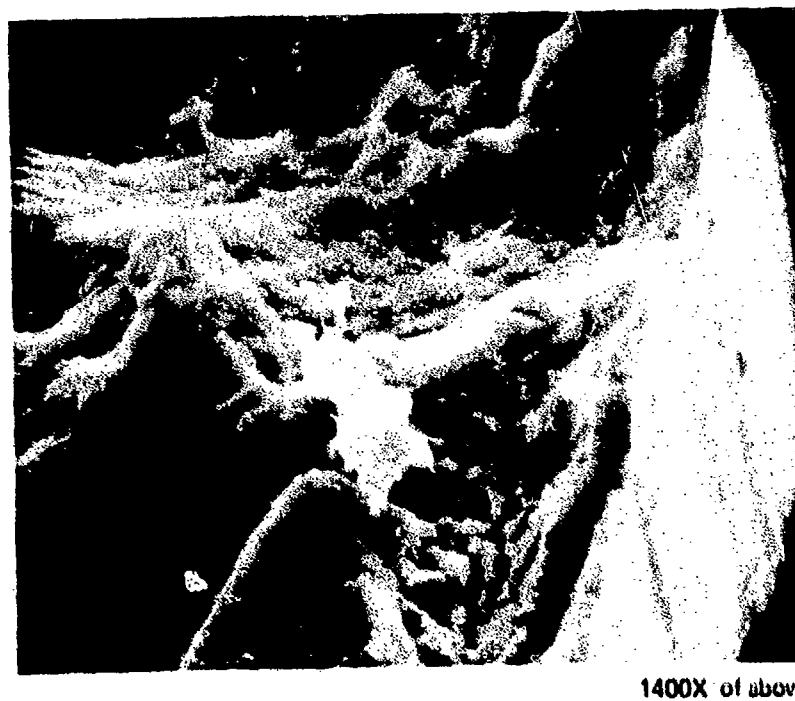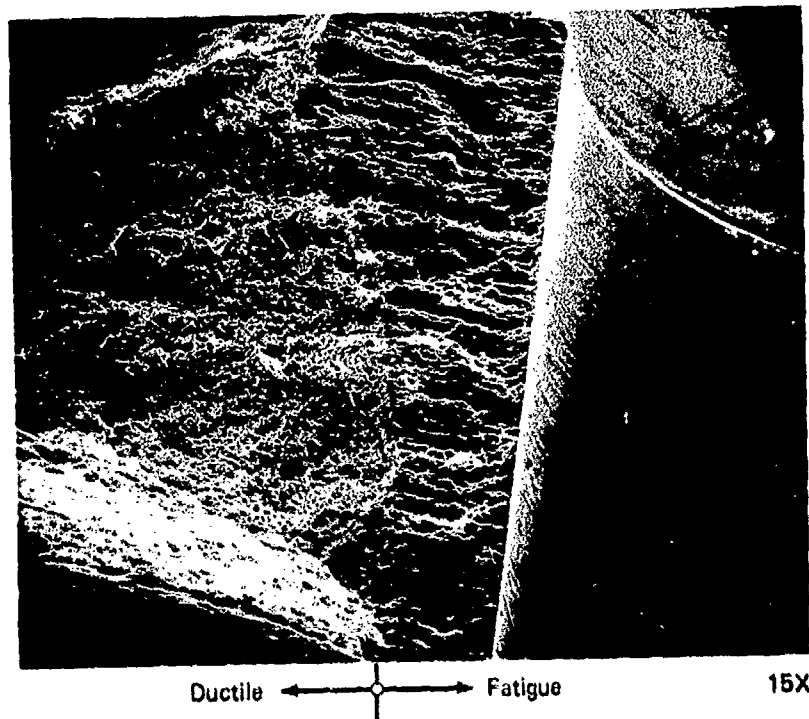
Figure 76. 3/8-In.-Diameter Hole Ti-6Al-4V Specimen

Fatigue ←——————→ Ductile

1

2

300X

2
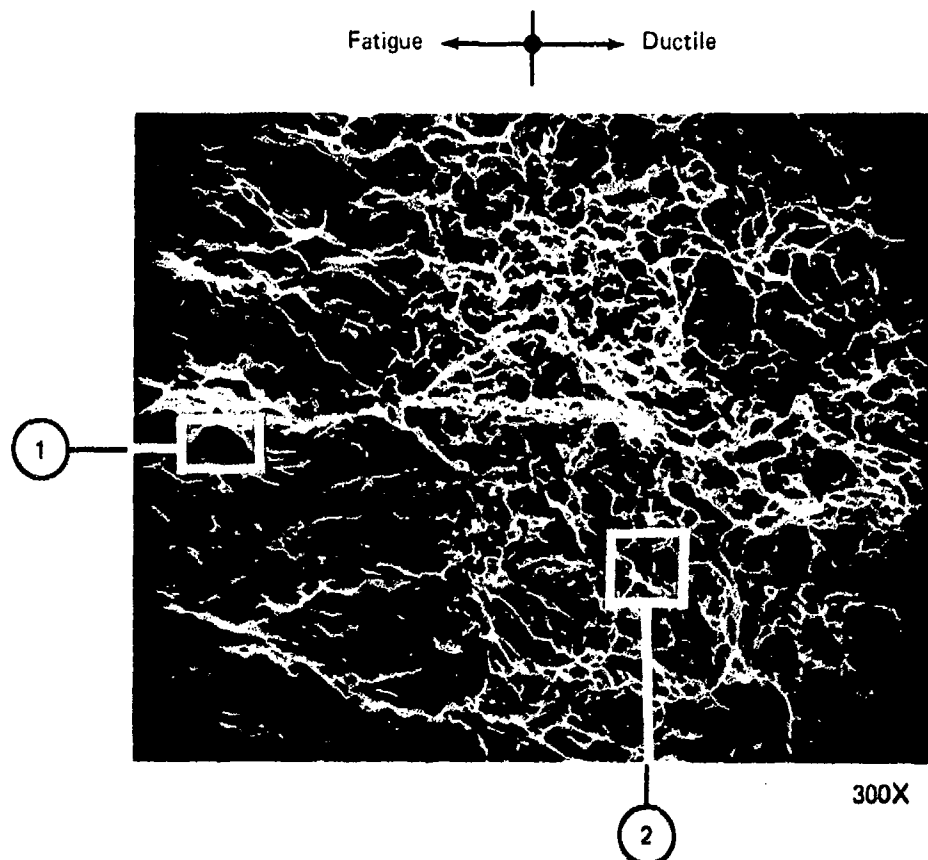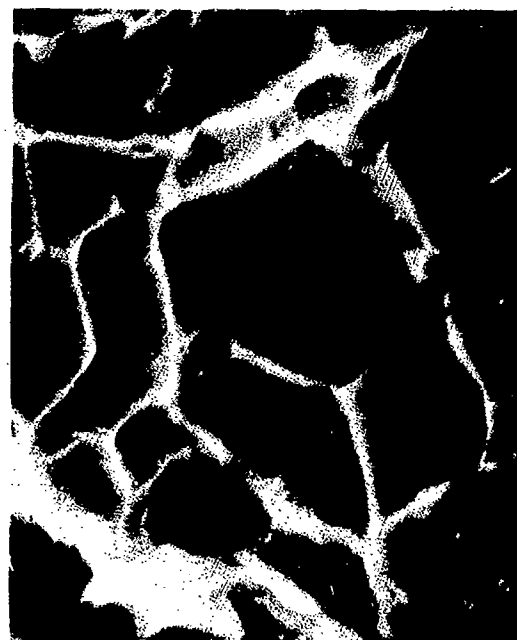
Fatigue Zone (1)   3000 X   Ductile Zone (2)   3000 X

Figure 77. Fatigue/Ductile Transition 3/8-In.-Diameter Hole, Ti-6Al-4V Specimen

10 X

Corner ⓑ 200 X

Fatigue Area ⓒ 2000 X
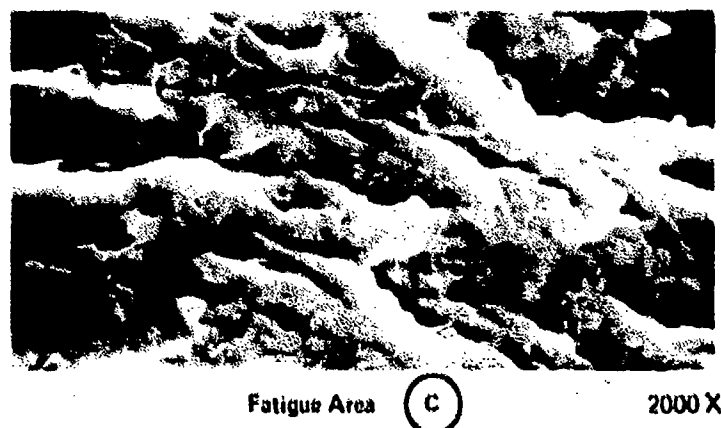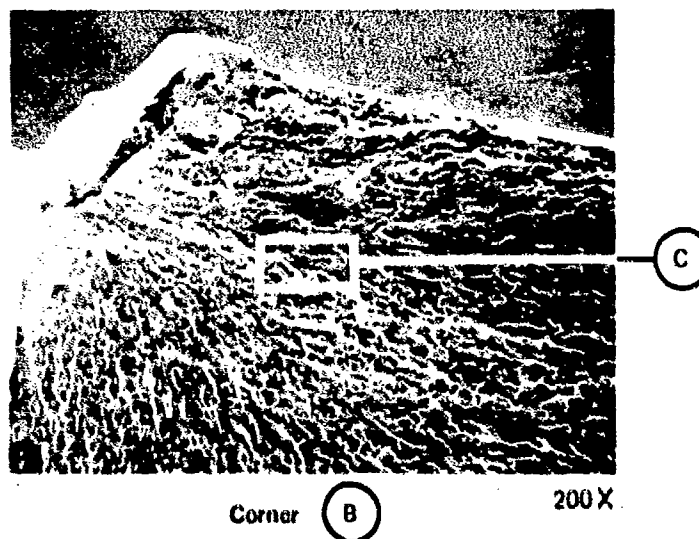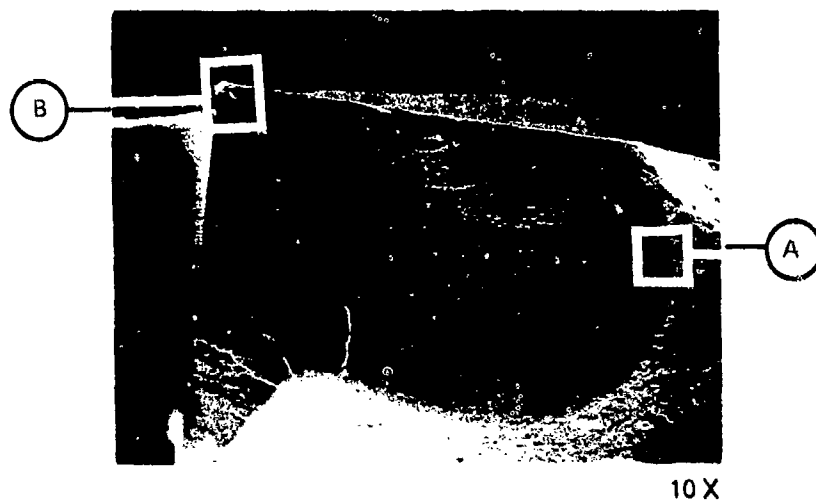
Figure 78. 3/4-In.-Diameter Hole - Ti-6Al-4V Specimen

Fatigue ← ● → Ductile

Fatigue/Ductile Transition (A) of Figure 78   200X

Fatigue Zone (D)   2000 X

Ductile Zone (E)   2000X
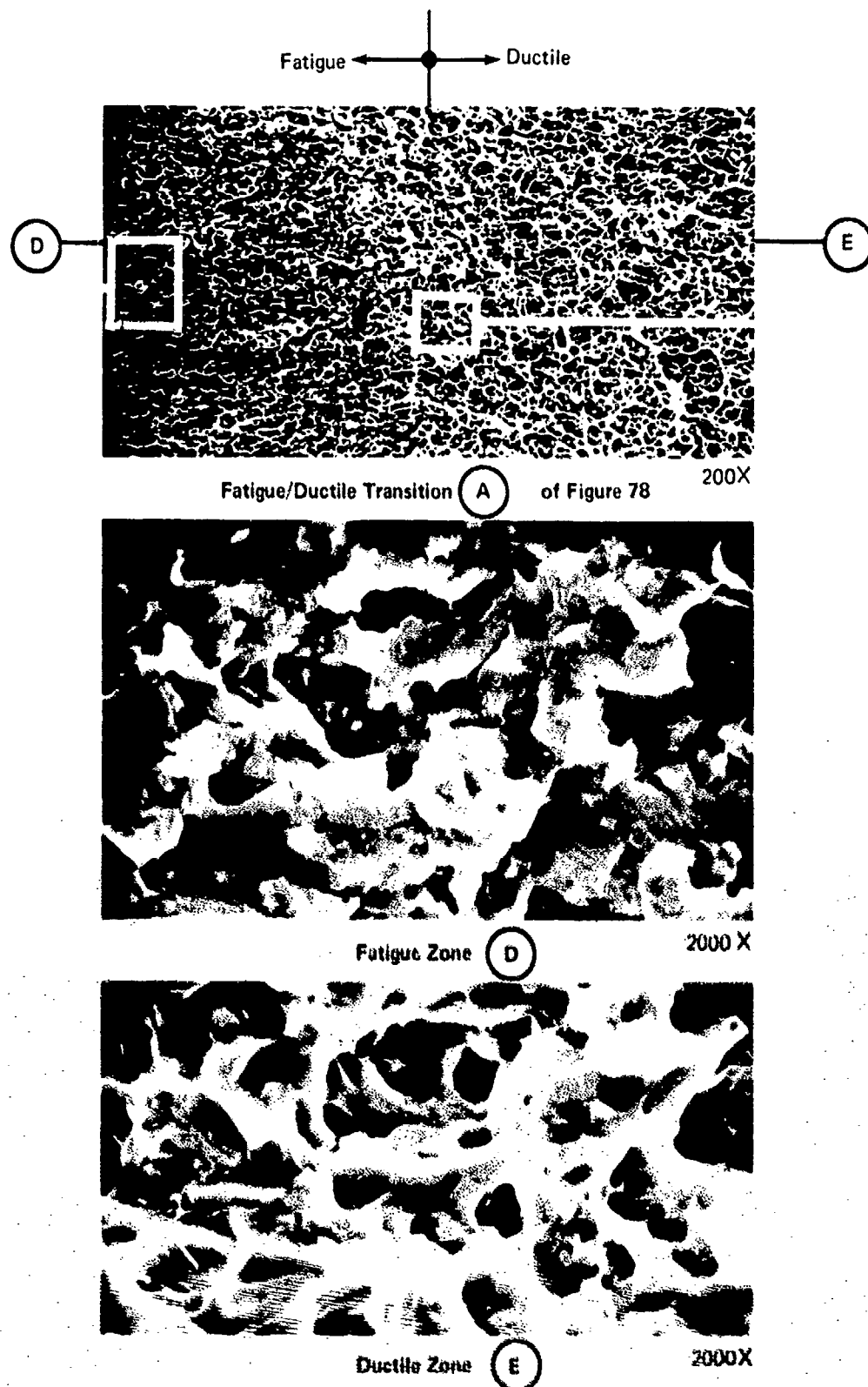
Figure 79. 3/4-In.-Diameter Hole Ti-6Al-4V Specimen Across Fatigue/Ductile Transition

163
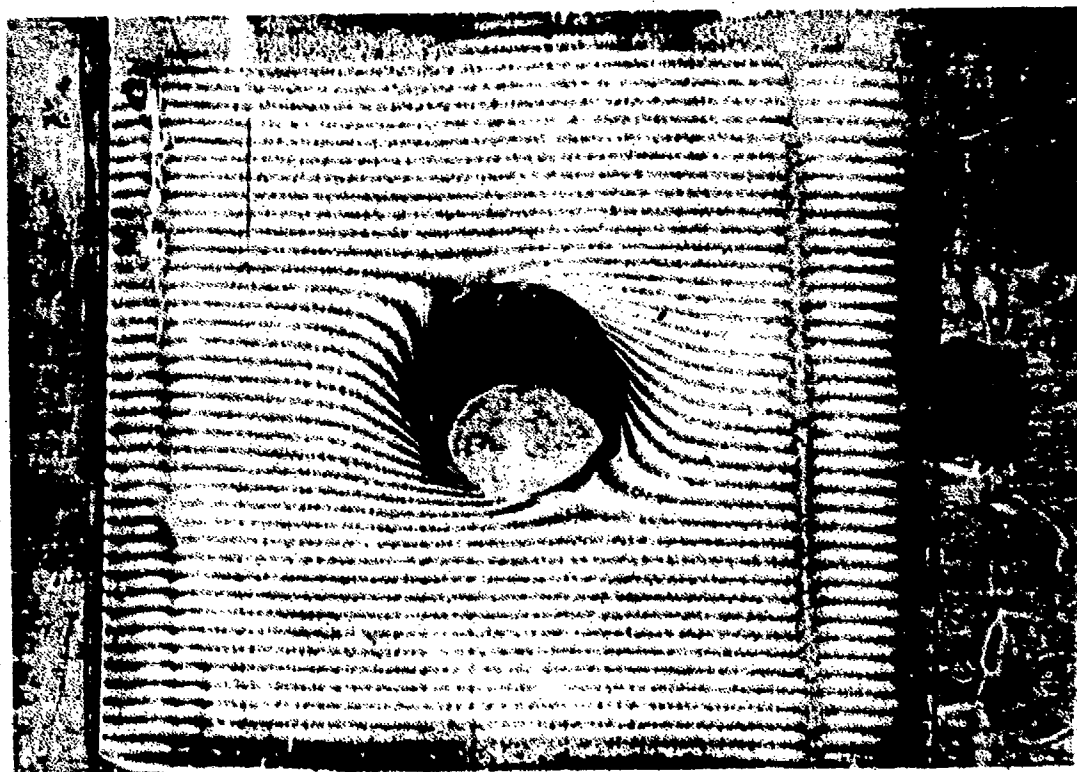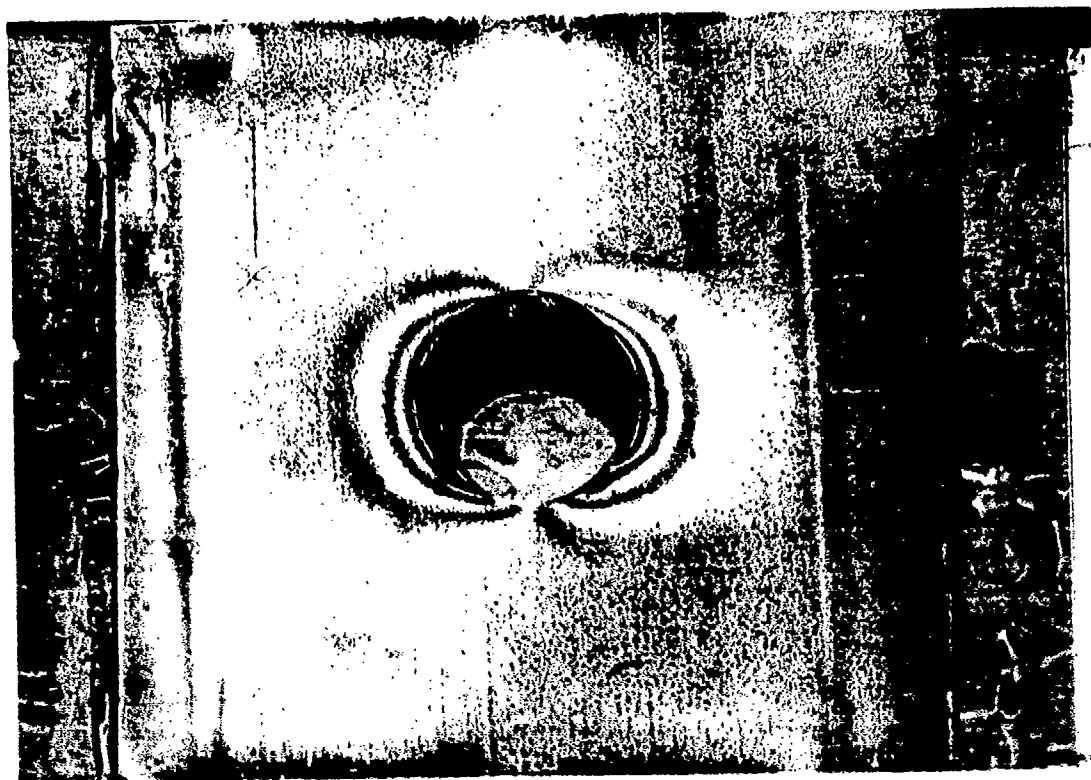
Figure 80. Moire Strain Tests

R = radial
T = tangential

Average strain (in.): .080, .060, .040, .020

Hole side	Entrance	Exit	Entrance	Exit	Entrance	Exit	Entrance	Exit
Coldwork interference (in.)	0.30	0.030	0.030	0.019	0.019	0.030	0.030	0.019
Average affected zone	0.40	0.40	0.55	0.40	0.40	0.75	0.40	0.40
Hole diameter (in.)	3/8	3/8	3/4	3/8	3/8	3/4	3/8	3/8
Material	2024-T851				Ti-6Al-4V, annealed		300M (270-300 ksi)	
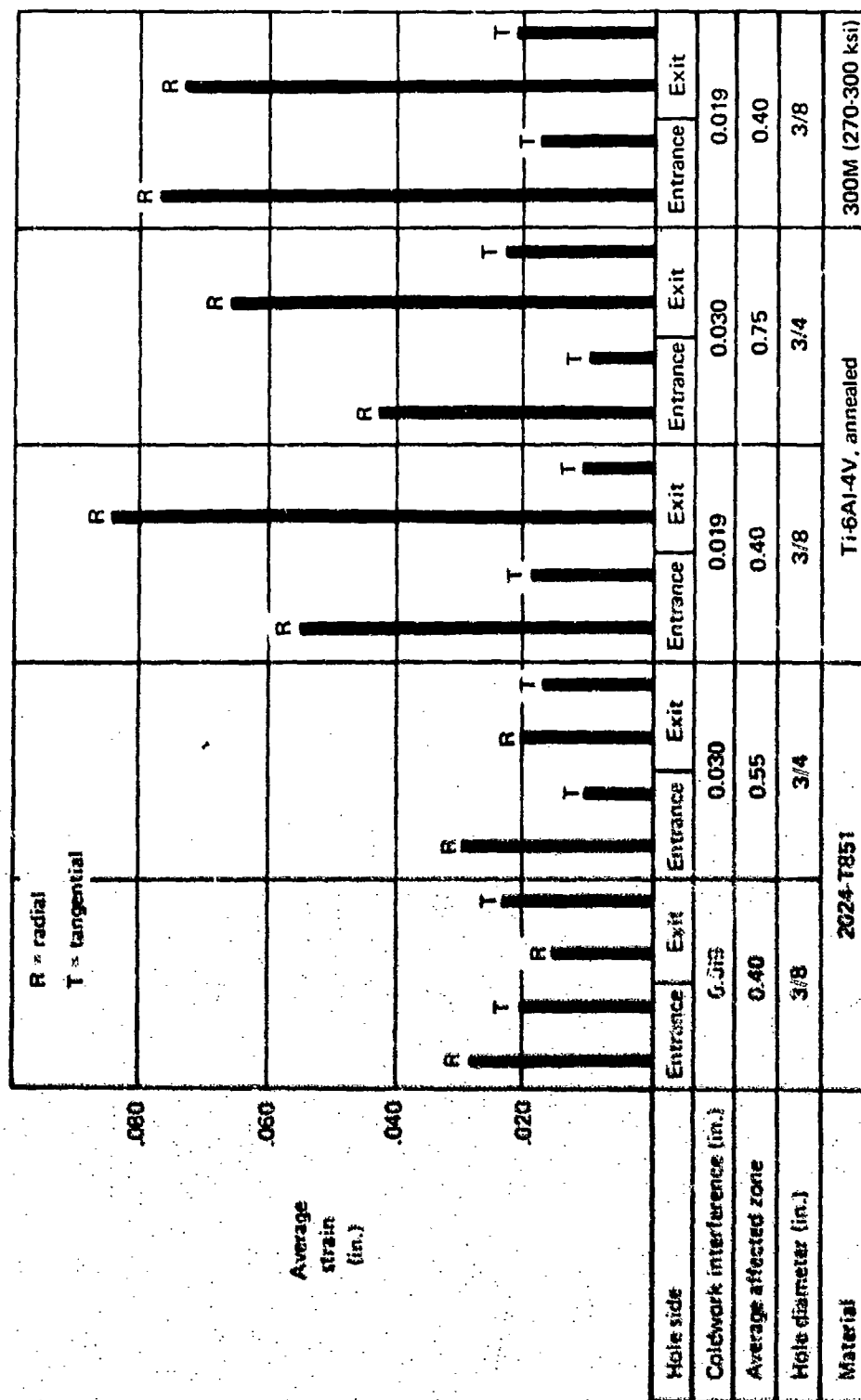
Figure 81. — Moire Strain Data

NDT INFORMATION REPORT

REQUESTED BY: _____J. Phillips_____   DATE __3-7-73__

ORGANIZATION: _____6-7310_____   PHONE:_____237-7155_____

OBJECTIVE: Search for cracks around holes as marked on two parts provided.

REFERENCE: Request to M. L. Phelps, 2-19-73

SUMMARY:

Subject parts were inspected by use of eddy current using both the ED-520 and the NDT-6 instruments and by using three different penetrant inspection methods, which included use of fluorescent and Hi-Rez penetrant in both standard application and special application methods ("wink" method).

No cracks were detected by any of the inspection methods.

Engineer: _____

Lead Engineer: _____

Supervisor: _____

CC: Ron Neufeld

Figure 82.—NDT Information Report
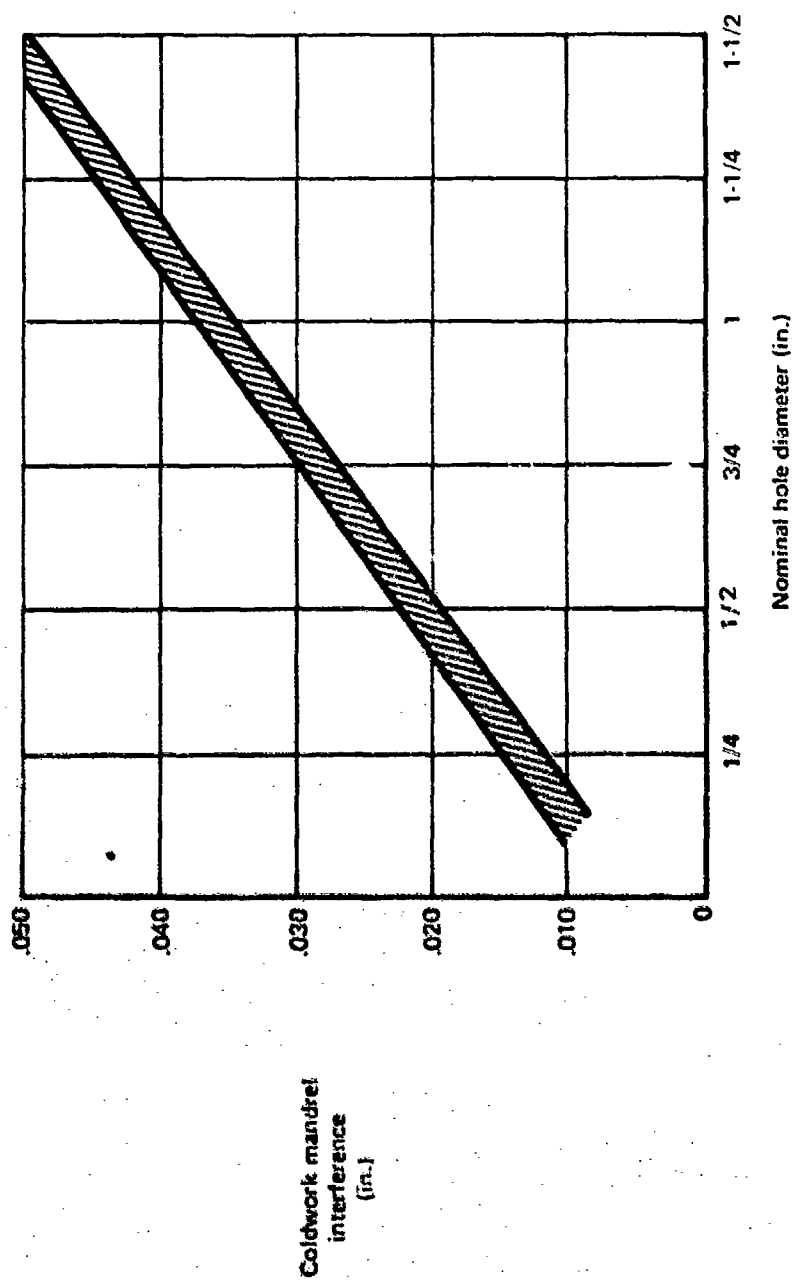
Figure 83.—Projected Optimum Mandrel Interference—Ti-6Al-4V, Annealed
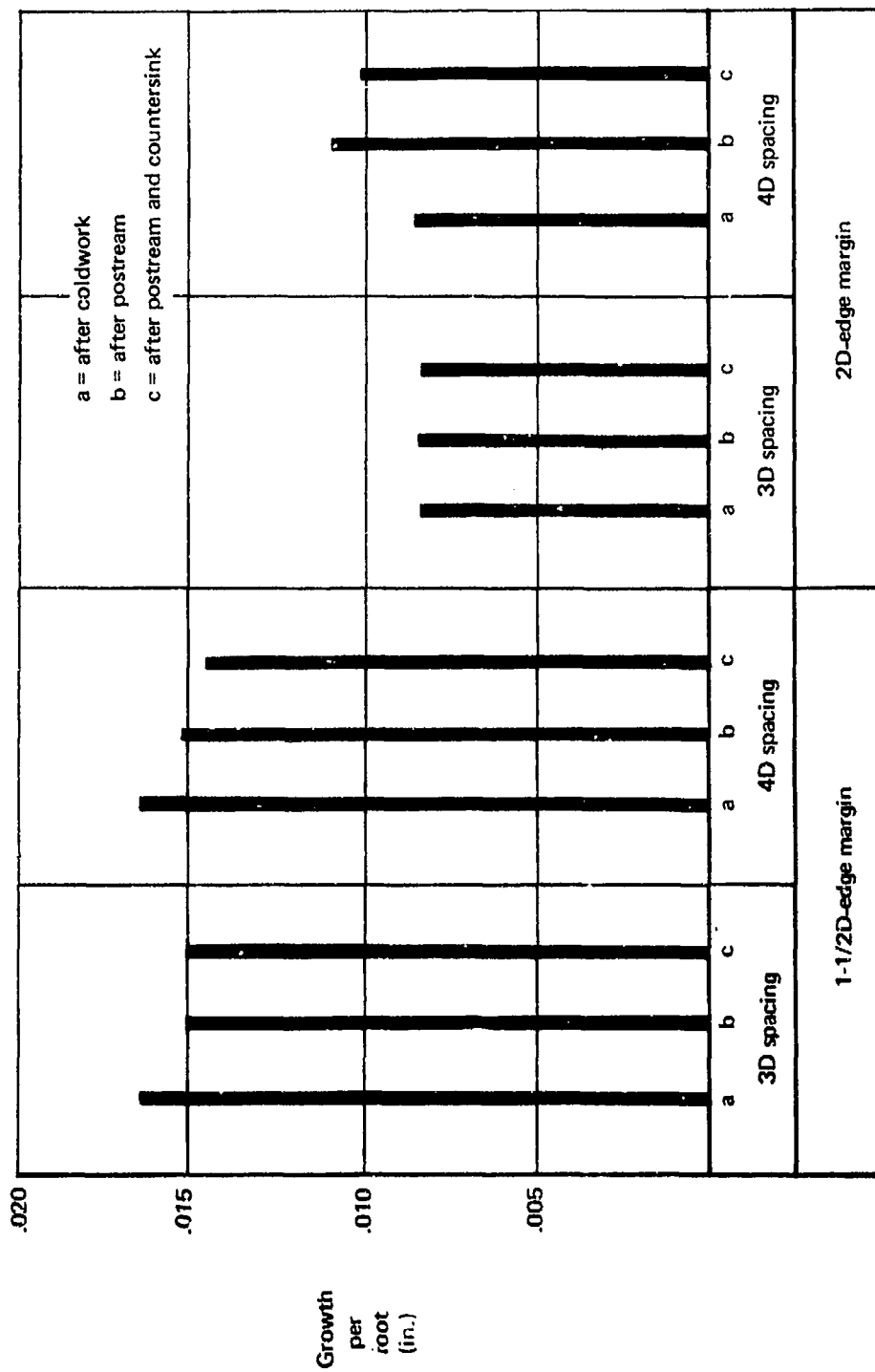
Figure 84.—Lineal Growth—3/8-In. Plate, 3/8-In.-Diameter Holes, 0.019-In. Interference, 2024-T851
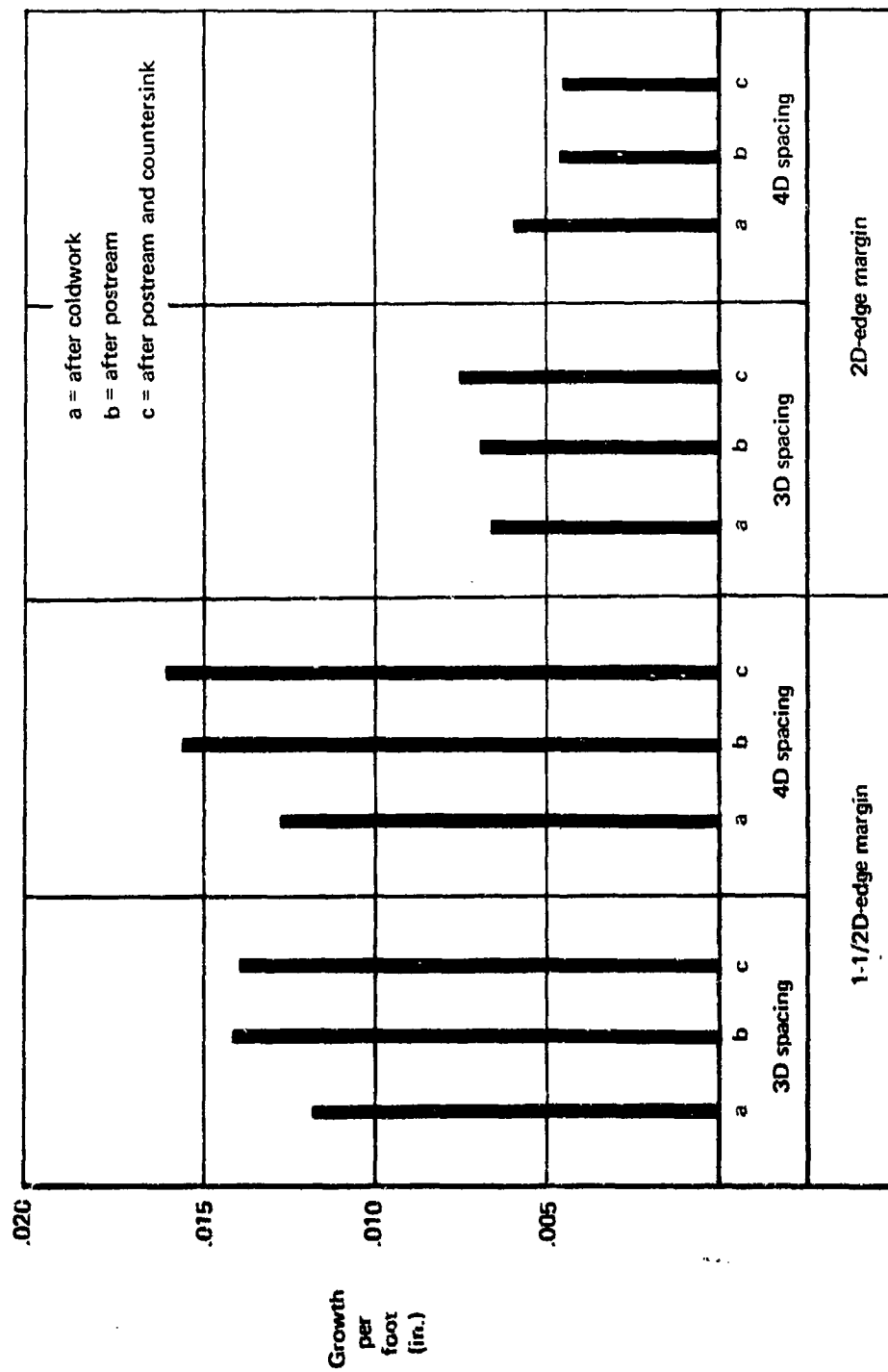
Figure 85. — Lineal Growth – 3/4-In. Plate. 3/4-In.-Diameter Hole. 0.030-In. Interference. 2024-T851
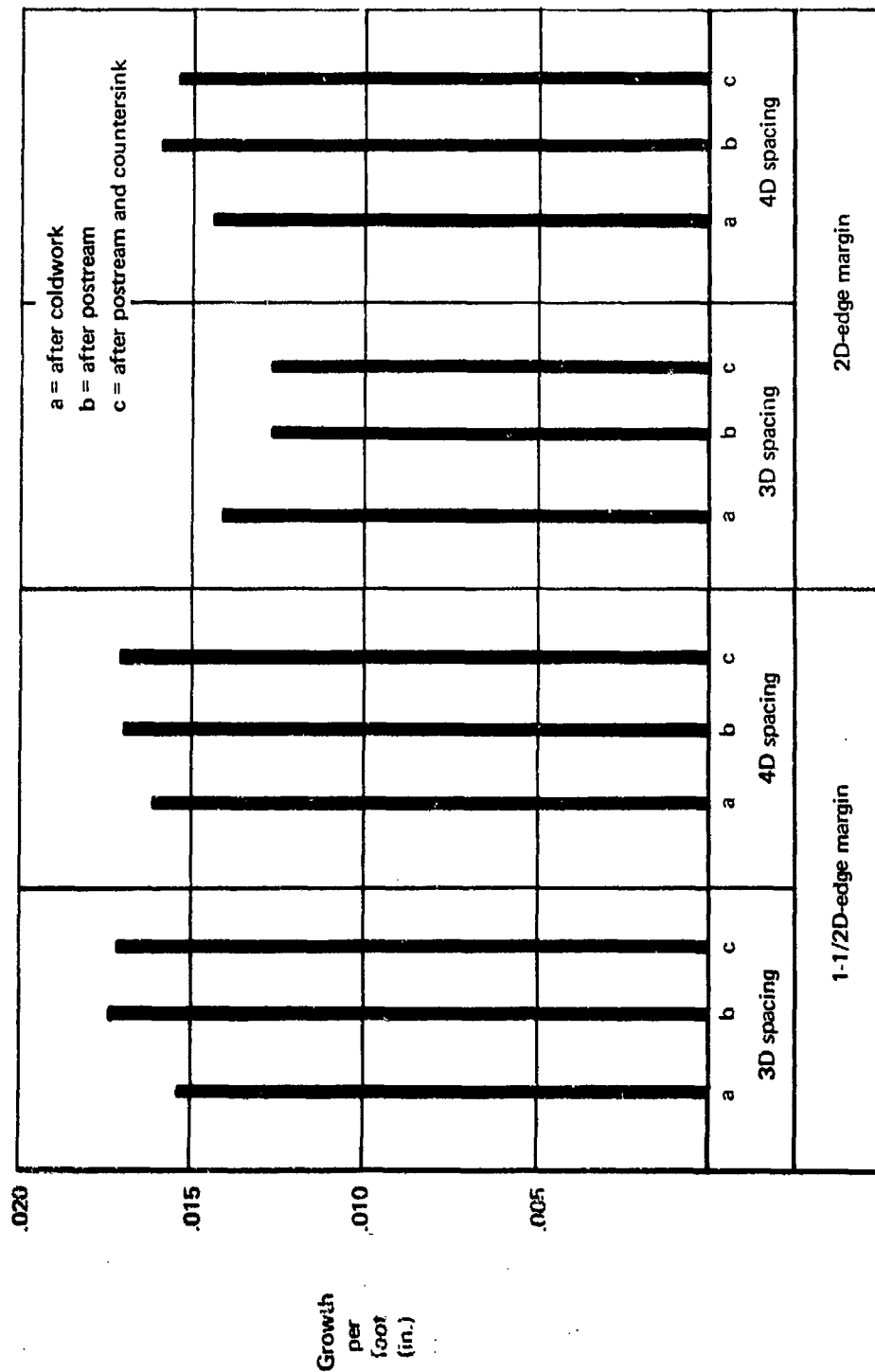
Figure 86. – Lineal Growth–3/8-In. Plate, 3/8-In.-Diameter Hole, 0.018-In. Interference, Ti-6Al-4V
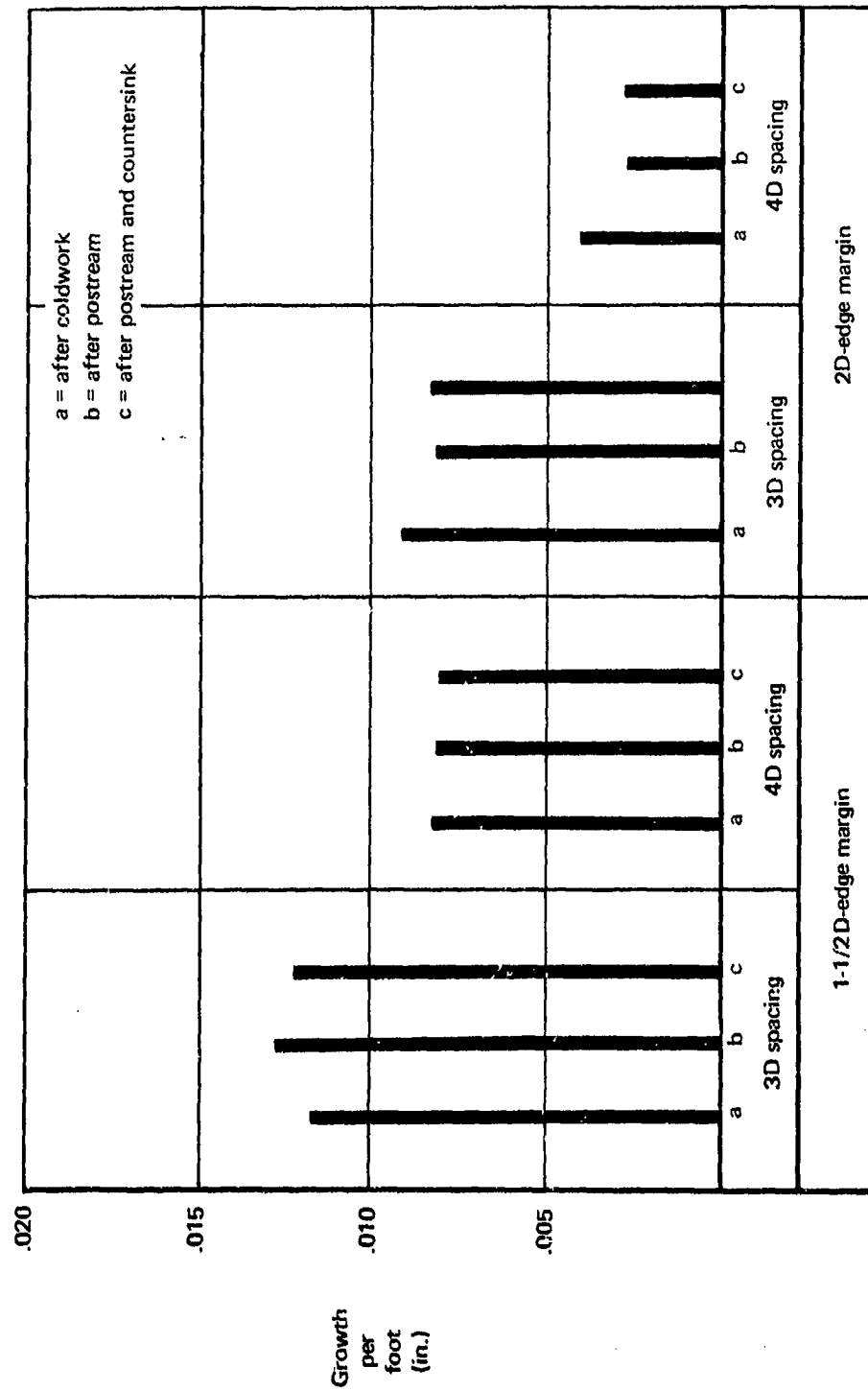
Figure 87. – Lineal Growth – 3/4-In. Plate. 3/4-In.-Diameter Hole. 0.029-In. Interference. Ti-6Al-4V
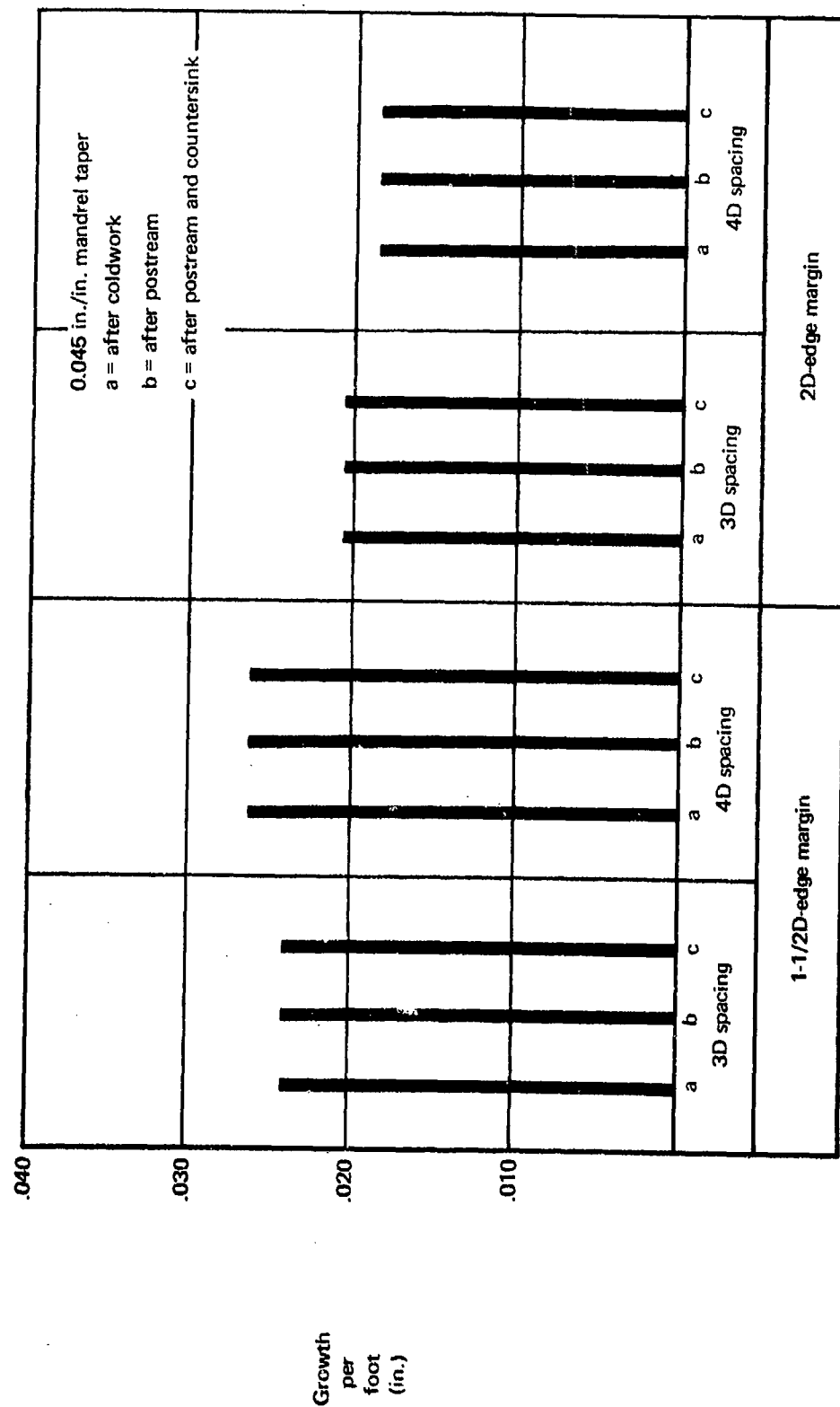
Figure 88.–Lineal Growth–3/8-In.-Diameter Hole, 0.023-In. Interference, 300M Steel (270-300 KSI)

172
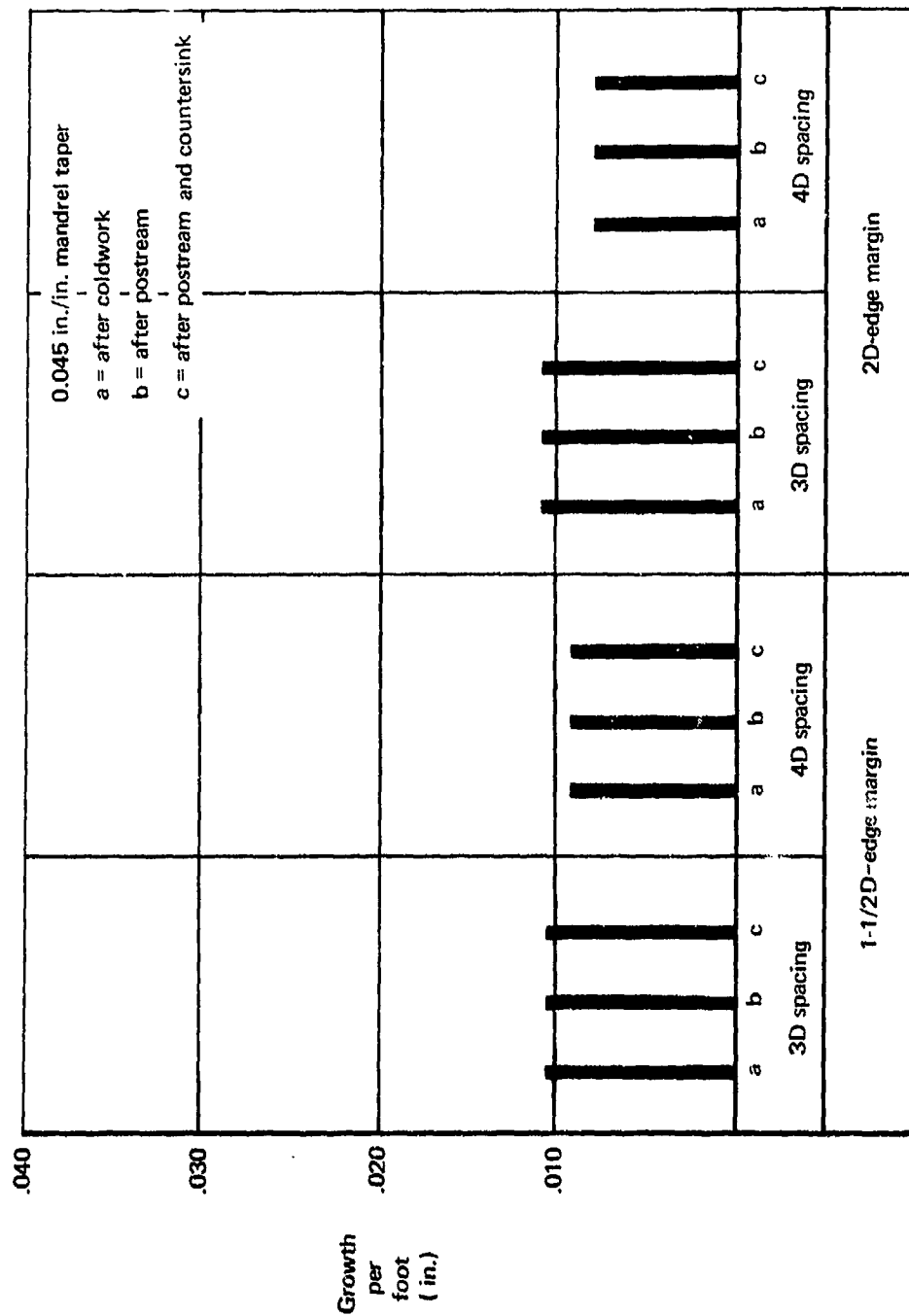
Figure 89.—Lineal Growth—3/4-In. Plate, 3/4-In.-Diameter Hole, 0.030-In. Interference, 300M Steel (270–300 KSI)
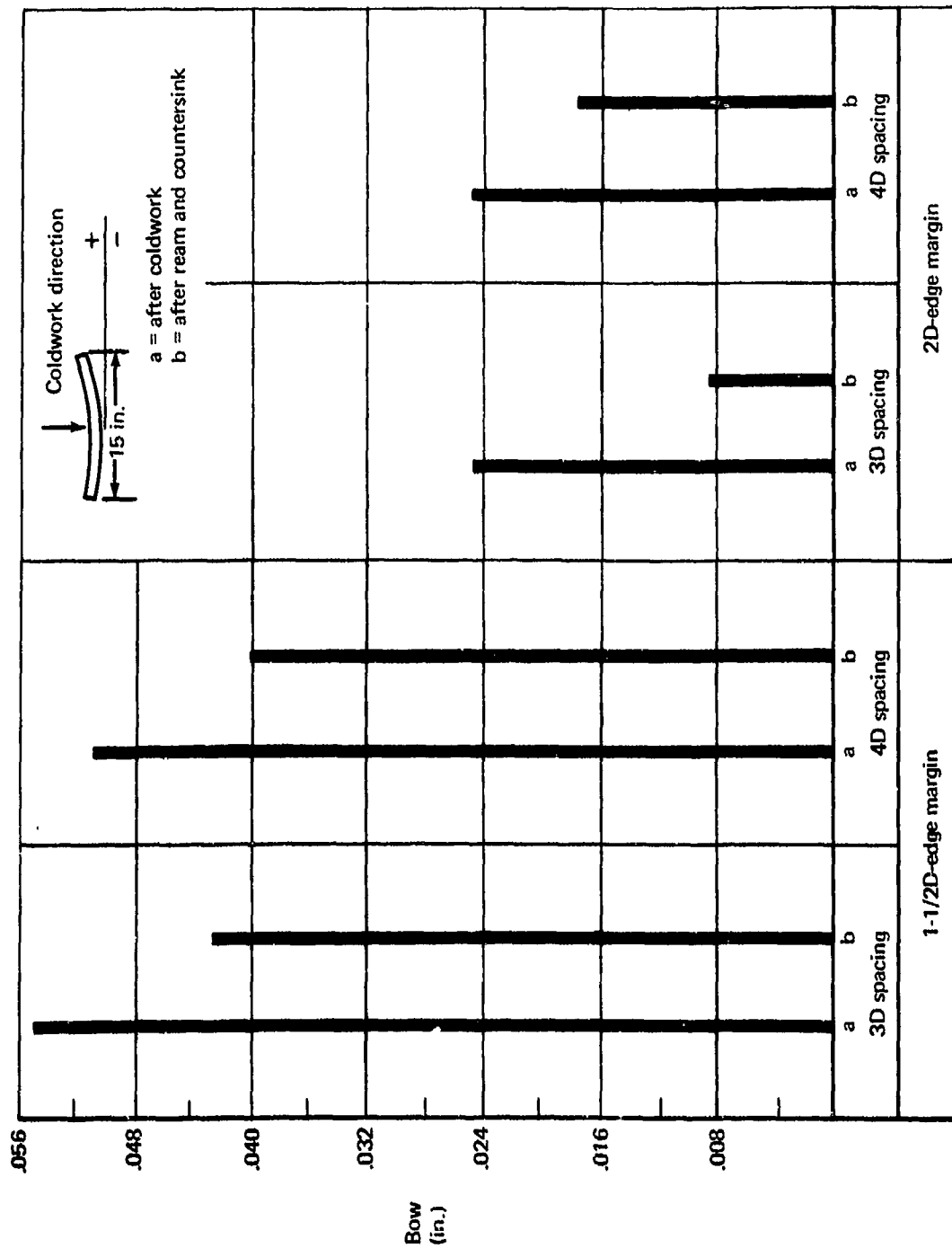
Figure 90.—Specimen Bow—3/8-In. Plate, 3/8-In.-Diameter Holes, 2024-T851

174
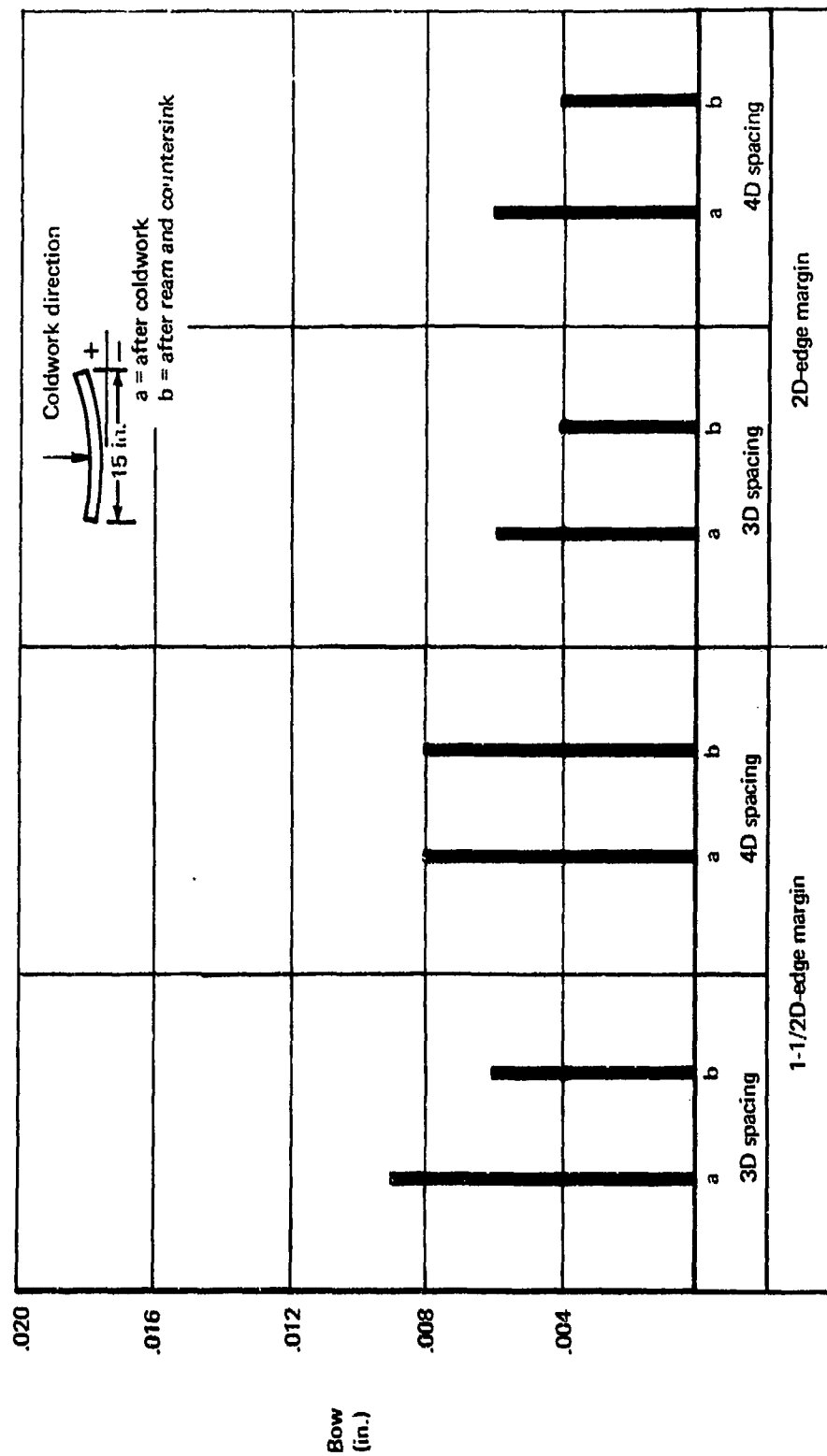
Figure 91.—Specimen Bow—3/4-In. Plate. 3/4-In.-Diameter Holes, 2024-T851
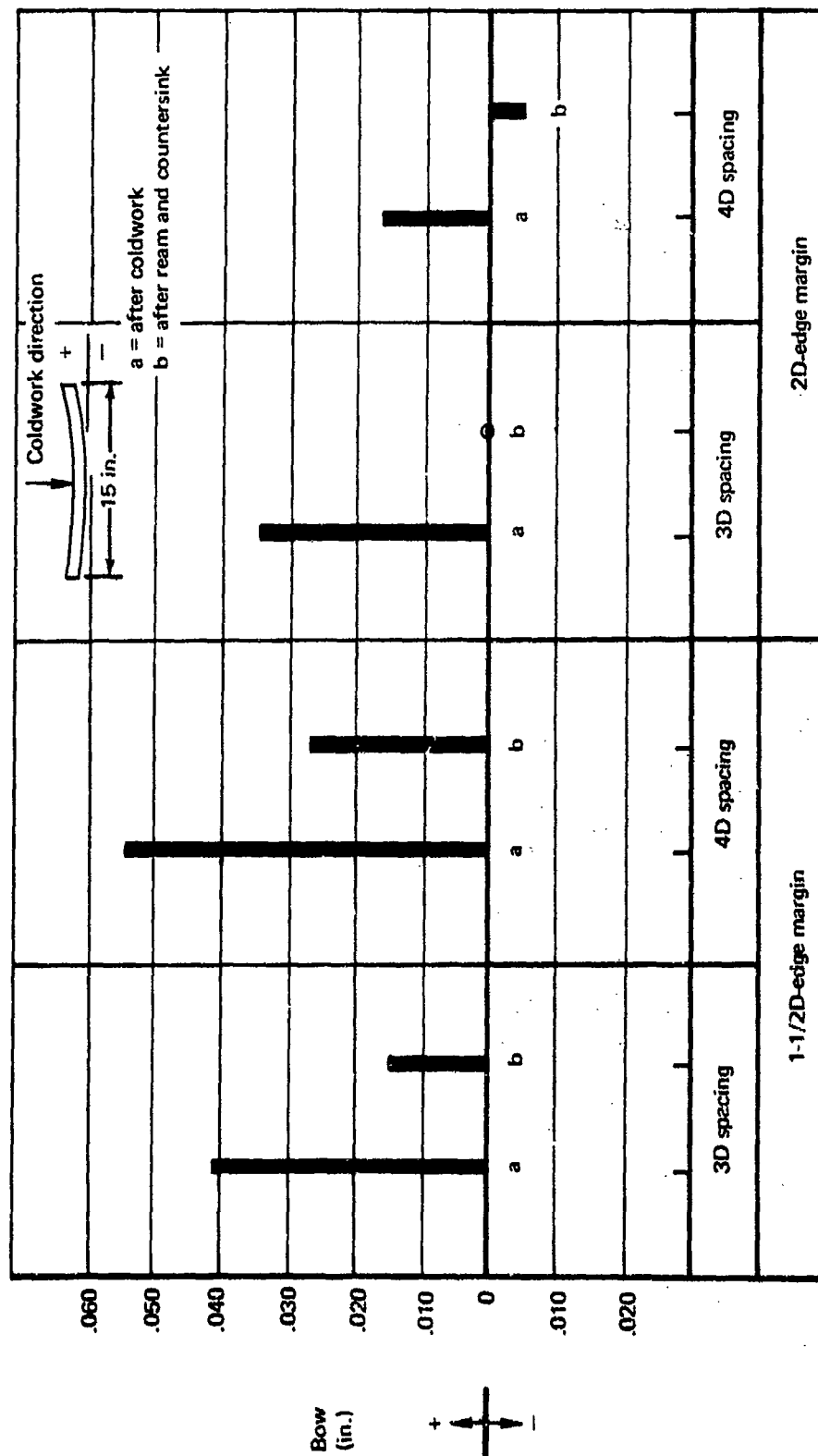
Figure 92.—Specimen Bow—3/8-In. Plate. 3/8-In.-Diameter Holes. Ti-6Al-4V

Figure 93. —Specimen Bow—3/4-In. Plate. 3/4-In.-Diameter Holes, Ti-6Al-4V
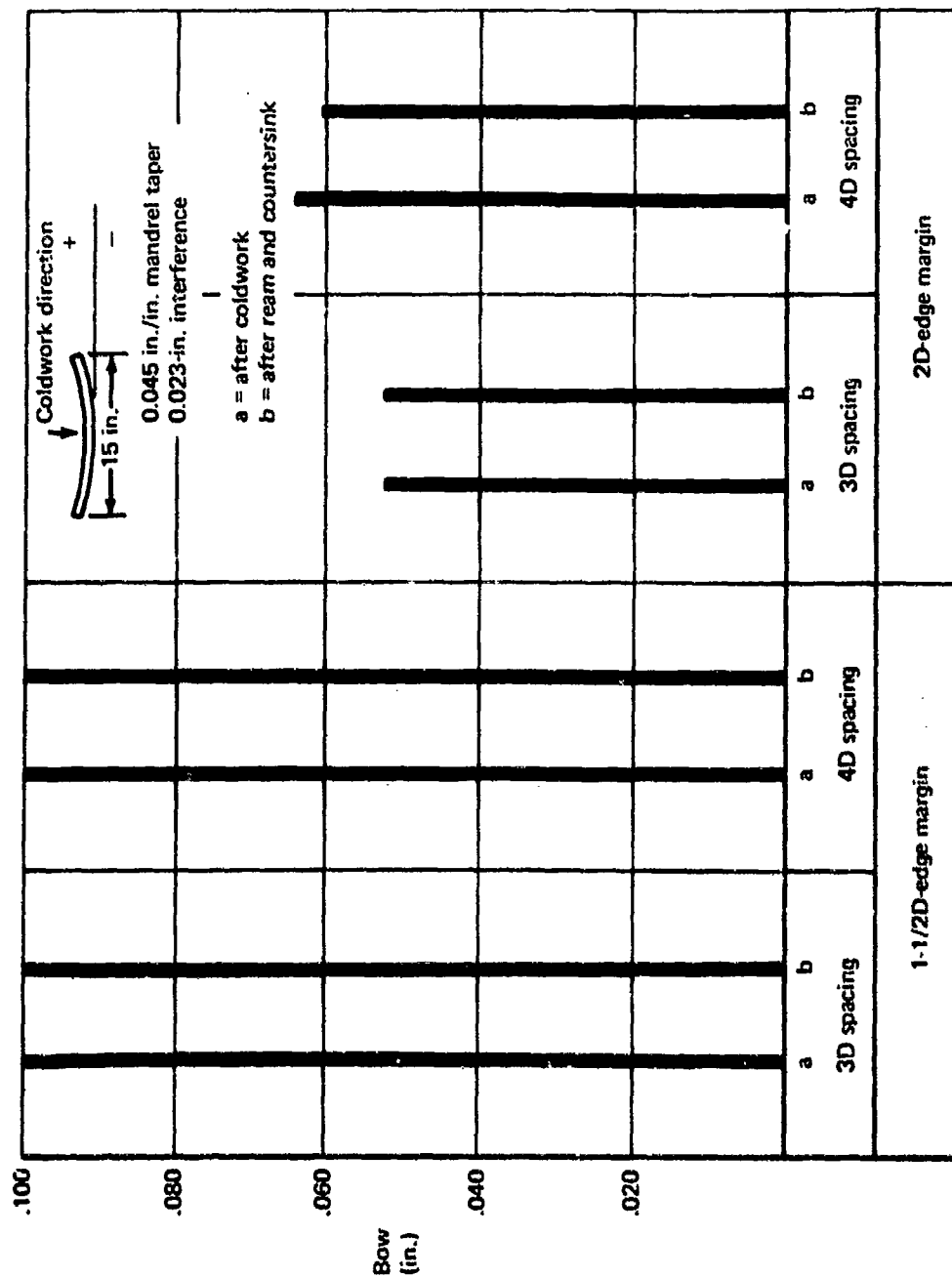
Figure 94.—Specimen Bow—3/8-In. Plate. 3/8-In.-Diameter Holes. 300M Steel (270-300 KSI)
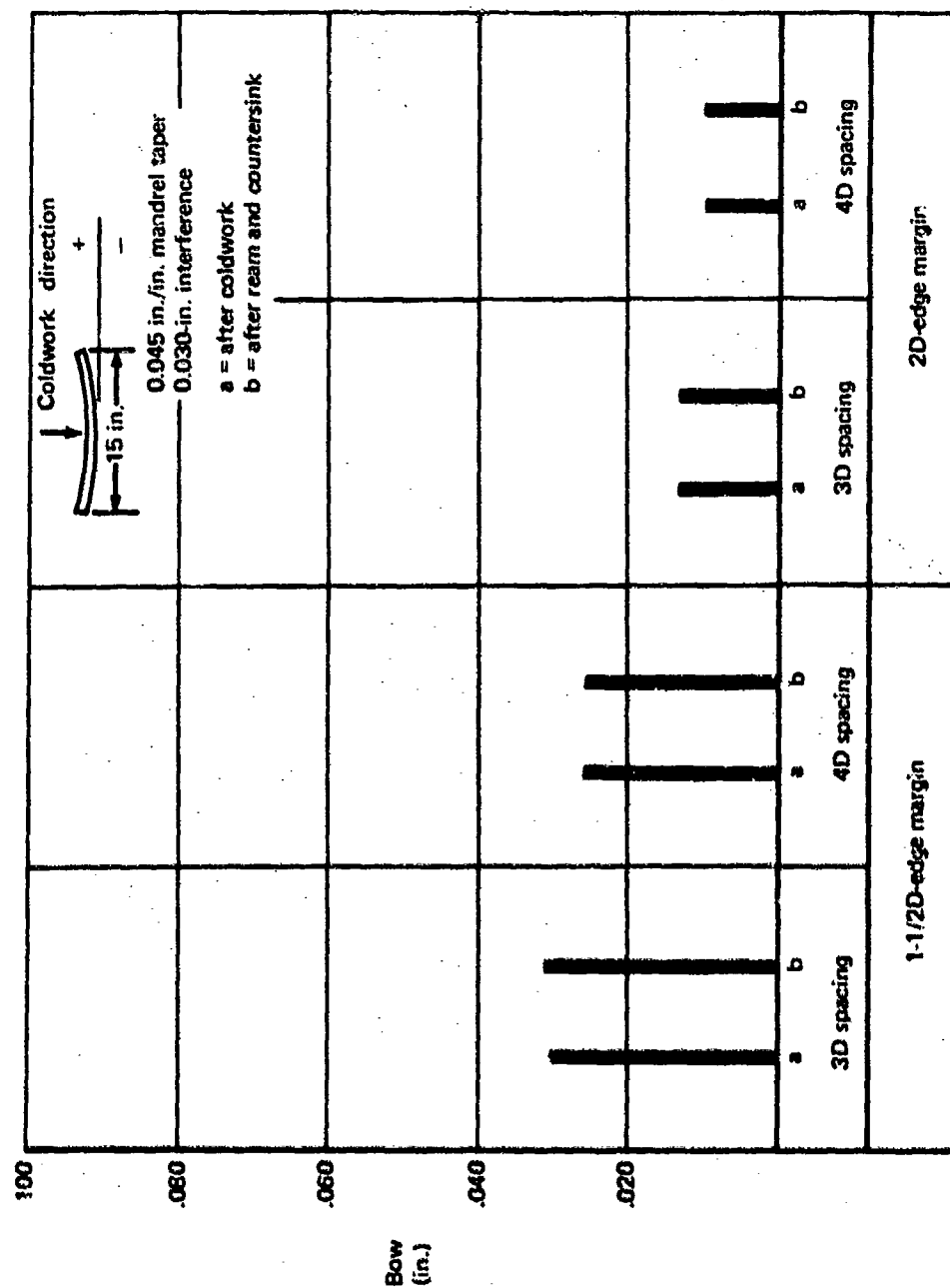
Figure 95.—Specimen Bow—3/4-In. Plate, 3/4-In.-Diameter Holes, 300M Steel (270-300 KSI)

Average edge bulge (in.)

.005
.004
.003
.002
.001

a = 3D-hole spacing
b = 4D-hole spacing

Hole diameter (in.)	a 3/8 b	a 3/4 b	a 3/8 b	a 3/4 b
Interference (in.)	0.018	0.030	0.018	0.030
Edge margin	1-1/2D		2D	
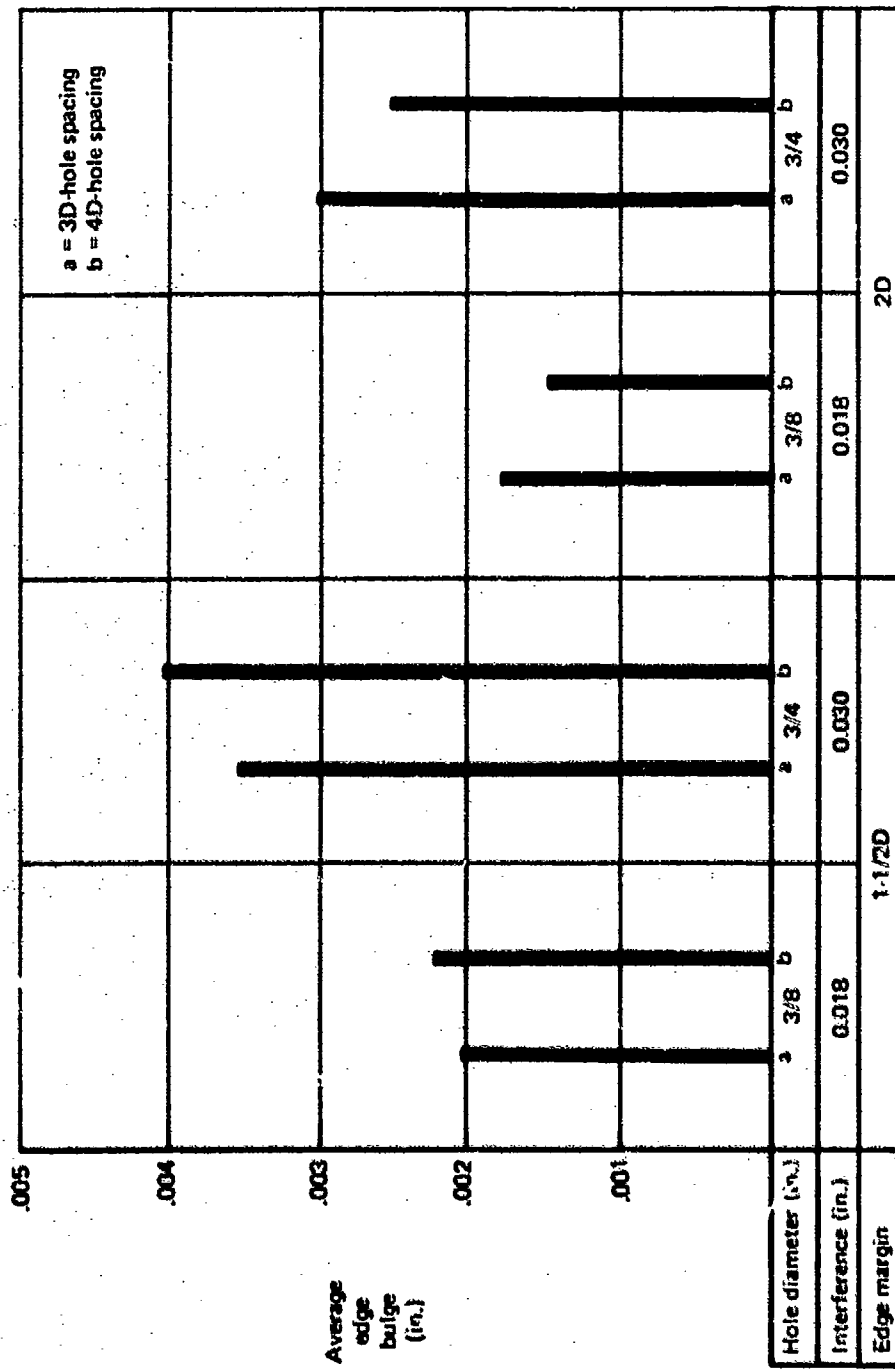
Figure 96. – Edge Bulge at Holes—2024-T851
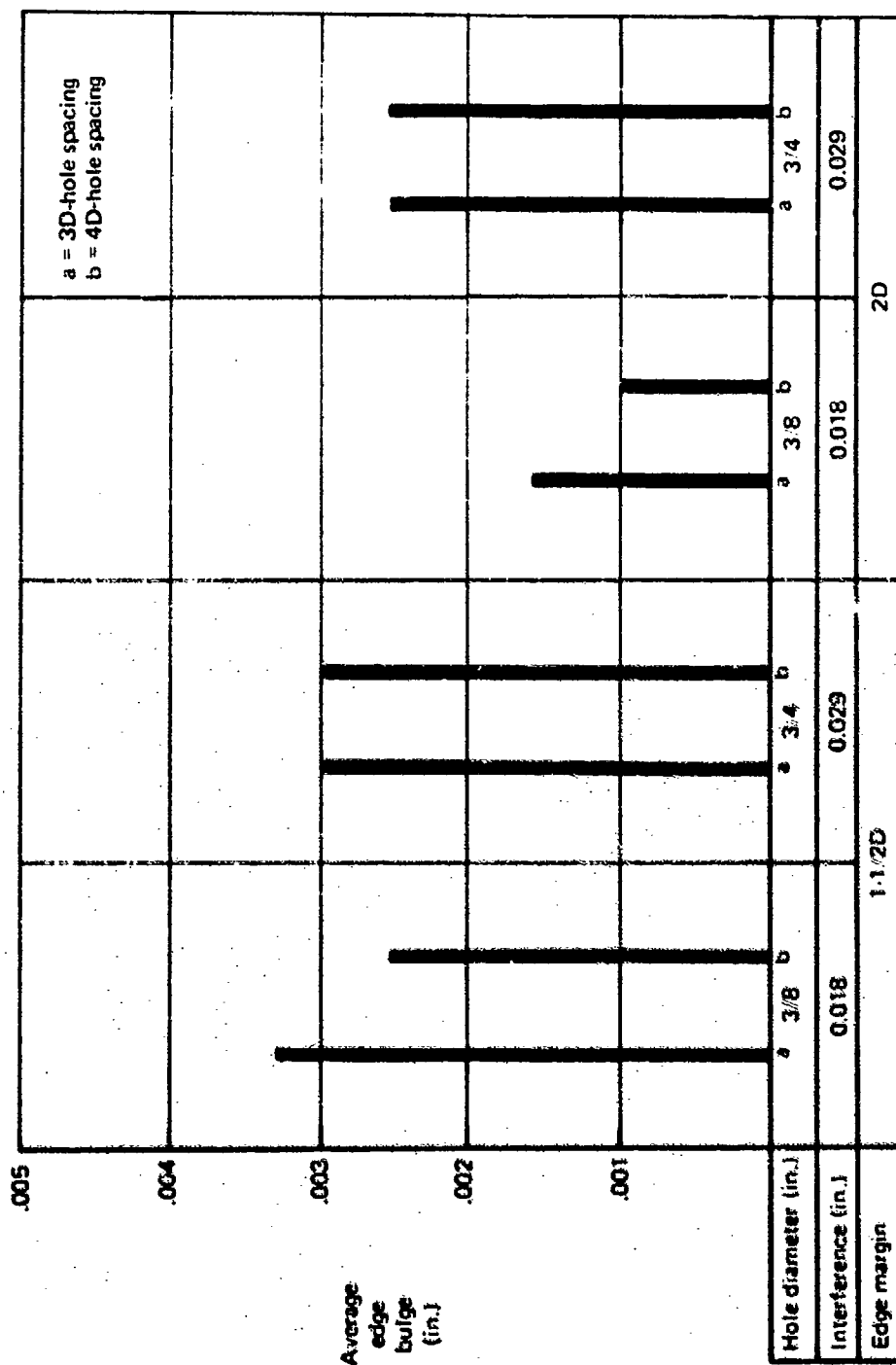
Figure 97.—Edge Bulge at Holes—Ti-6Al-4V

Hole diameter (in.)	a 3/8	b	a 3/4	b	a 3/8	b	a 3/4	b
Interference (in.)	0.018		0.029		0.018		0.029	
Edge margin	1.1/2D				2D			

a = 3D-hole spacing
b = 4D-hole spacing

Average edge bulge (in.)

.005
.004
.003
.002
.001
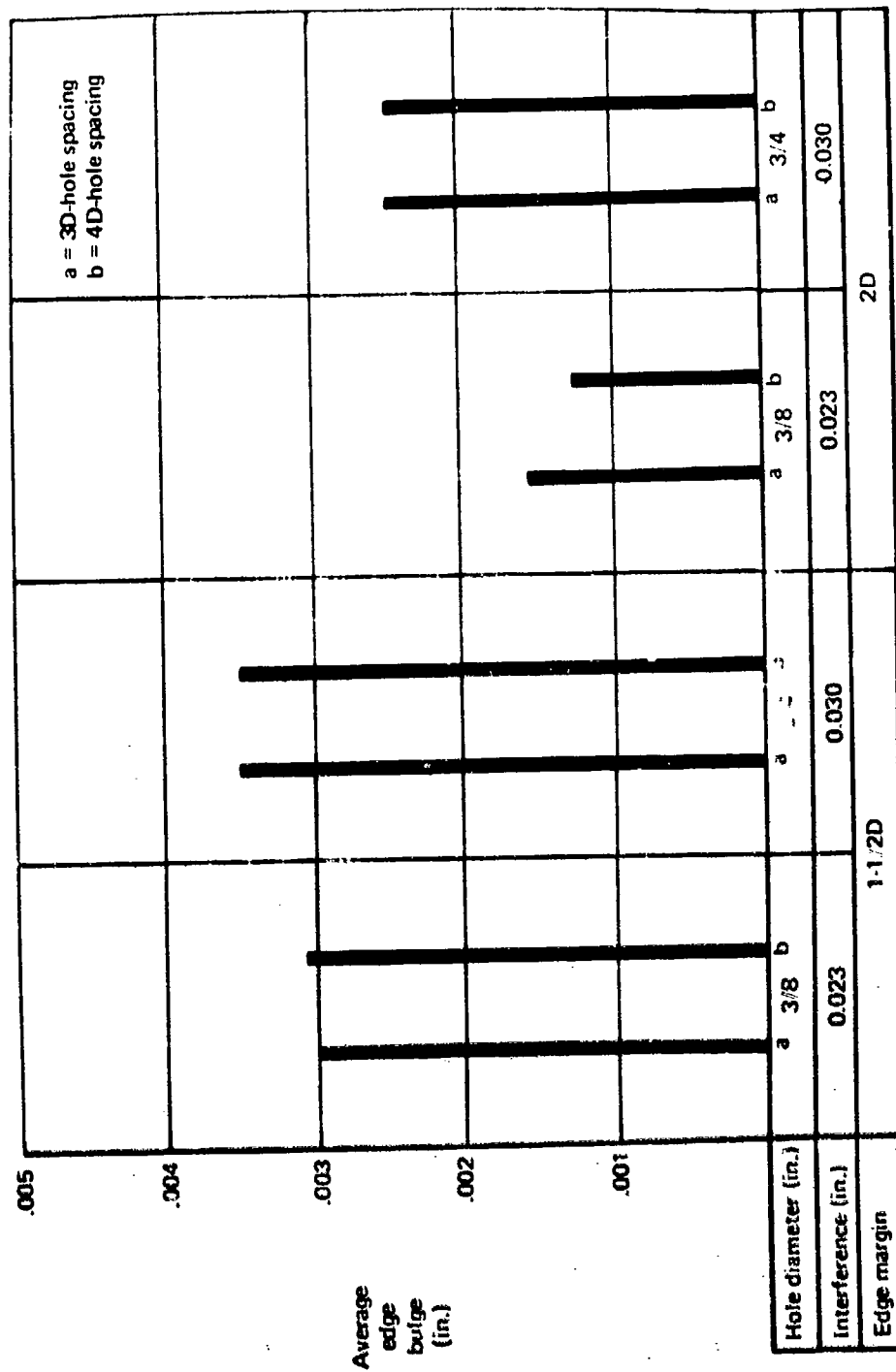
Figure 98. — Edge Bulge at Holes—300M Steel
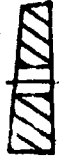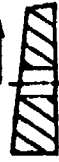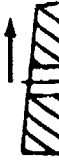
Material	Surface angle (deg)	Centerline shift (in.)	Direction of shift
2024-T851 aluminum	2	0.0035	
2024-T851 aluminum	4	0.0035	
Ti-6Al-4V titanium	2	0.0020	
Ti-6Al-4V titanium	4	0.0030	
300M steel (270-300 ksi)	2	0.0008	
300M steel (270-300 ksi)	4	0.0017	

Figure 99. —Surface Angle Effect

183
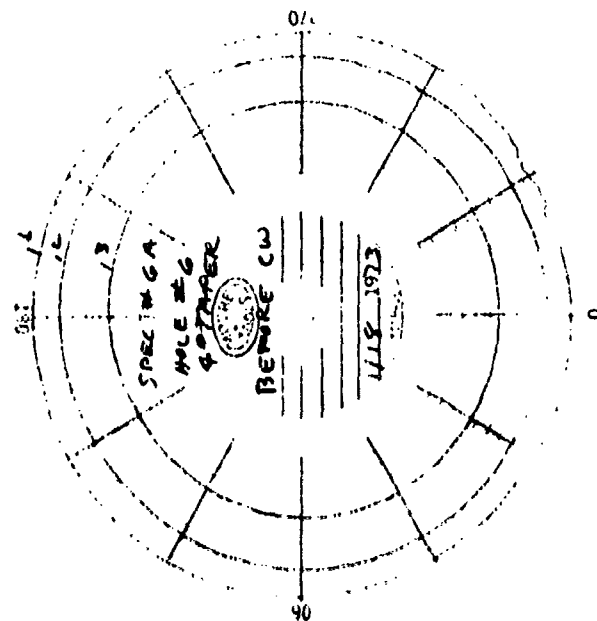
Hole Traces
Before Coldwork
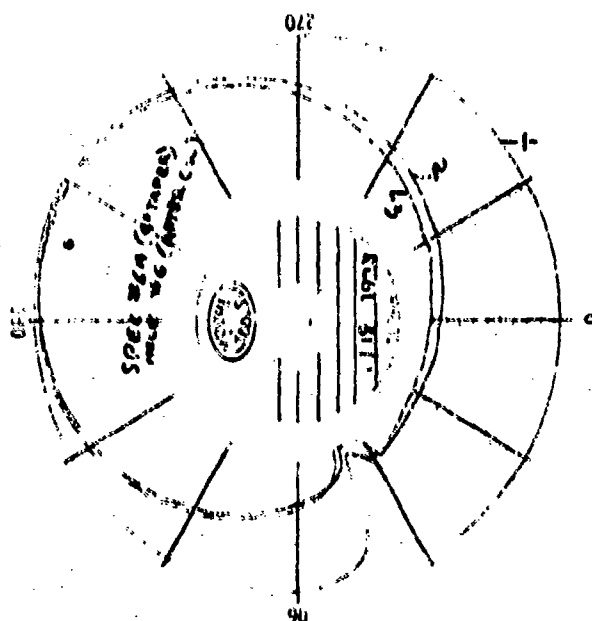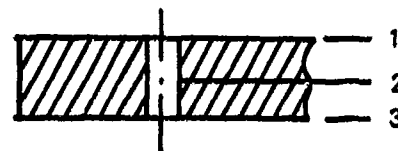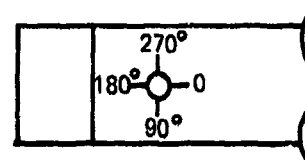
Hole Traces
After Coldwork

Figure 100.—Surface Taper Effect—4°-Surface Taper, 2024-T851

Material	Nominal hole diameter (in.)	Coldworking interference (in.)	Material gage (in.)	Mandrel taper (in./in.)	Midpoint hole size (in.)		
					Immediately after postream	One hr after postream	24 hr after postream
2024-T851 aluminum	3/8	0.019	3/4	0.045	0.3753/0.3754	0.3752/0.3753	0.3752/0.3753
Ti-6Al-4V titanium	3/8	0.019	3/4	0.045	0.3753/0.3754	0.3752/0.3753	0.3752/0.3753

Figure 101.—Hole Diameter Creep

185
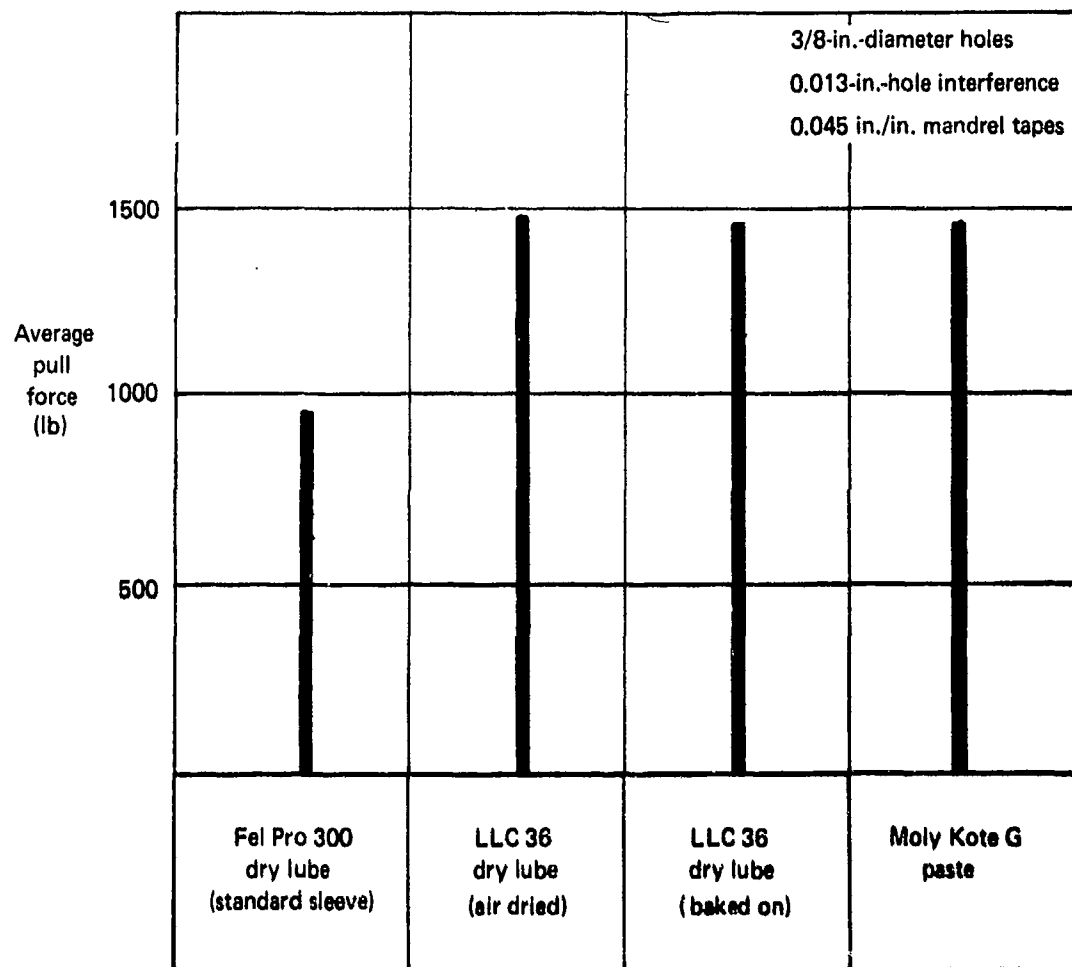
Figure 102.—Basic Sleeve Lubricants—2024-T851, 3/8-In. Thick
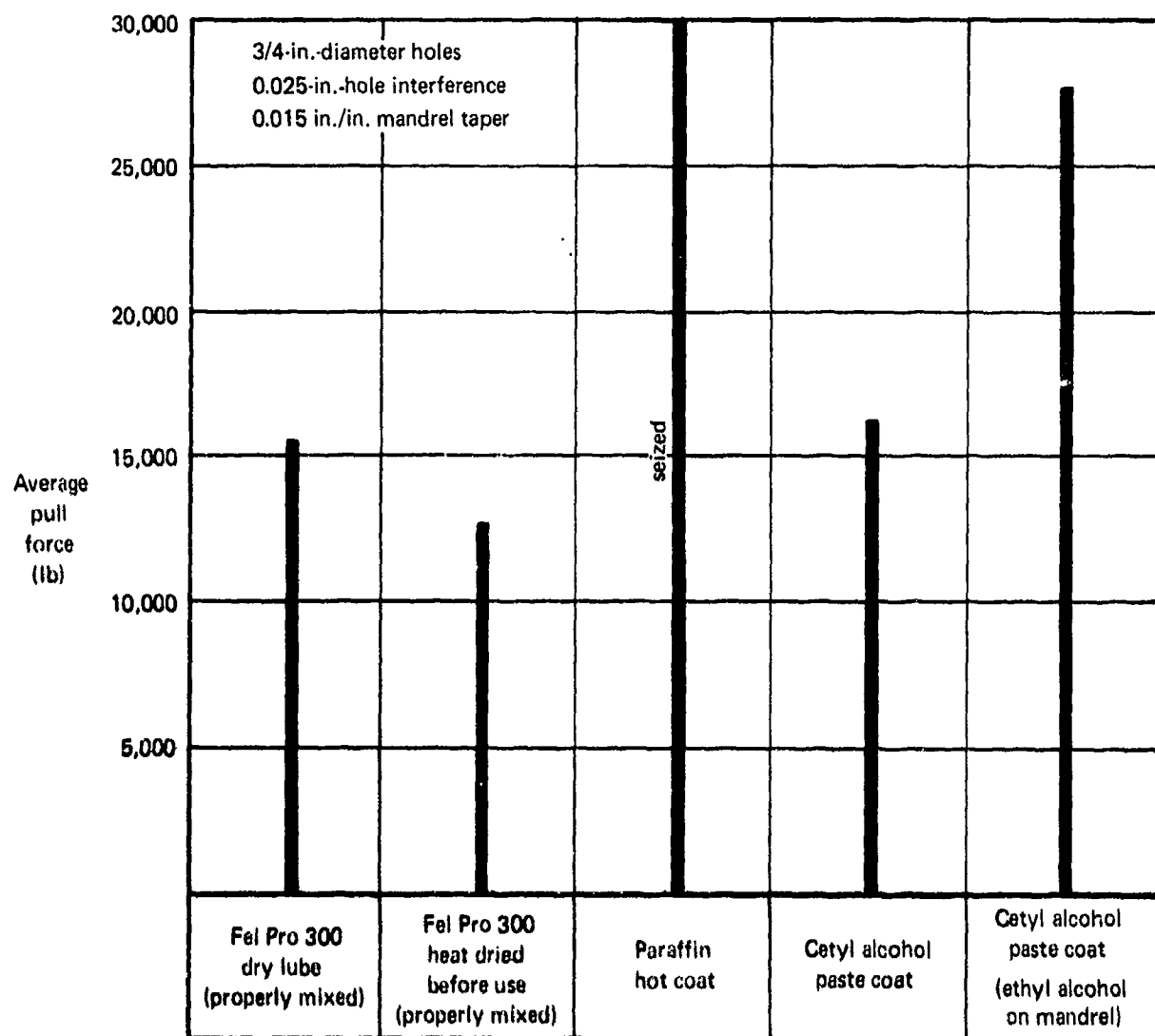
Figure 103.—Basic Sleeve Lubricants—7075-T651, 2 In. Thick

187
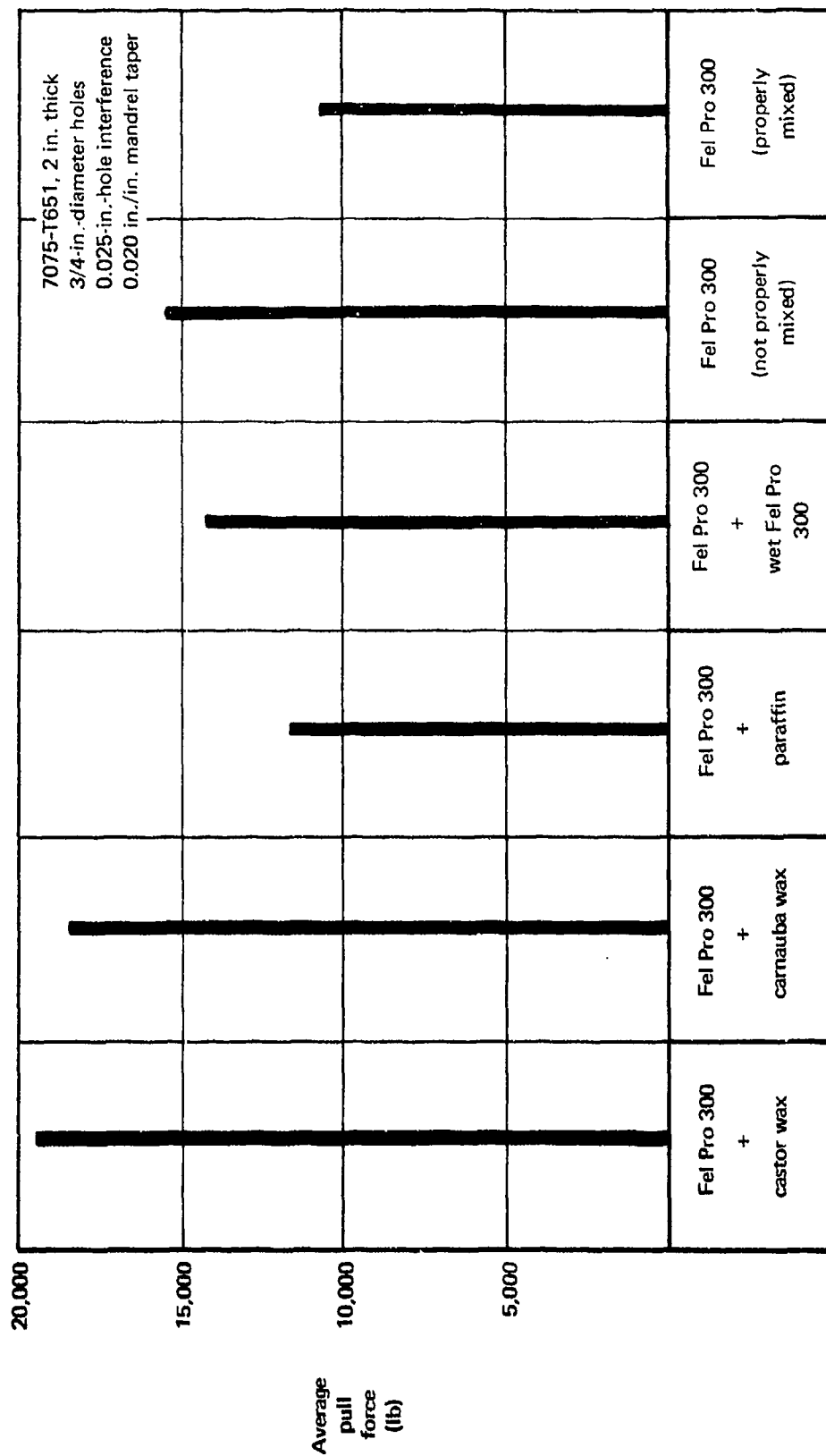
Figure 104.—Sleeve Lubricants—Fel Pro 300 Variations
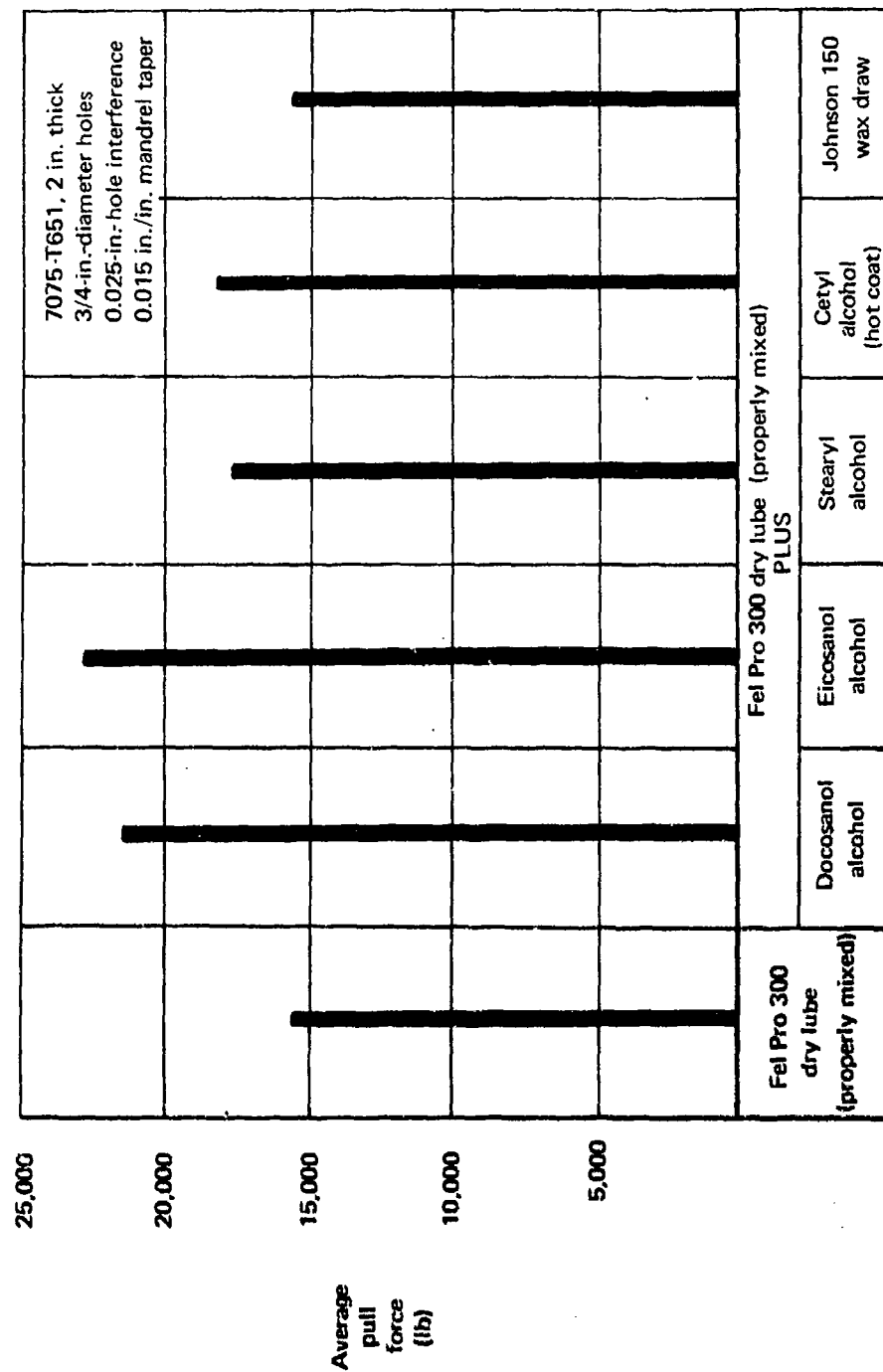
Figure 105. —Sleeve Lubricants—Fel Pro 300 Variations
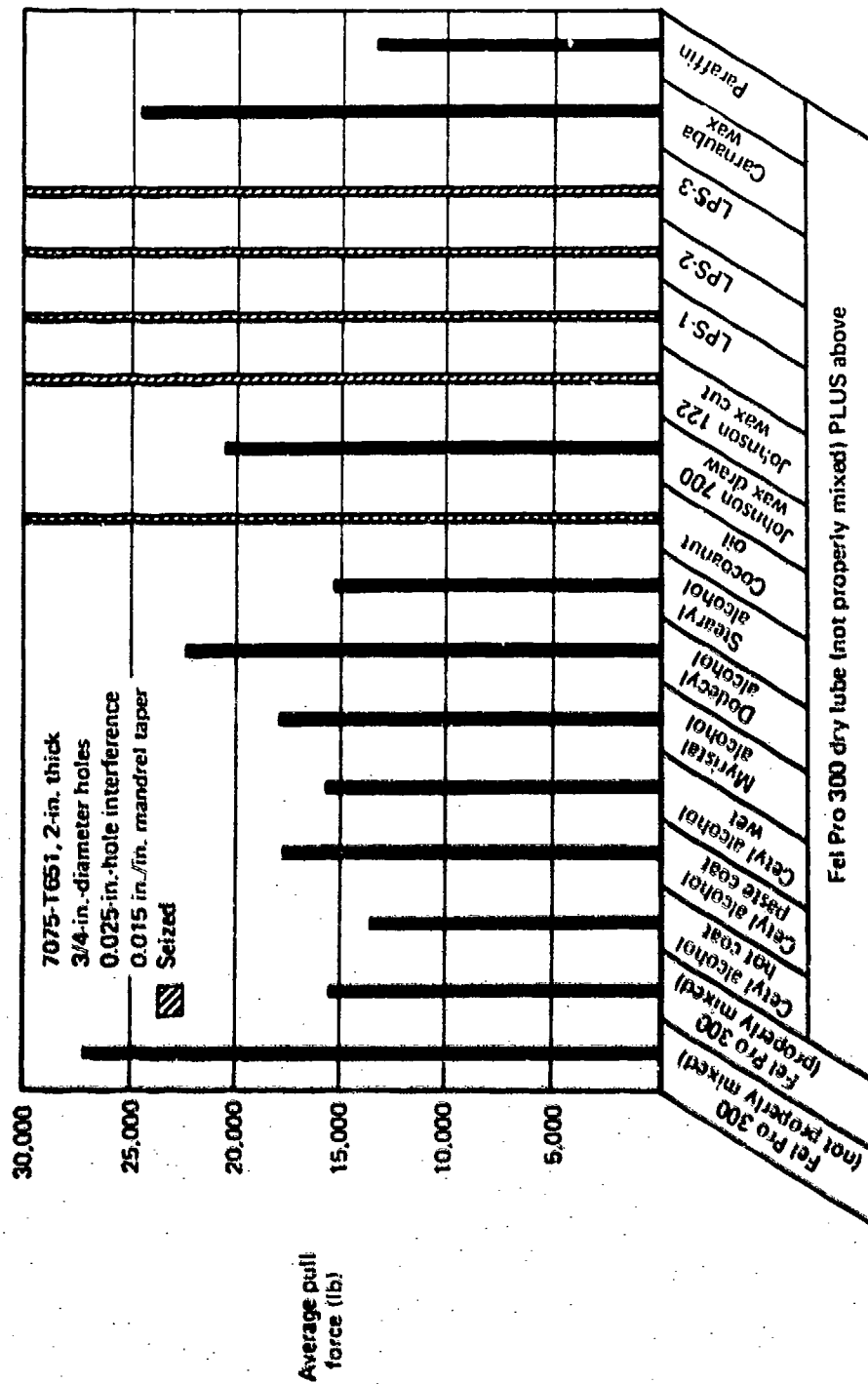
Figure 106.—Sleeve Lubricants—Fel Pro 300 Variations

Mandrel finish	None	Vapor blast + Fel Pro 300	None	Vapor blast + Fel Pro 300
Material	2024-T851 aluminum		TI-6AI-4V titanium	
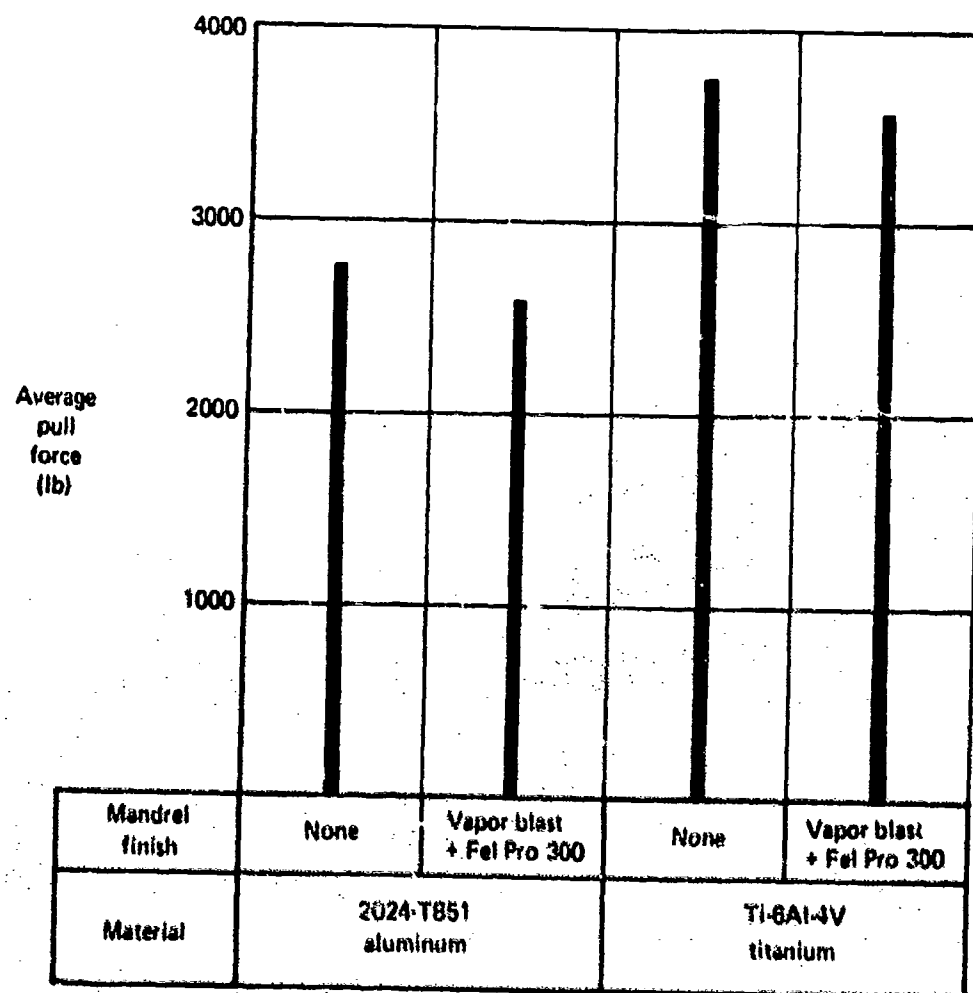
Figure 107.—Mandrel Finish Variation—3/8-In.-Diameter Holes, Fel Pro 300-Lubricated Sleeves
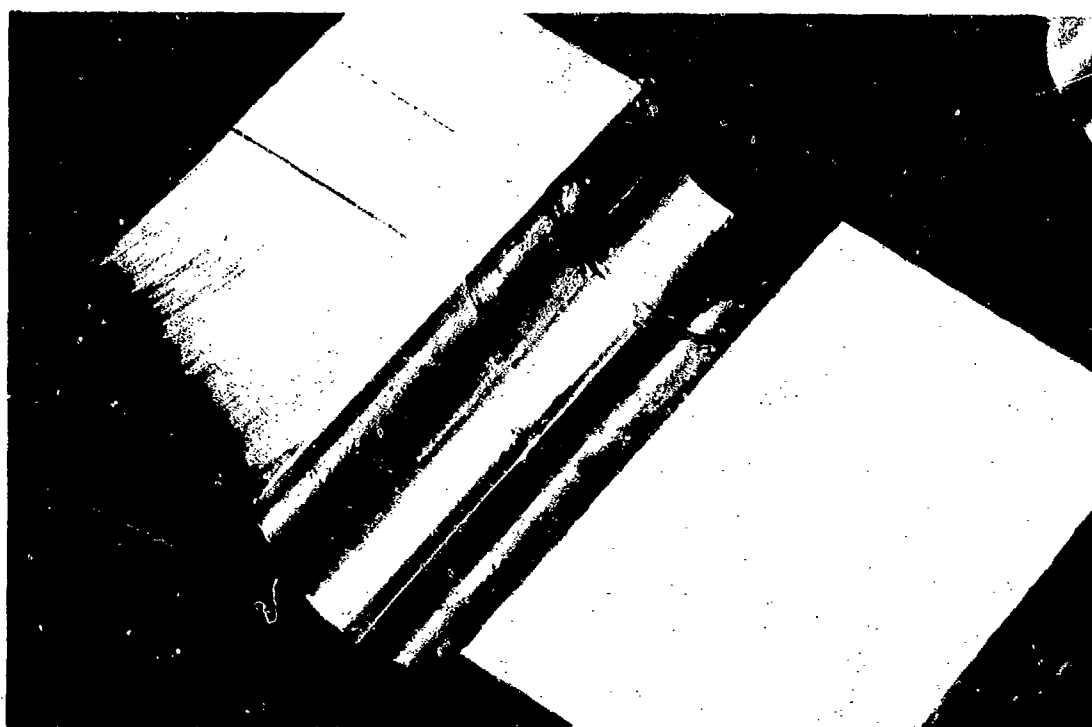
Figure 168. Ridge From Two Axial Split Sleeves
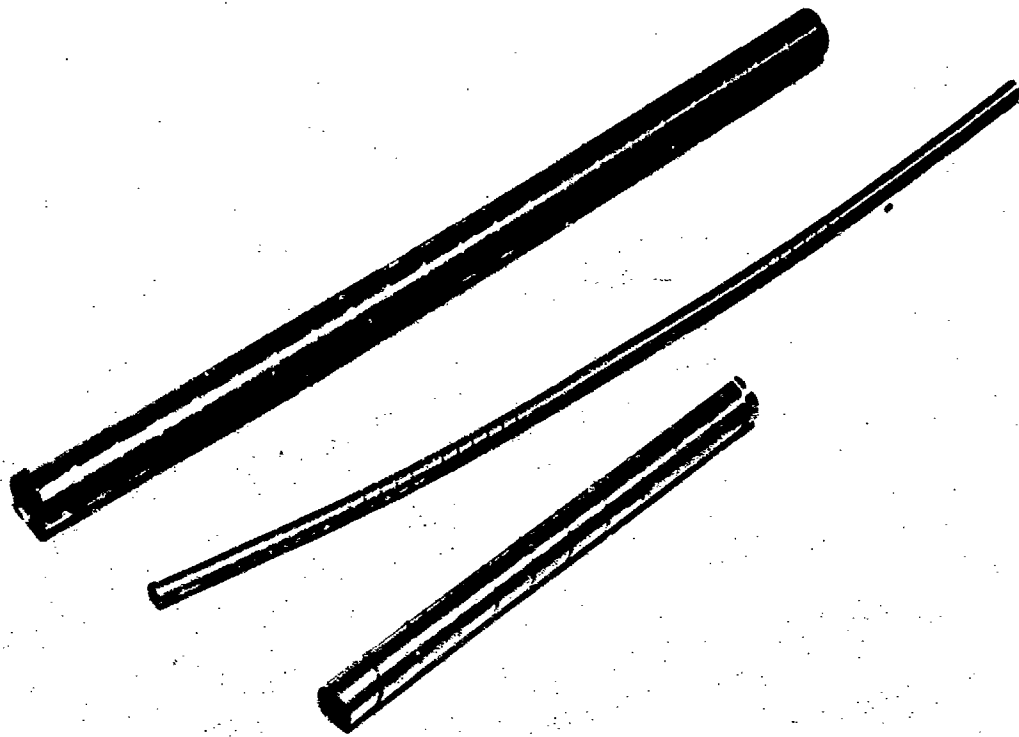
Figure 109. Helical Sleeves As Wound

Figure 110.—Helical Sleeves—Cut to Length
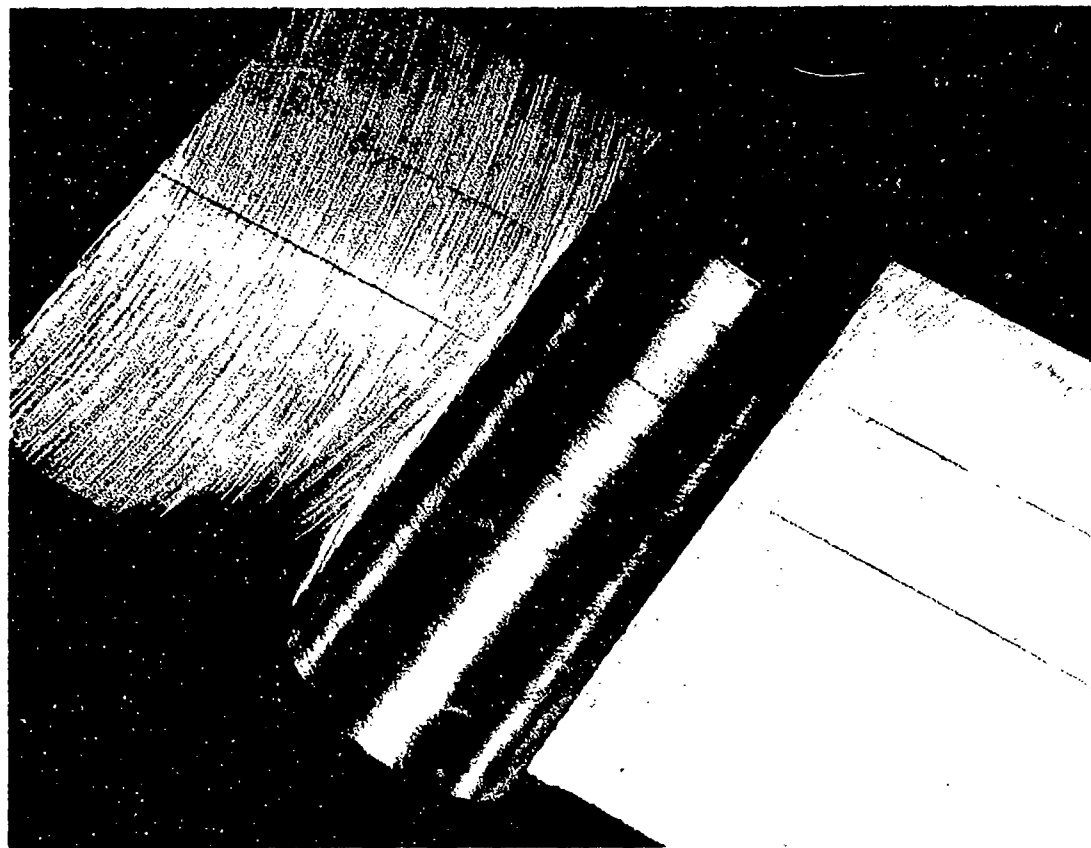
Figure 111.—Ridge From Helical Sleeve
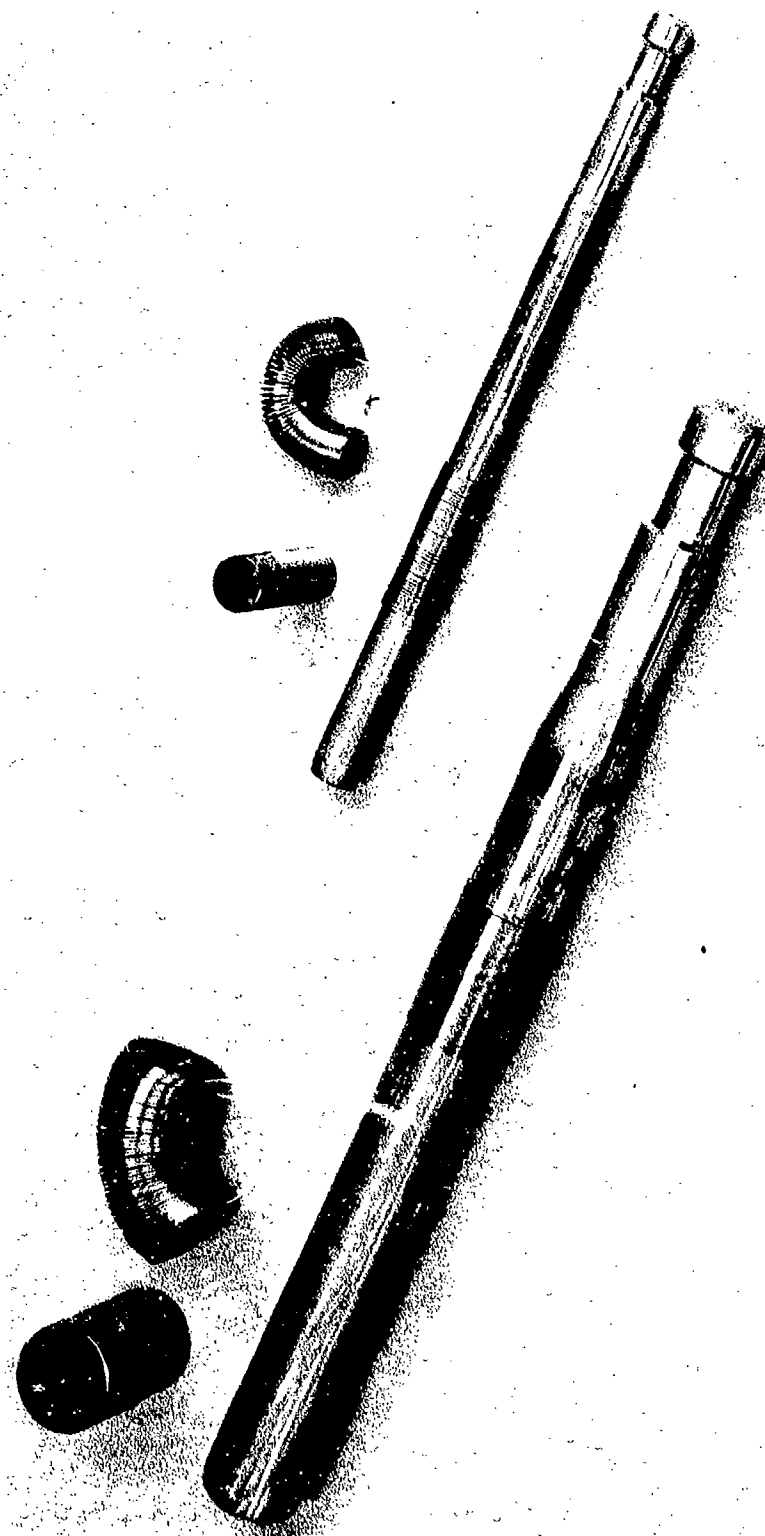
Figure 112.—Square Wire Sleeves and Mandrels
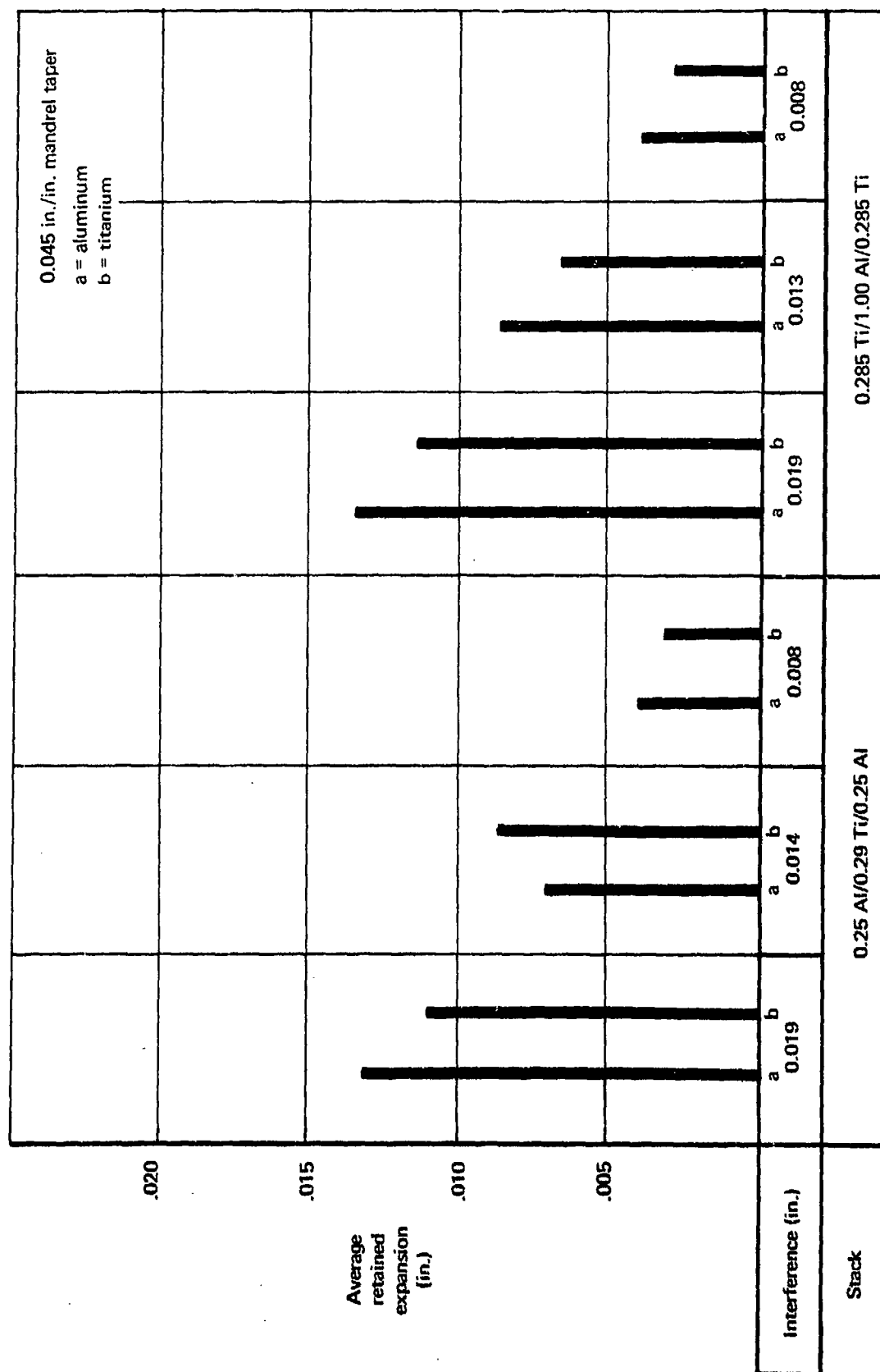
Figure 113.—Multimaterial Stacks—Retained Expansion
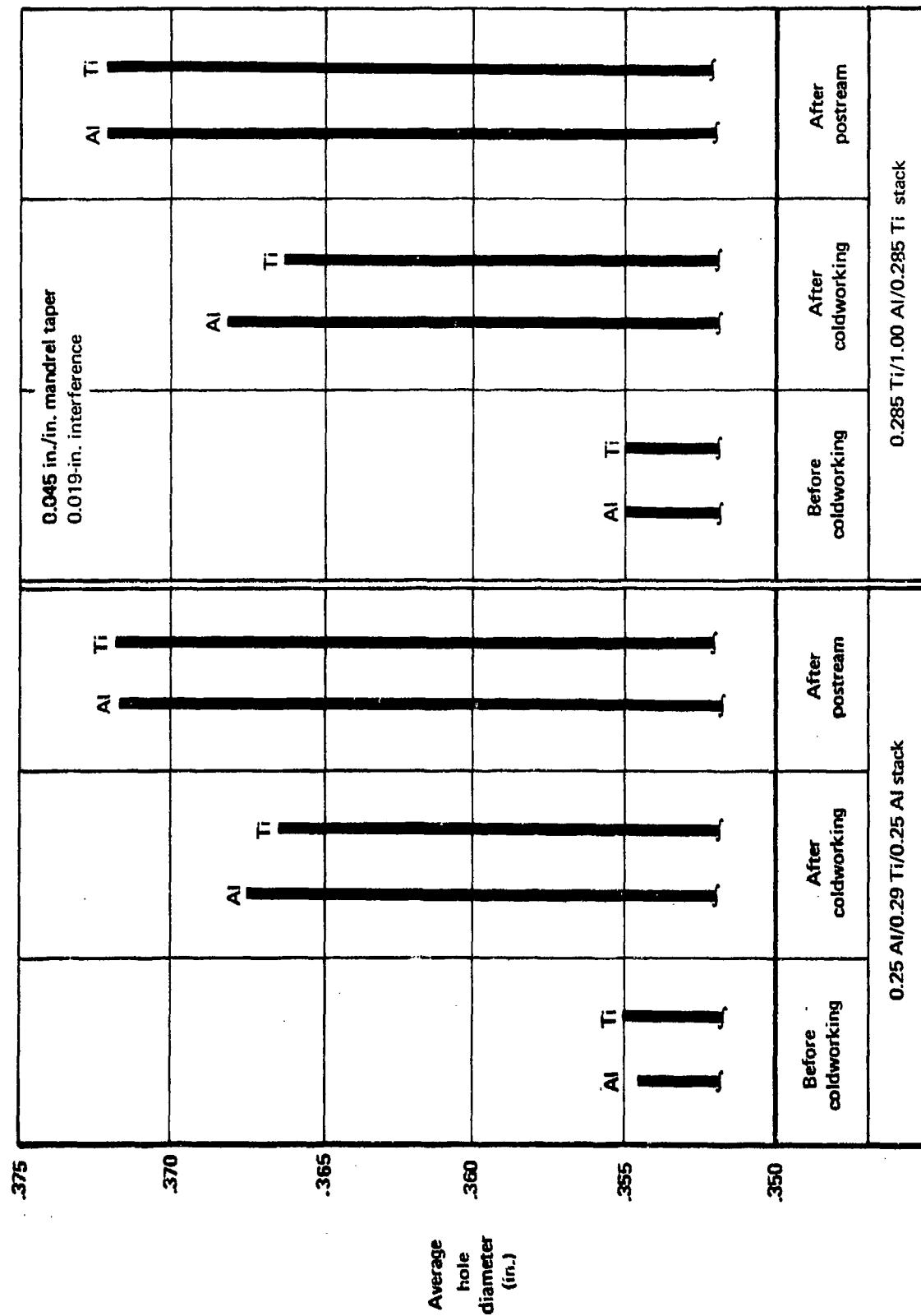
Figure 114.—Multimaterial Stacks—Diameter Effects

*To allow 0.010-in. postream below 1/2 in. and 0.015-in. postream above 1/2 in. when using recommended optimum coldworking interference

Nominal finished hole diameter (in.)

Nominal diameter reduction for starting hole* (in.)
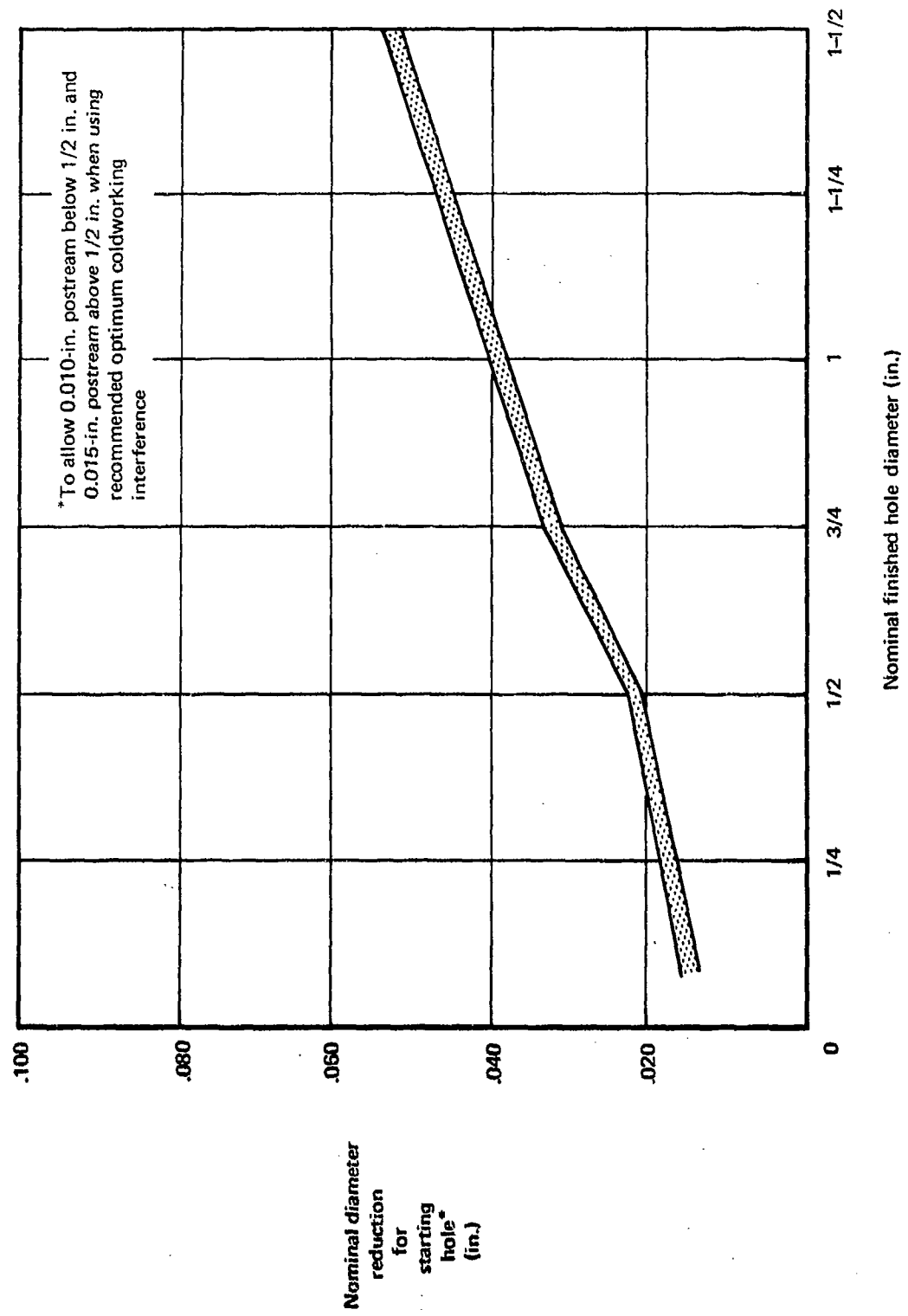
Figure 115.—Starting Hole Diameter—2024-T851 and Ti-6Al-4V

Nominal diameter reduction for starting hole* (in.)

*To allow 0.010-in. postream below 1/2 in. and 0.015-in. postream above 1/2 in. when using recommended optimum coldworking interference; (see fig. 70 for further clarification)

For theoretical optimum interference

For practical limit interference

Nominal finished hole diameter (in.)
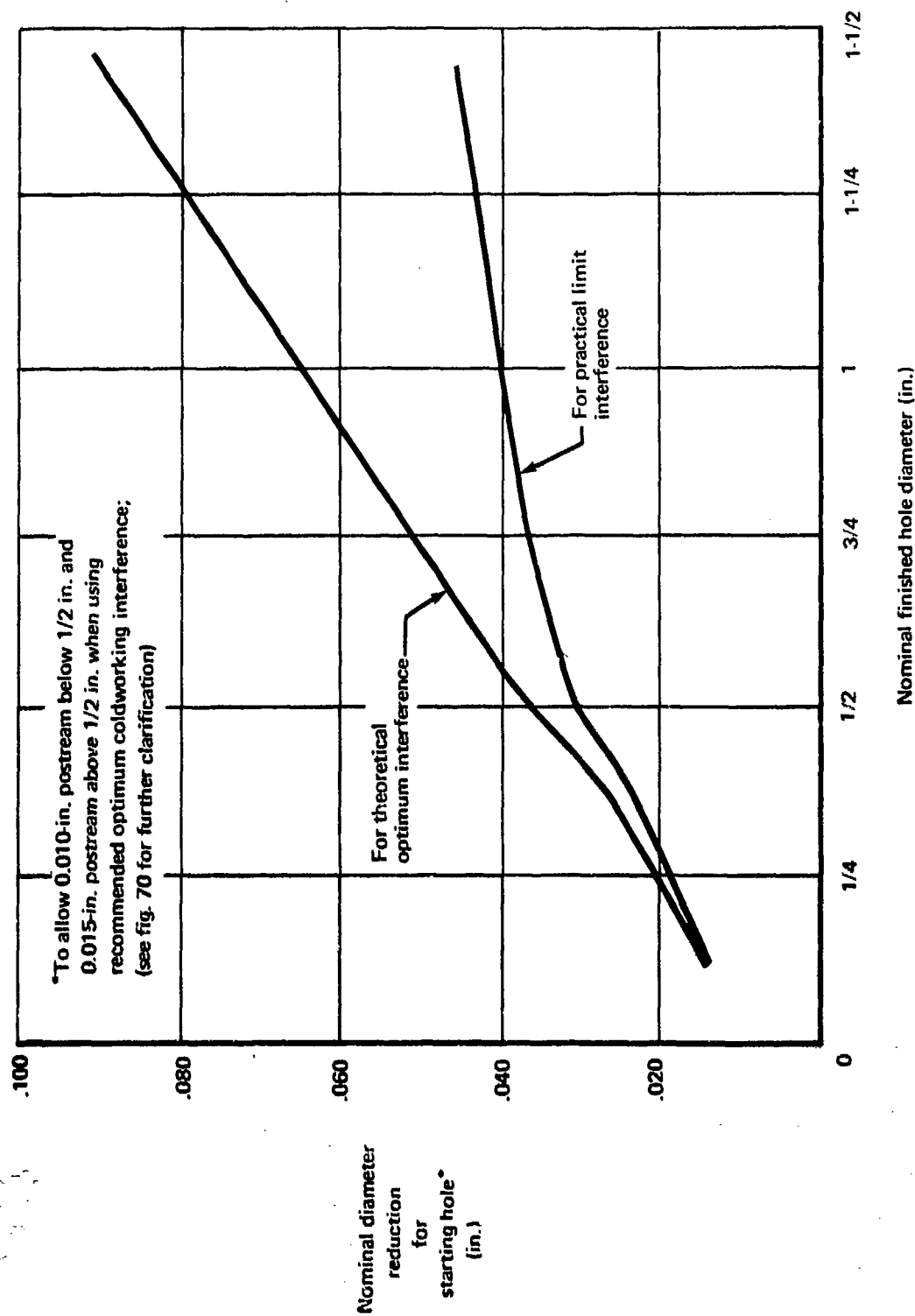
Figure 116.—Starting Hole Diameter—300M Steel (270-300 KSI)

200
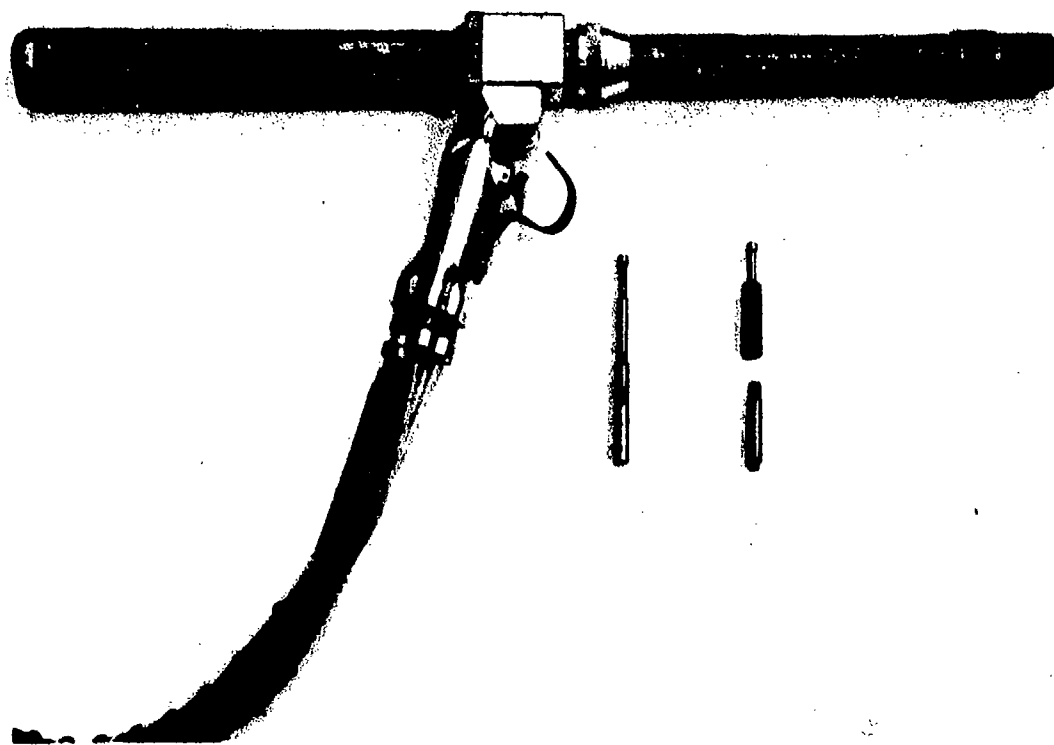
Figure 117.—CP 659 Pull Gun
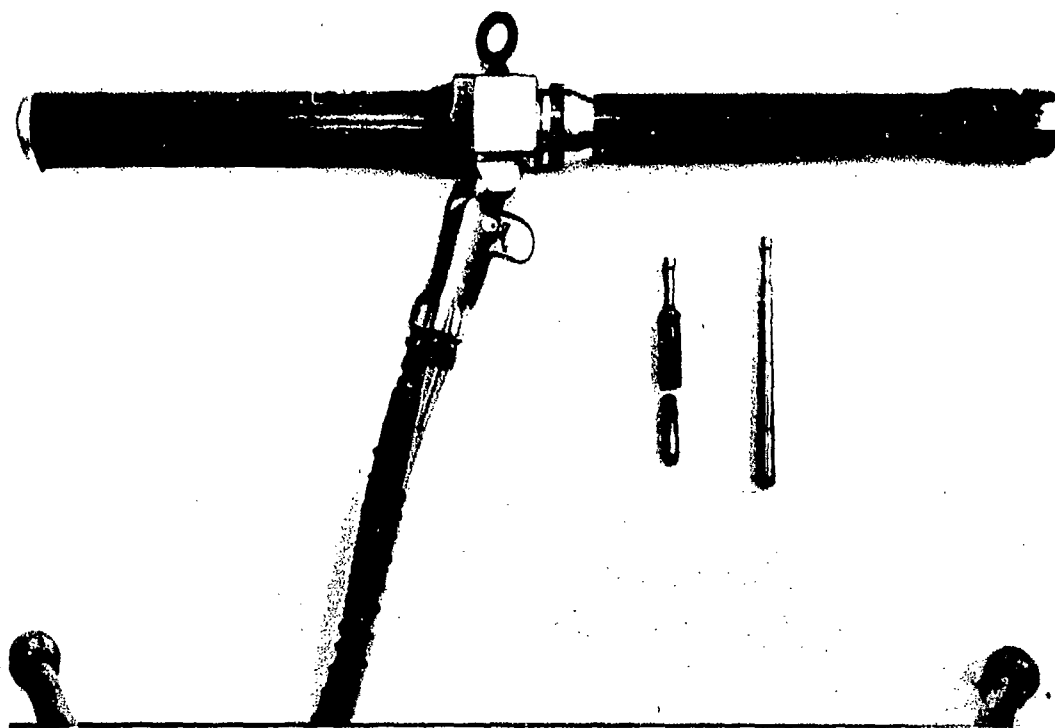
Figure 118.—CP 660 Pull Gun

Current Mandrel Design

Proposed Mandrel Design
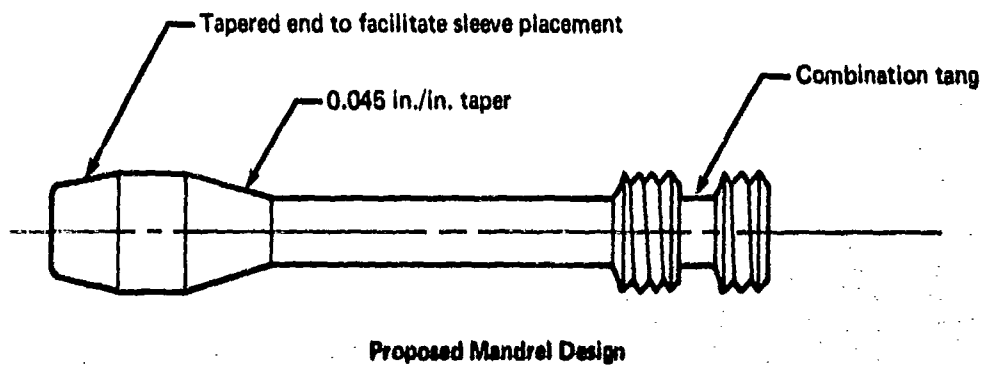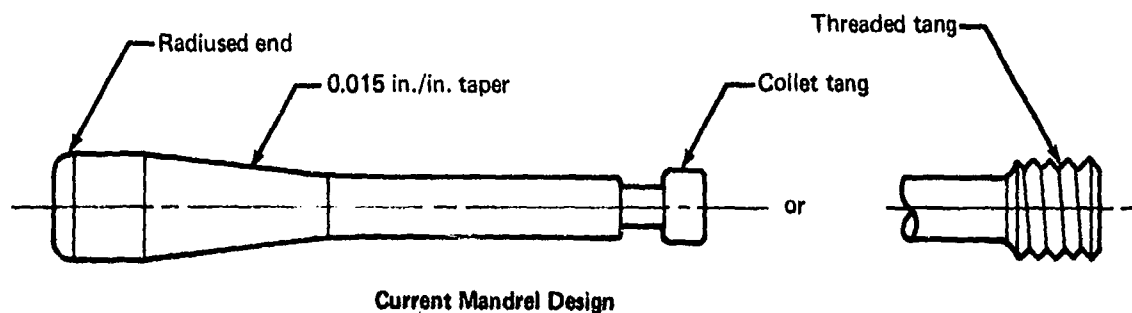
Figure 119.—Mandrel Design
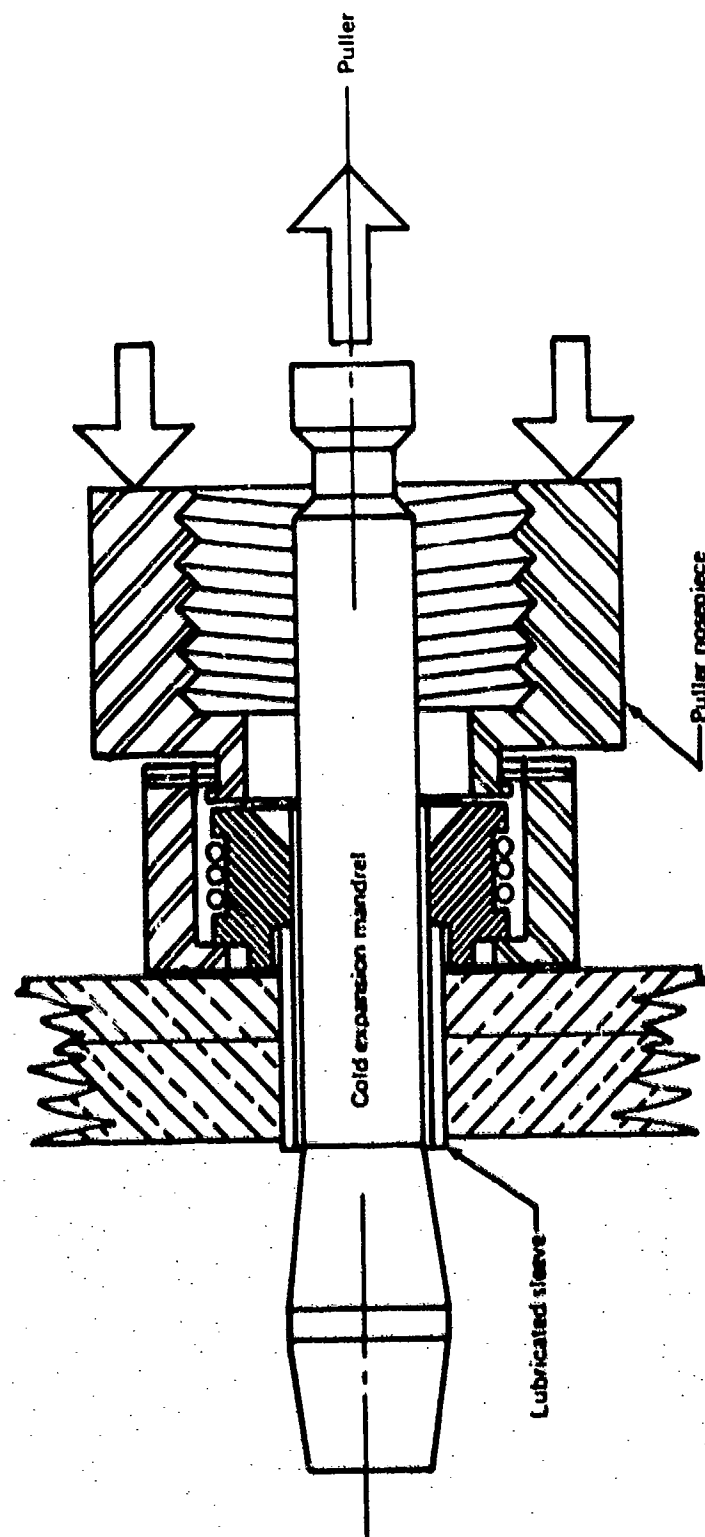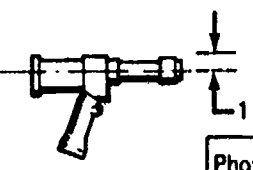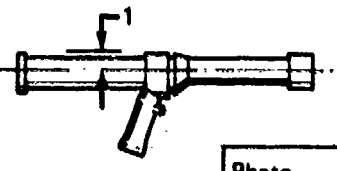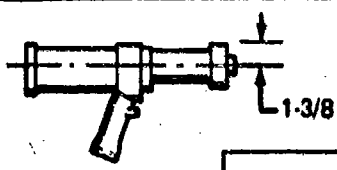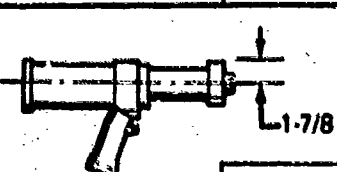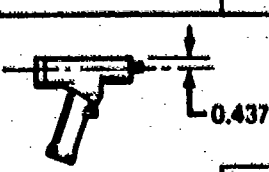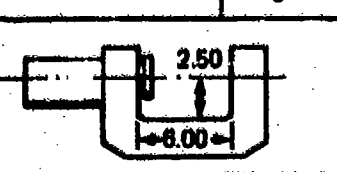
Figure 1.20. —Schematic Representation of Coldworking Tool Setup

Puller

Puller nosepiece

Cold expansion mandrel

Lubricated sleeve

Puller and squeezer units		Stroke (in.)	Force capability with 7000 psi (lb)	Force capability with 10000 psi (lb)	Oil volume requirement (in.^{3})
Drawing (dimensions in inches)	Designation				
	ST 1350A-032	3-1/8	7,000	10,000	4
Photo— figs.124 and 125	ST 1350A-055	5-1/2	7,000	10,000	6
	CP 659	9 & 14	5,500	7,800	7½ & 12
Photo· figs.117 and 118	CP 660	12	11,000	15,700	20
Photo— fig. 127	ST 1350A-B	6-3/8	18,000	25,700	17
Photo— fig.128	ST 1350A-C	6-3/8	25,000	35,700	23
Photo— fig. 138	ST 1350A-RA-1	1	4,700	6,700	1
Photo— fig. 131	ST 1350B	5	35,000	50,000	25

Note: All pullers use air for return stroke and hydraulics for power stroke

Figure 131.—Coldworking Puller and Squeezer Units

Puller or squeezer units	Maximum coldworking diameter capacity at 7000 psi* (in.)									Maximum coldworking diameter capacity at 10,000 psi* (in.)								
	2024-T851			Ti-6Al-4V			300M (270-300 ksi)			2024-T851			Ti-6Al-4V			300M (270-300 ksi)		
	1/4-in. thick	1/2-in. thick	1-in. thick	1/4-in. thick	1/2-in. thick	1-in. thick	1/4-in. thick	1/2-in. thick	1-in. thick	1/4-in. thick	1/2-in. thick	1-in. thick	1/4-in. thick	1/2-in. thick	1-in. thick	1/4-in. thick	1/2-in. thick	1-in. thick
ST 1350A	7/8	11/16	1/2	1/2	7/16	3/8				1	7/8	3/4	3/4	9/16	7/16			
ST 1350A-B	1-1/2	1-1/4	7/8	7/8	13/16	3/4				2	1-3/4	1-3/8	1-1/4	15/16	7/8			
ST 1350A-C	2	1-3/4	1-3/8	1-1/4	15/16	7/8				2-5/8	2-1/2	1-3/4	1-1/2	1-1/4	15/16			
ST 1350A-RA-1	3/4	1/2	7/16	7/16	3/8	5/16				7/8	11/16	1/2	1/2	7/16	3/8			
CP 659	3/4	5/8	7/16	1/2	7/16	3/8				7/8	3/4	5/8	5/8	1/2	7/16			
CP 660	1-1/8	15/16	13/16	3/4	5/8	7/16				1-1/2	1-1/4	7/8	7/8	3/4	5/8			
ST 1350B							1	7/8	3/4							1-1/2	1-1/4	7/8

*For 0.045 in./in. mandrel taper only; smaller taper angles reduce capacity; 25% excess capacity included

Figure 122 — Tool Coldworking Capacity

Puller unit	Hole diameter (in.)					
	1/4	1/2	3/4	1	1-1/4	1-1/2
ST 1350A-032	2-1/2	2-1/4	2	1-7/8	1-3/4	1-1/2
ST 1350A-055	4-7/8	4-5/8	4-3/8	4-1/4	4-1/8	3-7/8
ST 1350A-B	5-3/4	5-1/2	5-1/4	5-1/8	5	4-3/4
ST 1350A-C	5-3/4	5-1/2	5-1/4	5-1/8	5	4-3/4
ST 1350A-RA-1	3/8	1/8	—	—	—	—
CP 559	13-3/8	13-1/8	12-7/8	12-3/4	12-5/8	12-3/8
CP 660	11-3/8	11-1/8	10-7/8	10-3/4	10-5/8	10-3/8

Note: Reflects only stroke capability, not force capability

Figure 123 - Maximum Thickness Capability
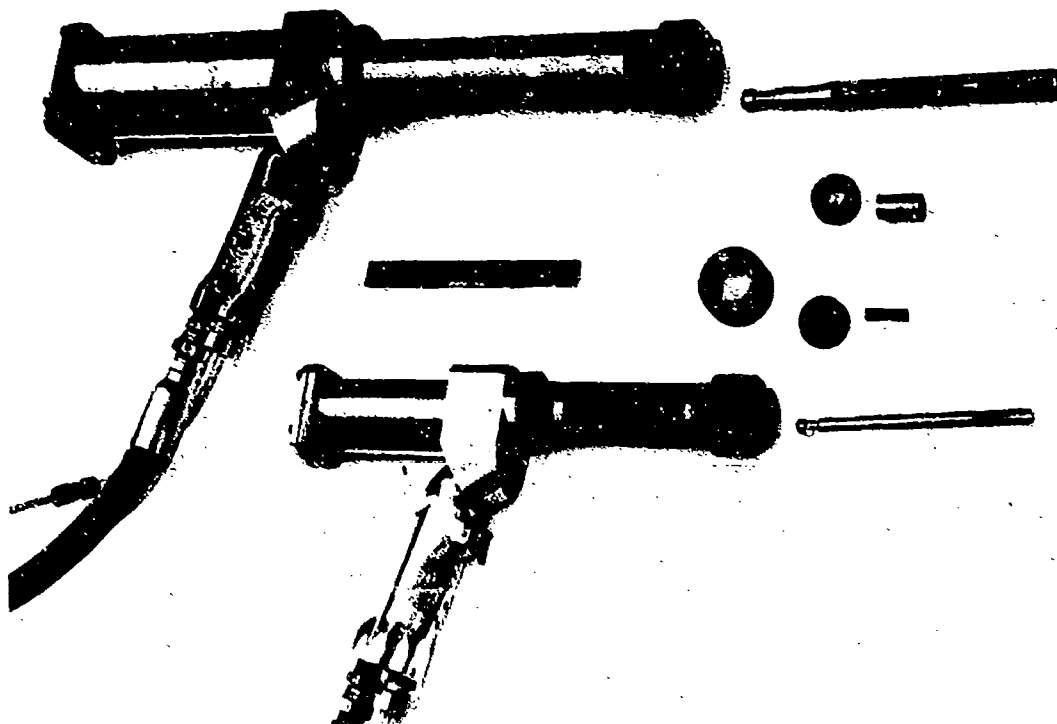
Figure 124.—ST 1350A and 1350A-C—Coldwork Pull Guns With Mandrels, Nosepieces, and Sleeves

Figure 125.--ST 1350A Coldwork Pull Gun in Production Use for Sleeve Coldworking
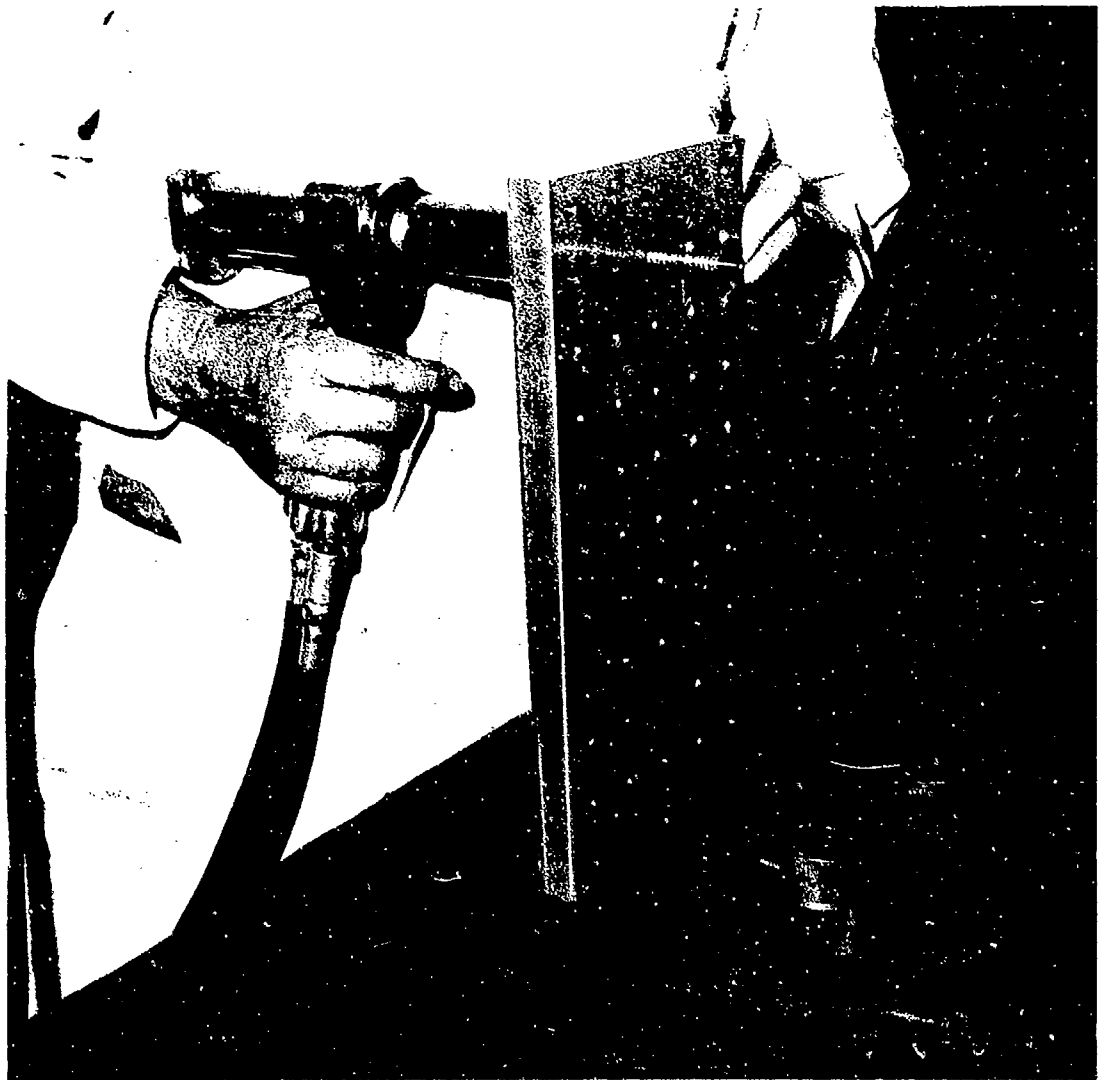
Figure 126.—ST 1350A Pull Gun Being Used to Pull Broach for Postsizing
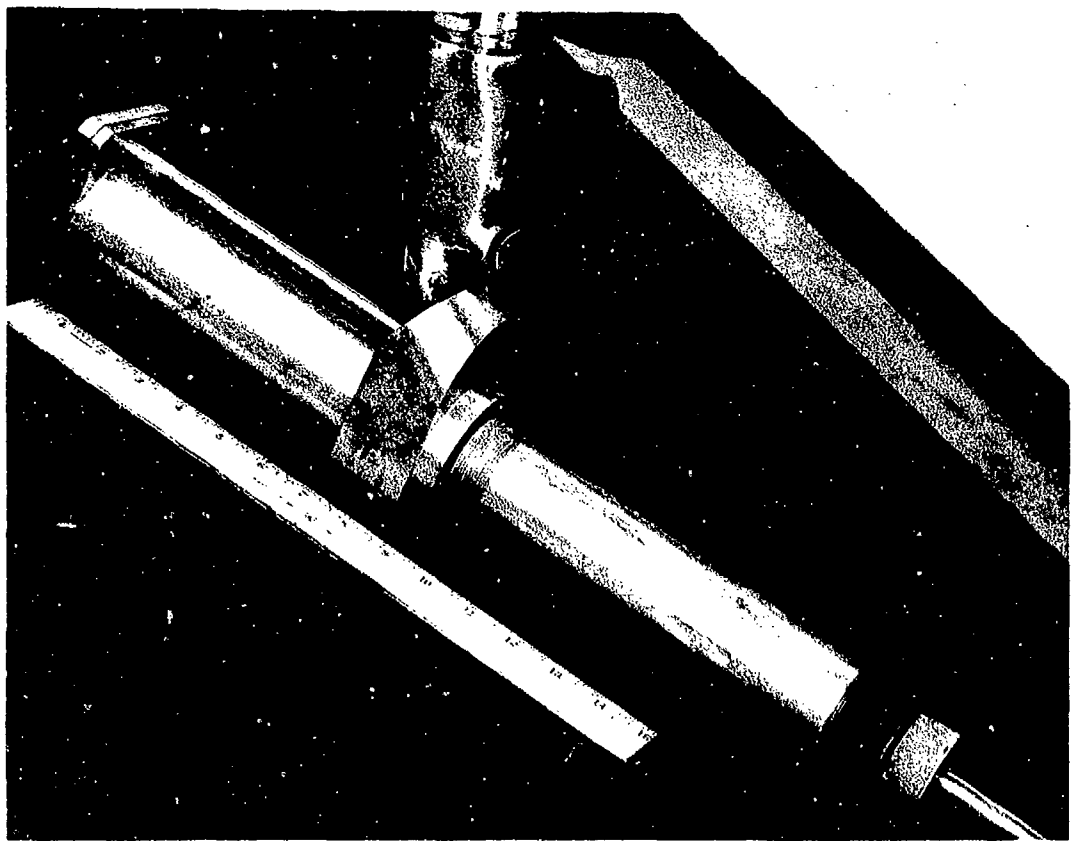
Figure 127. ST 1350A-B Coldwork Pull Gun
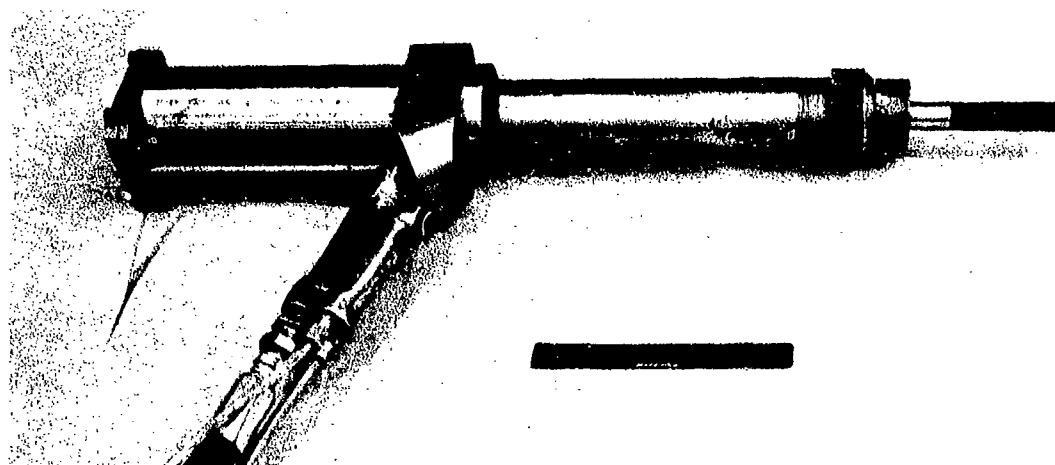
Figure 128.—ST 1350A-C Coldwork Pull Gun
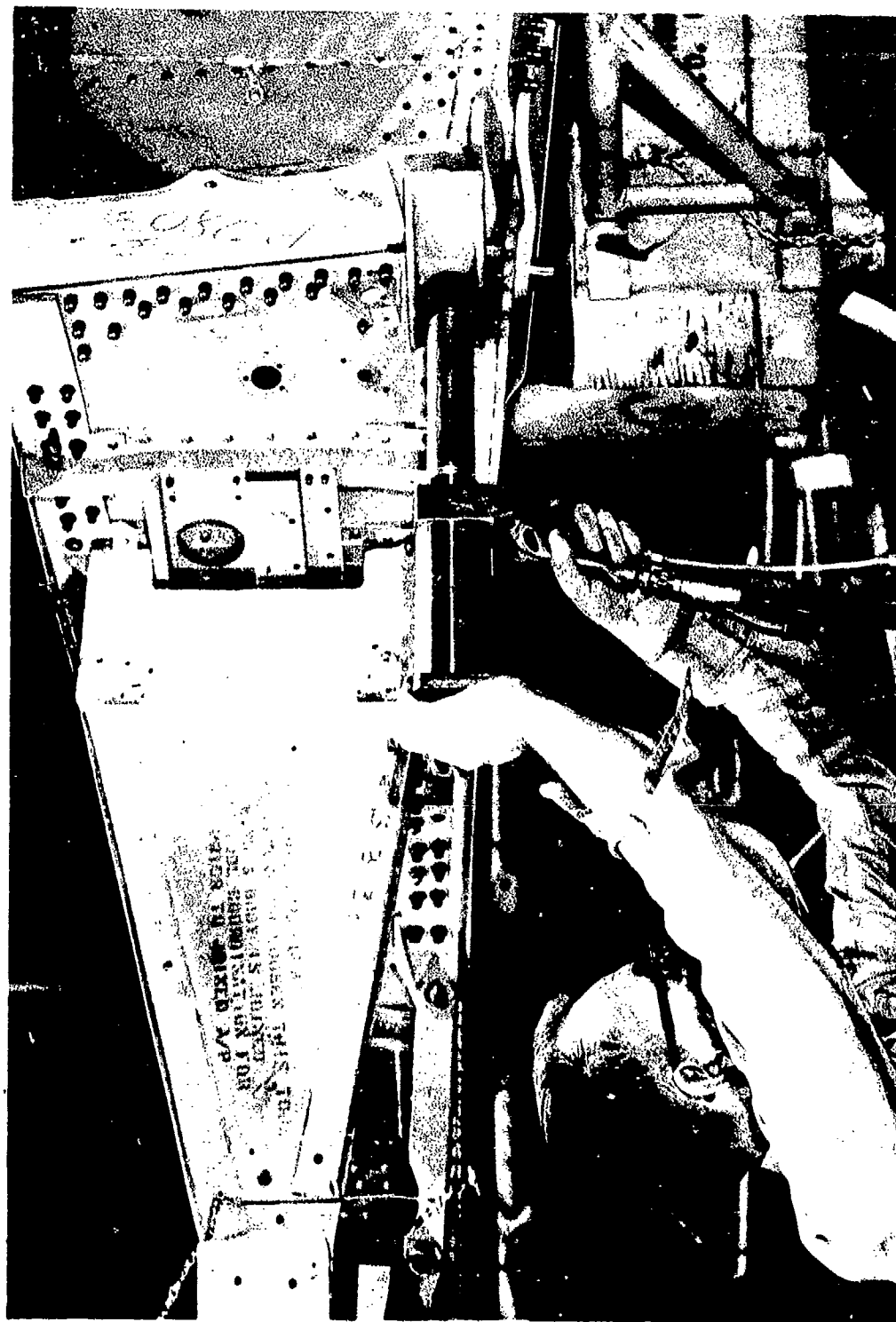
Figure 129.--ST 1 350A-C Coldwork Pull Gun in Production Use for Sleeve Coldworking— Horizontal Position
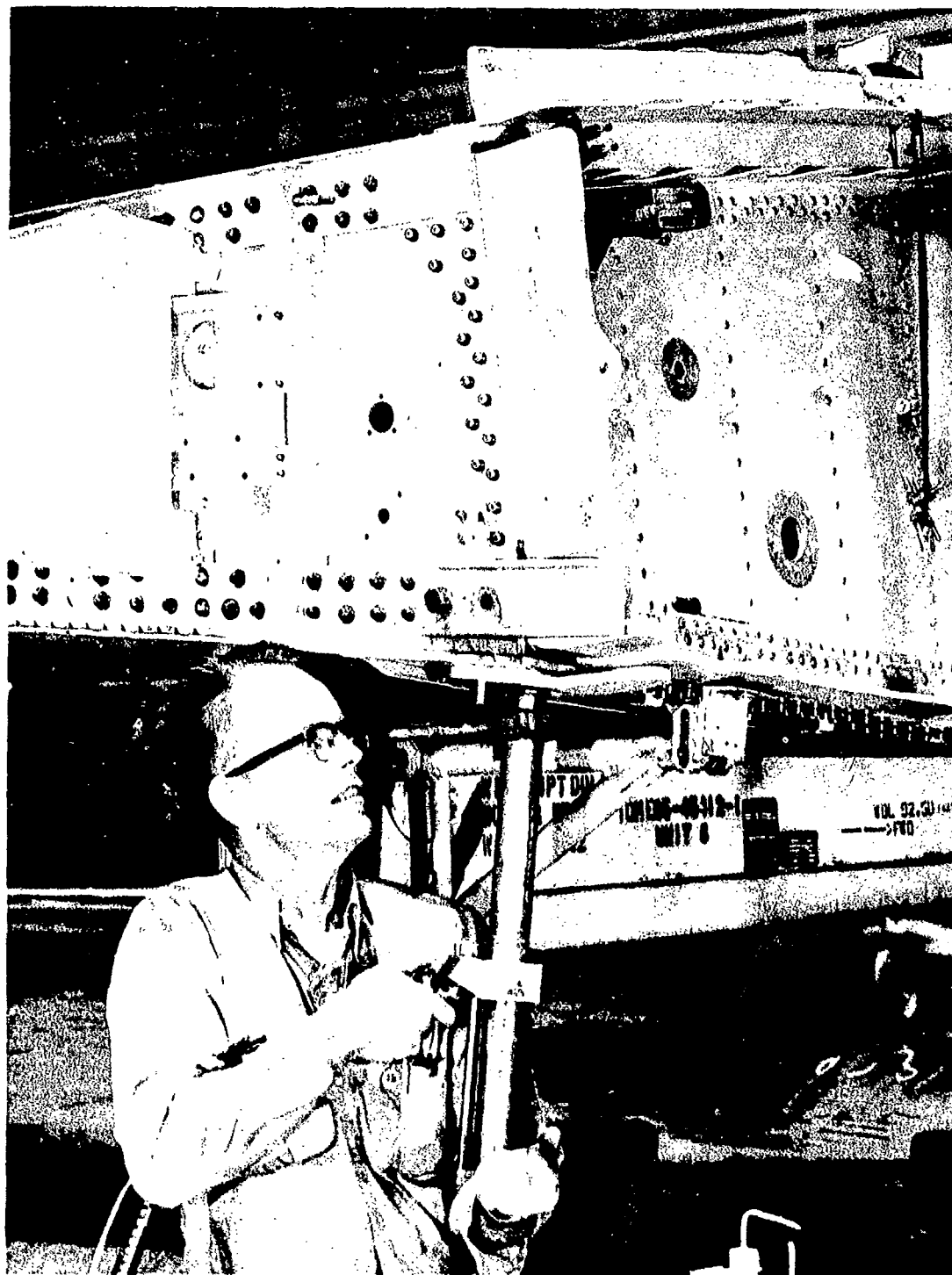
Figure 130. ST 1350A-C Coldwork Pull Gun in Production Use for Sleeve Coldworking Vertical Position
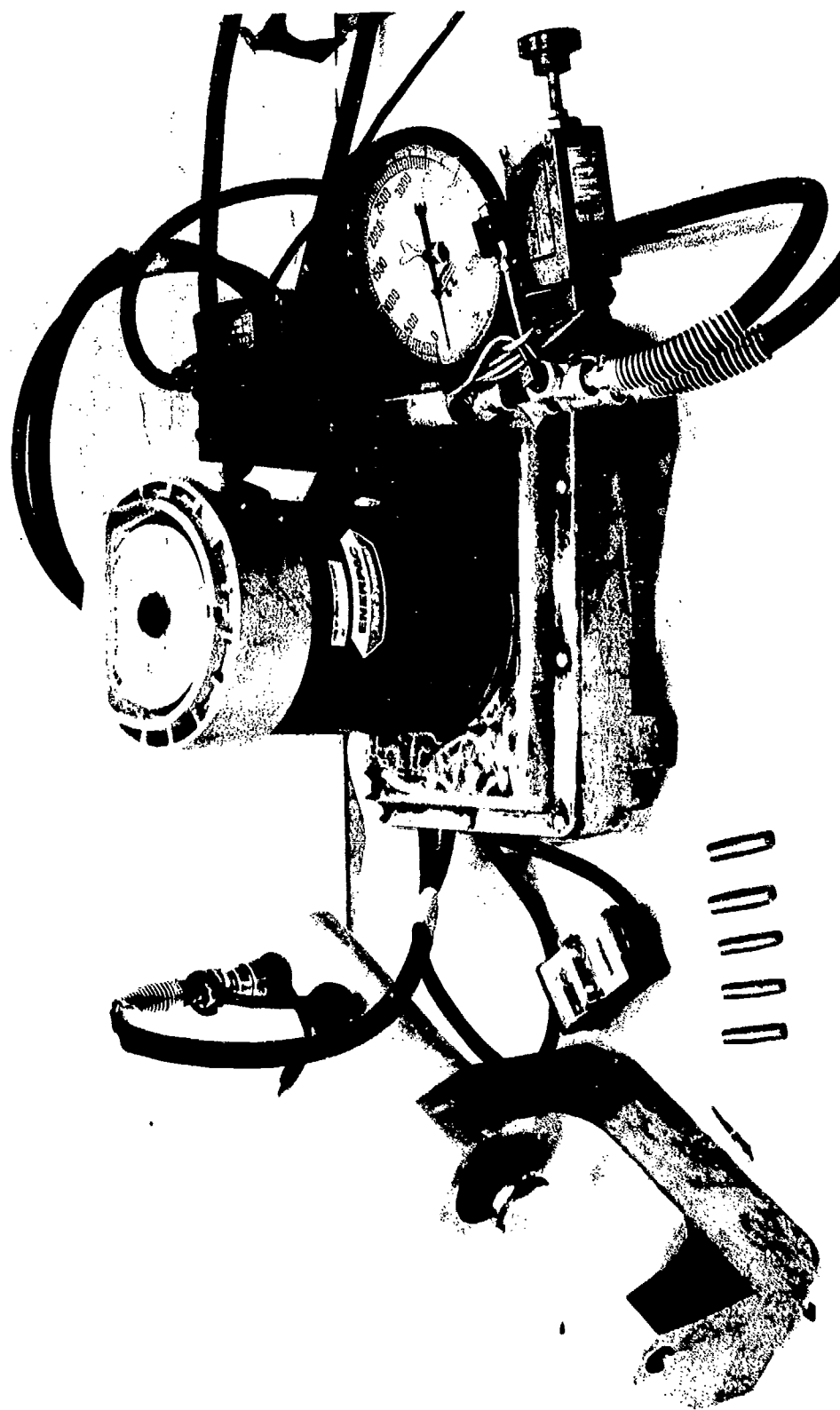
Figure 131. — Enerpac Electrohydraulic Power Unit With Squeeze Yoke and Carbide Mandrels for Steel Coldworking
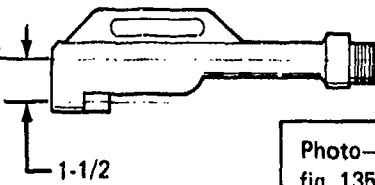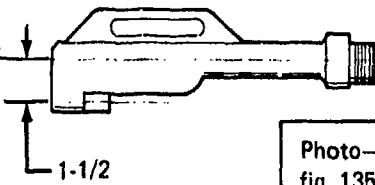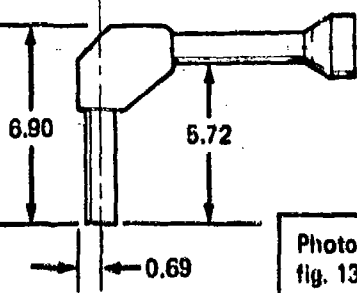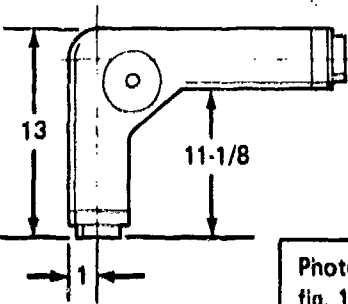
Drawing	Designation	For use with	Stroke (in.)	Capacity (lb)
3.96 / Photo—fig. 133	ST 1350A-B1-031 offset adapter	ST 1350A-B1-031	3-1/8	7,000
	ST 1350A-B-055 offset adapter	ST 1350A-B1-055	5-1/2	7,000
1-1/2 / Photo—fig. 135	ST 1350A-C-A offset adapter	ST 1350A-C	6-3/8	25,000
13 / 11-1/8 / 1 / Photo—fig. 136	ST 1350A-ARA2 angle head with self-aligning nosepiece	ST 1350A-ARA2	7	22,600
6.90 / 5.72 / 0.69 / Photo—fig. 138	ST 1350A-RAA angle puller	ST 1350A-055 or ST 1350A-RAA angle head puller assembly	5-1/2	7,000
2.58 / 3 / Photo—fig. 138	ST 1350A-RA-A offset adapter	ST 1350A-RA-1	1	4,500

Figure 132.—Puller Unit Accessories
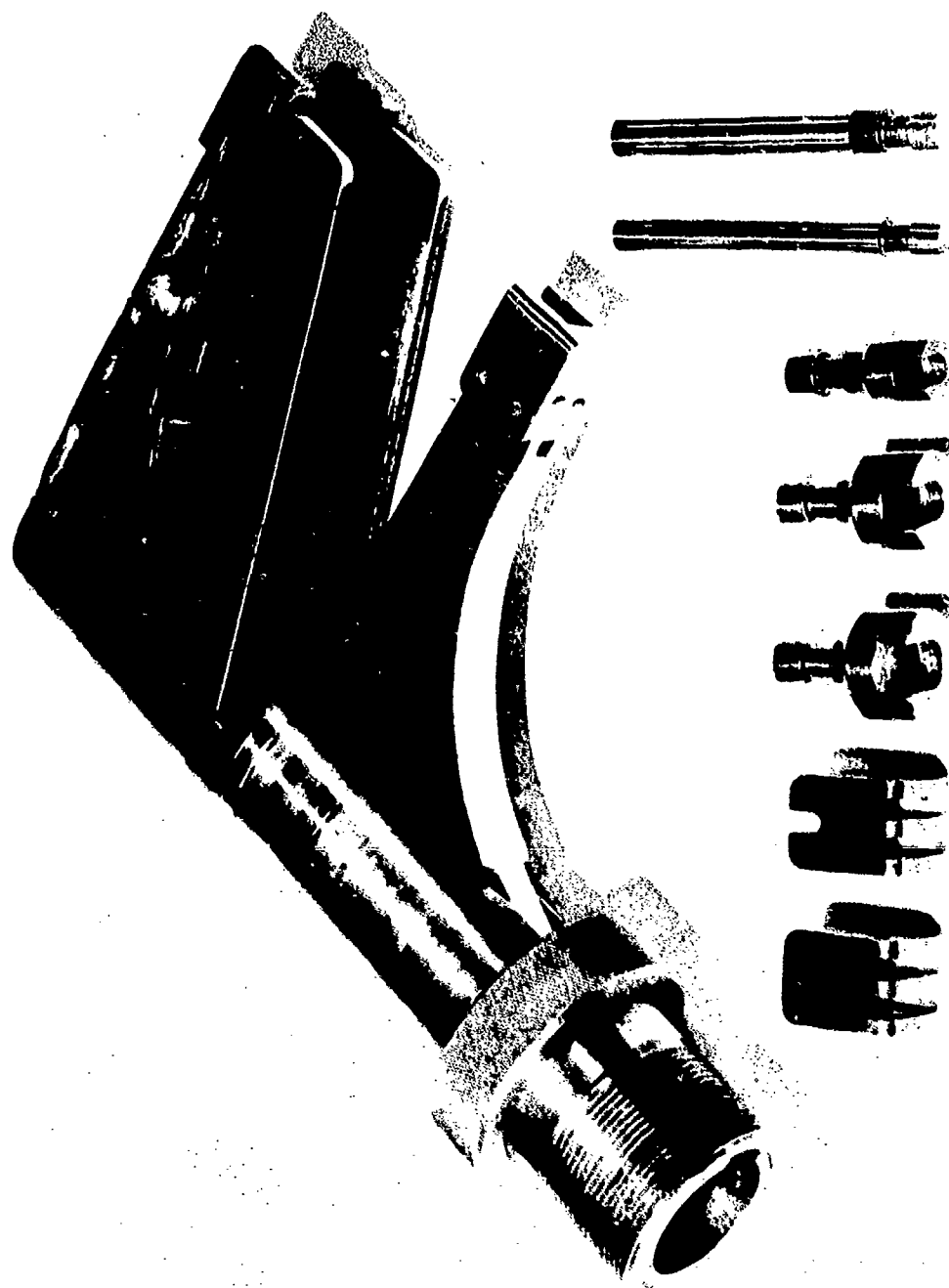
Figure 133.--ST 1350A-B1 Offset Adapter
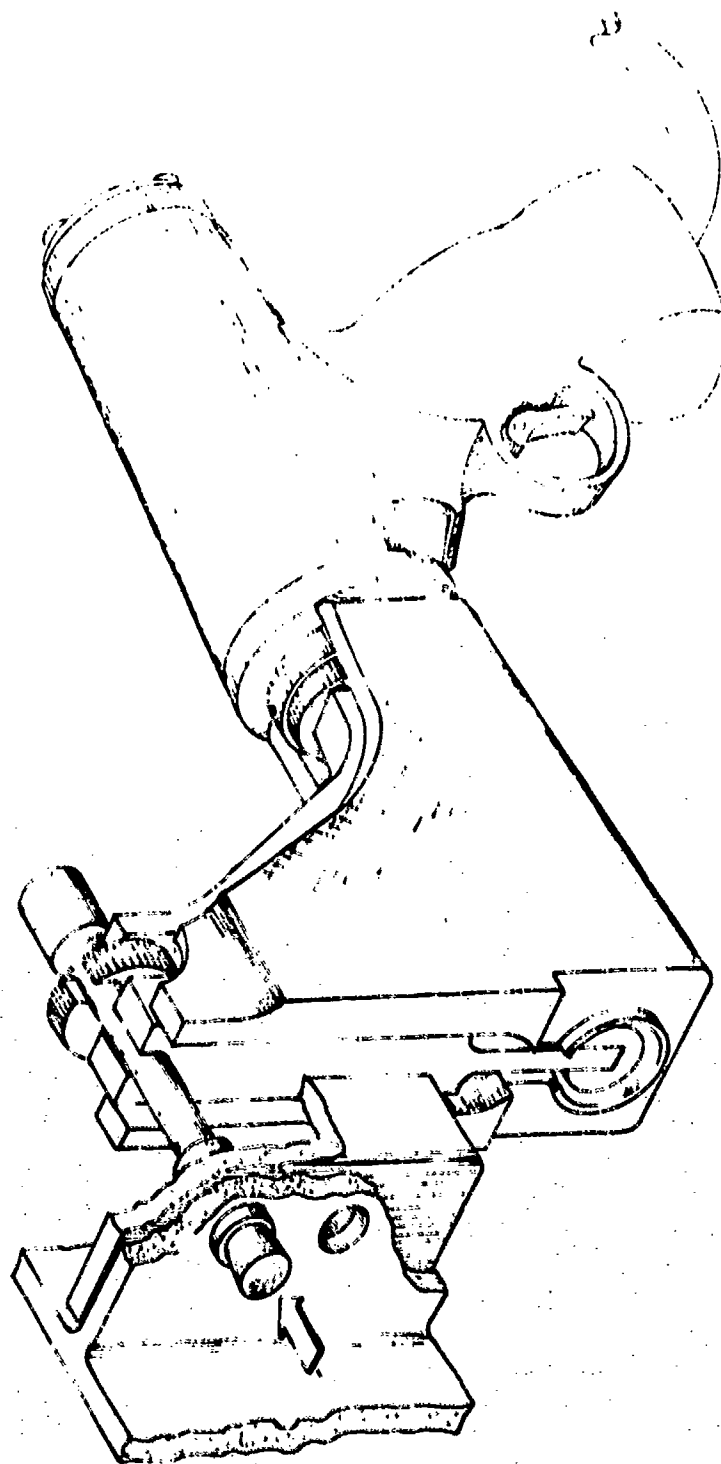
Figure 134.—Schematic of Offset Adapter in Use
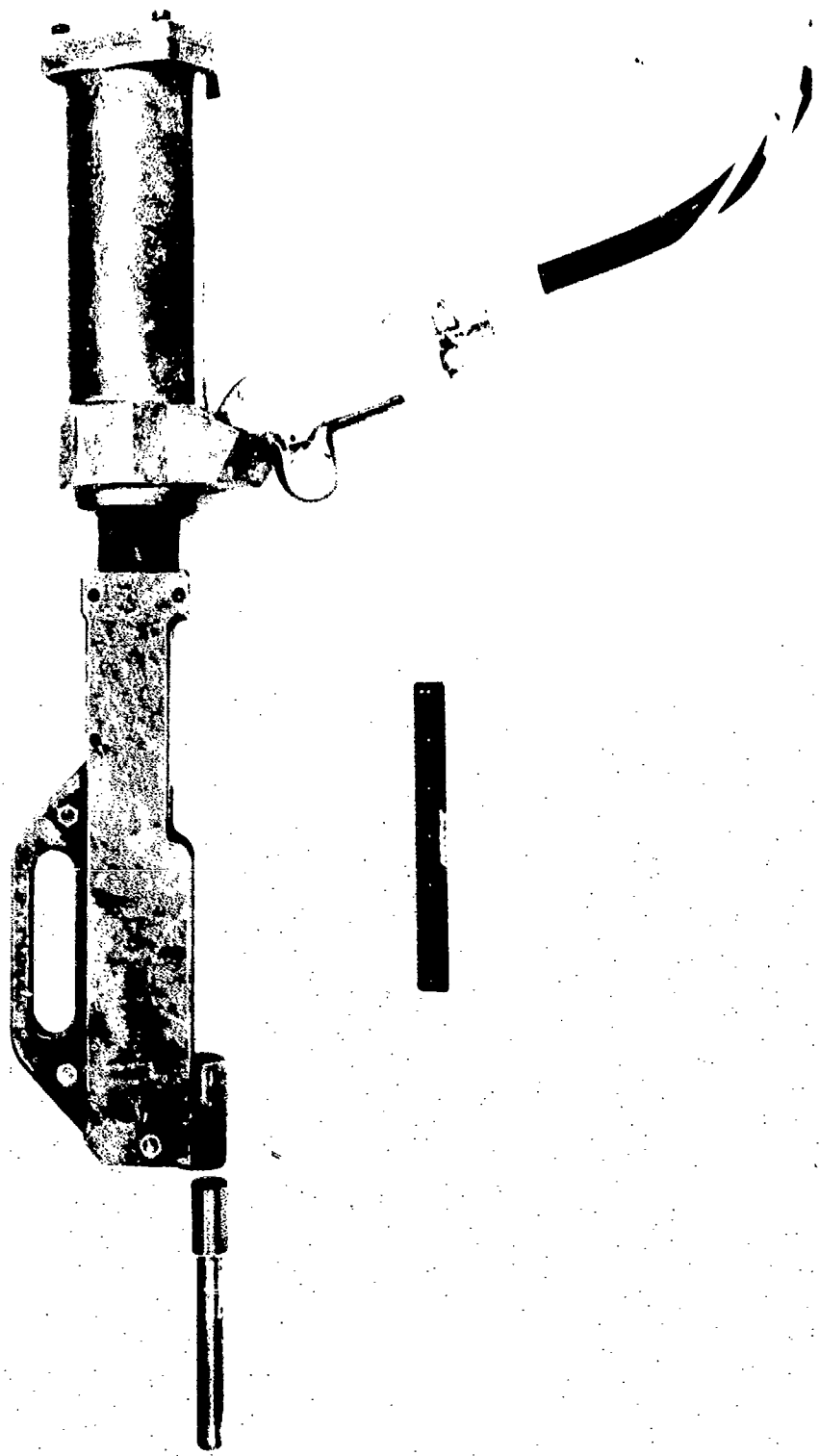
Figure 135. ST 1350A-C-A Offset Adapter
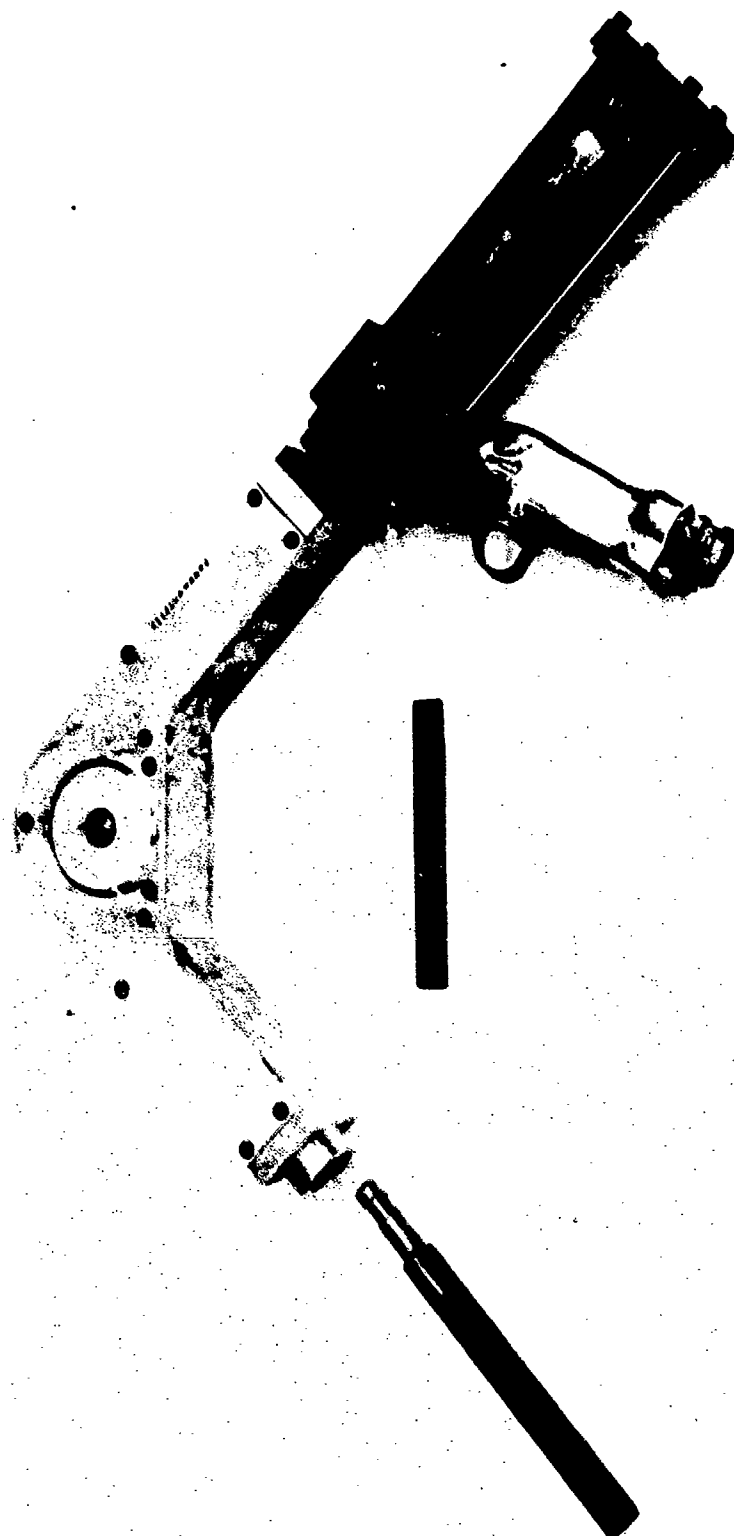
Figure 136.—ST 1350A-ARA2 Angle Head
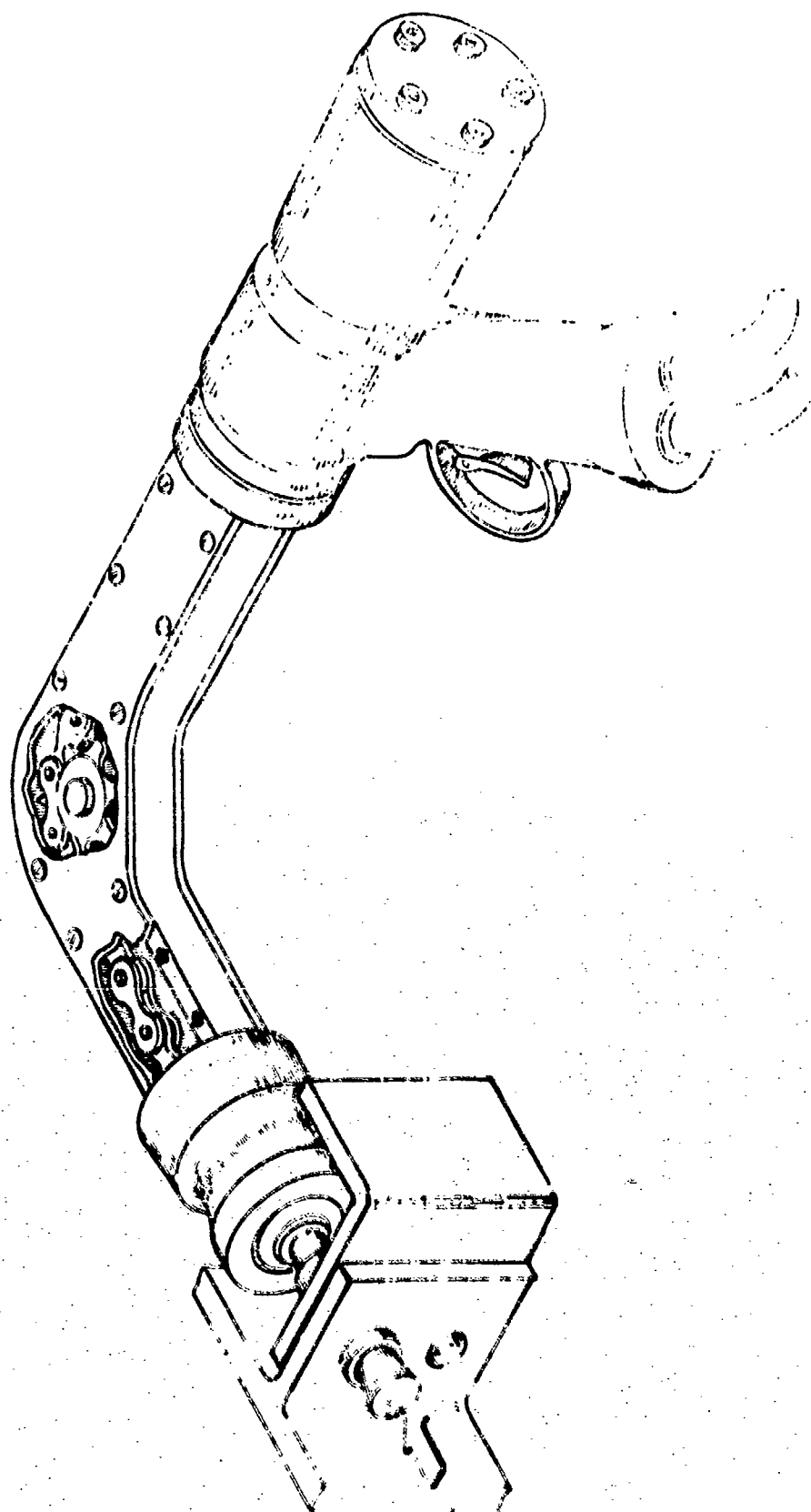
Figure 137. – Schematic of Angle Head in Use
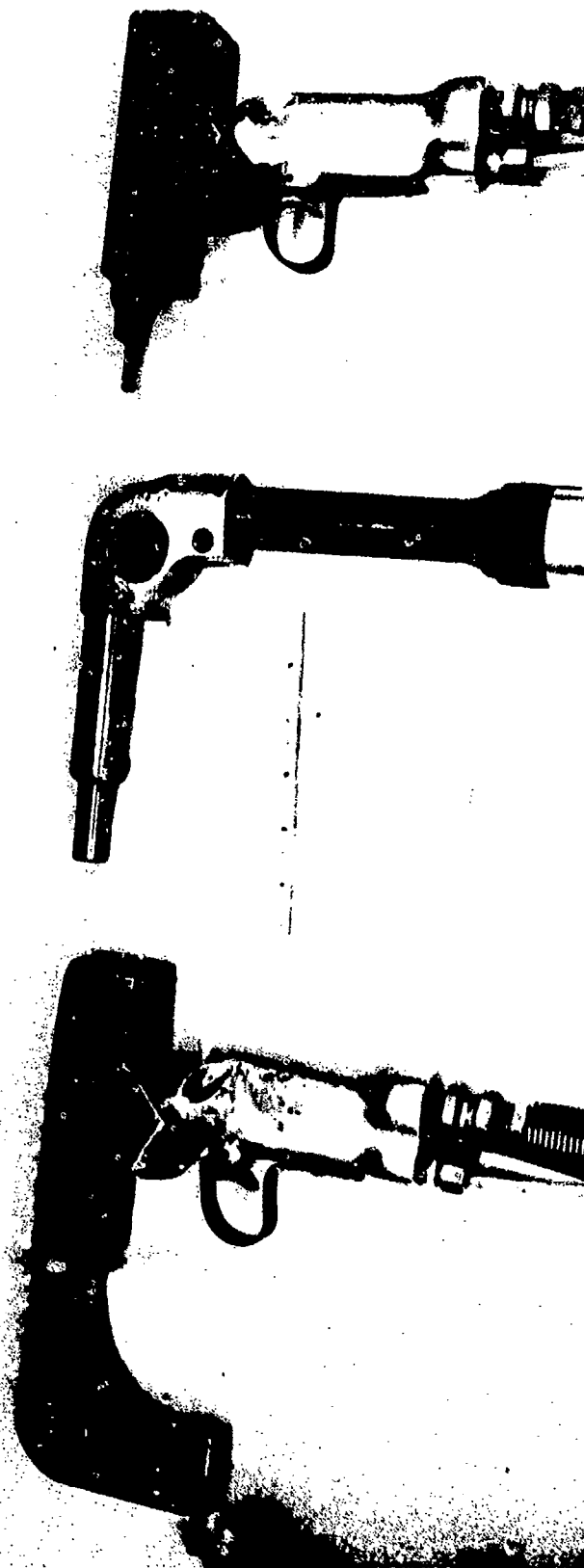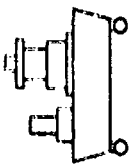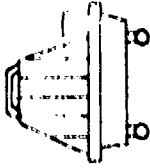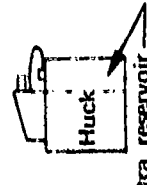
Figure 138.—*ST 1350A-RA-A Offset Adapter on ST 1350A-RA-1 Pull Gun, ST 1350A-RAA Angle Head, and ST 1350A-RA-1 Pull Gun*

Power units		Photo fig.	Maximum psi	Output at maximum psi (in.^{3})	Oil available per cycle (in.^{3})	Type pumping	Input power	Type unit	Approximate weight (lb)	1973 list price
Drawing	Designation									
	Chicago Pnuematic CP 805 (turtle)	140	7,000 (std)	20	80	Pulsating	Air (90 psi)	Floor	58	$1425
	Enerpac PA 621 with remote control modification	141	10,000	30	150	Continuous	Air (90 psi)	Floor	60	$1100
	Enerpac Pam 3022 with remote control modification	—	10,000	30	300	Continuous	Air (90 psi)	Floor	100	$1200 (modified)
	Enerpac PA-130 with remote control modification	142 and 143	10,000	—	24	Pulsating	Air (90 psi)	Floor	Approx. 20 (modified)	$600 (modified)
	Huck 970 power rig with reservoir modification	144 and 145	7,000	NA	25 (modified)	Pulsating	Air (90 psi)	Belt	Approx. 15 (modified)	Approx. $800 (modified)

Note: Any hydraulic power source with 7000-10,000 psi capacity can be used; above have been used

Figure 139. – Portable Hydraulic Power Sources

223
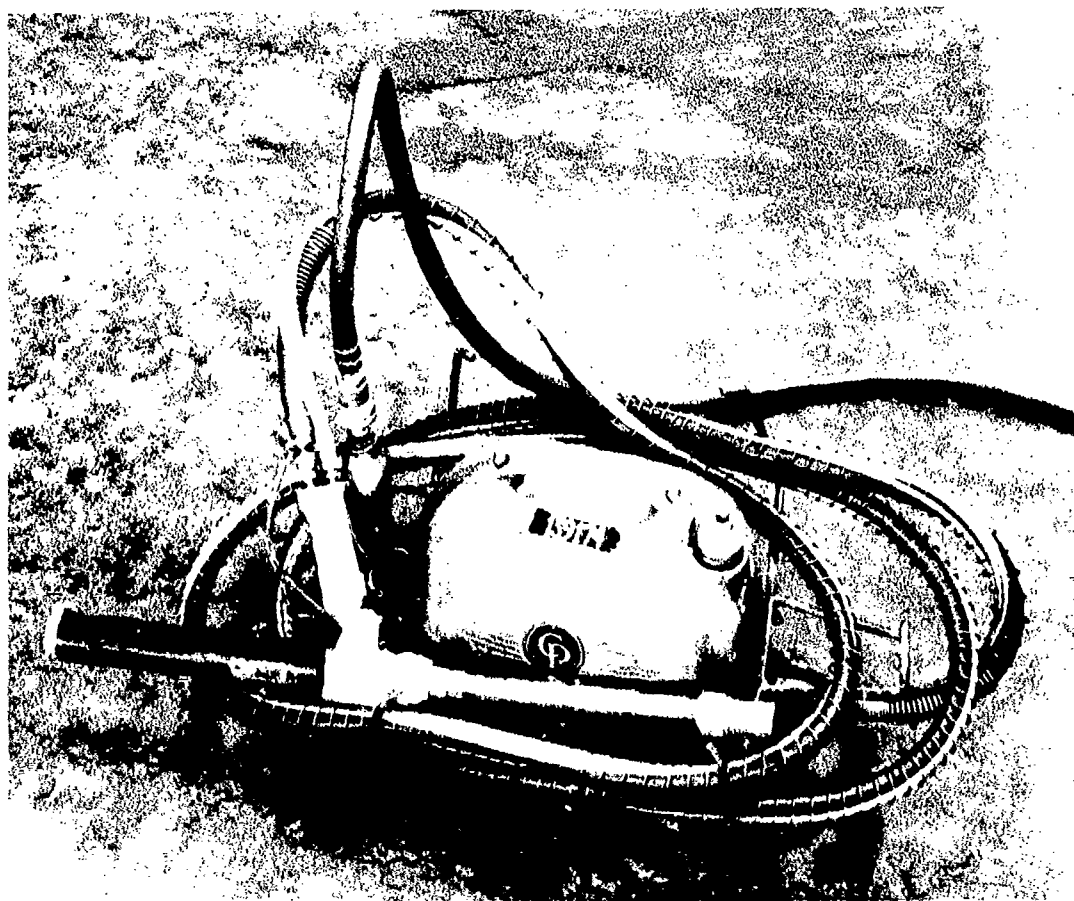
Figure 140.   CP 805 Pneudraulic Power Unit and CP 659 Pull Gun
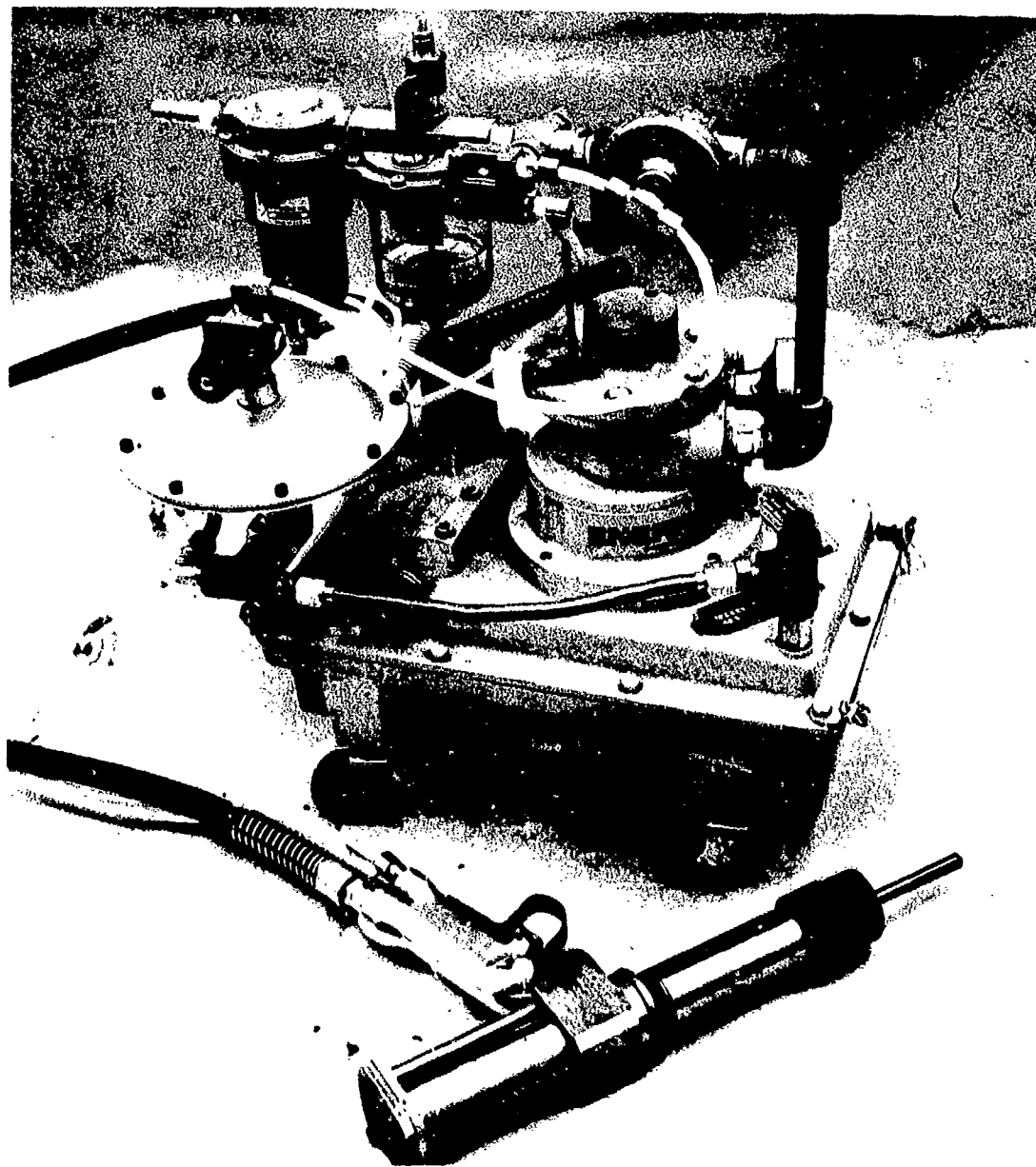
Figure 141. Enerpac Air-Hydraulic Power Pack PA621 With Remote Control
Modification, and ST 1350A Pull Gun

225
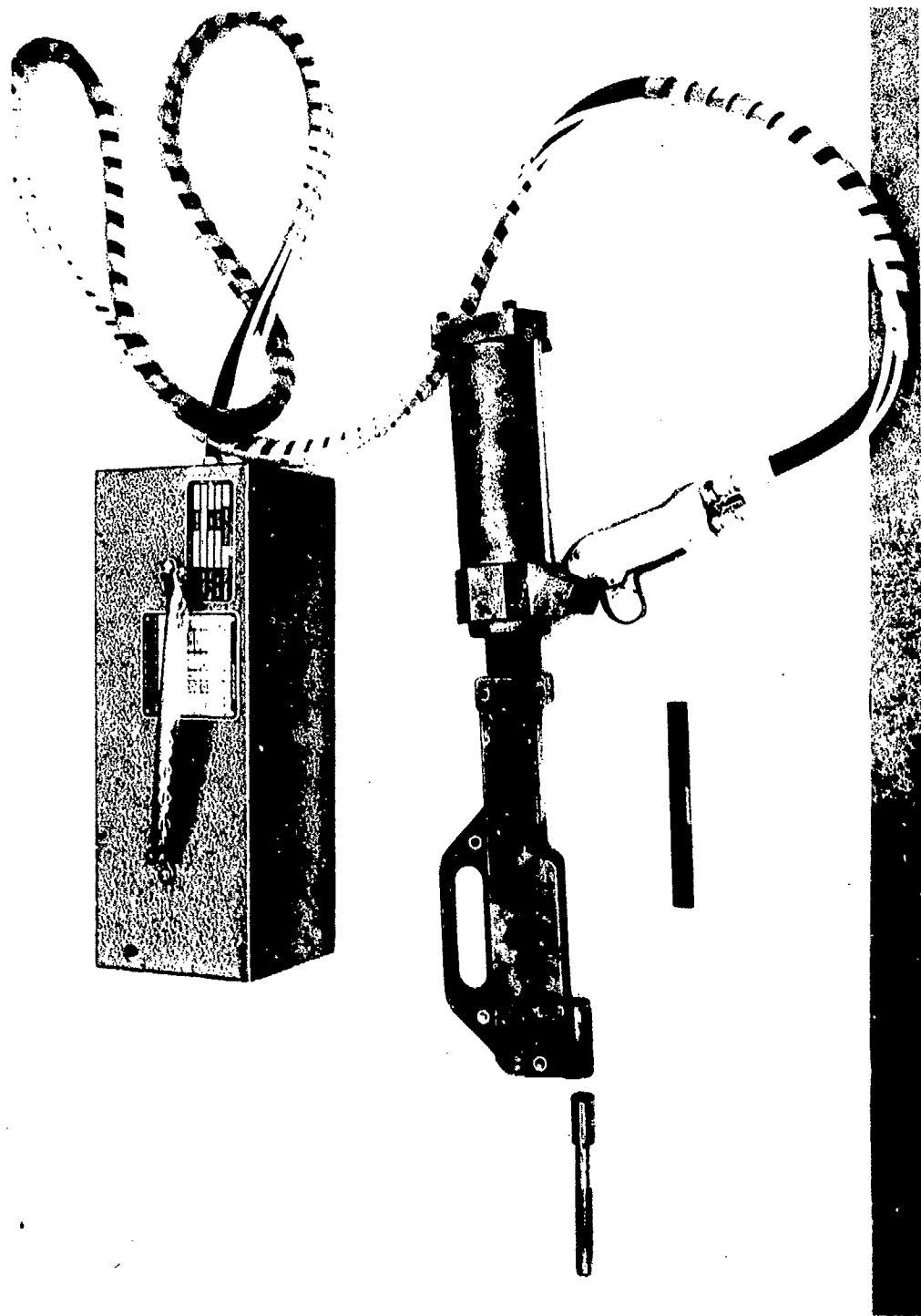
Figure 142. Enerpac Pneudraulic Power Pack PA-1 30 (in Case) With Remote Control Modification and ST 1 350A-C-A Pull Gun With ST 1 350A-C-A Offset Adapter
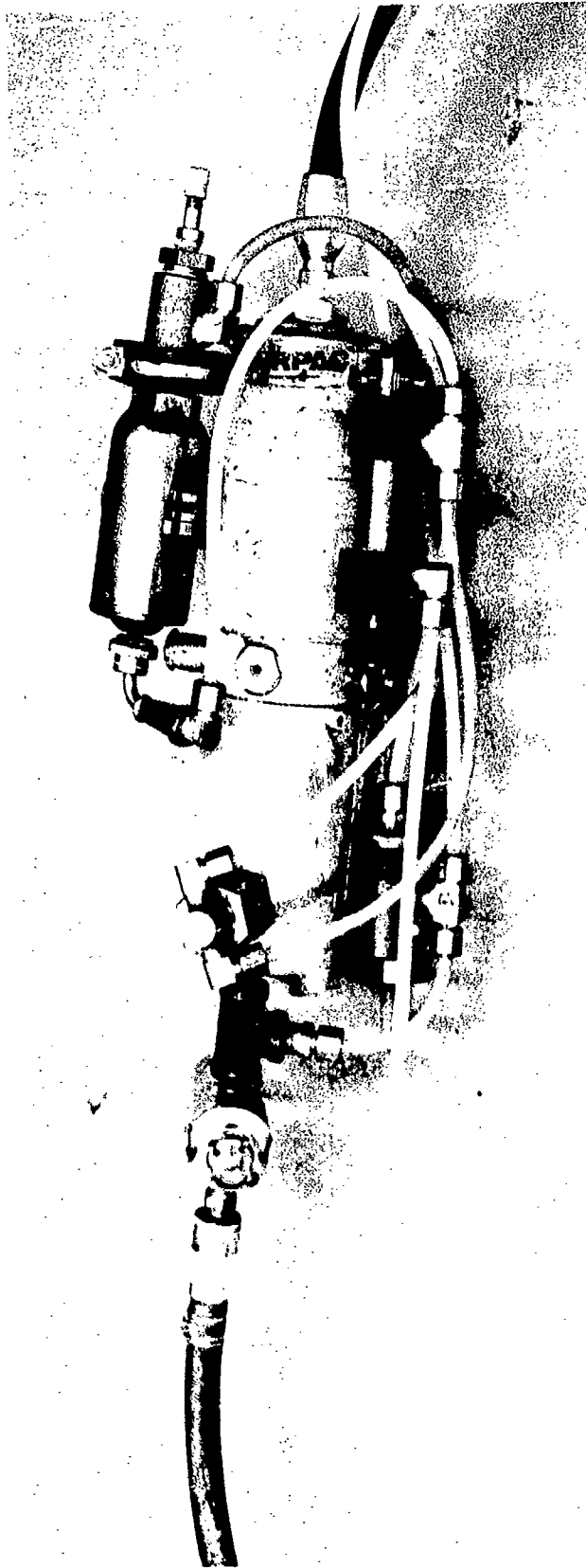
Figure 143.—Enerpac Pneudraulic Unit PA-130 Out of Case Showing Automatic Actuation Adaptation
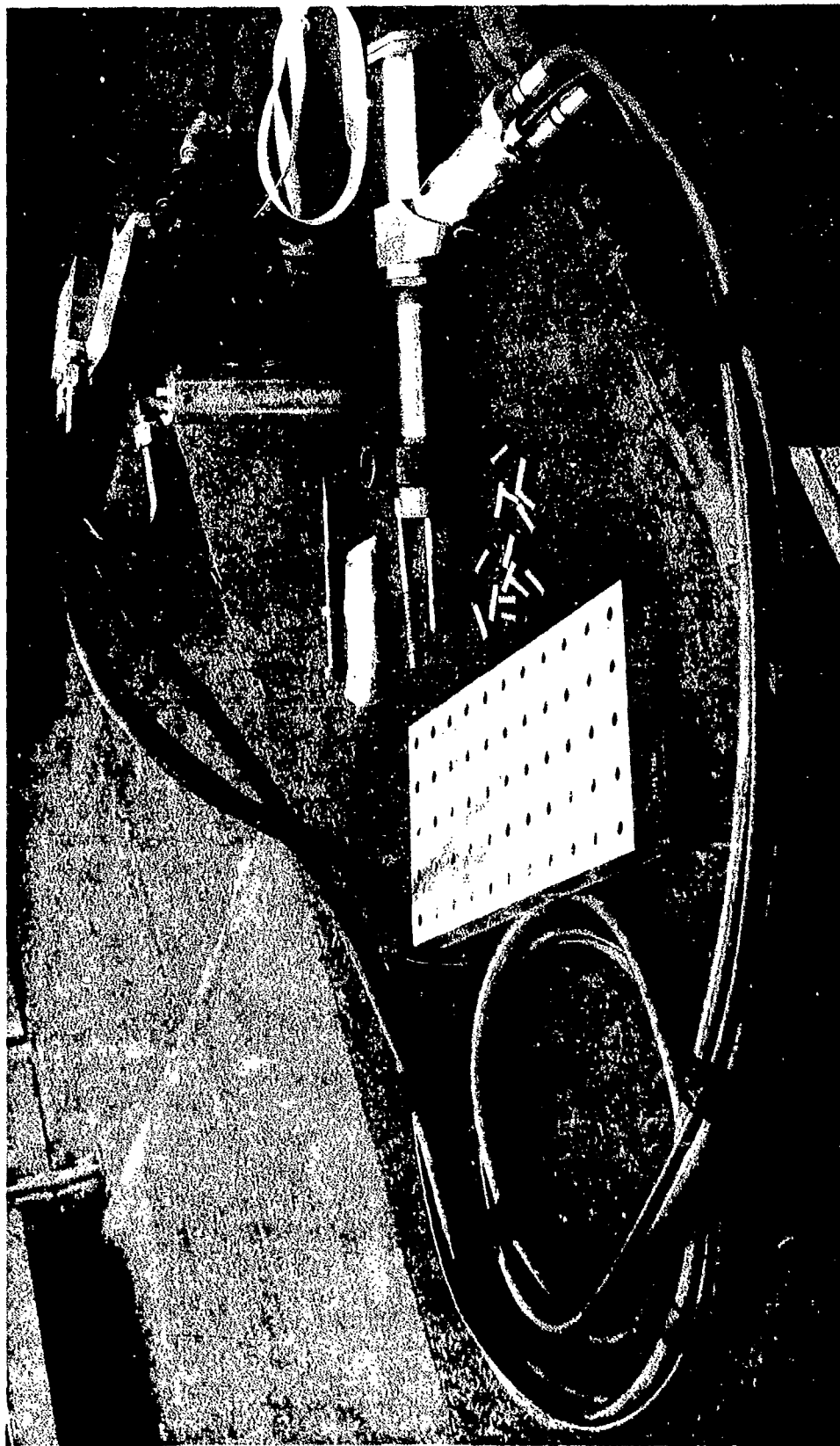
Figure 144. Huck 970 Pneudradlic Power Rig With Reservoir   laptation and ST 1350A Pull Gun

Figure 145. Huck 970 Pneudraulic Power Rig in Use as Portable Strap-On Unit
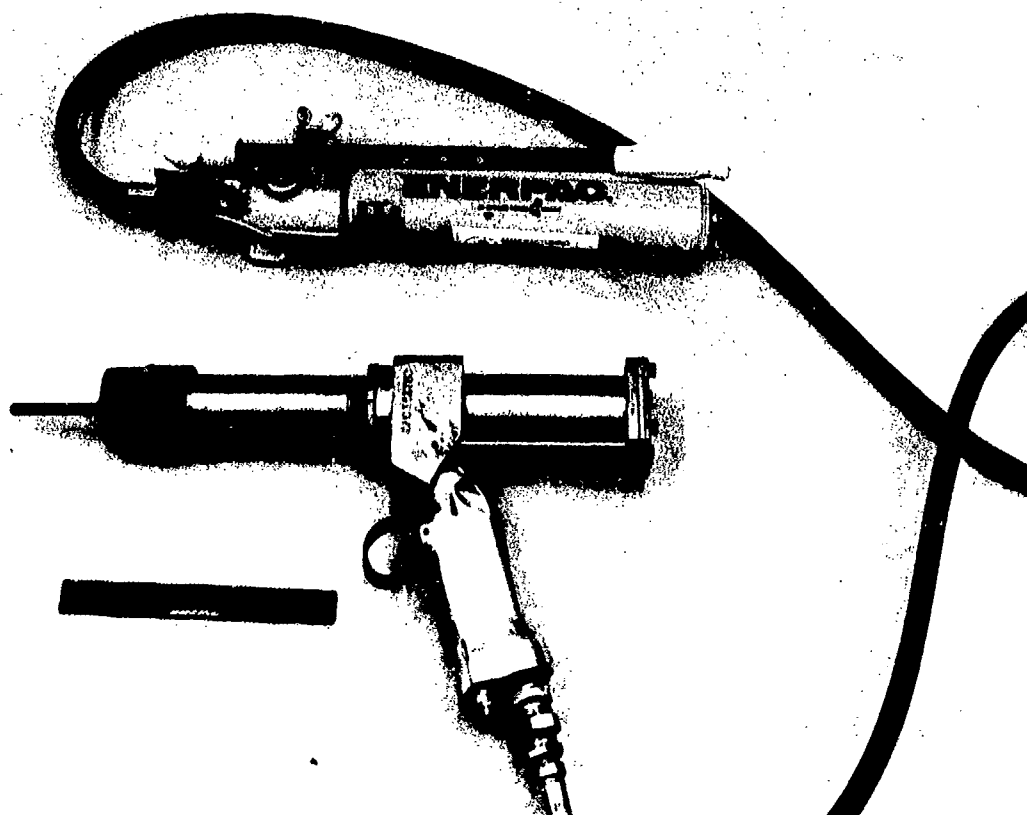
Figure 146. ST 1350A Pull Gun With Enerpac Hand Pump

Figure 147.—CP 660 Broach Puller Model A
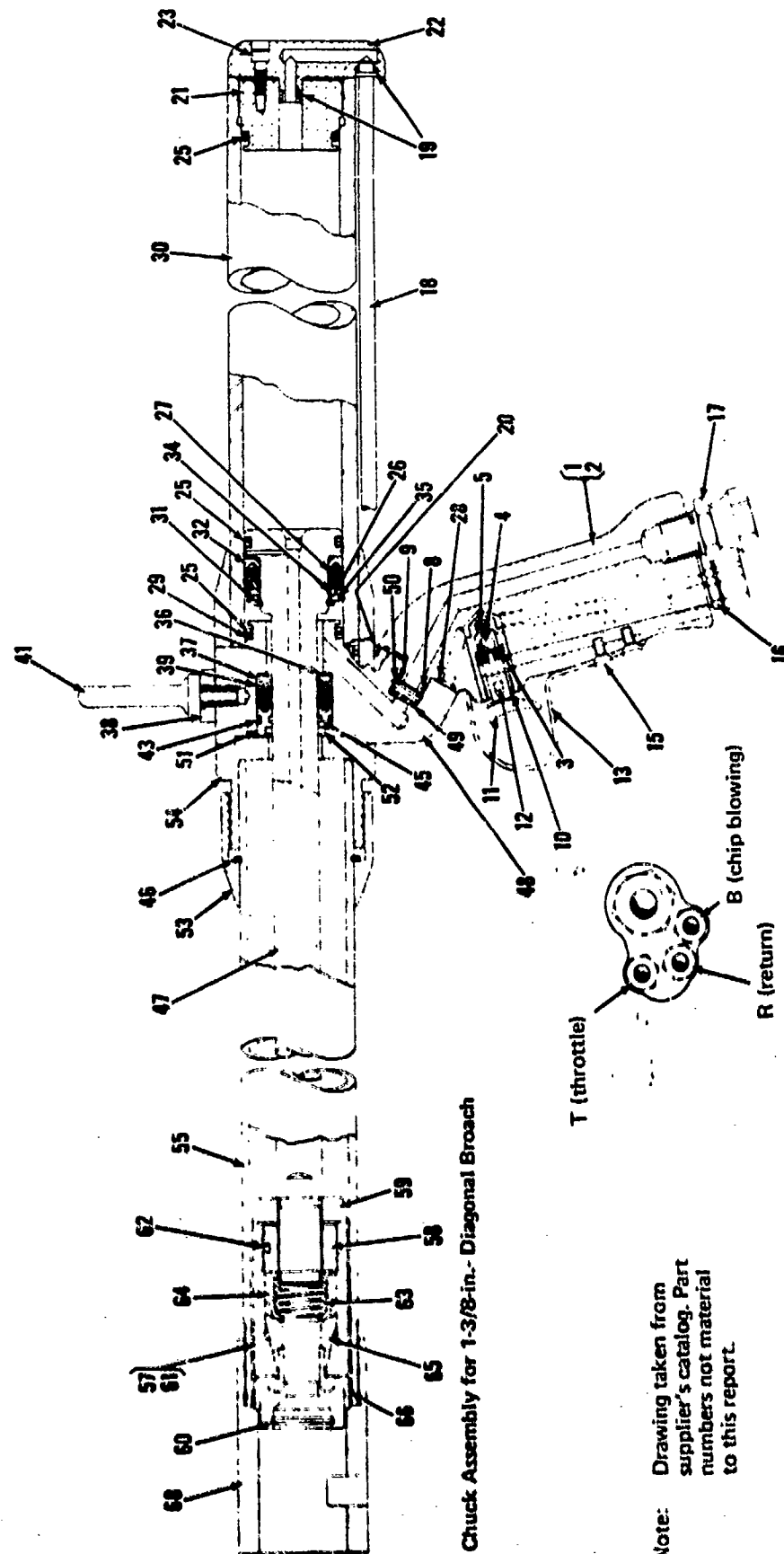
Chuck Assembly for 1-3/8-in.- Diagonal Broach

Note: Drawing taken from
supplier's catalog. Part
numbers not material
to this report.

T (throttle)

B (chip blowing)

R (return)
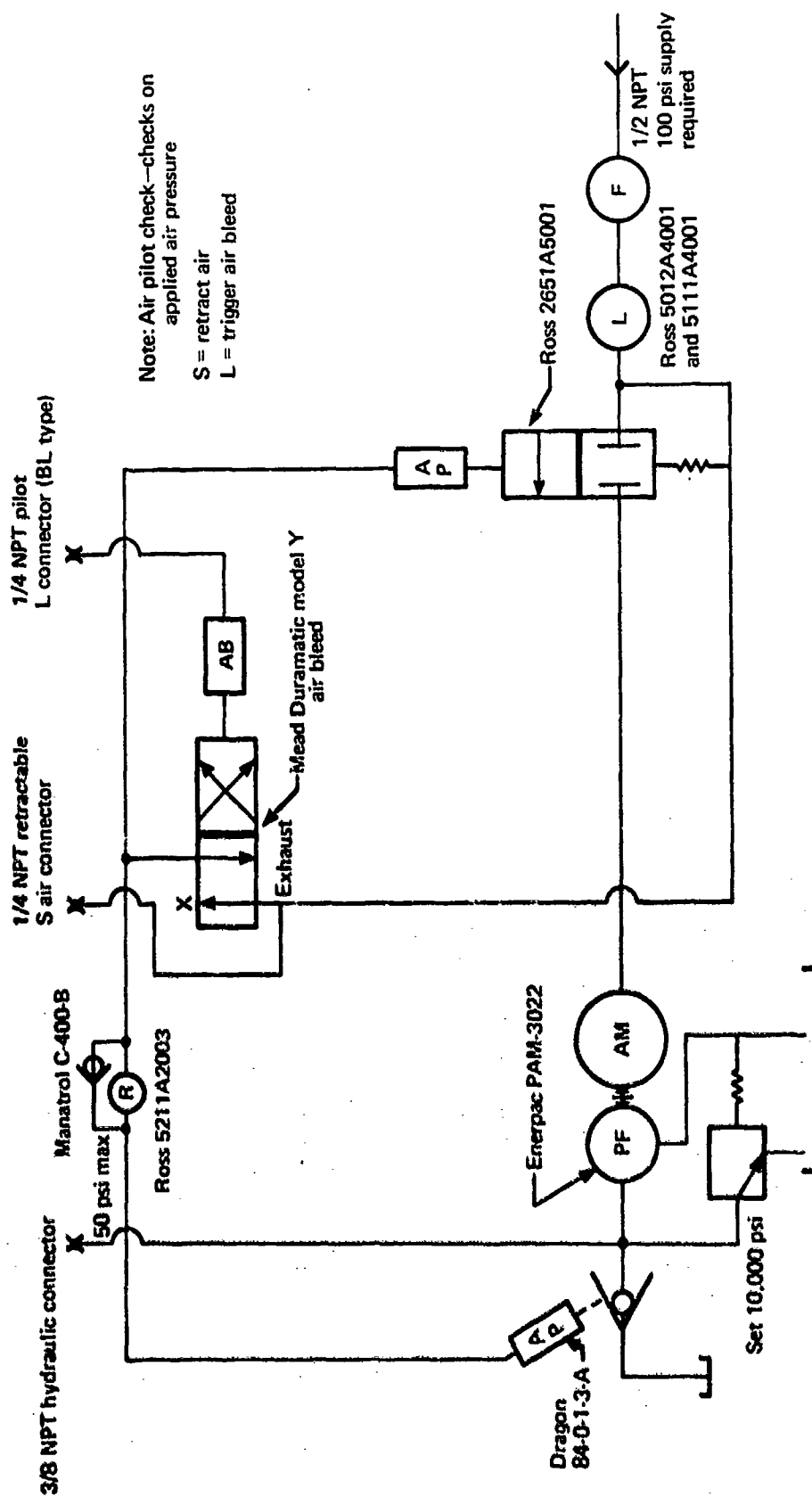
Figure 148.—Schematic of Automatic Adaptation for Enerpac Units

Note: Air pilot check—checks on applied air pressure

S = retract air
L = trigger air bleed

1/2 NPT
100 psi supply required

Ross 2651A5001

Ross 5012A4001 and 5111A4001

1/4 NPT pilot L connector (BL type)

Mead Duramatic model Y air bleed

1/4 NPT retractable S air connector

Exhaust

Manatrol C-400-B

50 psi max

Ross 521 1A2003

3/8 NPT hydraulic connector

Enerpac PAM-3022

Set 10,000 psi

Dragon 84-0-1-3-A

232

Figure 149. Base Metal S-N Scatter Curve 2024-T851 Aluminum
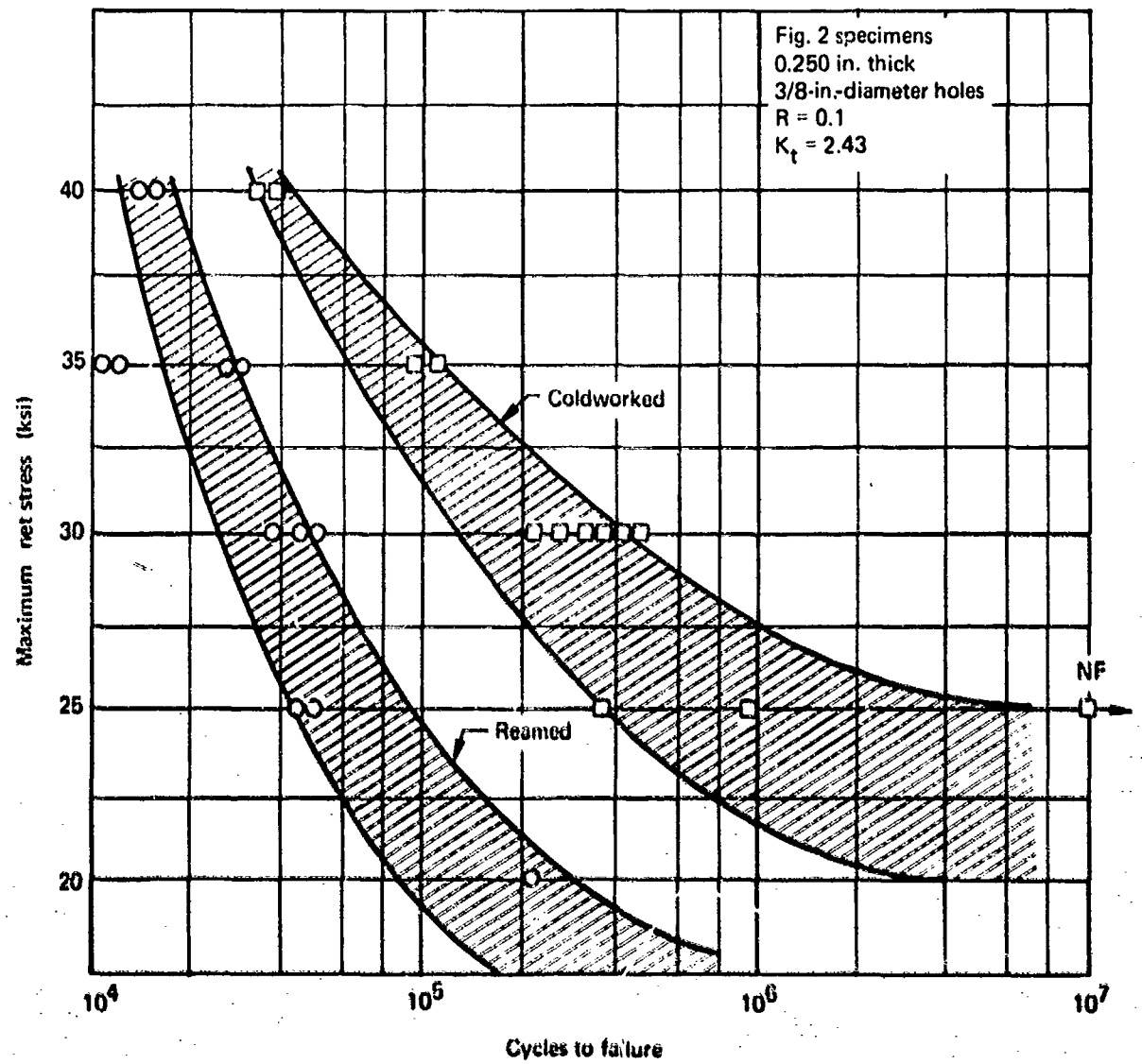
Figure 150.—S-N Scatter Curves - Zero Load Transfer Open Holes - 2024-T851 Aluminum

The chart text:

Fig. 2 specimens
0.250 in. thick
3/8-in.-diameter holes
R = 0.1
K_t = 2.43

Coldworked

Reamed

NF

Maximum net stress (ksi)

Cycles to failure
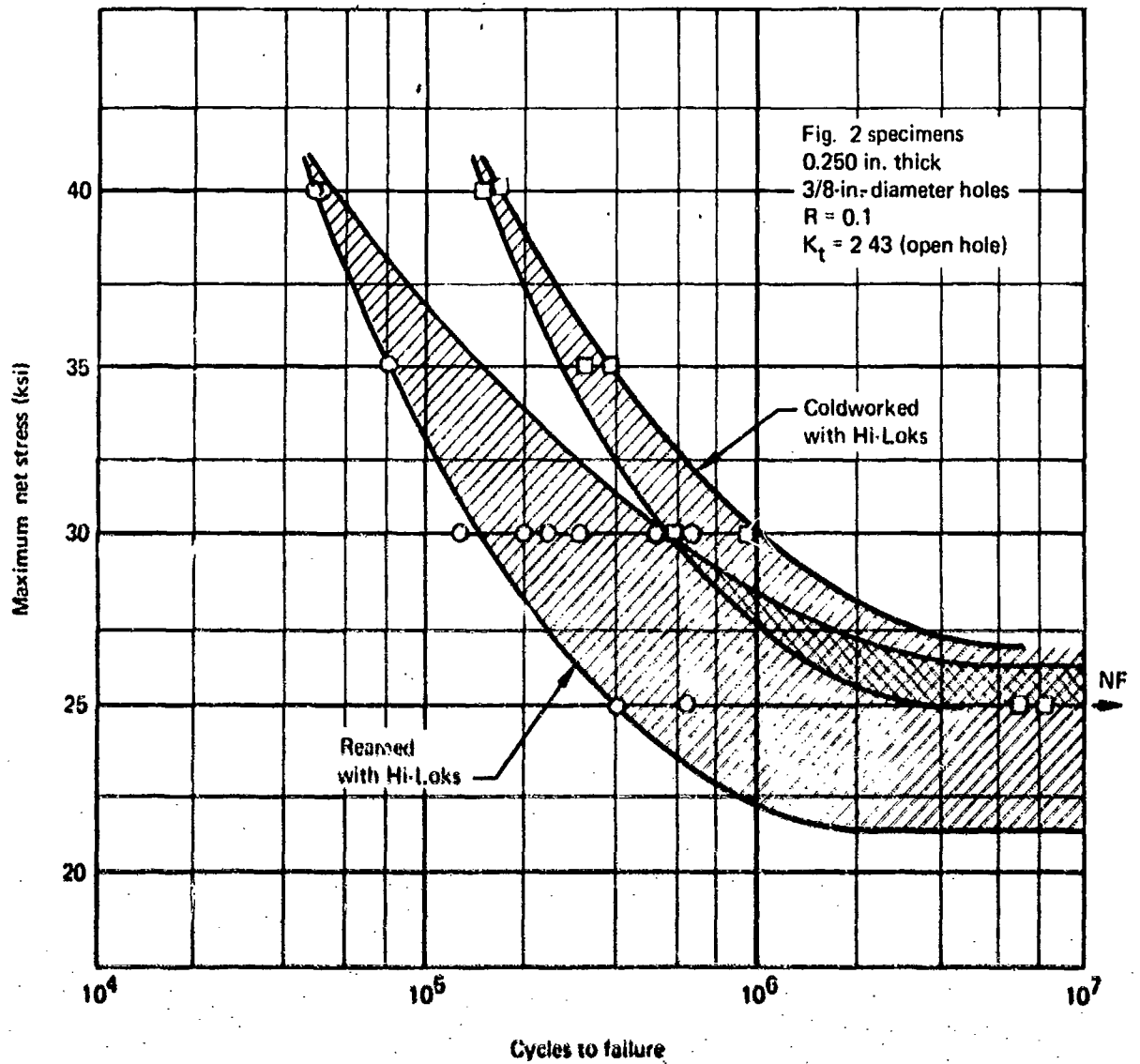
Figure 151. Hi-Lok S-N Scatter Curves—Zero Load Transfer Filled Holes—2024-T851 Aluminum

235
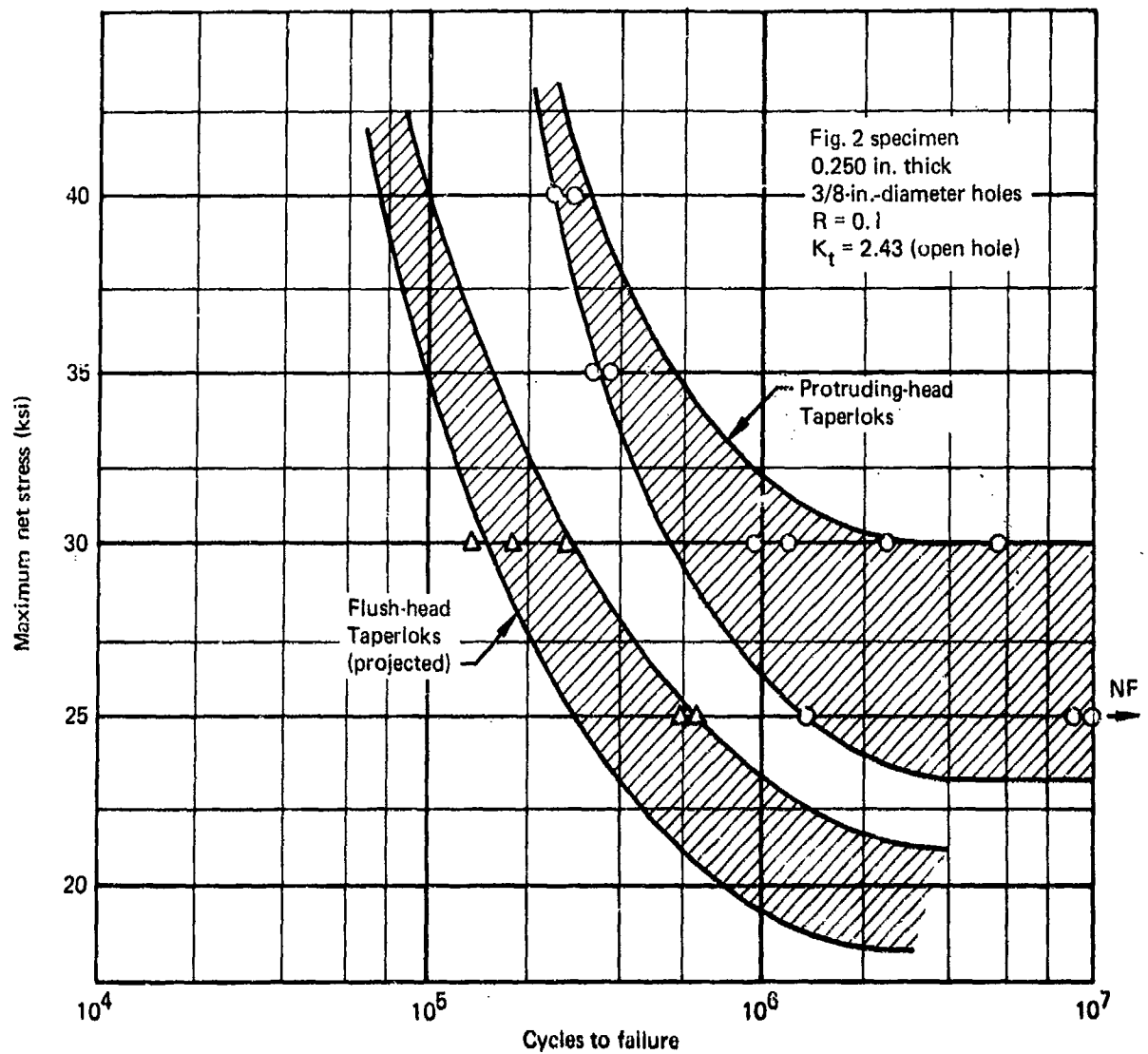
Figure 152. — Taper-Lok S-N Scatter Curves—Zero Load Transfer Filled Holes—2024-T851 Aluminum

The figure contains the following labels:

Maximum net stress (ksi)

Fig. 2 specimen
0.250 in. thick
3/8-in.-diameter holes
R = 0.1
K_t = 2.43 (open hole)

Protruding-head
Taperloks

Flush-head
Taperloks
(projected)

NF

Cycles to failure
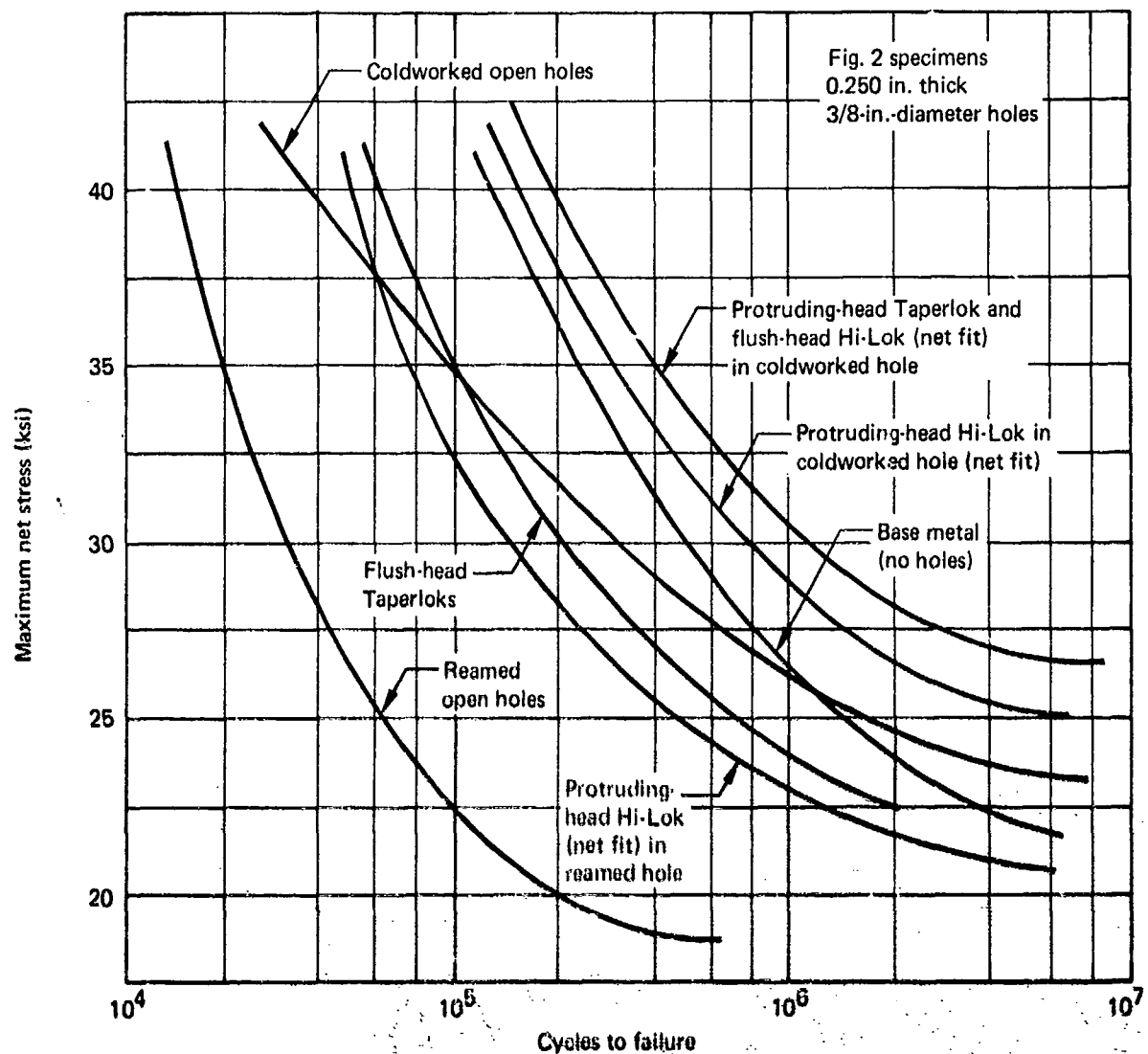
Figure 15.3. Log Mean S-N Curves (Net Stress) Zero Load Transfer.
Fatigue Tests 2024-T851 Aluminum

237
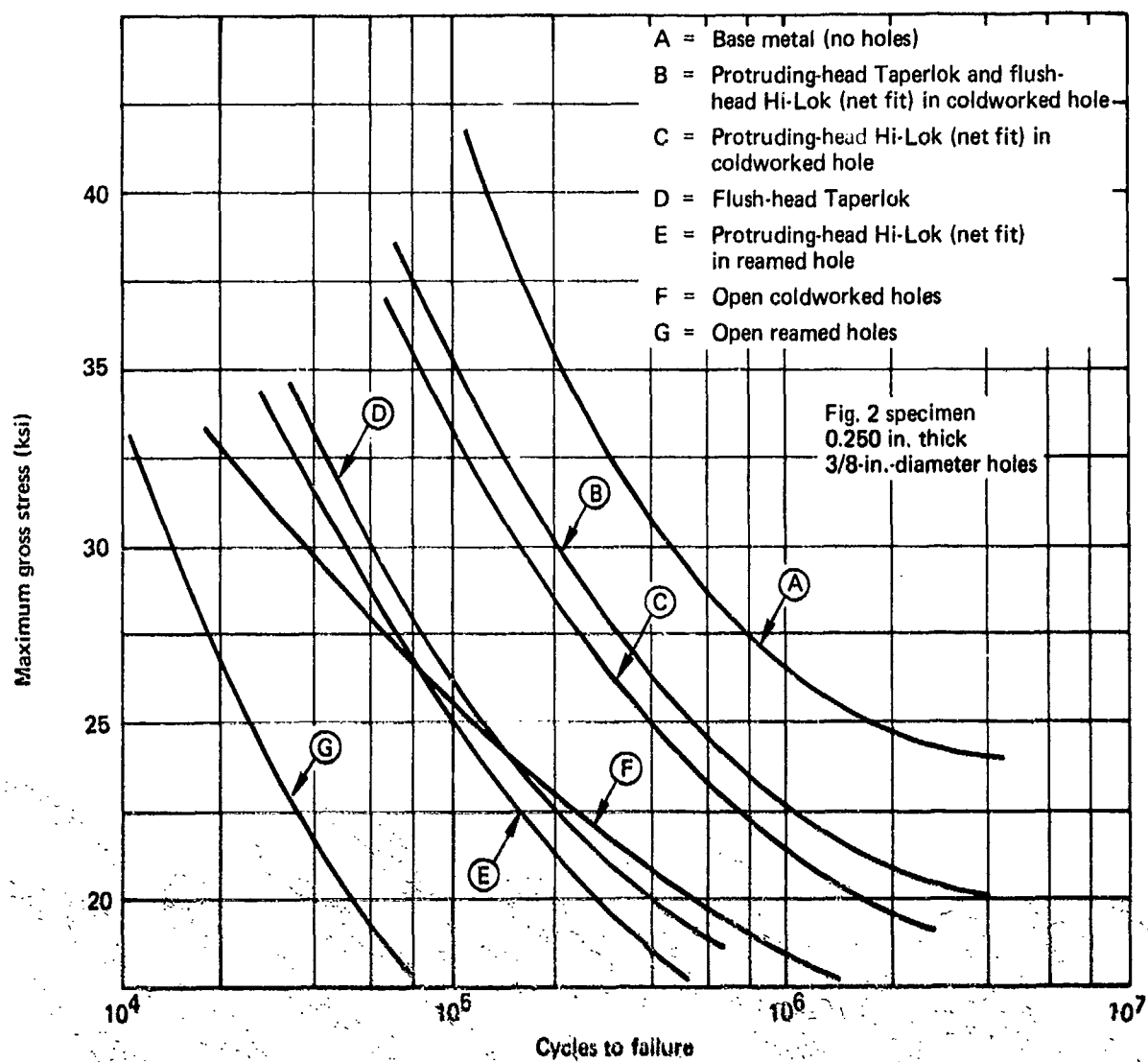
Figure 154. Log Mean S-N Curves (Gross Stress) Zero Load Transfer Fatigue Tests 2024-T851 Aluminum
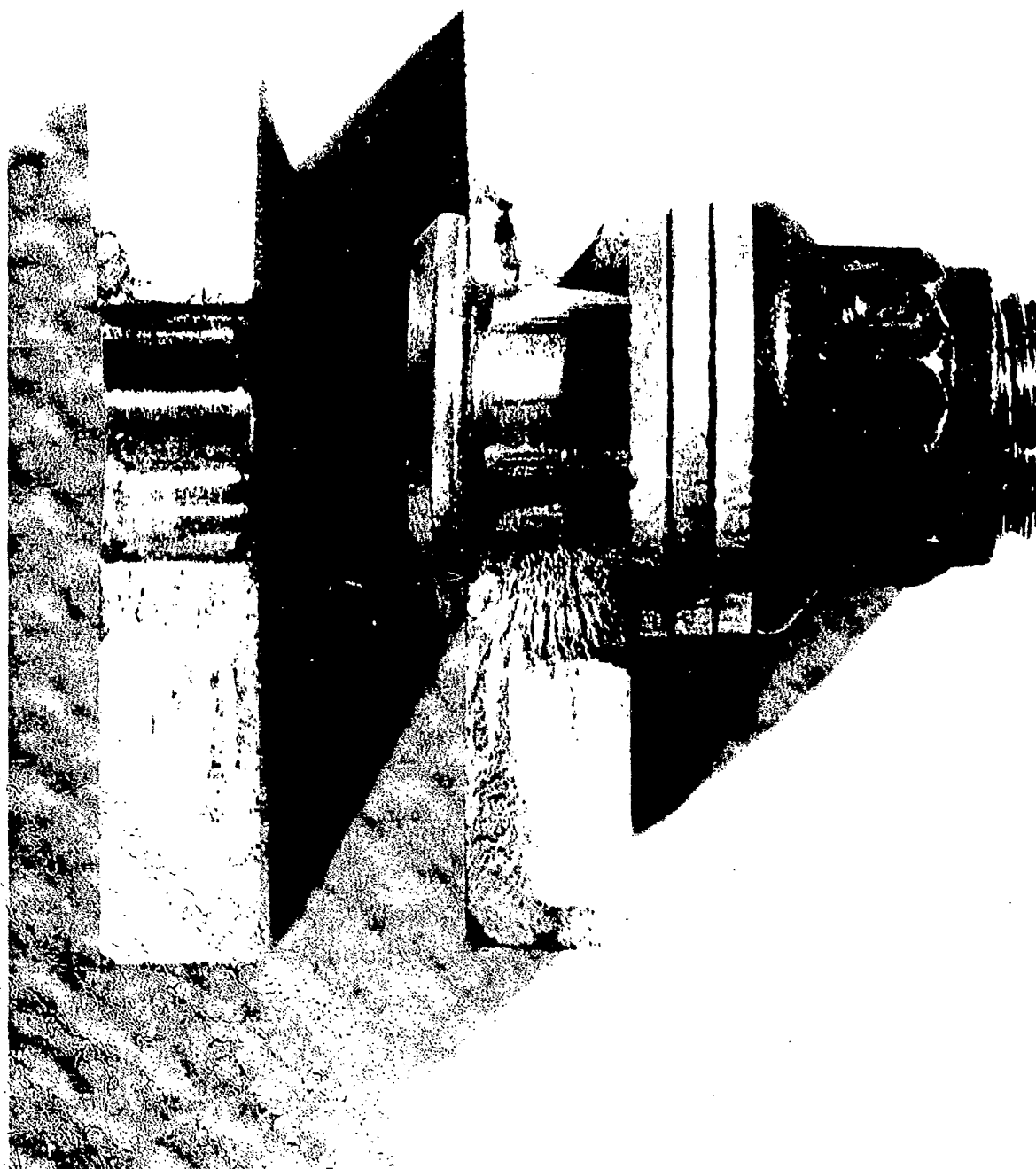
Figure 155   Ti-Lok in Reamed Hole   Fatigue Fracture Origin Along Shank
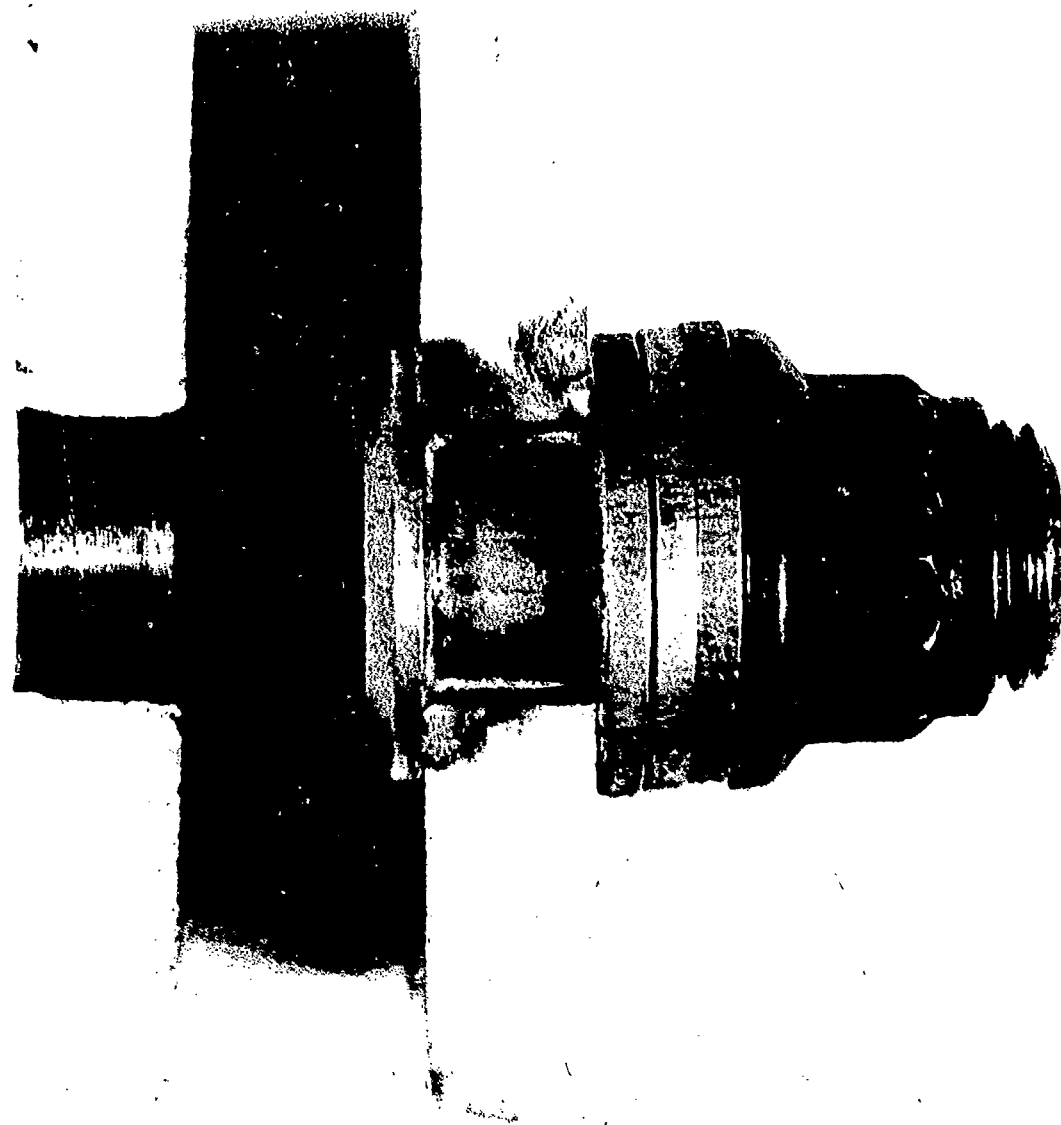
Figure 150 — Hi-Lok in Sleeve Coldworked Hole. Fatigue Fracture Origin At Outer Corner
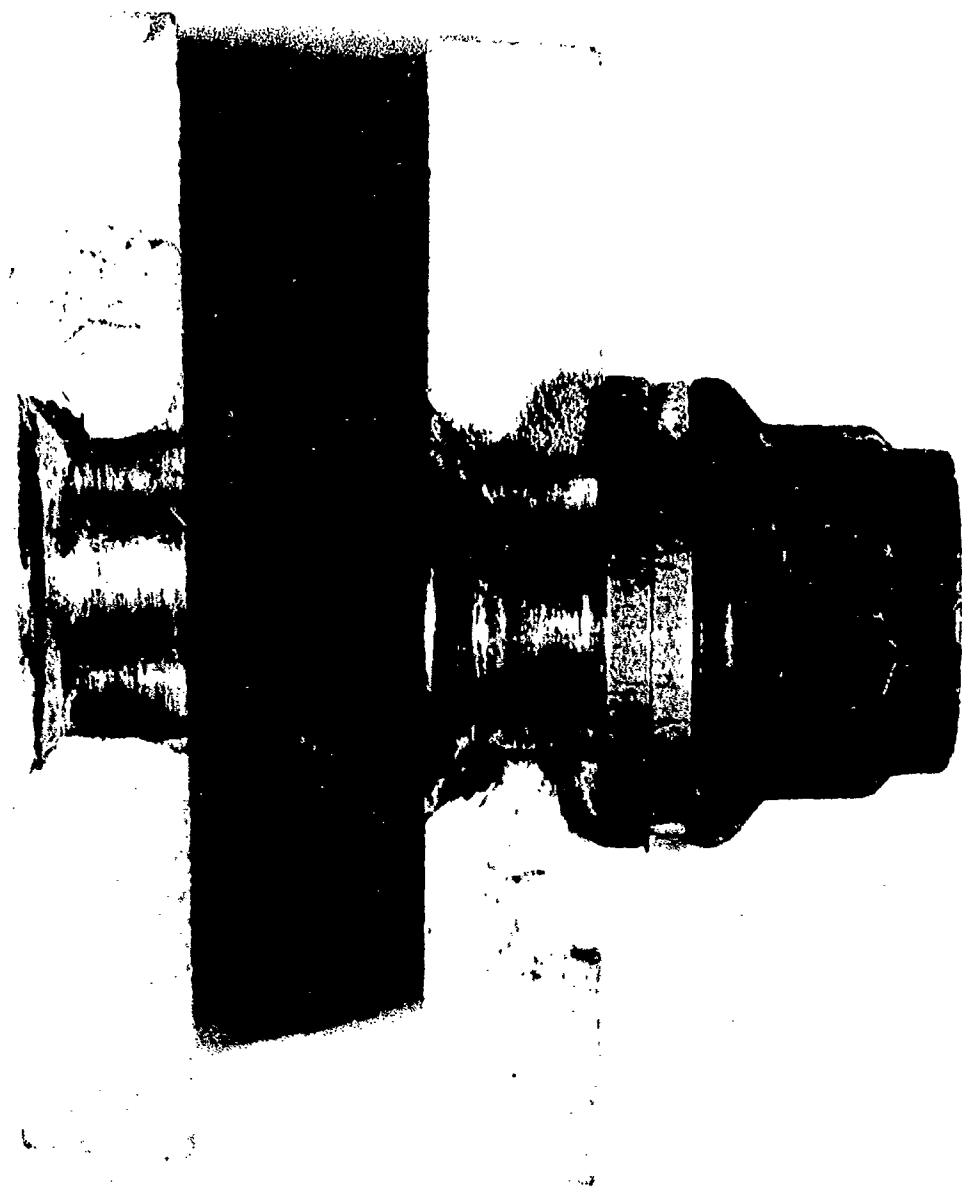
Figure 15.   Flush Head Taper-Lok   Fatigue Fracture Origin at Top of Countersink

Figure 158.—Alloy Comparison—Zero Load Transfer Fatigue Tests—2024-T851 and 7175-T736

Cycles to failure at 30-ksi maximum net stress
R = 0.1, K_t = 2.43

Line	Condition	10^4	10^5	10^6
1	Base metal (no holes)			O OO
2	Reamed only	O OO		
3	Reamed and honed	O OO		
4	0.009-in. coldworked and postreamed	O	O	
5	0.014-in. coldworked and postreamed		OOO	
6	0.019-in. coldworked and postreamed			OOO O
7	0.024-in. coldworked and postreamed			OO O

All holes 3/8-in. diameter
All specimens per fig. 2

Figure 159.—Zero Load Transfer Open-Hole Fatigue Tests—2024-T851

243
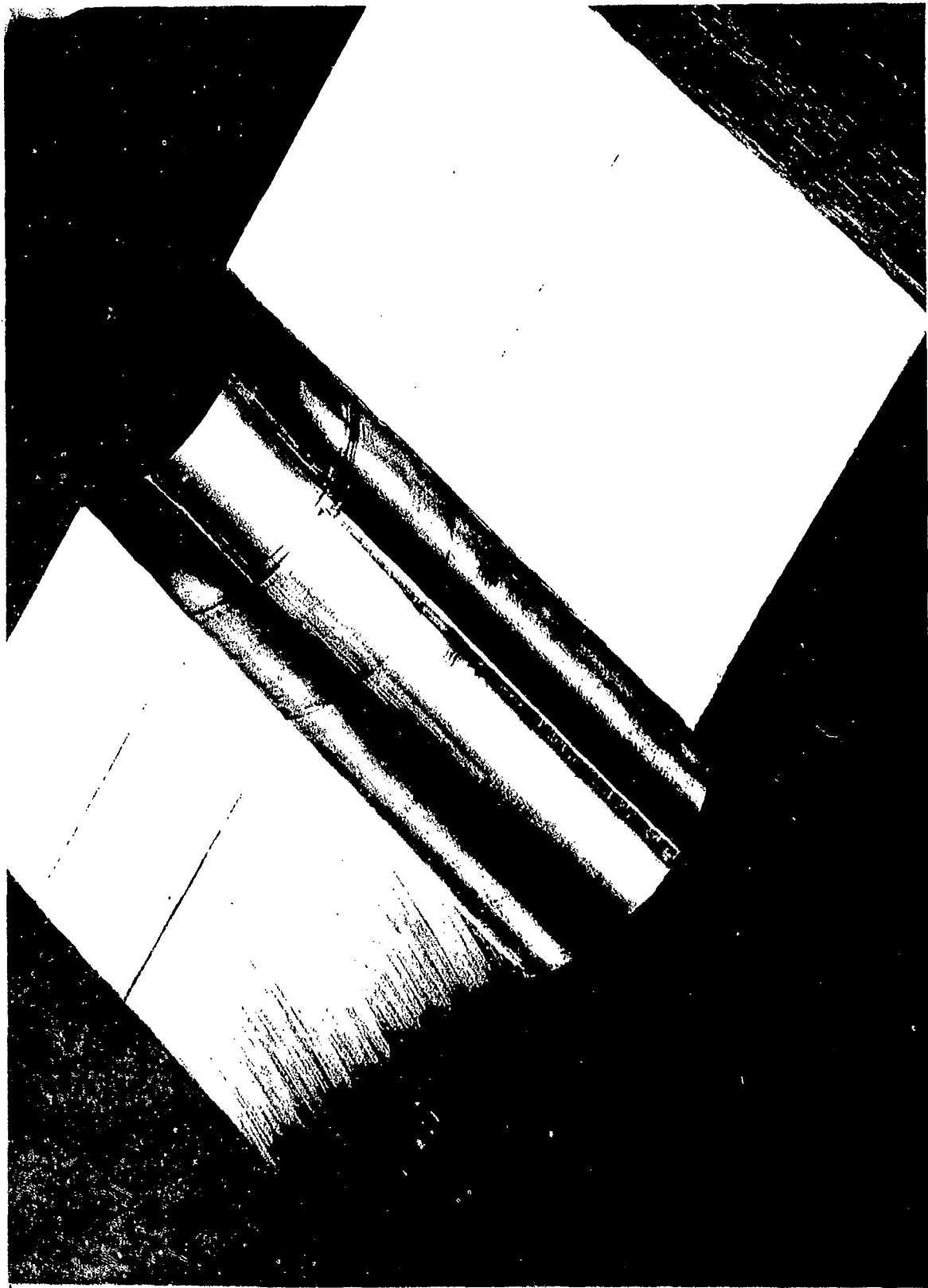
Figure 160. Ridges from Splits in End-to-End Stacked Sleeves in Coldworked Hole

Cycles to failure at 30-ksi maximum net stress
$R = 0.1$, $K_t = 2.43$

Line	Condition
1	Reamed only
2	Coldworked and postreamed, 0° split[a]
3	Coldworked and postreamed, 90° split[a]
4	Coldworked and postreamed in as-drilled hole
5	Coldworked and postreamed in abusively drilled hole
6	Coldworked only, no postream
7	Coldworked and postreamed, one hole postscored
8	Coldworked and 1/64-in.-postreamed
9	Coldworked and 1/32-in.-postreamed
10	Coldworked and 1/16-in.-postreamed
11	Coldworked and postreamed square wire sleeve

(x-axis: 10^4, 10^5, 10^6, 10^7)

All holes 3/8-in. diameter
All coldworked to 0.019-in. interference
All specimens per fig. 2

[a] Orientation of sleeve split to specimen axis
[b] All failure origins opposite split
[c] All failures in nonscored holes

Figure 161.- Process Variables, Zero Load Transfer Open-Hole Fatigue Tests--2024-T851 Aluminum

Cycles to failure at 30-ksi maximum net stress
$R = 0.1$, $K_t = 2.43$

Line	Condition	Specimen thickness (in.)
1	Base metal (no holes)	0.250
2	Coldworked and postreamed	0.250
3	Reamed only	0.250
4	Coldworked and postreamed	0.060

10^4 10^5 10^6 10^7

All holes 3/8-in. diameter
All specimens per fig. 2

All coldworked to 0.019-in. interference

Figure 162. Thin-Sheet Comparison--Open-Hole Zero Load Transfer Fatigue Tests--2024-T851 Aluminum

Figure 163. Zero-Load Transfer Open-Hole Edge-Margin and Hole-Spacing Fatigue Tests—2024-T851

Line	Coupon type (figure number)	Edge margin	Hole spacing
1	2	2 D	4 D
2	7a	1-1/2 D	5-1/4 D
3	7b	2 D	5-1/4 D
4	7c	2-1/2 D	5-1/4 D
5	7d	2-1/2 D	3 D
6	7e	2-1/2 D	4 D

Cycles to failure at 30-ksi maximum net stress R = 0.1,

All holes 3/8-in. diameter

Cycles to failure at 30-ksi maximum net stress
$R = 0.1$, $K_t = 2.43$ (open hole)

Line	Condition
1	Base metal (no holes)
2	Reamed only
3	Coldworked and postreamed
4	Protruding-head Taperlok
5	100°-head Taperlok
6	100°-countersink after coldwork and postream
7	100°-countersink before coldwork and postream
8	70°-countersink after coldwork and postream
9	Coldworked and postreamed, 0.002-in. clearance, Hi-Lok
10	Coldworked and postreamed, 0.002-in. interference Hi-Lok
11	One hole not coldworked and postreamed
12	0.030-in. crack before coldworkd and postreamed [a]

Horizontal axis: 10^4, 10^5, 10^6, 10^7

All holes 3/8-in. diameter
All coldworked to 0.019-in. interference
All specimens per fig. 2
All holes filled with net-fit Hi-Loks unless otherwise noted

a 0.021-in. crack after postream
b Actual precrack 0.120-0.240 in.

Figure 164   Zero Load Transfer Filled-Hole Fatigue Tests—2024-T851 Aluminum

248

Cycles to failure at 40 ksi maximum net stress
$R = 0.1$, $K_t = 2.43$ (open hole)

Line	Condition
1	Fig. 2 — two-hole coupon Coldworked and postreamed Net-fit Hi-Loks
2	Figure 9 — 15-hole coupon Coldworked and postreamed Net-fit Hi-Loks
3	Fig. 8 — 15-hole coupon Coldworked and postreamed production technique Net-fit Hi-Loks
4	Fig. 8 — 15-hole coupon Coldworked—no postream production technique Net-fit Hi-Loks

10^4 10^5 10^6 10^7

Figure 165. Zero Load Transfer Versus Low Load Transfer and Postream Versus No Postream Methods 2024-T851
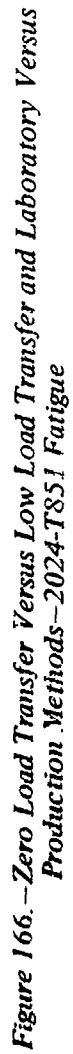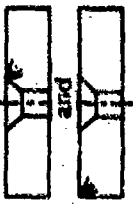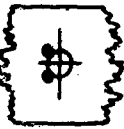
Figure 166.—Zero Load Transfer Versus Low Load Transfer and Laboratory Versus Production Methods—2024-T851 Fatigue

Cycles to failure at 30 ksi maximum net stress
R = 0.1, K_t = 2.43 (open hole)

Line	Condition
1	Fig. 2—two-hole coupon Coldworked and postreamed Net-fit Hi-Loks
2	Fig. 8—15-hole coupon Coldworked and postreamed, one at time Net-fit Hi-Loks
3	Fig. 8—15-hole coupon Coldworked and postreamed production method Net-fit Hi-Loks

10^4 10^5 10^6 10^7

Line	Condition	Coupon type (figure number)	Load transfer	Interface shim[a]	Interface upset removed
1	Base metal (no holes)	2	Zero	–	–
2	Reamed only, net-fit, protruding-head, Hi-Lok	2	Zero	–	–
3	Coldworked and postreamed, net-fit, protruding-head, Hi-Lok	2	Zero	–	–
4	Reamed only net-fit, protruding-head, Hi-Lok	10	High	0.010 smooth	No
5	Coldworked and postreamed, net-fit, protruding-head, Hi-Lok	10	High	0.010 smooth	No
6	Coldworked and postreamed, 0.002-in. clearance, protruding-head, Hi-Lok	10	High	0.010 smooth	No
7	Coldworked and postreamed, 0.002-in interference, protruding-head, Hi-Lok	10	High	0.010 smooth	No
8	Coldworked and postreamed, net-fit, flush-head Hi-Lok	10	High	0.010 smooth	No
9	Protruding-head Taperlok	10	High	0.010 smooth	No
10	Flush-head Taperlok	10	High	0.010 smooth	No
11	Coldworked and postreamed net-fit, protruding-head Hi-Lok	10	High	0.050 rough	No
12	Coldworked and postreamed, net-fit, protruding-head Hi-Lok	10	High	No	No
13	Coldworked and postreamed, net-fit, protruding-head Hi-Lok	10	High	No	Yes

Cycles to failure at 30-ksi maximum net stress
R = 0.1, K_t = 2.43 (open hole)

10^4 10^5 10^6 10^7

All holes 3/8-in. diameter
All coldworked to 0.019-in. interference

[a] Micarta

Figure 167. – Filled-Hole Load-Transfer Comparisons—2024-T851 Fatigue Tests

251

ZLT[a], reamed, open hole		ZLT, coldworked, flush head, filled hole, 70°
ZLT, coldworked, open hole		ZLT, protruding-head Taperlok
ZLT, reamed, protruding head, filled hole		ZLT, flush head Taperlok
ZLT, coldworked, protruding head, filled hole, net fit		HLT[b], filled hole, net fit, with shim
ZLT, coldworked, protruding head, filled hole, interference fit		HLT, filled hole, net fit, without shim
ZLT, coldworked, protruding head, filled hole, clearance fit		HLT, filled hole, interference fit with shim
ZLT, coldworked, flush head, filled hole, 100° postcountersunk		HLT, Taperlok

[a]ZLT = zero load transfer
[b]HLT = high load transfer

Figure 168. – Typical Failure Origins – 2024-T851
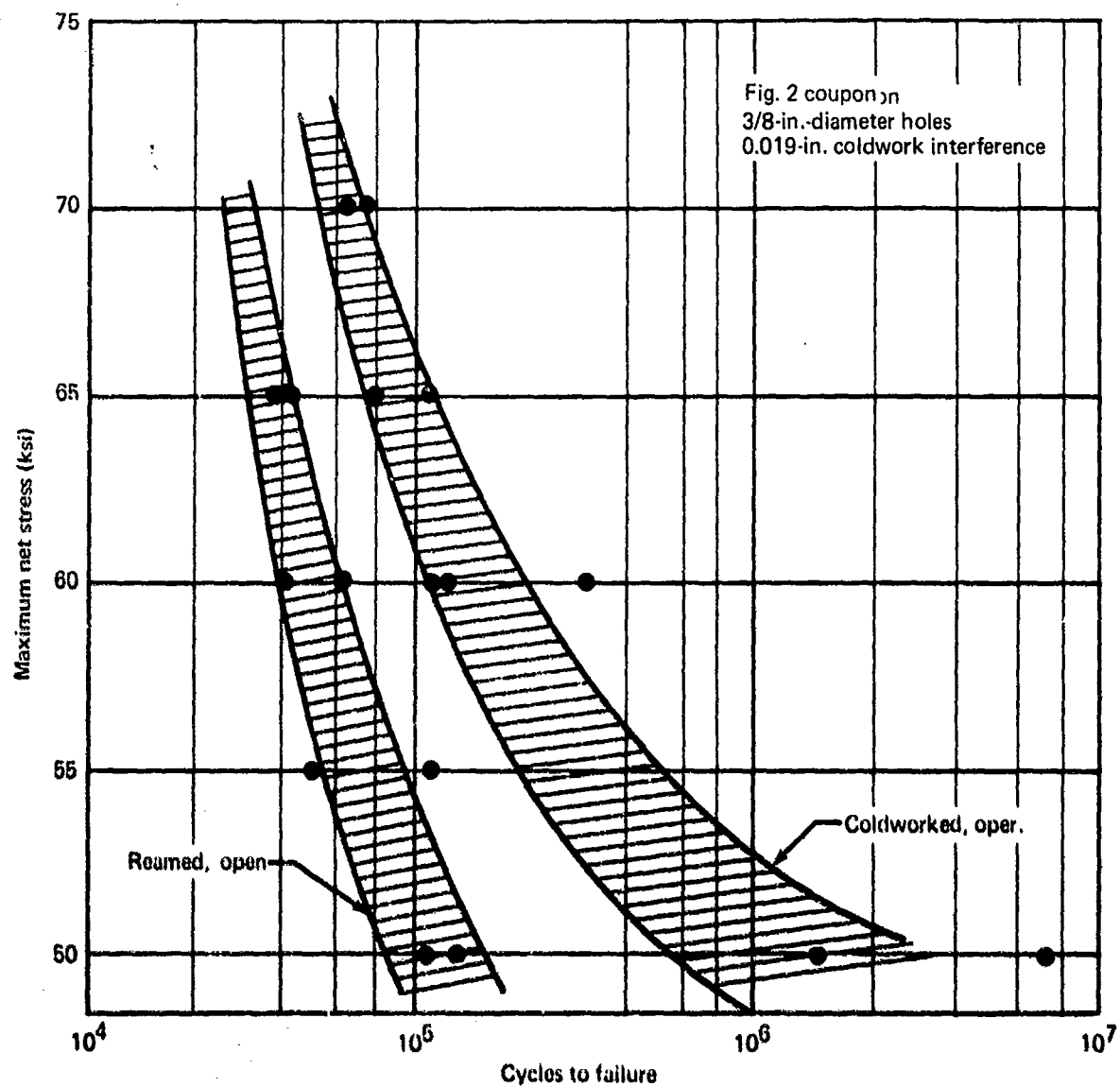
Figure 169 - ZLT Fatigue Scatter Bands Ti-6Al-4V Annealed, Open Holes

Line	Condition	Alloy	Heat treatment	Cycles to failure at 115-ksi maximum net stress, R = 0.1
1	Base metal	Ti-6Al-4V	Annealed	
			STA	
			STOA	
2	Base metal	Ti-6Al-6V-2Sn	Annealed	
			STA	
			STOA	

Figure 170. – Base Metal Titanium Alloy Fatigue Comparison

All specimens per fig. 2

254

Figure 171. Titanium Alloy Fatigue Comparison—Reamed Holes

Line	Condition	Alloy	Heat treatment
1	Reamed open holes	Ti-6Al-4V	Annealed
			STA
			STOA
2	Reamed open holes	Ti-6Al-6V-2Sn	Annealed
			STA
			STOA
3	Reamed holes with Hi-Loks	Ti-6Al-4V	Annealed
			STA
			STOA
4	Reamed holes with Hi-Loks	Ti-6Al-6V-2Sn	Annealed
			STA
			STOA

Cycles to failure at 70-ksi maximum net stress
$R = 0.1$, $K_t = 2.43$ (open hole)

10^4 10^5 10^6 10^7

All holes 3/8-in. diameter
All specimens per fig. 2
All Hi-Loks net fit

Line	Condition	Alloy	Heat treatment	Cycles to failure at 70-ksi maximum net stress $R = 0.1$, $K_t = 2.43$ (open hole)
1	Coldworked and postreamed open hole	Ti-6Al-4V	Annealed	
			STA	
			STOA	
2	Coldworked and postreamed open hole	Ti-6Al-6V-2Sn	Annealed	
			STA	
			STOA	
3	Coldworked and postreamed with Hi-Lok	Ti-6Al-4V	Annealed	
			STA	
			STOA	
4	Coldworked and postreamed with Hi-Lok	Ti-6Al-6V-2Sn	Annealed	
			STA	
			STOA	

All holes 3/8-in. diameter
All specimens per figure 2
Coldworked to 0.019-in. interference
All Hi-Loks net fit

Figure 172.—Titanium Alloy Fatigue Comparison—Coldworked Holes
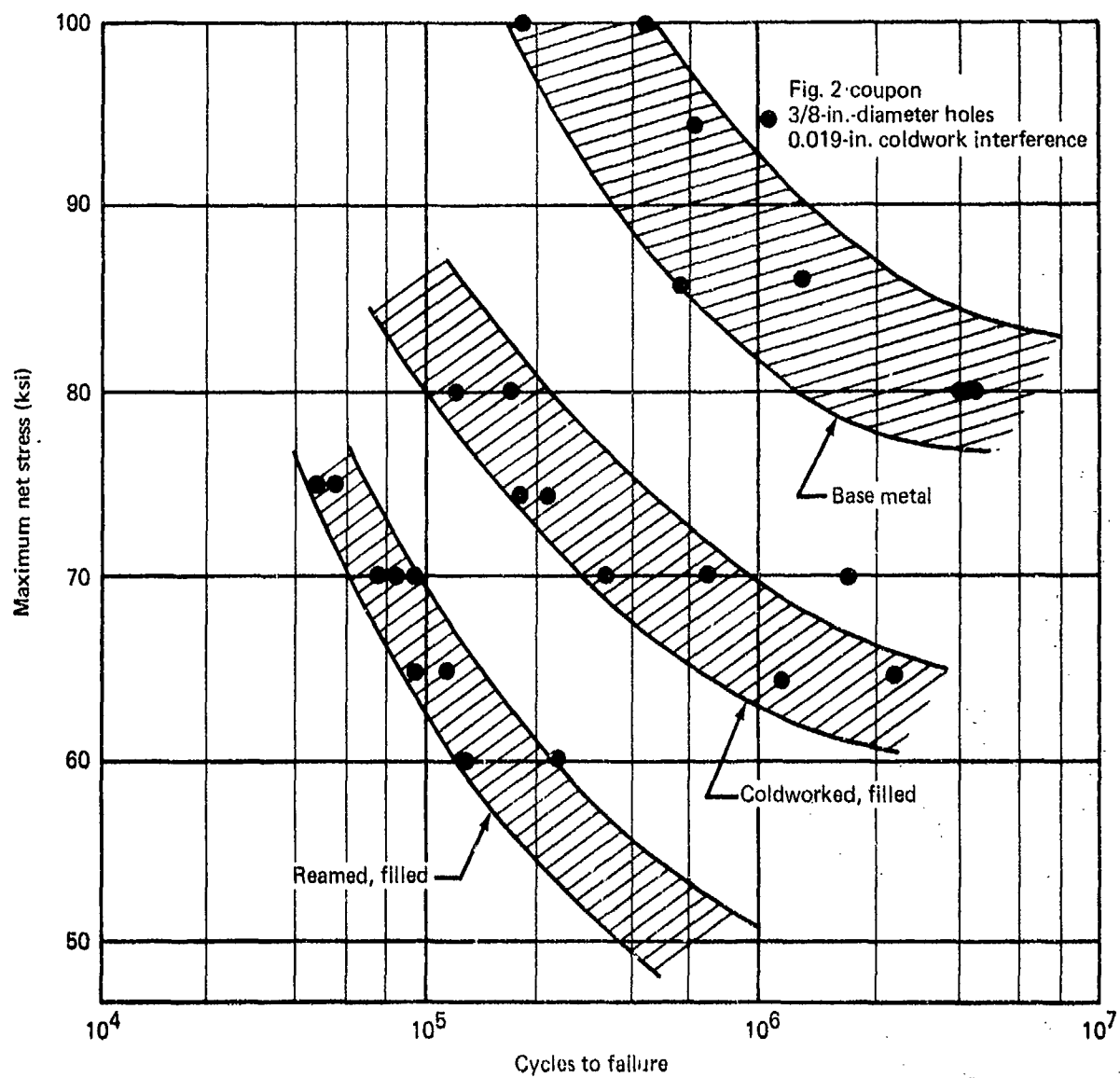
Figure 173.—Filled Hole and Base Metal ZLT Fatigue
Scatter Bands Ti-6Al-4V, Annealed
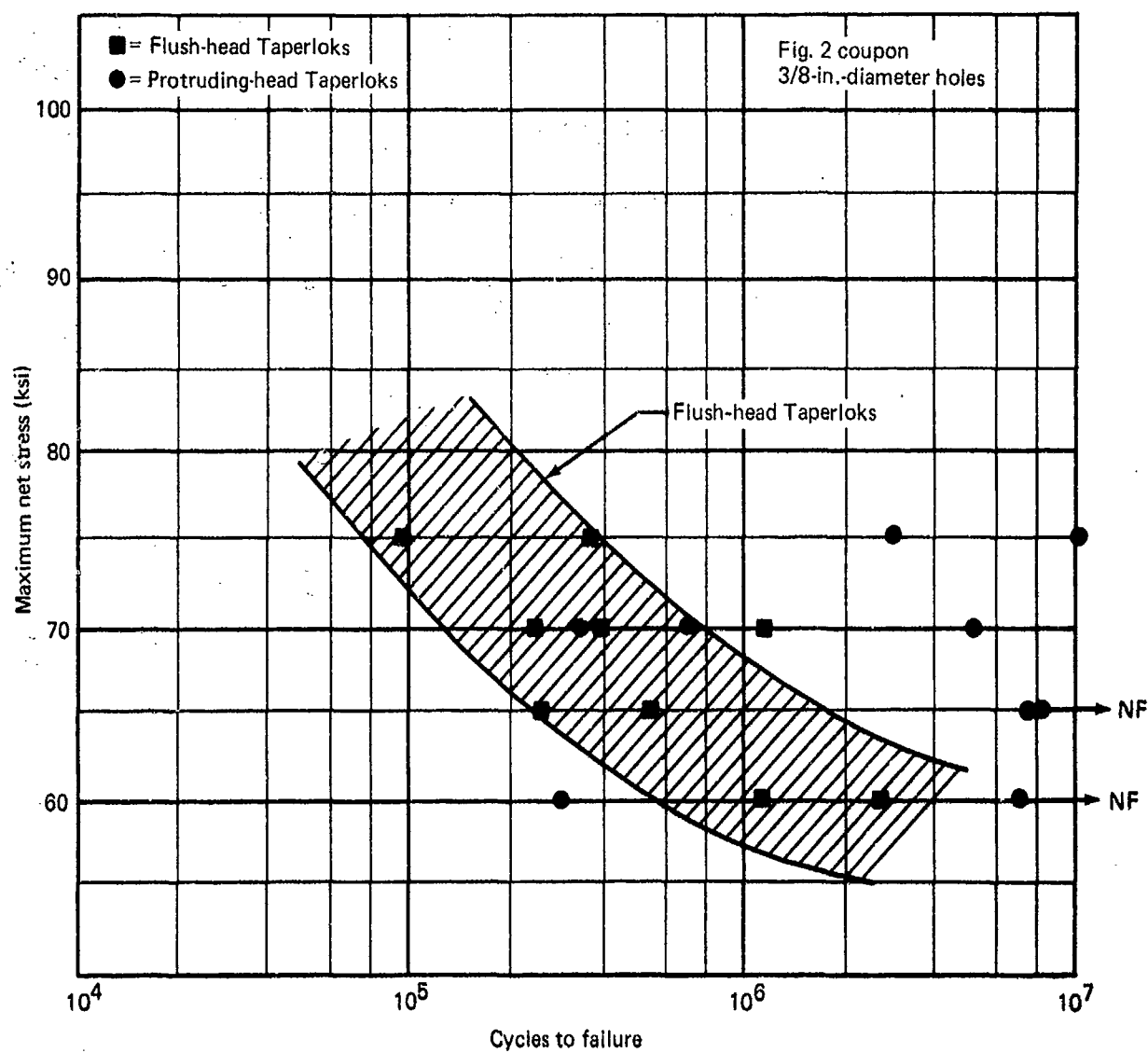
Figure 174. — S-N Scatter Curves - Ti-6Al-4V, Annealed, Tapered Fasteners

258

Line	Condition																	
1	Honed only																	
2	Reamed only																	
3	Coldworked and postreamed																	

Cycles to failure at 65-ksi maximum net stress
$R = 0.1$, $K_t = 2.43$

10^4 10^5 10^6 10^7

All holes 3/8-in. diameter
Coldworking to 0.019-in. interference
All specimens per fig. 2

Figure 175.—Zero Load Transfer Open-Hole Fatigue Tests for Precision Hole Generation Program Comparisons— Ti-6Al-4V, Annealed

259

Cycles to failure at 70-ksi maximum net stress
$R = 0.1$, $K_t = 2.43$

Line	Condition	10^4 — 10^7 (data points)
1	Reamed only	O O
2	Coldworked and postreamed, 0°-split(a)	
3	Coldworked and postreamed, 90°-split(a)	
4	Coldworked and postreamed in as-drilled hole	
5	Coldworked and postreamed in abusively drilled hole	
6	Coldworked only, no postream	
7	Coldworked and postreamed, one hole postscored	
8	Coldworked and 1/64-in. postream	
9	Coldworked and 1/32-in. postream	
10	Coldworked and 1/16-in. postream	
11	Coldworked and postreamed with square wire sleeve	Sleeves failed—not tested

All holes 3/8-in. diameter
All coldworked to 0.019-in. interference
All specimens per fig. 2

(a) Orientation of sleeve split to specimen axis
(b) Failure origins both sides of hole
(c) Failure origins at score

Figure 176. – Zero Load Transfer Open-Hole Fatigue Tests—Ti-6Al-4V. Annealed

Line	Condition	Specimen thickness (in.)
1	Base metal (no holes)	0.250
2	Coldworked and postreamed	0.250
3	Reamed only	0.250
4	Coldworked and postreamed	0.060

All holes 3/8-in. diameter
All specimens per fig. 2
Holes coldworked to 0.019-in. interference

Cycles to failure at 70-ksi maximum net stress
$R = 0.1, K_t = 2.43$

10^4 10^5 10^6 10^7

NF

Figure 177.—Thin-Sheet Comparison—Open-Hole Zero Load Transfer Fatigue Test—Ti-6Al-4V, Annealed

Cycles to failure at 70-ksi maximum net stress
R = 0.1

Line	Coupon type (figure number)	Edge margin	Hole spacing
1	2	2 D	4 D
2	7a	1-1/2 D	5-1/4 D
3	7b	2 D	5-1/4 D
4	7c	2-1/2 D	5-1/4 D
5	7d	2-1/2 D	3 D
6	7e	2-1/2 D	4 D

All holes 3/8-in. diameter
All holes coldworked to 0.019-in. interference

Figure 178.--Zero Load Transfer Open-Hole Edge Margin and Hole Spacing Fatigue Tests--Ti-6Al-4V (Annealed)

Cycles to failure at 70-ksi maximum net stress
R = 0.1, K_t = 2.43 (open hole)

Line	Condition
1	Reamed only
2	Coldworked and postreamed
3	Coldworked and postreamed, 0.002-in. clearance, Hi-Lok
4	Coldworked and postreamed, 0.002-in. interference, Hi-Lok
5	One hole not coldworked and postreamed
6	100° countersink after coldwork and postream
7	100° countersink before coldwork and postream
8	70° countersink after coldwork and postream
9	Protruding-head Taperlok
10	100°-head Taperlok
11	80,000 cycles fatigue before coldwork and postream
12	Fatigue cracked first, then coldworked and postreamed

10^4 10^5 10^6 10^7

All holes 3/8-in. diameter
All coldworking to 0.019-in. interference
All specimens per fig. 2
All holes filled with net-fit Hi-Loks unless otherwise noted

[a] 0.030-in. precrack
[b] 0.020-in. precrack
[c] 0.010-in. precrack

Figure 179. Zero Load Transfer Filled-Hole Fatigue Tests—Ti-6Al-4V (Annealed)

263
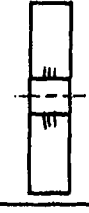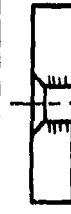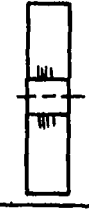
Line	Condition	Coupon type (figure number)	Skin material	Stringer material	Net stress (ksi) Ti	Net stress (ksi) Al
1	Single coupon, coldworked and postreamed	Two-hole (2)	Ti	—	70	—
2	Single coupon, coldworked and postreamed	Two-hole (2)	Al	—	—	40
3	Single coupon, coldworked and postreamed	15-hole (9)	—	Ti	70	—
4	Dual coupon, coldworked and postreamed	15-hole (8)	Ti	Ti	70	70
5	Dual coupon, coldworked and no postream	15-hole (8)	Ti	Ti	70	70
6	Dual coupon, coldworked and postreamed	15-hole (8)	Ti	Al	64	40

All coupons with net-fit Hi-Loks
Two-hole coupons tested at 6000 cpm; 15-hole coupons at 600 cpm
Failure origins in line 6 primarily in titanium skin portion of coupon

Figure 180. – Low Load Transfer Fatigue Test – Ti-6Al-4V and Ti-6Al-4V/2024-T851

Line	Condition	Coupon type (figure number)	Load transfer	Interface shim (Micarta)	Interface upset removed	Cycles to failure at 70-ksi maximum net stress R = 0.1
1	Reamed only	2	Zero	—	—	
2	Coldworked and postreamed	2	Zero	—	—	
3	Reamed only	10	High	0.010	No	
4	Coldworked and postreamed	10	High	0.010	No	
5	Coldworked and postreamed 0.002-in. clearance, Hi-Lok	10	High	0.010	No	
6	Coldworked and postreamed 0.002-in. interference, Hi-Lok	10	High	0.010	No	
7	Coldworked and postreamed 100°-head, Hi-Lok	10	High	0.010	No	
8	Coldworked and postreamed	10	High	None	No	
9	Coldworked and postreamed	10	High	None	Yes	
10	Protruding-head Taperlok	10	High	0.010	No	
11	100°- head, Taperlok	10	High	0.010	No	

All holes 3/8-in. diameter
All coldworking to 0.019-in. interference
All fasteners protruding head net fit Hi-Loks unless otherwise noted

Figure 181. – High-Load Transfer Filled-Hole Fatigue Test–Ti-6Al-4V (Annealed)

265

Figure 182. – Typical Fatigue Failure Origins—Ti-6Al-4V

ZLT[a],
reamed open hole

ZLT,
reamed hole with net-fit
protruding head Hi-Lok

ZLT,
coldworked open hole

ZLT,
coldworked hole with
net-fit protruding head Hi-Lok

ZLT,
coldworked hole with clearance-
fit protruding-head,Hi-Lok

ZLT,
coldworked hole with interference-
fit protruding-head,Hi-Lok

ZLT,
coldworked precountersunk hole
with net-fit 100°-head,Hi-Lok

ZLT,
coldworked postcountersunk hole
with net-fit 100°-head,Hi-Lok

ZLT,
coldworked postcountersunk hole
with net-fit 70°-head,Hi-Lok

ZLT,
protruding-head,Taperlok

ZLT,
100°-head Taperlok

HLT[b],
reamed hole with net-fit
protruding-head,Hi-Lok and shim

HLT,
coldworked hole with net-fit
protruding-head,Hi-Lok and shim

HLT,
coldworked hole with clearance-
fit protruding-head,Hi-Lok and shim

HLT,
coldworked postcountersunk hole with
net-fit 100°-head,Hi-Lok and shim

HLT,
coldworked hole with net-fit
protruding-head,Hi-Lok and no shim

HLT,
coldworked hole with interference-
fit protruding-head,Hi-Lok and shim

HLT,
coldworked hole with net-fit protruding-
head,Hi-Lok, no shim and no upset

HLT,
protruding-head,Taperlok

HLT,
100°-head,Taperlok

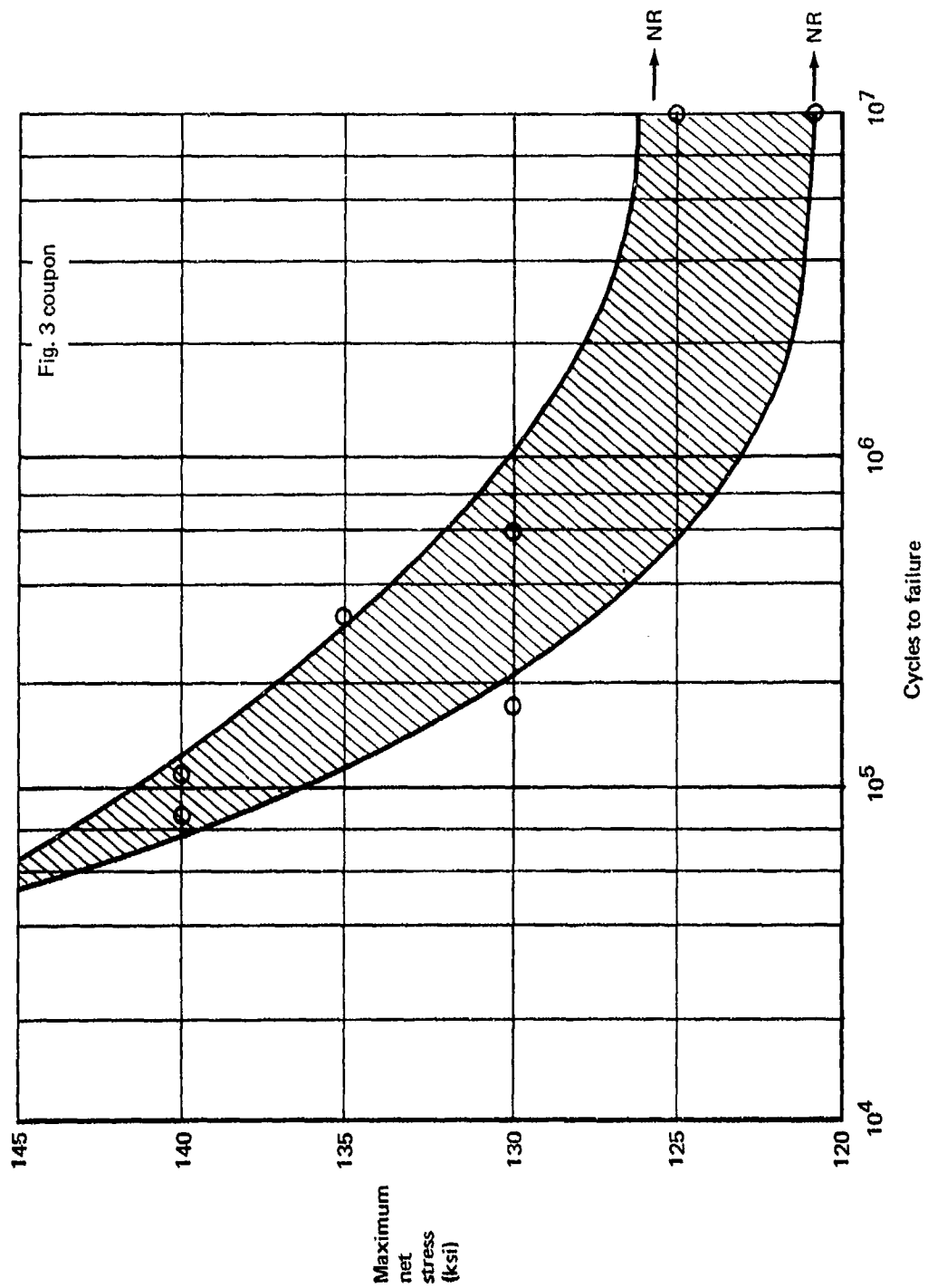aZLT = zero load transfer
bHLT = high load transfer

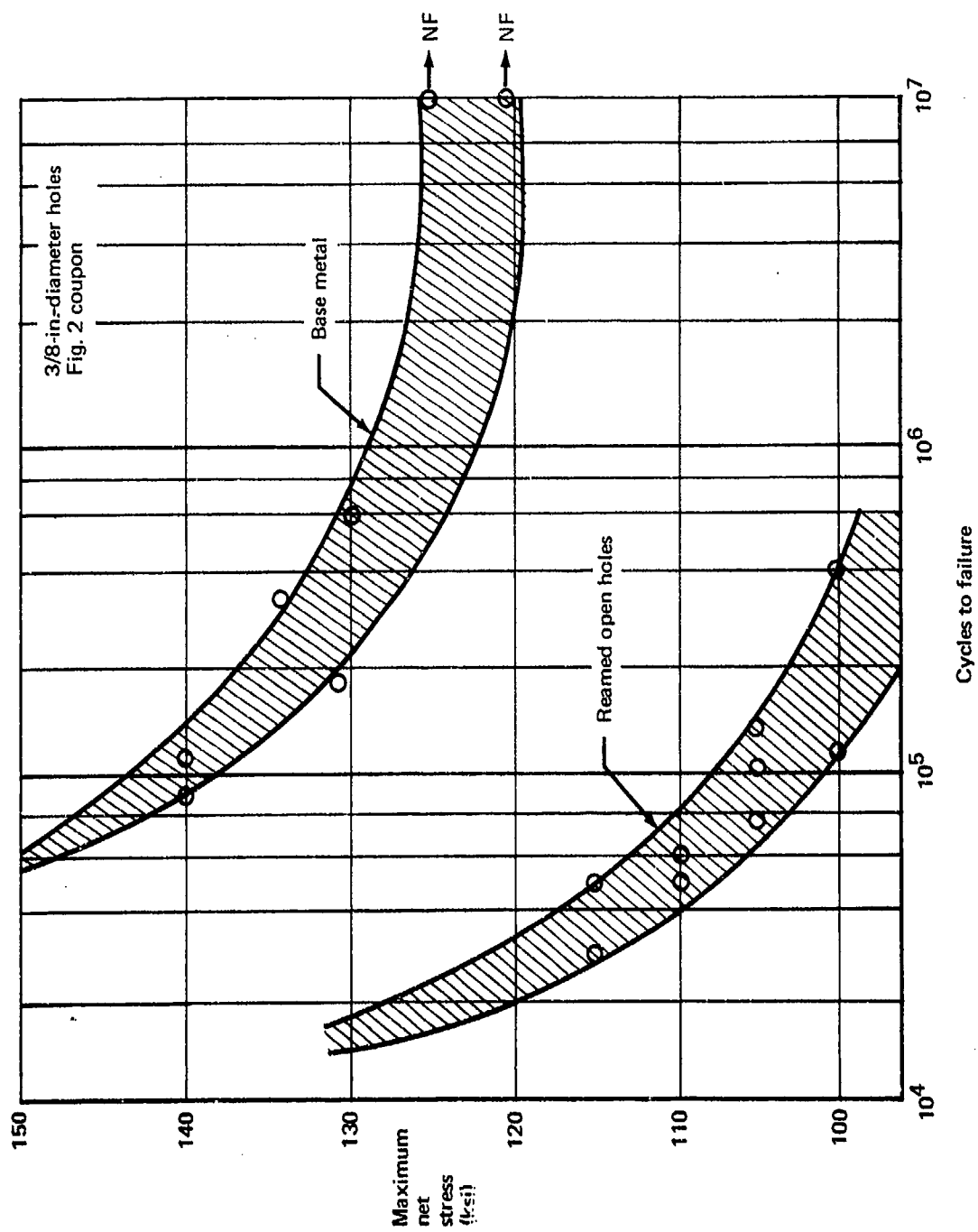*Figure 183. – Base Metal S-N Scatter Curve – 300M Steel (270-300 KSI)*

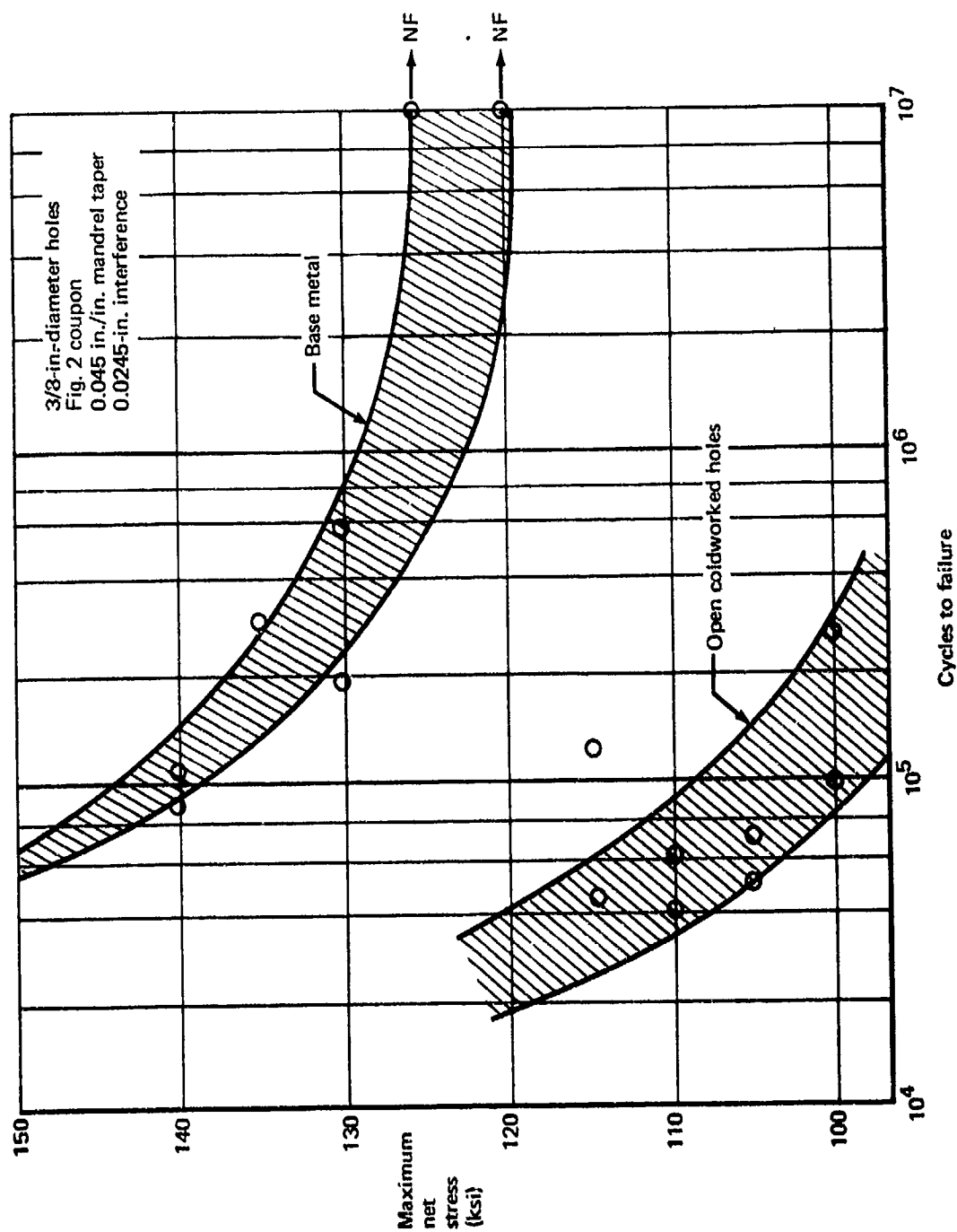Figure 184.—Reamed Open Holes and Base Metal S-N Scatter Curves—300M Steel (270-300 KSI)

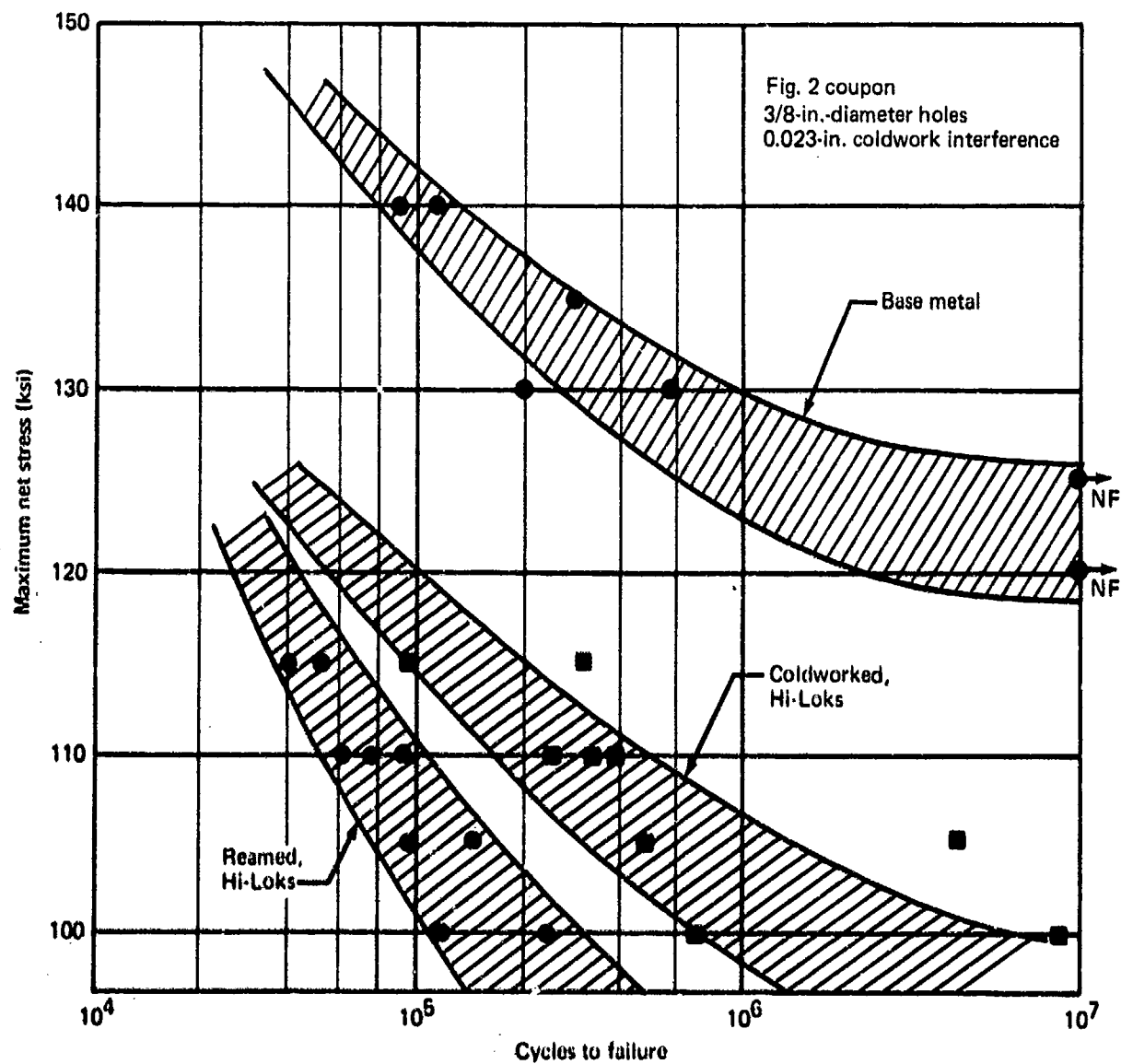Figure 185. —Coldworked Open Holes and Base Metal S-N Scatter Curves—300M Steel (270-300 KSI)

Figure 186. Filled Holes and Base Metal S-N Scatter Curves - 300M Steel

Line	Condition	Test stress (ksi)	Mandrel taper (in./in.)	Coldworked interference (in.)	Cycles to failure R = 0.1, K_t = 2.43 (open hole)
1	Honed open	105	—	—	
2	Reamed open	105	—	—	
3	Reamed open	110	—	—	
4	Coldworked open	110	0.045	0.0245	
5	Reamed filled	110	—	—	
6	Coldworked filled	110	0.015	0.023	
7	Coldworked filled	110	0.030	0.0245	
8	Coldworked filled	110	0.045	0.020	
9	Coldworked filled	110	0.045	0.023	
10	Coldworked filled	110	0.045	0.0245	

All holes 3/8-inch diameter in fig. 2 coupons

All filled holes have net fit, cadmium-plated steel Hi-Loks

Figure 187.--Open- and Filled-Hole Fatigue Performance, Honing, Reaming, and Coldworking, With Mandrel Taper and Interference Variations--300M Steel (270-300 KSI)

271

Cycles to failure at 110-ksi maximum net stress
R = 0.1, K_t = 2.43

Line	Condition
1	Reamed only
2	Coldworked and postreamed in reamed hole
3	Coldworked and postreamed in as-drilled hole
4	Coldworked and postreamed in abusively drilled hole
5	Coldworked and postreamed, one hole postscored
6	Coldworked only, no postream
7	Coldworked and 1/64-in. postream
8	Coldworked and 1/32-in. postream
9	Coldworked and 1/16-in. postream

10^4 10^5 10^6 10^7

All holes 3/8-in. diameter
All holes coldworked to 0.023-in. interference (carbide mandrels—no sleeve)
All specimens per fig. 2

Figure 188.—Zero Load Transfer Open-Hole Fatigue Tests—300M Steel (270-300 KSI)

Cycles to failure at 110-ksi maximum net stress
R = 0.1, K_t = 2.43

Line	Condition	Specimen thickness (in.)
1	Base metal (no holes)	0.250
2	Coldworked and postreamed	0.250
3	Reamed only	0.250
4	Coldworked and postreamed	0.060

All holes 3/8-in. diameter
All specimens per fig. 2
Holes coldworked to 0.023-in. interference

NF

10^4 10^5 10^6 10^7

Figure 189. Thin-Sheet Comparison—Open-Hole Zero Load Transfer Fatigue Test—300M Steel (270-300 KSI)

Figure 190.—Zero Load Transfer Open-Hole Edge-Margin and Hole-Spacing Fatigue Tests—300M (270-300 KSI)

Cycles to failure at 110-ksi maximum net stress
R = 0.1, K_t = 2.43 (open hole)

Line	Condition
1	Base metal (no holes)
2	Reamed only
3	Coldworked and postreamed carbide mandrel, no sleeve
4	Coldworked and postreamed HSS mandrel, 0° sleeve
5	Coldworked and postreamed HSS mandrel, 90° sleeve

All holes 3/8-in. diameter
Coldworking interference: carbide = 0.023 in.; HSS = 0.018 in.
All holes filled with net-fit Hi-Loks unless otherwise noted
All specimens per fig. 2

10^4 10^5 10^6 10^7

Figure 191. Zero Load Transfer Filled-Hole Fatigue Tests—Pull Process versus Push Process—300M Steel (270-300 KSI)

Cycles to failure at 110-ksi maximum net stress
R = 0.1, K_t = 2.43 (open holes)

Line	Condition	10^4	10^5	10^6	10^7
1	Reamed only		ooo		
2	Coldworked and postreamed			o oo	
3	100° csk after coldwork and postream			o	
4	100° csk before coldwork and postream	o oo			
5	70° csk after coldwork and postreamed			o o o	
6	Coldworked and postreamed with 0.002-in. clearance, Hi-Lok			oo o	
7	Coldworked and postreamed with 0.002-in. interference Hi-Lok			o o	o
8	One hole not coldworked and postreamed	o oo			
9	80,000-cycle prefatigue before coldwork and postream			o	o→ NF
10	0.030-in. crack before coldwork and postream			o	o→ NF

All holes 3/8-in. diameter
All coldworking to 0.023 in. interference
All holes filled with net-fit Hi-Loks unless otherwise noted
All coldworking with carbide mandrels—no sleeves
All specimens per fig. 2

Figure 192. Zero Load Transfer Filled-Hole Fatigue Tests—300M Steel (270-300 KSI)

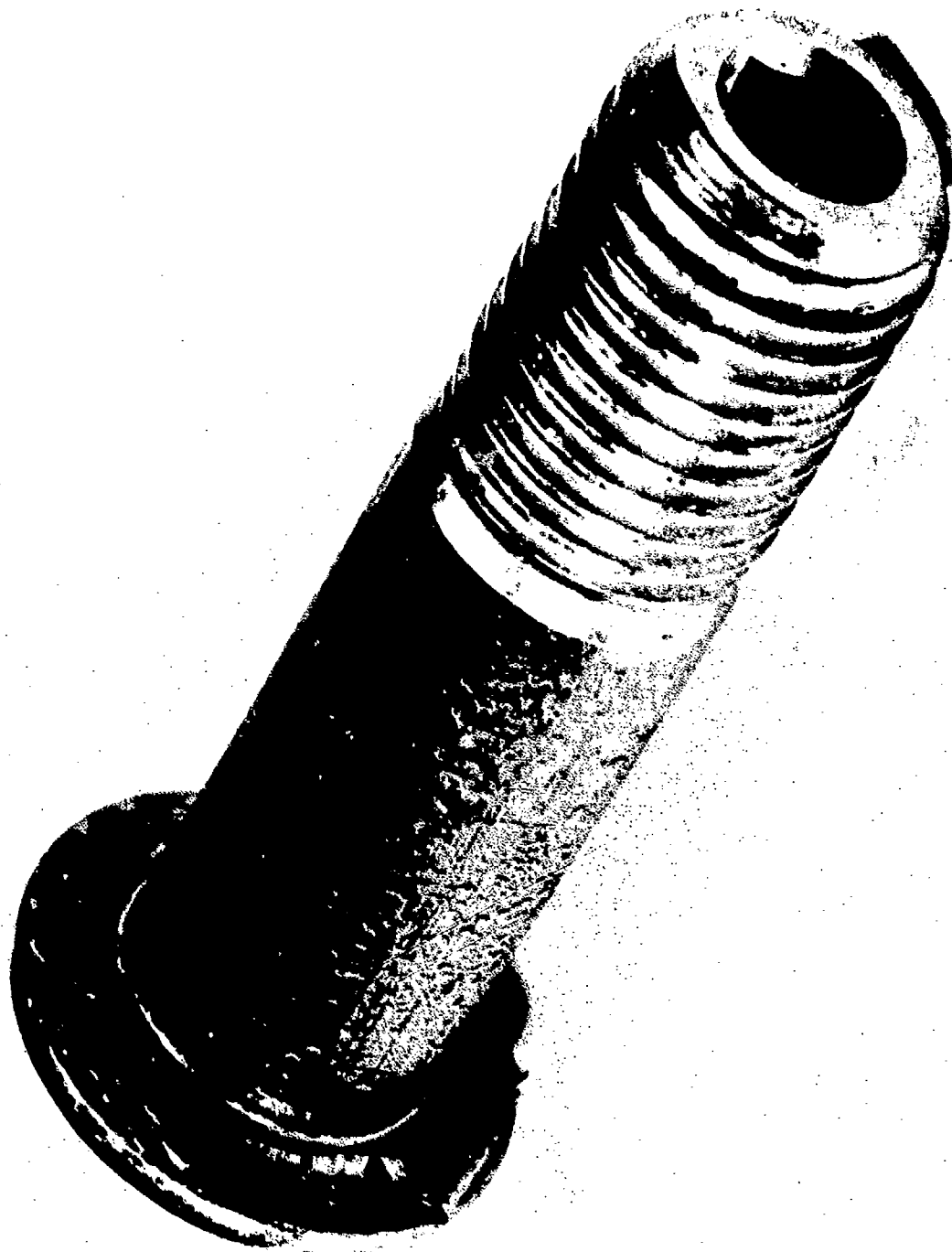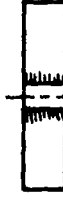Figure 193 – Bolt After Interference-Fit Installation in 300M Steel (270-300 KSI)

Line	Condition	Coupon type (figure number)	Load transfer	Interface shim (micarta)	Cycles to failure at 110-ksi maximum net stress R = 0.1
1	Reamed only	2	Zero	—	
2	Coldworked and postreamed	2	Zero	—	
3	Reamed only	10	High	0.020 in.	
4	Coldworked and postreamed with	10	High	0.020 in.	
5	Coldworked and postreamed with 0.002-in. clearance, Hi-Lok	10	High	0.020 in.	
6	Coldworked and postreamed with 0.002-in. interference, Hi-Lok	10	High	0.020 in.	
7	Coldworked and postreamed 100° head, Hi-Lok	10	High	0.020 in.	
8	Coldworked and postreamed	10	High	None	

All holes 3/8-in. diameter
All holes net-fit Hi-Lok unless otherwise stated

Figure 194. — High Load Transfer Filled-Hole Fatigue Test – 300M Steel (270-300 KSI)

Figure 195. Typical Fatigue Failure Origins—300M Steel (270-300 KSI)
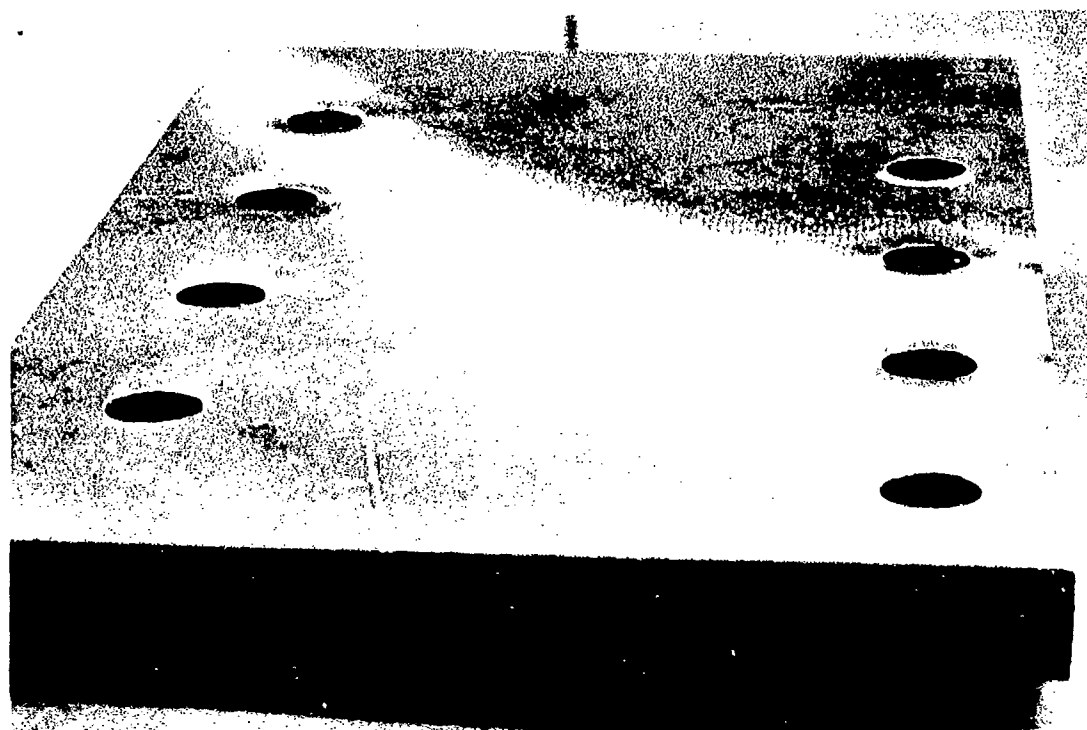
Before Testing

After 888 Hours of Testing

Figure 196. 300M Steel Stress Corrosion Coupon—Before and After Testing
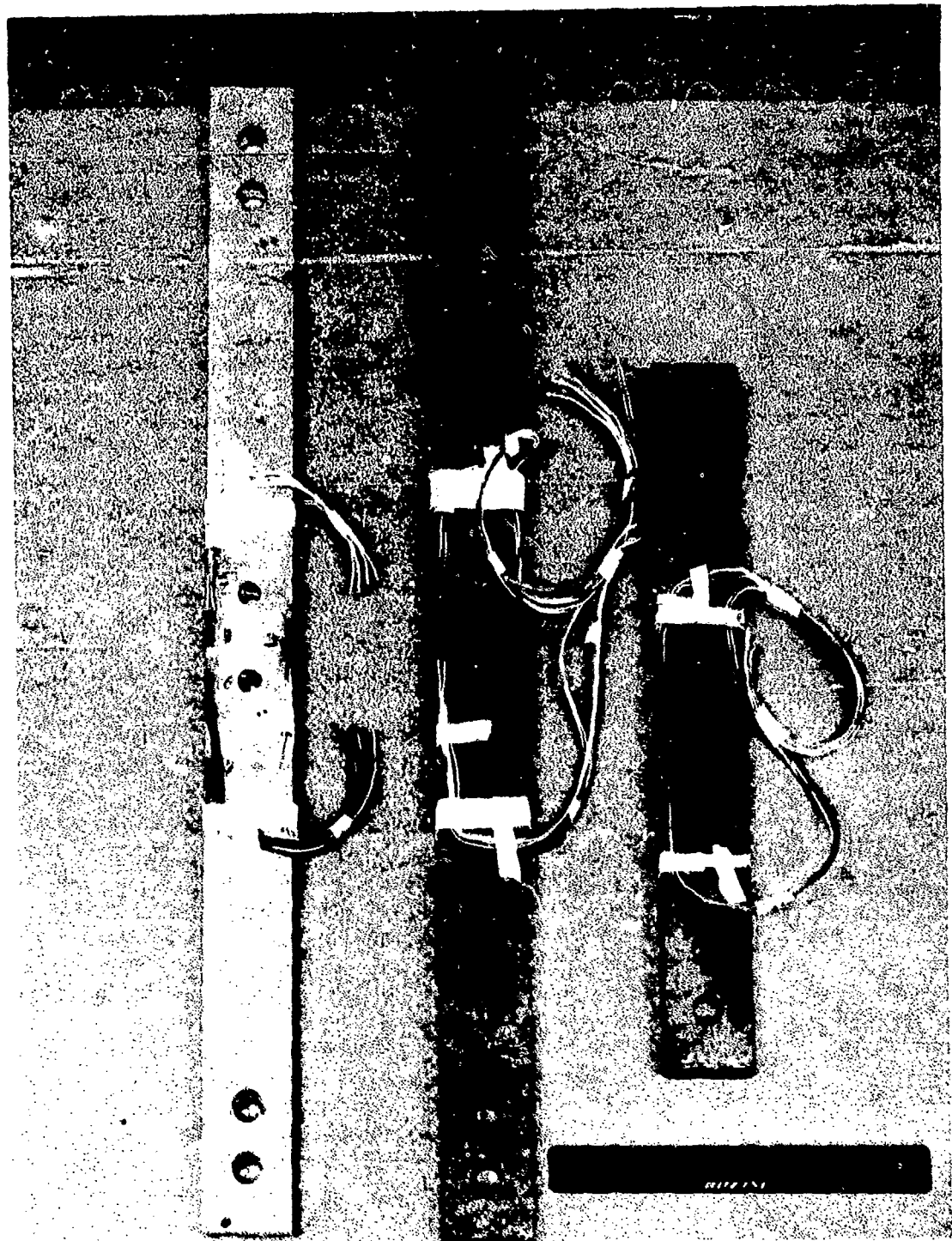
Figure 197. Edge Strain Coupons
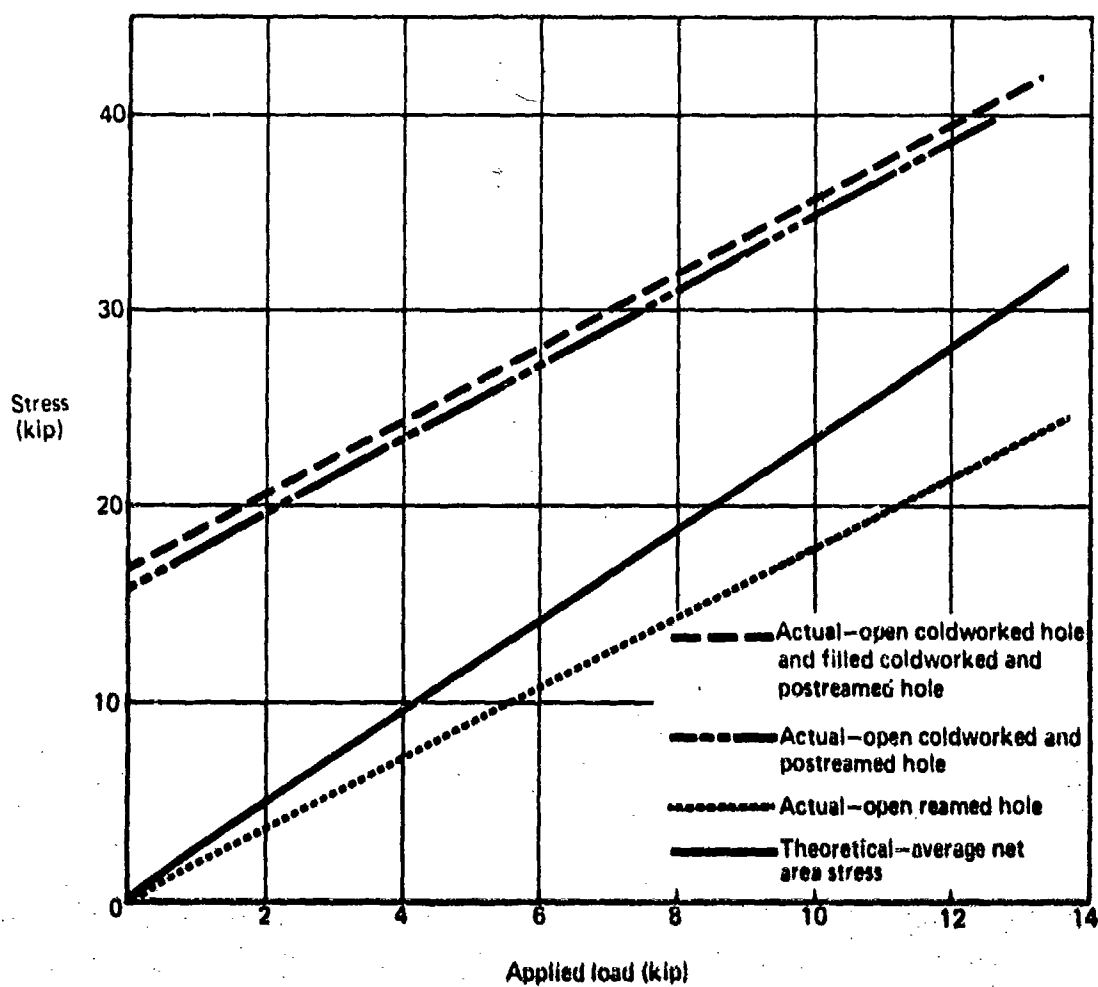
Figure 198.—Stress at Specimen Edge Adjacent to Hole—2024 T851

Legend (within figure):
- Actual—open coldworked hole and filled coldworked and postreamed hole
- Actual—open coldworked and postreamed hole
- Actual—open reamed hole
- Theoretical—average net area stress

Axis labels: Stress (kip) (vertical), Applied load (kip) (horizontal)
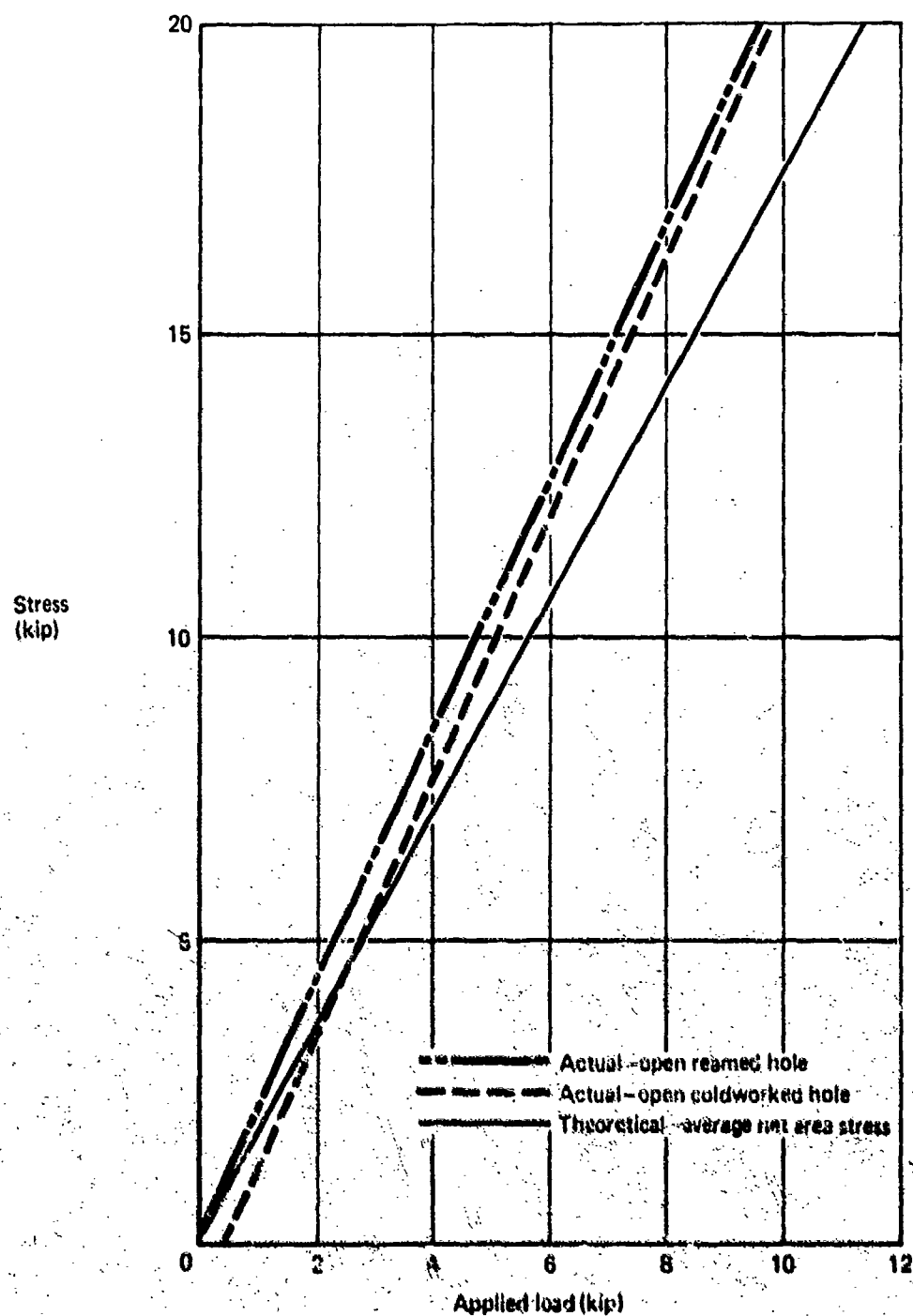
Figure 199.—Stress at Specimen Edge Between Holes—2024-T851
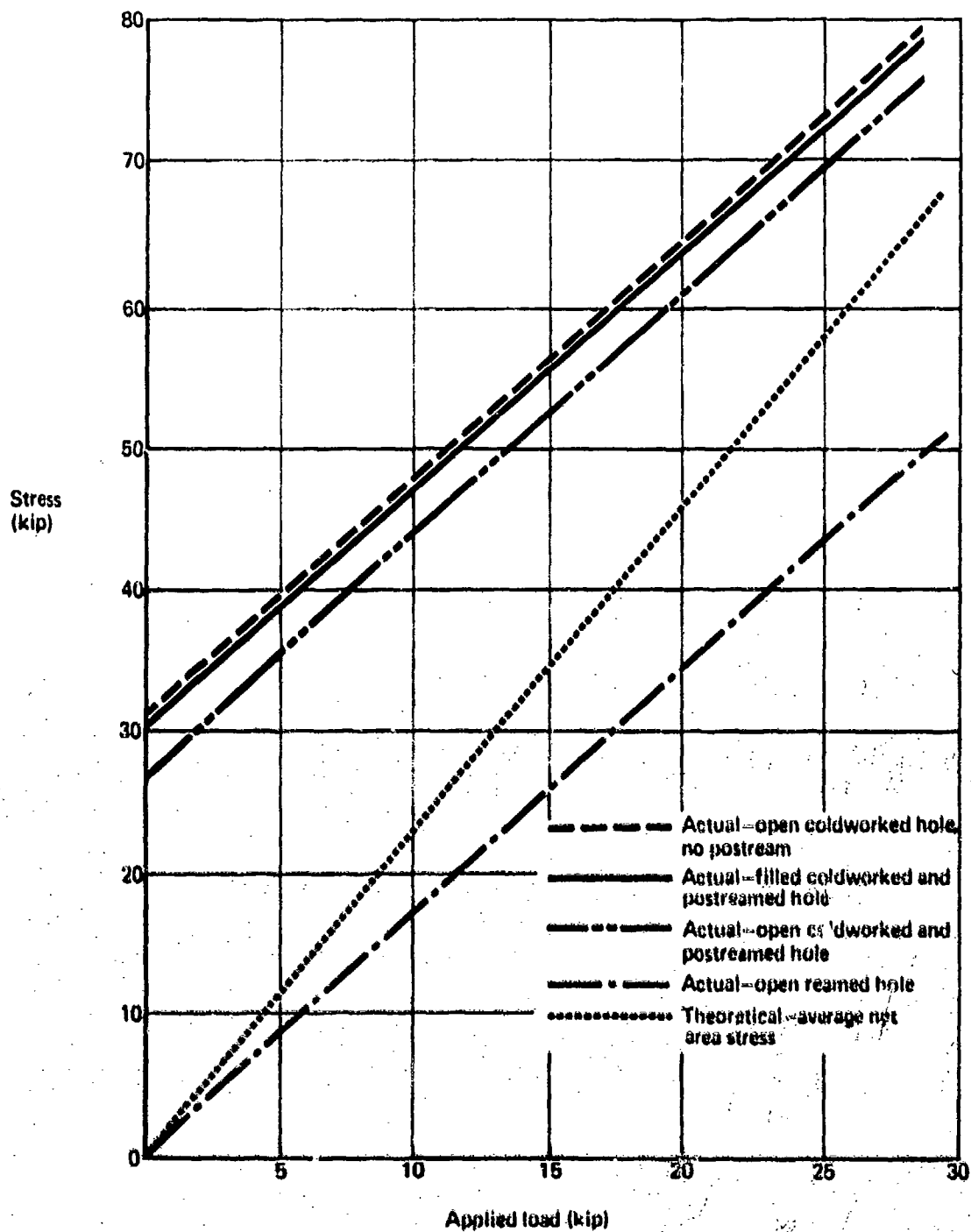
Figure 200.—Stress at Specimen Edge Adjacent to Hole—Ti-6Al-4V
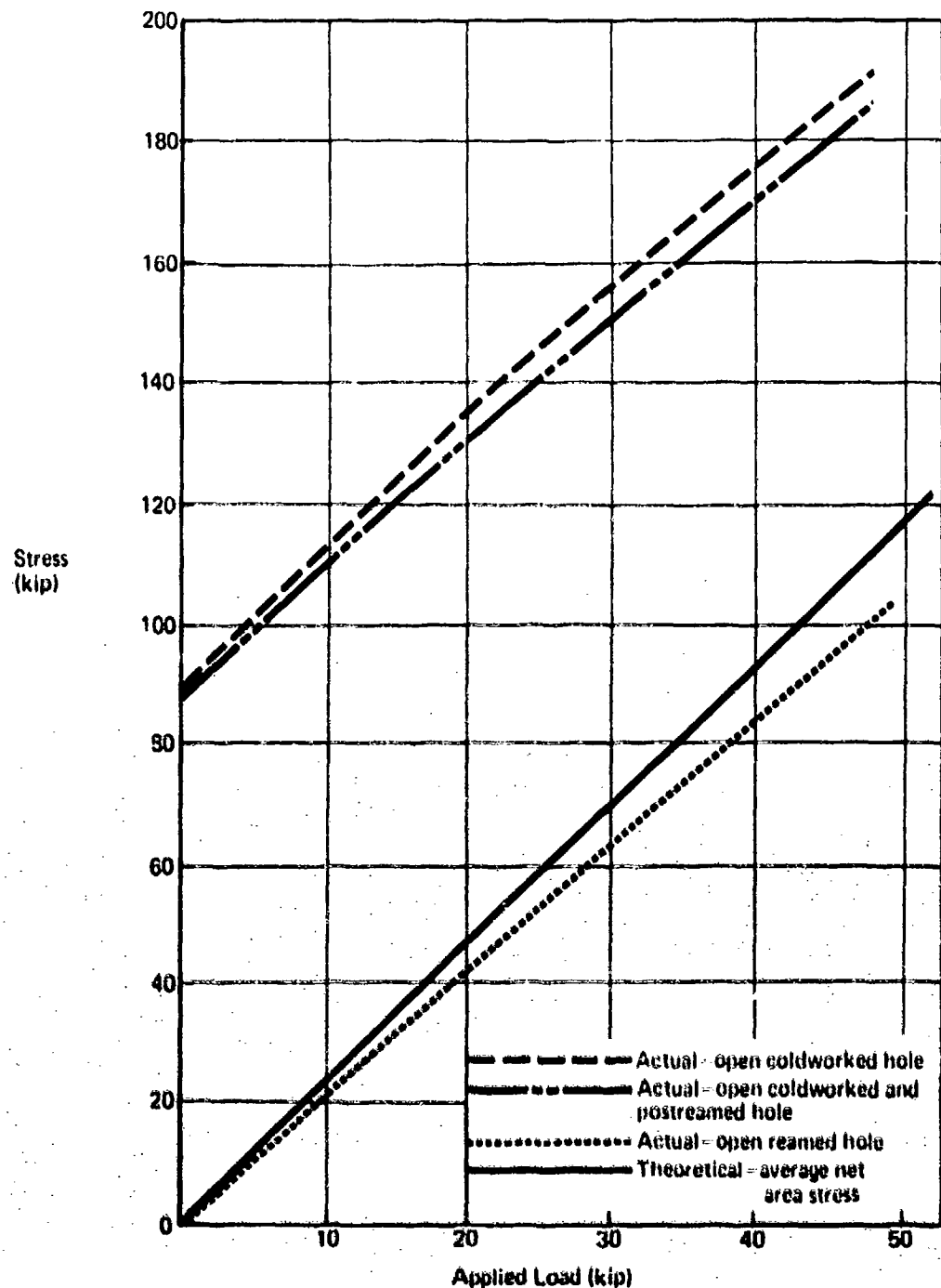
Figure 201. Stress at Specimen Edge Adjacent to Hole 300M Steel (270-300 KSI)

Material	Hole diameter (in.)	Coldworking interference (in.)	Stress increase (psi)	Yield strength (psi)
2024-T851	3/8	0.019	17,000	58,000
Ti-6Al-4V (annealed)	3/8	0.019	31,500	136,000
300M (270-300 ksi)	3/8	0.023	89,000	250,000

Figure 202. – Tensile Stress Increase From Coldworking at Point Adjacent to Hole on Edge of 2D Edge Margin Specimen

C/W; 2.50D·E/M
C/W; 2D E/M
C/W; 1.75D·E/M
C/W, 2D·E/M
C/W;2D·E/M

5D

C/W; 2D E/M

4D

C/W, 2D·E/M

3D

C/W; 2D·E/M

C/W; 2D·E/M

4D

C/W; 2D·E/M

4D

C/W; 2D·E/M

3D

C/W; 2D·E/M

C/W; 2D·E/M

2 PLACES,
3D and 4D
spacing

C/W,2D·E/M

C/W; 2D·E/M
csk far side after C/W

C/W; 2D·E/M
csk far side before C/W

0.375·In. Diameter Holes 0.019 C/W Interference

Figure 20.3   Photo Stress Coupon, 20°T·T·S·1   Aluminum   Entrance Side

C.W. 2D E/M

↕ 4D

C/W. 2D E/M

↕ 4D

C.W. 2D E/M

↕ 3D

C.W. 2D E/M

2 places,
3D and 4D
ream only

C/W. 2D E/M

Csk after
C/W. 2D E/M

Csk before
C/W. 2D E/M

C.W. 2.5D E/M

C/W. 2D E/M

C/W. 1.75D E/M

C.W. 1.50D E/M

C.W. 2D E/M

↕ 5D

C/W. 2D E/M

↕ 4D

C.W. 2D E/M

↕ 3D

C/W. 2D E/M

0.375-In. Diameter Holes — 0.019 C/W Interference

Figure 204   Photo Stress Coupon 2014-T851 Aluminum — Exit Side
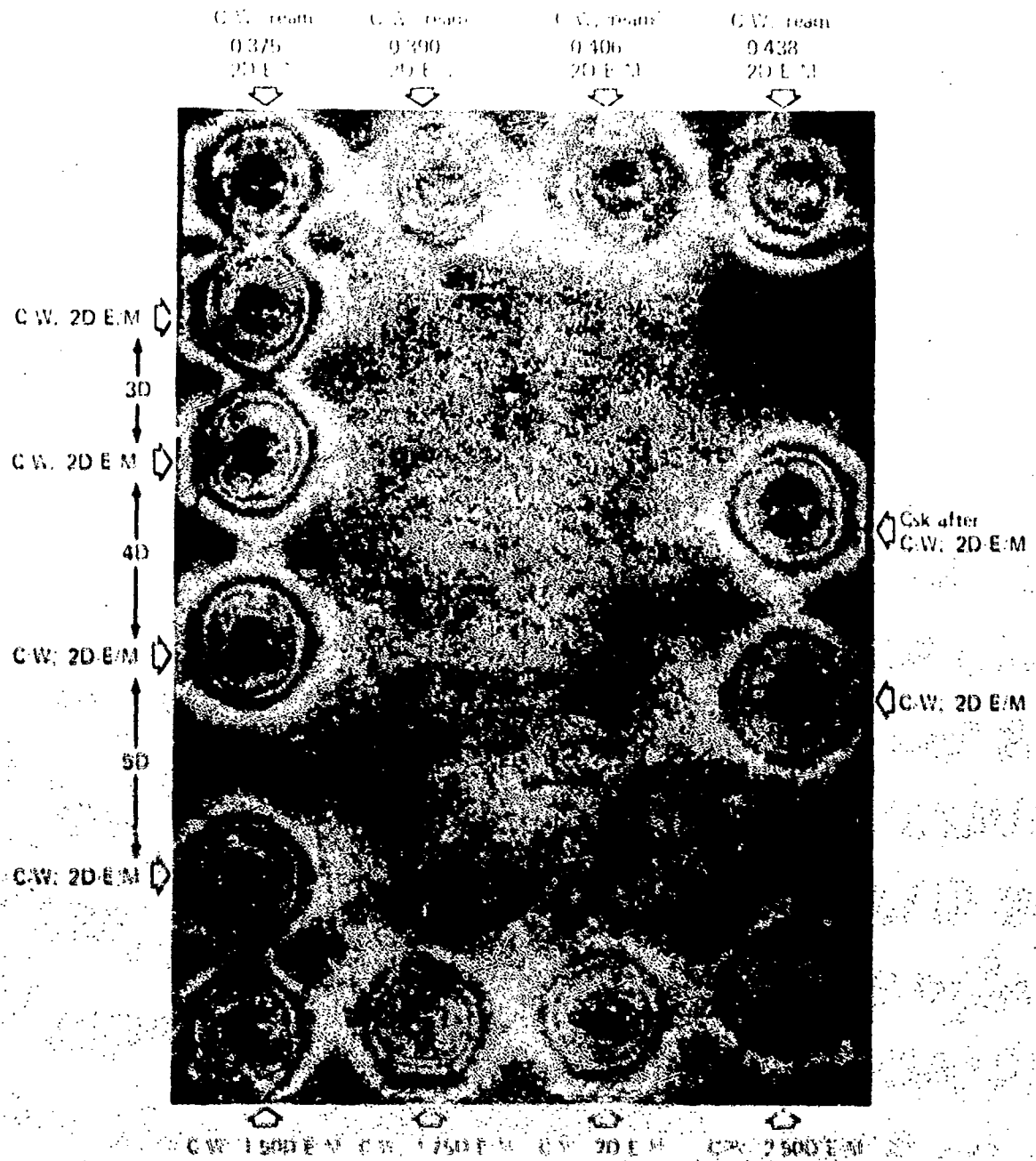
0.375-in. Diameter Holes 0.019 C/W Interference

Figure 205. Photo Stress Comparison Test 11-11 (Bacchus) D. Entrance Side

C/W; ream 0.438 2D-E/M

C/W; ream 0.406 2D-E/M

C/W; ream 0.390 2D-E/M

C/W; ream 0.375 2D-E/M

C/W; 2D-E/M

3D

C/W; 2D-E/M

4D

C/W; 2D-E/M

5D

C/W; 2D-E/M

Csk far side after C/W; 2D-E/M

C/W; 2D-E/M

C/W; 2.5D-E/M   C/W; 2D-E/M   C/W; 1.75D-E/M   C/W; 1.50D-E/M
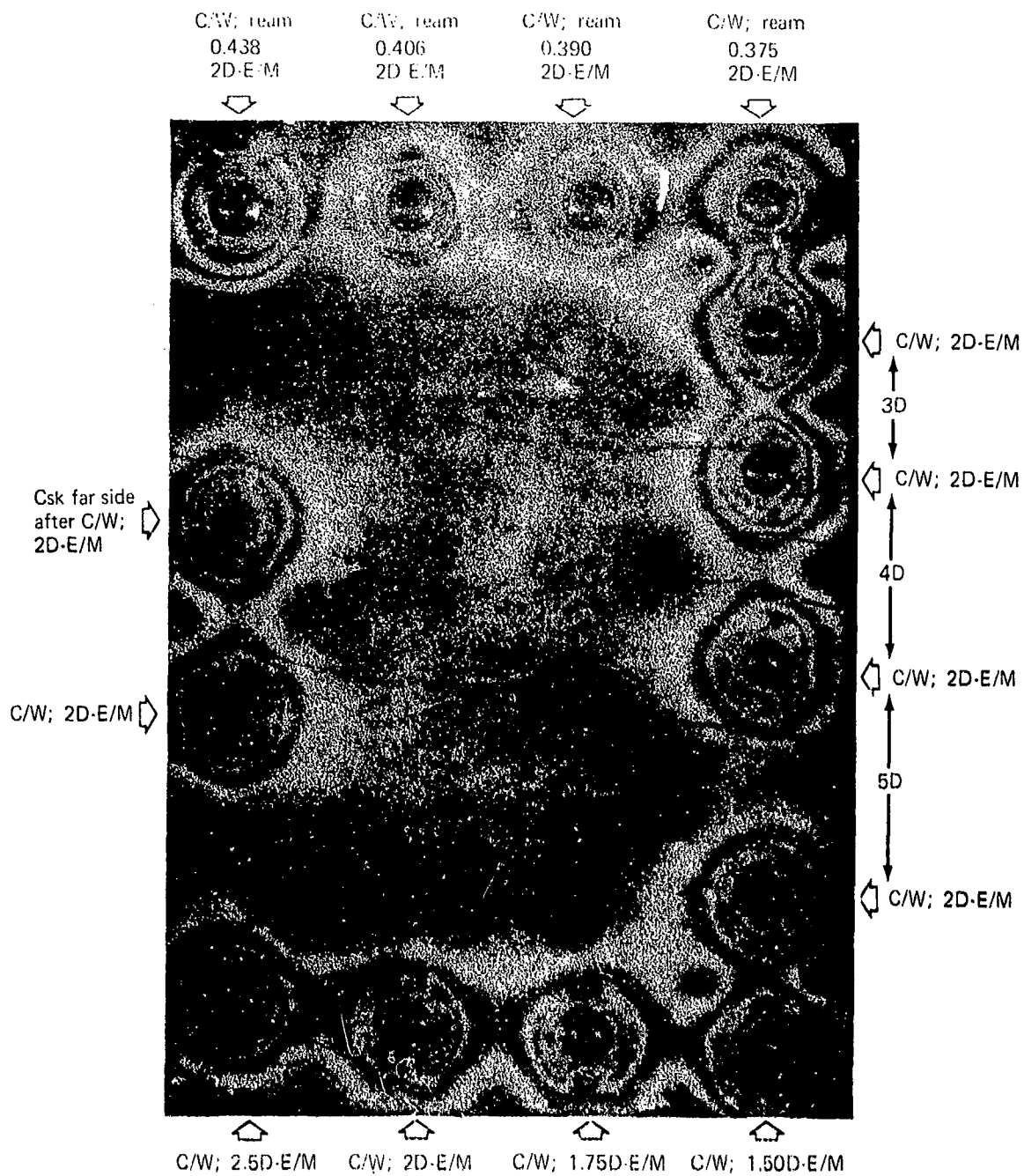
0.375-In. Diameter Holes—0.019 C/W Interference

Figure 206   Photo Stress Coupon Ti-6Al-4V (Condition I) Exit Side
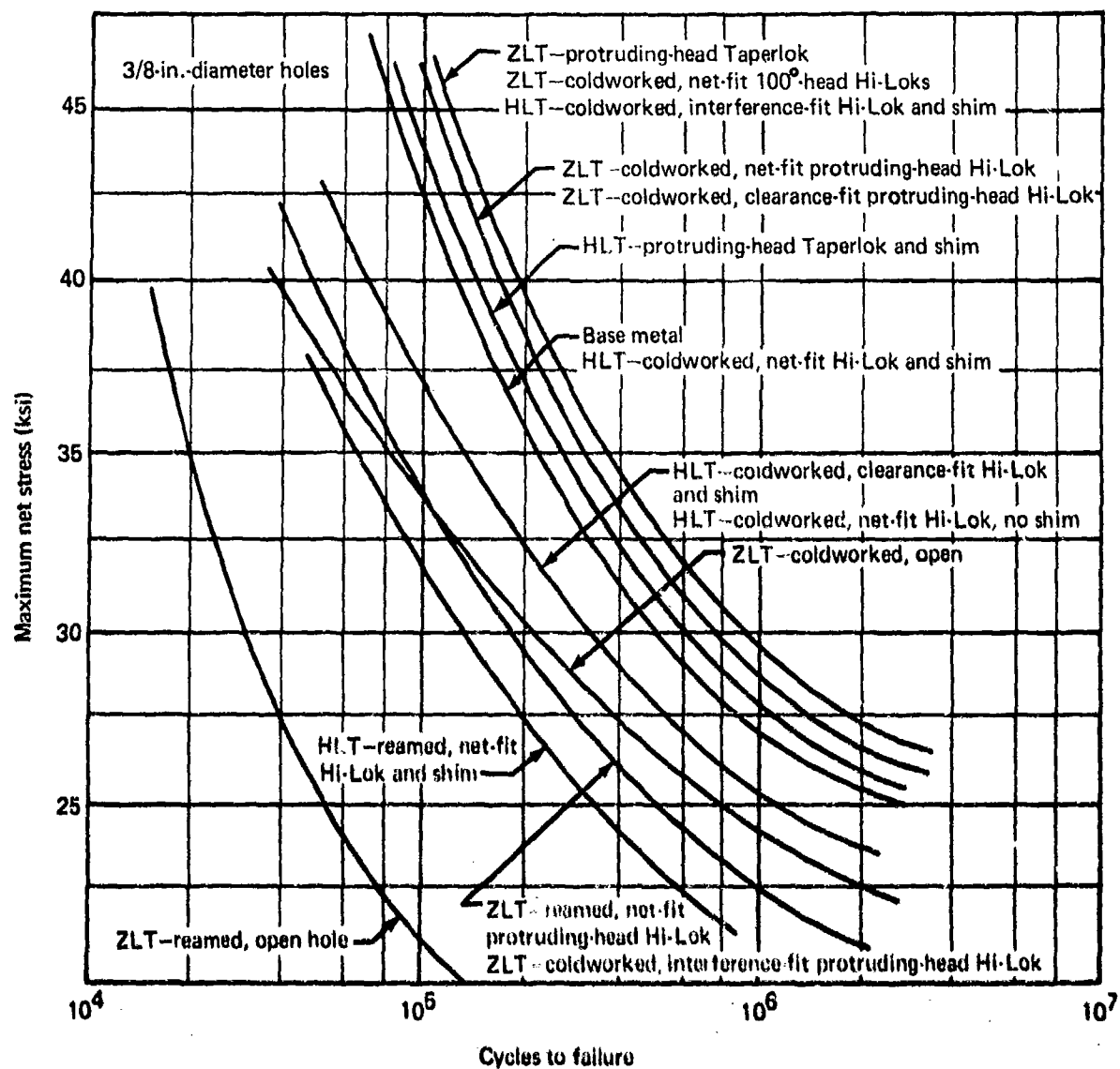
Figure 207. – Extrapolated S-N Curves – 2024-T851

Figure 208. Extrapolated S-N Curves—Ti-6Al-4V

The graph axes and labels:
- Y-axis: Maximum net stress (ksi), ranging from 45 to 100
- X-axis: Cycles to failure, ranging from 10^4 to 10^7
- Top right label: 3/8-in.-diameter holes

Curve labels (top to bottom, right side):
- Base metal
- ZLT—coldworked, interference fit
- ZLT—coldworked, net fit
- ZLT—coldworked, clearance fit
- ZLT—reamed, net fit
- ZLT—coldworked, open and HLT Taperlok
- ZLT—reamed, open and HLT interference fit

Curve labels (left side):
- HLT—no shim, net fit
- HLT—reamed
- HLT—coldworked, net fit and shim

NOTES: ZLT Taperloks not included (excessive scatter).
See section IV, B, 1. for perspective.

Figure 209.—Extrapolated S-N Curves—300M Steel (270-300 KSI)

The chart is labeled as follows:

Y-axis: Maximum net stress (ksi), with gridlines at 140, 130, 120, 110, 100

X-axis: Cycles to failure, from 10^3 to 10^7

Curve labels:
- Base metal
- ZLT–coldwork, filled (pull process)
- ZLT–reamed, Hi-Loks
- ZLT–coldworked, open
- ZLT–coldworked, 100° postcountersunk Hi-Loks
- ZLT–coldworked, net-fit and clearance-fit Hi-Loks
- ZLT–coldworked, open hole, no postream
- ZLT–reamed, open
- ZLT–coldworked, 100° precountersunk Hi-Loks
- HLT–coldworked (a)
- HLT–reamed

Legend box:
3/8-in.-diameter holes
All Hi-Loks net fit unless otherwise noted
All coldworked holes postreamed unless noted

aNet fit, clearance fit, interference fit with and without shim.

293

Condition and performance

Material	Maximum net stress (ksi)	Load transfer	Reamed, open		Reamed, Hi-Lok		Coldworked, open		Coldworked, Hi-Lok		Coldworked and countersunk Hi-Lok		Countersunk and coldworked, Hi-Lok	
			Average cycles	Origin	Average cycles	Origin	Average cycles	Origin	Average cycles	Origin	Average cycles	Origin	Average cycles	Origin
2024-T851	30	Zero	45,000	A	150,000	A	300,000	B	800,000	C	1,200,000	C	200,000	E
		High	--		150,000	A	--		500,000	B	--		--	--
300M	110	Zero	50,000	B	70,000	B	50,000	B	325,000	B	10,000,000 NF	E	30,000	D/E
		High	--		4,000	A	--		17,000	A/B	8,000	D	--	--
Ti-6Al-4V (annealed)	70	Zero	30,000	A	80,000	A	70,000	A/B	500,000	A	300,000	A	800,000	A
		High	--		15,000	A	--		30,000	A	10,000	D	--	--

All fasteners net fit   Failure origin locations:

Figure 210.—Material Fatigue Trends and Comparisons

Material	Maximum net stress (ksi)	Load transfer	Averages cycles to failure				
			Reamed Protruding-head	Coldworked protruding-head	Coldworked flush-head	Protruding-head Taperlok	Flush-head Taperlok
2024-T851	30	Zero	150,000[a]	800,000[a]	1,200,000[a][c]	1,200,000	200,000
		High	150,000[a]	800,000[b]	—	700,000	—
Ti-6Al-4V (annealed)	70	Zero	80,000[a]	4,000,000[b]	800,000[a][d]	1,000,000[e]	300,000[e]
		High	15,000[a]	25,000[b]	10,000[a][c]	70,000	9,000

[a]Net fit
[b]Interference fit
[c]Countersunk after coldwork
[d]Countersunk before coldwork
[e]Wide scatter

Figure 211.—System Performance Comparisons

Condition	2024-T851			Ti-6Al-4V			300M (270-300 ksi)		
	ZLT	LLT	HLT	ZLT	LLT	HLT	ZLT	LLT	HLT
Base metal	42	--	--	110	--	--	140	--	--
Reamed open	22	--	-	52	--	--	105	--	--
C/W open	33	--	--	63	--	--	100 118[a]	--	.
Reamed only with net-fit protruding-head Hi-Lok	33	No data	32[b]	66	No data	46[b]	105	No data	73[b]
C/W and postreamed with net-fit protruding-head Hi-Lok	46	42	37 42[b]	86	67	56 48[b]	120	No data	84 84[b]
C/W--no postream, with net-fit protruding-head Hi-Lok	No data	42	No data	No data	64	No data	No data	No data	No data
C/W and postreamed with clearance-fit protruding-head Hi-Lok	46	No data	37[b]	77	No data	48[b]	120	No data	84[b]
C/W and postreamed with interference-fit protruding-head Hi-Lok	33	No data	52[b]	98	No data	52[b]	115	No data	84[b]
Pre-csk, C/W, and postreamed with net-fit 100-head Hi-Lok	33	No data	No data	87	No data	No data	95	No data	No data
C/W, postreamed and post-csk with net-fit 100-head, Hi-Lok	47	No data	No data	83	No data	42[b]	130	No data	78[b]
Protruding-head Taperlok	47	No data	43[b]	91	No data	65[b]	No data	No data	No data
100-head Taperlok	35	No data	No data	82	No data	42[b]	No data	No data	No data

[a] No postream
[b] With micarta shim

Figure 212.—Allowable Average Operating Stress (KSI) Within 2D Zone of Fastener To Produce 100,000 Cycles (No Safety Factor)
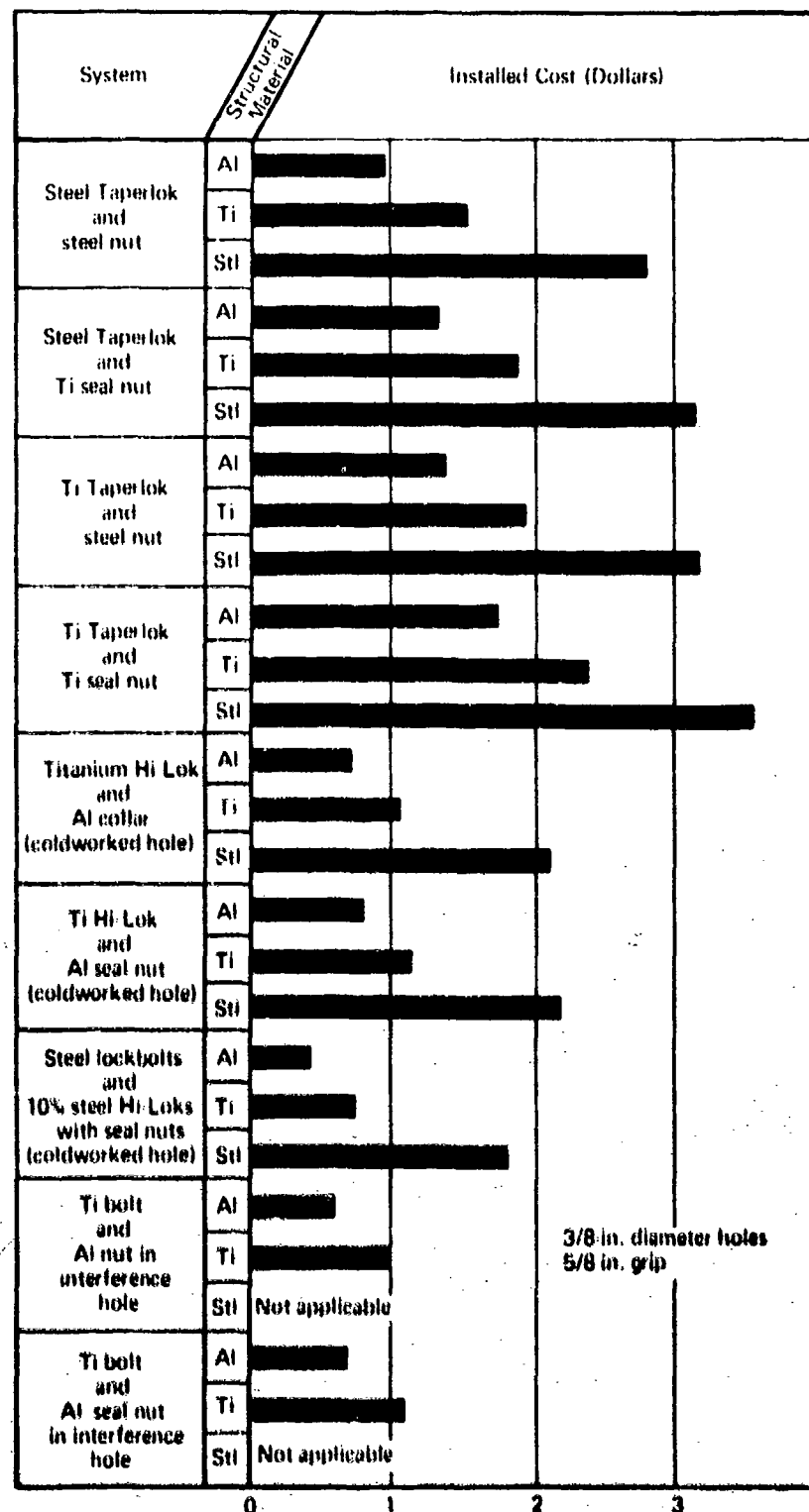
Figure 213.—Installed Cost for Different Fatigue-Rated Fastener Systems
in Aluminum, Titanium, and Steel

DISTRIBUTION LIST

DEPARTMENT OF THE AIR FORCE

AFML/MXA
WPAFB, OH 45433

AFML/MX (Librarian)
WPAFB, OH 45433

AFML/LTM
WPAFB, OH 45433

AFFDL/FBS
Attn: Applied Mechanics Branch
WPAFB, OH 45433

AFLC/MAUT
Attn: Lt. Col. S. G. Martin
WPAFB, OH 45433

AFLC/MME
Attn: Mr. A. B. Richter
WPAFB, OH 45433

ASD/SDXE
Attn: Mr. Ray Ingram
WPAFB, OH 45433

ASD/ENFS
Attn: Mr. Dick Stewart
WPAFB, OH 45433

ASD/YAEF
Attn: Mr. Harold W. Howard
C-5A SPO Bldg. 52
WPAFB, OH 45433

AFFDL
Attn: Mr. Clark Beck
WPAFB, OH 45433

AFFDL/FBT
Attn: Mr. R. L. Cavanagh
WPAFB, OH 45433

AFFDL/FBS
Attn: Mr. J. F. Nicholson
WPAFB, OH 45433

AFFDL/FBA
Attn: Mr. V. Russo
WPAFB, OH 45433

HA USAF/RDPI
Attn: Maj. T. F. Kennedy, Jr.
Washington, DC 20330

HQ AFSC
Andrews AFB
Washington, DC 20332

HQ USAF/RDPS
Washington, DC 20330

AIR MATERIALS AREAS (AMAs)

OOAMA/NME
Hill AFB, UT 84401

OCAMA/NME
Tinker AFB, OK 73145

SAAMA/NME
Kelly AFB, TX 78241

WRAMA/NME
Robins AFB, GA 31093

SMAMA/NME
McClellan AFB, CA 95652

SMAMA/MMEAS
Attn: Lt. Col. Schneider
McClellan AFB, CA 95652

DEPARTMENT OF THE ARMY

U. S. Army Production Equipment Agency
Rock Island Arsenal
Attn: Mfg. Technology Div. AMXPE-MT
Rock Island, IL 61201

DEPARTMENT OF THE NAVY

Commander
Naval Air Systems Command
Headquarters (AIR-50181)
Washington, DC 20360

Commanding Officer
Naval Air Development Center
(Aero Materials Department)
Johnsville
Warminster, PA 18974

Naval Air Development Center
Air Vehicle Technology Dept. Structures Div.
Attn: Code 30332-PK
Warminster, PA 18974

Director
Naval Research Laboratory (Code 2020)
Washington, DC 20360

DEPARTMENT OF DEFENSE

Defense Metals Information Center
Battelle Memorial Institute
Attn: Library
505 King Avenue
Columbus, OH 43201

OTHER GOVERNMENT AGENCIES

National Aeronautics and Space Adm.
Langley Research Center
Attn: Mr. Robert Baucom
Hampton, VA 23365

NASA/Langley Research Center
Attn: Mr. John Crews, Jr.
Mail Stop 465
Hampton, VA 23665

NASA/Lewis Research Center
Structures and Manufacturing R&D
21000 Brookpark Road
Cleveland, OH 44135

National Adacemy of Sciences
National Research Council
Materials Advisory Board
2101 Constitution Ave., N. W.
Washington, DC 20418

DEFENSE CONTRACTORS

Aerojet-General Corporation
Dept. 4923, Building 160
Attn: Technical Library
1100 West Hollyvale
Azusa, CA 91702

Aeronca Manufacturing Company
Attn: Technical Library
1712 Germantown Road
Middletown, OH 45042

Aeroprojects, Inc.
Attn: Mr. Phil Krause
310 E. Rosedale Ave.
West Chester, PA 19380

AiResearch Manufacturing Co.
Attn: Technical Library
9851-9951 Sepulveda Blvd.
Los Angeles, CA 90045

Amerace Corporation
ESNA Division
Attn: Mr. Frank E. Sisson
2330 Vauxhall Road
Union, NJ 07083

Air Industries Corporation
Attn: Mr. Ernest A. Morales
12570 Knott St.
Garden Grove, CA 92640

Aluminum Company of America (ALCOA)
Attn: Mr. Gregory B. Barthold
Manager, Technical Programs
1200 Ring Building
Washington, DC 20036

Avco Corporation
Aerospace Structures Division
Attn: Mr. Harold Black, V. P.
Nashville, TN 37202

Avibank Mfg., Inc.
Attn: Mr. E. L. Thorp
210 South Victory Bldv.
Burbank, CA 91503

Battelle Memorial Institute
Attn: Mr. Steve Ford
505 King Avenue
Columbus, OH 43201

The Boeing Aerospace Company
Attn: Mr. A. White, Manager
Manufacturing R&D
Mail Stop 1F-41
P. O. Box 3707
Seattle, WA 98124

Boeing Commercial Airplane Company
Attn: Mr. J. Phillips
Manufacturing R&D
Mail Stop 64-05
PO. Box 3707
Seattle, WA 98124

Boeing Commercial Airplane Company
Attn: Mr. H. E. Buffum
Director, Engineering Operations
Mail Stop 77-31
P. O. Box 3707
Seattle, WA 98124

Boeing Commercial Airplane Company
Attn: Mr. J. Chocola
Mail Stop 77-16
P. O. Box 3707
Seattle, WA 98124

The Boeing Vertol Company
Attn: Mr. M. Rohner, Manager
Manufacturing R&D
Boeing Center
P. O. Box 16858
Philadelphia, PA 19142

The Boeing Wichita Company
Attn: Mr. V. Gerstner, Manager
Manufacturing R&D
Mail Stop K14-38
3801 S. Oliver
Wichita, KS 67210

The Boeing Wichita Company
Attn: Mr. J. Wherry, Chief Structures
Mail Stop K16-24
3801 S. Oliver
Wichita, KS 67210

Beech Aircraft Corporation
Attn: Technical Library
Wichita, KS 67202

The Bendix Corporation
Bendix Products Aerospace Div.
Technical Library
South Bend, IN 46624

Bell Aerosystems Company
Attn: Technical Library
P. O. Box 1
Buffalo, NY 14205

Bell Helicopter Company
Attn: Technical Library
P. O. Box 482
Fort Worth, TX 76101

Cherry Rivet Division
Townsend Company
Attn: Mr. W. B. Causey
Manager, Technical Services
1224 East Warner Avenue
Santa Ana, CA 92707

Cherry Rivet Division
Townsend Company
Attn: Mr. Larry G. Kaps
1224 East Warner Avenue
Santa Ana, CA 92707

Cherry Rivet Division
Townsend Company
Attn: Mr. Glenn R. Willey, Engineer
1224 East Warner Avenue
Santa Ana, CA 92707

Curtiss-Wright Corporation
Wright-Aeronautical Division
Attn: Mr. J. D. Sverdlik
              Supvr. Mfg. Research
Wood Ridge, NJ 07075

Detroit Diesel-Allison
Attn: Mr. K. K. Hanin, Manager
              Engineering Operations
P. O. Box 894
Indianapolis, IN 46206

Douglas Aircraft Company (1-18)
Attn: Mr. Ed Pampy
3855 Lakewood Boulevard
Long Beach, CA 90846

Douglas Aircraft Company
Attn: Mr. J. D. Van Dyke
              Chief Engineer
AMST Prototype Program YC-15
Mail Code 41-41
3855 Lakewood Blvd.
Long Beach, CA 90846

Fairchild Industries
Attn: Technical Library
Hagerstown, MD 21740

Convair Aerospace Div/San Diego Oper.
General Dynamics Corp.
Attn: Technical Library
P. O. Box 1950
Lindbergh Field
San Diego, CA 92112

Convair Aerospace Division
General Dynamics Corporation
Attn: Dr. M. G. Miller
Mail Zone 643-20
P. O. Box 80847
San Diego, CA 92138

Convair Aerospace Division
Attn: Mr. Fiske Hanley
P. O. Box 748
Fort Worth, TX 76101

Convair Aerospace Div/Ft. Worth Oper.
General Dynamics Corp.
Attn: Technical Library
P. O. Box 748
Fort Worth, TX 76101

Dresser Industries, Inc.
Attn: Mr. W. P. Etheridge
Marketing Division Tool Group
12115 E. Slauson Avenue
Santa Fe Springs, CA 90670

General Electric Company
Attn: Mr. M. R. J. Kerzlenik
          Process Technology Programs
Aircraft Engine Group
Cincinnati, OH 45215

General Electric Company
Attn: Mr. Gy Bellows
Aircraft Engine Group
Cincinnati, OH 45215

General Electric Company
Attn: Mr. A. Sundberg
Cincinnati, OH 45215

Grumman Aerospace Corporation
Attn: Mr. John Huber
South Oyster Bay Road
Bethpage, NY 11714

Grumman Aerospace Corporation
Attn: Technical Library Plant 35
Bethpage, L. I., NY 11714

Grumman Aerospace Corporation
Attn: Mr. Carl Micillo, Manager
Adv. Mats and Processes Dev.
Plant 12
Bethpage, L. I., NY 11714

Hi-Shear Corporation
Attn: Mr. Neil R. Gore
P. O. Box 141
Baldwin, MO 63011

Hi-Shear Corporation
Attn: Mr. Frank Gill
2600 Skypark Drive
Torrance, CA 90509

Hi-Shear Corporation
Attn: Mr. Ed Hatter
2600 Sky Park Drive
Torrance, CA 90509

Huck Manufacturing Company
Attn: Mr. Paul A. Tibbals
Manager, Fastener Development
2500 Bellevue Avenue
Detroit, MI 48207

Hughes Aircraft Division
Attn: Technical Library
Florence and Teale Streets
Culver City, CA 90230

Industrial Designers, Inc.
Attn: Mr. P. E. Gunderson, Gen. Mgr.
6406 S. 143rd St.
Tukwila, WA 98168

Kaynar Mfg. Co., Inc.
Attn: Mr. Joseph P. Zupan
800 So. State College Blvd.
Fullerton, CA 92631

Lockheed-California Company
Central Library Dept. 72-35
Building 63-1
Burbank, CA 91503

Lockheed-California Company
Lockheed Aircraft Corporation
Attn: Mr. Robert L. Vaughn
Rotary Wing Projects
Burbank, CA 91503

Lockheed-California Company
Lockheed Aircraft Corporation
Attn: Mr. John H. Wooley
R&D Program Coordinator
Burbank, CA 91503

Lockheed-California Company
Lockheed Aircraft Corporation
Attn: Mr. Robert B. Urzi
Senior Research Engineer
Burbank, CA 91503

Lockheed-Georgia Company
Division of Lockheed Aircraft Corp.
Attn: Technical Library
Marietta, GA 30061

Lockheed-Georgia Company
Attn: Mr. J. R. Beard, Jr.
Marietta, GA 30060

Lockheed-Georgia Company
Attn: Mr. Hugh Davis
86 South Cobb Drive
Marietta, GA 30060

Lockheed-Georgia Company
Attn: Mr. T. Nelson Bridges
Dept. 42-11
Marietta, GA 30060

Kaman Aircraft
Attn: Mr. W. N. Stone
Bloomfield, CT 06002

John O. King, Inc.
Attn: Mr. John O. King
711 Trabert Ave. N. W.
Atlanta, GA 30318

LVT Aerospace Corporation
Vought Aeronautics Division
Attn: Mr. W. W. Wood, Chief of Mfg.
         Research and Development
P. O. Box 5907
Dallas, TX 75222

Metcut Research Associates Inc.
3980 Rosslyn Drive
Cincinnati, OH 45209

McDonnell Aircraft Company
Attn: Mr. Ed P. Bonney
Lambert St. Louis Municipal Airport
P. O. Box 516
St. Louis, MO 63166

McDonnell Douglas Corporation
Attn: Mr. Howard Siegel, Manager
         Material and Process Dev.
P. O. Box 516
St. Louis, MO 63166

McDonnell Douglas Corporation
Attn: Technical Library
3855 Lakewood Blvd.
Long Beach, CA 90801

Marquardt Corporation
Attn: Technical Library
16555 Saticoy Street
Van Nuys, CA 91408

The Martin-Marietta Company
Attn: Engineering Library
         M. P. 30
P. O. Box 5837
Orlando, FL 32802

The Martin-Marietta Corp.
Attn: Technical Library
Baltimore, MD 21233

North American Rockwell
Attn: Mr. Michael L. Hansen
Supervisor, B-1 Division
International Airport
Los Angeles, CA 90009

North American Rockwell
Los Angeles Division
Attn: Mr. T. R. Dutko
Structural Projects
Research and Engineering
International Airport
Los Angeles, CA 90009

North American Rockwell Corp. (2 copies)
Los Angeles Division
Attn: Technical Library
Los Angeles, CA 90009

Northrop Norair
Attn: Technical Information
3901 W. Broadway
Hawthorne, CA 90250

Northrop Corporation
Attn: Mr. R. H. Pugh
Manufacturing R&D
3901 West Broadway
Hawthorne, CA 90250

Northrop Corporation
Aircraft Division
Attn: Mr. Al Langlois
Manufacturing R&D
3901 West Broadway
Hawthorne, CA 90250

Northrop Corporation
Aircraft Division
Attn: Mr. B. Gaiennie, Manager
Manufacturing R&D
Dept. 5205, Zone 16
3901 W. Broadway
Hawthorne, CA 90250

Olympic Fastening Systems, Inc.
Attn: Mr. James K. Leeg
11445 So. Dolan Street
Downey, CA 90241

Omark Industries, Inc.
Attn: Mr. A. Leach
2100 S. E. Millport Road
Portland, OR 97222

Omark Industries, Inc.
Attn: Mr. John Bingham,
Vice President
1415 East Grand Avenue
El Segundo, CA 90246

Omark Industries
Aerospace Tooling Division
Attn: Mr. Larry Salinas,
Sales Engineer
1415 East Grand Avenue
El Segundo, CA 90245

Rockwell International/Palmdale
Attn: Mr. Jim Pierce
Site 1, AF Plant 42
1500 Avenue M
Palmdale, CA 93550

Rohr Aircraft Corporation
Attn: Technical Library
P. O. Box 878
Chula Vista, CA 92101

Rohr Aircraft Corporation
Attn: Materials and Process Dev.
P. O. Box 643
Riverside, CA 92502

Republic Aviation Division
Fairchild Industries
Attn: Mr. G. Pfanner, Chief
Mfg. Research and Processes
Farmingdale, L. I., NY 11741

Rust-Lick Incorporation
Attn: Mr. John S. Reeder, Jr.
Sales Manager
92 Taylor Street
Danbury, CT 06810

Ryan Aeronautical Company
Attn: Technical Library
2701 Harbor Drive
San Diego, CA 92101

Sikorsky Aircraft
Attn: Mrs. K. P. Lucas
Division Library
North Main Street
Stratford, CT 06602

Solar Division
International Harvester Company
Attn: Technical Library
2200 Pacific Highway
San Diego, CA 92112

Standard Pressed Steel Co.
Attn: Mr. Thomas Baumgartner
       Manager, Engineering
Precision Fastener Division
Jenkintown, PA 19046

Technical Information Center
Cincinnati Milacron
Cincinnati, OH 45209

Tiodize Co., Inc.
817 N. Lake Street
Burbank, CA 91502

TRW, Inc.
Attn: Technical Library
23555 Euclid Avenue
Cleveland, OH 44117

United Aircraft Corporation
Pratt & Whitney Aircraft Div.
Attn: Technical Library
Florida Research and Development Center
West Palm Beach, FL 33401

United Aircraft Corporation
Pratt & Whitney Aircraft Div.
Attn: Mr. Douglas H. Secord
400 Main Street
East Hardford, CT 06108

United Aircraft Corp.
Hamilton Standard Div.
Attn: Technical Library
Windsor Locks, CT 06096

Valley-Todeco, Inc.
Attn: Mr. Jagdish Sekhon
Engineering Manager—Fasteners
12975 Bradley Avenue
Sylmar, CA 91342

VOI-Shan
Division of VSI Corporation
Attn: Mr. William H. Trembley
       Director of Engineering
8463 Higuera Street
Culver City, CA 90230

DOCUMENT CONTROL DATA - R & D
(Security classification of title, body of abstract and indexing annotation must be entered when the overall report is classified)

1. ORIGINATING ACTIVITY *(Corporate author)*	2a. REPORT SECURITY CLASSIFICATION
Boeing Commercial Airplane Company P.O. Box 3707 Seattle, Washington 98124	Unclassified
	2b. GROUP

3. REPORT TITLE

SLEEVE COLDWORKING FASTENER HOLES
Volume I–Discussion and Summary

4. DESCRIPTIVE NOTES *(Type of report and inclusive dates)*

Final Technical Report   1 June 1972 through 30 November 1973

5. AUTHOR(S) *(First name, middle initial, last name)*

Joseph L. Phillips

6. REPORT DATE	7a. TOTAL NO. OF PAGES	7b. NO. OF REFS
February 1974	305	2

8a. CONTRACT OR GRANT NO.	9a. ORIGINATOR'S REPORT NUMBER(S)
F33615-72-C-1630	
b. PROJECT NO.	D6-26271-6
746-2	
c.	9b. OTHER REPORT NO(S) *(Any other numbers that may be assigned this report)*
d.	AFML-TR-74-10, Volume I

10. DISTRIBUTION STATEMENT

Distribution limited to U.S. Government agencies only; test and evaluation data; February 1974. Other requests for this document must be referred to Manufacturing Technology Division, Air Force Materials Laboratory, Wright-Patterson Air Force Base, Ohio 45433.

11. SUPPLEMENTARY NOTES	12. SPONSORING MILITARY ACTIVITY
See Volume II–Appendix	Fabrication Branch, Manufacturing Technology Division—Air Force Materials Laboratory, Wright Patterson Air Force Base, Ohio

13. ABSTRACT

In this 21-month program, optimized process parameters for sleeve coldworking of fastener holes have been developed, and the effects of process and application parameters on structural performance have been defined for selected aluminum, titanium, and high-strength steel alloys. The sleeve coldworking process for fastener holes is a process that uses a tapered mandrel in conjunction with a disposable, prelubricated sleeve to compressively prestress a significant size zone around each hole which offsets the stress concentration of the hole itself. The sleeve method allows higher degrees of prestressing than possible with other methods and offers potential for significant improvements in fatigue performance. In addition, it does not require precision controls germane to other fatigue-rated hole preparation/fastener installation systems. This technical report covers the results of this 21-month program. In addition to definition of optimized methods and the effects of process and application variations upon structural performance, the results include performance and economics comparisons for the process with other fatigue-rated hole preparation/fastener systems. Volume II contains test data sheets and other supporting data.

14. KEY WORDS	LINK A		LINK B		LINK C	
	ROLE	WT	ROLE	WT	ROLE	WT
Sleeve coldworking						
Fastener holes						
Coldworking						
Fatigue improvement						
Hole coldworking						
Hole prestressing						
Prestressing						
Coining						
Mandrel/sleeve prestressing						
Mandrel/sleeve coining						
Mandrel/sleeve coldworking						

THIS REPORT HAS BEEN DELIMITED
AND CLEARED FOR PUBLIC RELEASE
UNDER DOD DIRECTIVE 5200.20 AND
NO RESTRICTIONS ARE IMPOSED UPON
ITS USE AND DISCLOSURE.

DISTRIBUTION STATEMENT A

APPROVED FOR PUBLIC RELEASE;
DISTRIBUTION UNLIMITED.